Institute of Engineering Surveying and Space Geodesy
Department of Civil Engineering
Faculty of Engineering

Rapid Integer Ambiguity Resolution in GPS Precise Point Positioning

By
Jianghui Geng, BSc

Thesis submitted to the University of Nottingham for
the degree of Doctor of Philosophy
September 2010

Abstract

GPS precise point positioning (PPP) has been used in many scientific and commercial applications due to its high computational efficiency, no need for any synchronous measurements from a nearby reference receiver and homogeneous positioning quality on a global scale. However, these merits are devalued significantly by unresolved ambiguities and slow convergences of PPP. Therefore, this thesis aims at improving PPP's performance by resolving ambiguities for a single receiver and accelerating the convergences to ambiguity-fixed solutions in order to achieve a centimeter-level positioning accuracy with only a few seconds of measurements.

In recent years, ambiguity resolution for PPP has been developed by separating fractional-cycle biases (FCBs) from single-receiver ambiguity estimates. One method is to estimate FCBs by averaging the fractional parts of single-difference ambiguity estimates between satellites, and the other is to assimilate FCBs into clocks by fixing undifferenced ambiguities to integers in advance. The first method suffers from a large number of redundant satellite-pair FCBs and unnecessary 15-minute narrow-lane FCBs.

Therefore, this thesis suggests undifferenced FCBs and one narrow-lane FCB per satellite-pair pass over a regional area in order to reduce the size of FCB products and achieve comparable positioning quality with that of the original method. Typical tests show that ambiguity resolution dramatically reduces the RMS of differences between hourly and daily position estimates from 3.8, 1.5 and 2.8 cm in ambiguity-float solutions to 0.5, 0.5 and 1.4 cm in ambiguity-fixed solutions for the East, North and Up components, respectively. Likewise, the RMS for real-time position estimates are reduced from 13.7, 7.1 and 11.4 cm to 0.8, 0.9 and 2.5 cm.

Furthermore, this thesis improves the accuracy of narrow-lane FCBs with integer constraints from double-difference ambiguities. In a global network analysis, the RMS of differences for the East component between the daily and IGS weekly estimates is reduced from 2.6 mm in the solutions based on original FCBs to 2.2 mm in the solutions based on improved FCBs.

More importantly, for the first time, this thesis provides a theoretical proof for the equivalence between the ambiguity-fixed position estimates derived from the aforementioned two methods. This equivalence is then empirically verified by the overall minimal discrepancies of the positioning qualities between the two methods. However, these discrepancies manifest a distribution of geographical pattern, i.e. the largest discrepancies correspond to sparse networks of reference receivers. This comparison can provide valuable reference for the GPS community to choose an appropriate method for their PPP ambiguity resolution.

As the foremost contribution, an innovative method is originally developed in this thesis in order to effectively re-converge to ambiguity-fixed solutions with only a few seconds of measurements. Specifically, ionospheric delays at all ambiguity-fixed epochs are estimated and then predicted precisely to succeeding epochs in the case of re-convergences. As a result, the practicability of real-time PPP is greatly improved by eliminating the unrealistic requirement of a continuous open sky view in most PPP applications. Typical tests illustrate that over 90% of re-convergences can be achieved within five epochs of 1-Hz measurements, rather than the conventional 20 minutes, even if the latency for predicted ionospheric delays is up to 180 s. Moreover, for a van-borne receiver moving in a GPS-adverse environment where satellite number decreases significantly and cycle slips occur frequently, only when the above rapid re-convergence technique is applied can the rate of ambiguity-fixed epochs dramatically rise from 7.7% to 93.6% of all epochs.

Acknowledgements

This PhD project has been undertaken at the Institute of Engineering Surveying and Space Geodesy and fully funded by the University of Nottingham. A collaborative development of the Positioning and Navigation Data Analyst software is also performed with Wuhan University in China.

A very special thankyou to my supervisors, Dr Xiaolin Meng, Prof Alan H Dodson and Prof Norman Teferle, who have fully mentored and favoured me during my three years of study and living in a foreign land. I am quite grateful for their valuable guidance whenever I came into any difficulties in my research.

I would also like to thank Dr Maorong Ge from the GeoForschungsZentrum Helmholtz Center in Potsdam for his indispensable guidance on the technique development of my research. He has spent a lot of energy and helped me a lot for my future development and career plan. Thanks also go to Prof Jingnan Liu and Prof Chuang Shi at Wuhan University who have supported me during the past six years when I began to study GNSS techniques and their applications. They even kindly and generously paid my travel and living expense when I went back to China for a scientific conference. I am quite honored by Dr Jens Wickert and Dr Jan Douša's kind invitation for a professional visit to the GeoForschungsZentrum Helmholtz Center. I am also grateful to Prof T Marmont at Beacon Energy Ltd for his financial support.

Dr Richard Bingley as my internal assessor is acknowledged for his valuable suggestions on my 3-year research in IESSG. Dr Andy Sowter is appreciated for kindly reviewing my *GPS solutions* papers when I was deeply depressed by the journal editor's comments. Prof Terry Moore is specially thanked for paying my expenses during the IGS Workshop 2010 in Newcastle. Dr Chris Hill is thanked for his help when I got injured on my elbows. Dr Marcio Aquino is acknowledged for his help on the ionosphere issues. Dr Flavien Mercier from the Center National d'Etudes Spatiales, France is thanked for his patience when I had questions on his research. Prof Marek Ziebart as my external assessor is appreciated for spending his valuable time on reading this thesis.

Thanks also go to Mr Donglie Liu, Ms Yujie Jin, Mr Kai Wan, Dr Lei Yang and Dr Yidong Lou for their help and support during my living in the UK. Both Dr David Luff and Mr Craig Hancock are acknowledged for their help in reading and commenting my papers and thesis. I specially thank all IESSG staff and students for providing a nice environment for me during my PhD study.

Finally, I need to express my heartfelt thanks to my parents and brothers, Xiaolin's family and my lovely girlfriend Lin Xu for their emotional support without which I could have not focused on my study for three years.

Contents

List of Figures

List of Tables

Acronyms and abbreviations

3D	3-Dimensional
BIPM	Bureau International des Poids et Mesures
BKG	Bundesamt für Kartographie und Geodäsie, Federal Agency for Cartography and Geodesy
CHAMP	CHAllenging Minisatellite Payload
CODE	Center for Orbit Determination in Europe
CORS	Continuously Operating Reference Station
COSMIC	Constellation Observing System for Meteorology Ionosphere and Climate
CPU	Central Processing Unit
DCB	Differential Code Bias
DEOS	Delft–Institute of Earth-Oriented Space Research
DLR	Deutsches Zentrum für Luft- und Raumfahrt, German Aerospace Center
EGNOS	European Geostationary Navigation Overlay Service
EPN	EUREF Permanent Network
ERP	Earth Rotation Parameter
ESOC	European Space Operations Center
EUREF	European Reference Frame
EUREF-IP	EUREF-Internet Protocol
FCB	Fractional-Cycle Bias
FKP	Flächenkorrekturparameter, Area Correction Parameter
GDGPS	Global Differential GPS
GEO	Geosynchronous Earth Orbiter
GFZ	GeoForschungsZentrum
GIPSY-OASIS	GPS-Inferred Positioning SYstem and Orbit Analysis SImulation Software
GLONASS	Global'naya Navigatsionnaya Sputnikovaya Sistema
GMF	Global Mapping Function
GNSS	Global Navigation Satellite System
GPS	Global Positioning System
GPT	Global Pressure/Temperature
GRACE	GRAvity Climate Experiment
IERS	International Earth Rotation and Reference Systems Service
IESSG	Insitute of Engineering Surveying and Space Geodesy
IGS	International GNSS Service
INS	Inertial Navigation System
IRC	Integer-Recovery Clock

ITRF	International Terrestrial Reference Frame
JPL	Jet Propulsion Laboratory
KBR	K-Band Ranging
LAMBDA	Least-squares AMBiguity Decorrelation Adjustment
LEO	Low Earth Orbiter
LiDAR	Light Detection And Ranging
MAC	Master-Auxiliary-Concept
NAVSTAR	NAVigation Signal Timing And Ranging
NCTU	National Chiao Tung University
NGS	National Geodetic Survey
NRTK	Network RTK
OSGB	Ordnance Survey of Great Britain
PANDA	Positioning And Navigation Data Analyst
PPP	Precise Point Positioning
PRN	Pseudo-Random Noise
RINEX	Receiver INdependent EXchange
RMS	Root Mean Square
RTK	Real-Time Kinematic
SLR	Satellite Laser Ranging
SP3	NGS Standard Product – 3
TEC	Total Electron Content
TECU	Total Electron Content Unit
TEQC	Translation, Editing and Quality Check
UNAVCO	University NAVSTAR Consortium
US	United States
UT	Universal Time
UTC	Coordinated Universal Time
VMF	Vienna Mapping Function
VRS	Virtual Reference Station
VTEC	Vertical Total Electron Content
WAAS	Wide Area Augmentation System
ZTD	Zenith Tropospheric Delay

Chapter 1

Introduction

1.1 Precise GPS positioning

Since 1980s, the Global Positioning System (GPS) (McDonald 2002) has been recognized as an effective and valuable tool in acquiring positions on a global scale. Due to the low precision and the complicated error budget of GPS pseudorange measurements, the resulting accuracy of standard point positioning can only reach about 10 m (Alkan 2001). In differential GPS positioning where a reference receiver at a known position provides error corrections, however, the position estimate at a nearby receiver can usually achieve an accuracy of better than 1 m (Alkan 2001; Landau et al. 2007). This can be understood in terms of the spatial and temporal correlation of GPS errors in the satellite orbits and clocks, the tropospheric and ionospheric delays (Kaplan and Hegarty 2006). Hence, most measurement errors at the nearby receiver can be mitigated by the error corrections from the reference receiver. Unfortunately, this error mitigation deteriorates when the inter-receiver distance is increased. This is due largely to the spatial decorrelation of the atmospheric delays if the inter-receiver distance exceeds several tens of kilometers. In this case, a sparse network of reference stations can be established to both improve the accuracy of the satellite orbits and clocks, and generate a grid model for the ionospheric delays over a continental area (Kee et al. 1991). As a result, the positioning accuracy of around 1 m can be achieved even though the inter-receiver distance is up to a few hundred kilometers. Typical examples are the US (United States) Wide Area Augmentation System (WAAS) (Lawrence et al. 2007) and the European Geostationary Navigation Overlay Service (EGNOS) (Guida et al. 2007).

Nevertheless, GPS carrier-phase measurements have to be exploited if a centimeter-level positioning accuracy is required. Carrier-phase measurements are of millimeter-level precision, but suffer from their nuisance ambiguities which have to be estimated along with the other parameters of primary interest. A large number of ambiguities can considerably deteriorate the positioning quality. Fortunately, integer resolution of double-difference ambiguities can be routinely performed on baselines between a network of receivers by double differencing the carrier-phase measurements (e.g. Dong and Bock 1989). In this relative positioning, fixing ambiguities to integers can significantly improve the positioning quality, especially for the East component (Blewitt 1989; Dong and Bock 1989; Xu 2007). For example, Blewitt (1989) improved the daily baseline accuracy from 2.7, 1.0 and 3.6 cm to 1.0, 0.8 and 4.0 cm for the East, North and Up components, respectively, by applying integer ambiguity resolution to baselines of up to

2000 km; and at present, daily positioning accuracy can normally achieve millimeter level after a successful double-difference ambiguity resolution (e.g. Hill et al. 2009; King and Williams 2009; Puskas et al. 2007); furthermore, GPS measurements of only a few hours or even 5-15 minutes can lead to an ambiguity-fixed positioning accuracy of better than 2 cm for baselines of shorter than several tens of kilometers (e.g. Eckl et al. 2001; Ghoddousi-Fard and Dare 2006; Larson et al. 2001; Lazio 2007; Schwarz 2008; Soler et al. 2006; Wielgosz 2010); finally, centimeter-level positioning accuracy can also be obtained for ambiguity-fixed epoch-wise solutions, especially for the horizontal components, on short baselines of only a few tens of kilometers (e.g. Bouin et al. 2009; Han and Rizos 2000a; King 2009; Larson et al. 2007; Shan et al. 2007). For comparison, keeping float ambiguities can potentially jeopardize the final solutions. For example, King et al. (2003) indicated that keeping float ambiguities can introduce spurious periodic horizontal signals into a position time series. Tregoning and Watson (2009) reported that the spurious-signal amplitudes in the ambiguity-float position time series are significantly larger than those in the ambiguity-fixed ones.

Apart from these achievements in the post-processing mode, the real-time kinematic (RTK) positioning is also of great interest for the GPS community. Usually, ambiguity-fixed solutions can be achieved using a few seconds of measurements and the positioning accuracy is at the centimeter level if the baseline length is shorter than a few tens of kilometers (Dai 2000; Dai et al. 2007; Han 1997b). However, this convergence speed to an ambiguity-fixed solution is highly subject to the accuracy of atmospheric corrections, especially during an ionospheric storm characterized by irregular and heterogeneous properties over space and time (Dai et al. 2003; Kim and Tinin 2007; Pratt et al. 1997; Wielgosz et al. 2005). Hence, longer baselines will lead to lower success rates of instantaneous ambiguity resolution. In this case, a network of Continuously Operating Reference Stations (CORS) can be established to spatially interpolate the atmospheric corrections of which the accuracy is significantly improved over that provided by the normal RTK where only one reference station is employed (Fotopoulos and Cannon 2001; Musa et al. 2005; Pratt et al. 1997; Snay and Soler 2008). This service model is called network RTK (NRTK). As a result, the inter-station distance can be extended to 50-100 km, or even a few hundred kilometers (Grejner-Brzezinska et al. 2005; Landau et al. 2007; Park and Kee 2010). However, the deficiencies of NRTK are also obvious. On the one hand, interpolated atmospheric corrections are normally usable only within the coverage of the CORS network and the accuracy of atmospheric corrections is rapidly degraded when users locate far outside the CORS network (Grejner-Brzezinska et al. 2005, 2009). On the other hand, due largely to the costly establishment of CORS networks, NRTK can cover only a regional area and hence can hardly evolve into a precise positioning service on a global scale (Rizos 2007).

However, many real-time applications require high positioning accuracy of centimeter level on a wide-area or even a global scale. For example, in precision farming, the irrigation-conduit and seed-bed establishment, which require a positioning accuracy of better than 10 cm, may be conducted in an area of over hundreds of square kilometers (Mondal and Tewari 2007); the topographical surveying with photogrammetry or laser scanning requires centimeter-level positioning accuracy for airborne sensors over a large area where reference stations are not always available (Yuan et al. 2009); precise positioning in offshore and desert areas, e.g. ocean drilling, seafloor and sea-surface mapping, and geohazard mitigations for volcano eruptions and tsunami monitoring, normally cannot require any nearby reference stations to be built due to logistical feasibility and expense (e.g. Chadwell and Spiess 2008; Kato et al. 2005). Therefore, a

global positioning service providing instantaneous centimeter-level accuracy without establishing a global dense network of reference stations has become a strategic development direction in the GNSS-based (Global Navigation Satellite System) positioning technologies.

1.2 Precise point positioning (PPP)

Precise point positioning (PPP) is a GNSS positioning technique processing both undifferenced carrier-phase and pseudorange measurements at solely a single receiver by fixing known satellite orbits and clocks of centimeter-level accuracy (Zumberge et al. 1997). PPP is characterized by two aspects. On the one hand, PPP processes undifferenced carrier-phase and pseudorange measurements. Comparatively, the standard point positioning employs only pseudorange measurements and the precise relative positioning employs double-difference measurements. Note that the point positioning technique based on phase-smoothed pseudorange measurements actually applies the difference between epochs to carrier-phase measurements (Hatch 1982). On the other hand, PPP requires precise satellite orbits and clocks. For the positioning techniques shown in Section 1.1, however, this requirement is usually unnecessary.

1.2.1 Solution at a single receiver

In general, at a single receiver, its position, zenith tropospheric delay (ZTD), clock and ambiguities for all observed satellites are estimated in PPP (Kouba and Héroux 2001). For a dual-frequency receiver, the first-order ionospheric delays can be removed using the ionosphere-free combination observable (Hofmann-Wellenhof et al. 2001). The residual higher-order delays account for less than 0.1% of the total ionospheric delays and their impacts on the position estimates are presumed minimal, hence usually being ignored in PPP (see Hernández-Pajares et al. 2007; Petrie et al. 2010). For a single-frequency receiver, ionospheric delays are usually mitigated with a priori correction models (Le and Tiberius 2007; Øvstedal 2002), such as the IGS (International GNSS Service) Vertical Total Electron Content (VTEC) maps (Hernández-Pajares et al. 2009; Noll et al. 2009). Unfortunately, the errors of these maps can be up to 4.5 TECU (Total Electron Content Unit) on average which is approximately equal to 72 cm for the L1 frequency (Hernández-Pajares et al. 2009). Throughout this thesis, however, "PPP" always denotes "dual-frequency PPP" except when otherwise noted. Moreover, ZTD is projected with a specific mapping function to the slant direction in order to correct the tropospheric delays for all observed satellites (e.g. Boehm et al. 2006a,b; Guo and Langley 2003; Niell 1996). Finally, the receiver clock is estimated as white noise and the ambiguities are estimated as real-valued constants over continuous carrier-phase measurements.

Besides this estimation strategy, PPP is complicated by its state-of-the-art corrections including the antenna phase center offset and variation, the phase wind-up effect, the relativity effect, the tropospheric delay, the station displacement effects and the inter-pseudorange biases (Hofmann-Wellenhof et al. 2001; Kouba and Héroux 2001). For a satellite, its center of mass, referred to by its orbit, does not coincide with its antenna phase center. Hence, this phase center offset from the center of mass should be corrected (e.g. Cardellach et al. 2007; Dilssner et al. 2010; Ge et al. 2005b). Note that this correction is subject to the satellite attitude which is rather complicated and uncertain during eclipse periods (Bar-Sever 1996; Kouba 2009a). This correction also applies to the receiver antennas. Moreover, the actual phase center does not

coincide with the nominal one, but depends on the signal frequency and the relative position between the satellite and the receiver. This phase center variation is at the millimeter level. Since November 5th 2006, absolute phase centers, instead of the relative ones, have been applied to the IGS products (Schmid et al. 2007).

GPS satellites transmit right circularly polarized radio waves, and thus the incoming carrier-phase measurements depend on the mutual orientation between the satellite and receiver antennas. This effect is called phase wind-up (Wu et al. 1993). Specifically, a rotation of the receiver antenna around its boresight can change the carrier-phase measurements by up to one cycle (García-Fernández et al. 2008). For a mobile receiver, this wind-up effect is subject to the antenna attitude (Kim et al. 2006; Le and Tiberius 2006).

The relativity effect significantly affects the undifferenced GPS measurements (Hofmann-Wellenhof et al. 2001). On the one hand, the gravitational field results in a space-time curvature of the signal propagation. This propagation correction can be up to 18.7 mm for GPS satellites, but this correction is much smaller for the relative positioning (Zhu and Groten 1988). On the other hand, the satellite fundamental frequency is affected by the satellite motion and the difference of the gravitational fields at the satellite and the receiver, consequently changing the satellite clock. The resulting frequency shift under the assumption of circular orbits has been corrected in the emitted satellite clock frequency. The residual periodic effect due to this assumption can be up to 46 ns for the satellite clock, but cancels out in the relative positioning (Zhu and Groten 1988).

Tropospheric delays for the satellite signal propagation are divided into two parts, namely the hydrostatic delays caused by the dry atmosphere and the wet delays caused by the water vapor (Solheim et al. 1999). In order to simplify their impact on GPS positioning, a symmetric troposphere condition around a ground receiver is usually assumed and hence slant delays at the same elevation can be mapped to the vertical direction with identical mapping function. Typical mapping functions include the Niell mapping function by Niell (1996), the Global Mapping Function and the Vienna Mapping Function 1 by Boehm et al. (2006a,b). A priori zenith delays can be computed using the Hopfield or Saastamoinen models (Colombo 2006; Hopfield 1969; Jensen and Øvstedal 2008; Saastamoinen 1973). Normally, zenith hydrostatic delays can be modeled to an accuracy of a few millimeters if the surface meteorological measurements are known, whereas zenith wet delays can be modeled to only a few centimeters (Stoew et al. 2007; Tregoning and Herring 2006). As a result, residual zenith wet delays are usually estimated in PPP. Note that the residual tropospheric delays are larger at smaller elevations due to the inaccurate mapping functions, and ZTDs manifest a high correlation with the Up component of positions in the estimation (e.g. Munekane and Boehm 2010; Tregoning and Herring 2006; Wang et al. 2008). In addition, the asymmetry impact of the troposphere condition can be partly mitigated by estimating the horizontal troposphere gradients (Bar-Sever et al. 1998). Considering the inaccurate mapping functions, measurements from water vapor radiometers, lidar, etc. have also been investigated and used to correct tropospheric delays (e.g. Bock et al. 2001; Bosser et al. 2010; Fund et al. 2010; Hobiger et al. 2008; Ortiz de Galisteo et al. 2010).

A ground station undergoes sub-daily periodic movements which can be up to a few decimeters, especially in the vertical direction. These station displacements are mainly caused by the solid Earth tide, the ocean loading, the polar motion, the atmospheric pressure loading and the hydrological loading (McCarthy and Petit 2004). In order to generate position estimates that are compatible with the ITRF (International Terrestrial Reference Frame), one needs to correct

for these displacements. The displacements due to the solid Earth tide, the ocean loading and the polar motion can be precisely modeled to 0.1 mm according to McCarthy and Petit (2004). The atmospheric pressure loading effects can be interpolated from tabular values (Tregoning and van Dam 2005). The hydrological loading is still under investigation by the GPS community (van Dam et al. 2001).

Finally, hardware biases differ for different measurement types (Jefferson et al. 2001). Because the clock offsets are governed by the pseudorange biases and current official clocks are estimated using the P1-P2 ionosphere-free observable (Defraigne and Bruyninx 2007), other pseudorange types, namely C/A, C2, etc. have to be calibrated to keep their compatibility with the P1-P2 combination. Such calibrations are performed by applying the P1-C1 differential code biases (DCBs) to the raw pseudorange measurements (Jefferson et al. 2001; Leandro et al. 2007). Note that these DCBs are normally deemed quite stable over at least one month.

1.2.2 Satellite products

Satellite products comprise orbits and clocks. GNSS orbits are determined by numerically integrating all physical forces imposed on the satellites, such as the gravity from Earth, Sun and Moon, the solar radiation pressure, the Earth radiation pressure and the thrust force (Montenbruck and Gill 2000). The unknown model parameters describing these forces are estimated using the GNSS measurements from a network of ground reference stations (e.g. Beutler et al. 2003; Geng et al. 2006). On the other hand, satellite clocks are determined using the undifferenced ionosphere-free observable of pseudorange and carrier-phase measurements from a network of reference stations (e.g. Hauschild and Montenbruck 2009). Pseudorange and carrier-phase measurements share the same clock parameters. To avoid the rank defect of the resulting normal equations, a receiver clock or the sum of a group of receiver clocks are constrained to zero (Kouba and Springer 2001). Due to the ambiguous nature of carrier-phase measurements, the absolute clock offsets are actually determined with pseudorange measurements, whilst carrier-phase measurements govern the relative accuracy between epoch-wise clocks (Defraigne and Bruyninx 2007; Defraigne et al. 2008).

Since 1994, the IGS has been routinely providing precise GPS satellite products generated by combining the individual products from several analysis centers including CODE (Center for Orbit Determination in Europe), GFZ (GeoForschungsZentrum) and JPL (Jet Propulsion Laboratory). The products have been evolving to be of better accuracy, shorter latency and greater variety (Dow et al. 2009; Steigenberger et al. 2009). Table 1.1 presents a summary of the quality of the latest GPS satellite products issued by the IGS. We can see that the final products have the highest accuracy, but with a latency of 12 to 18 days; comparatively, the rapid products have much shorter latency of a few tens of hours, but their clock sample interval is enlarged from 30 s to 5 minutes; the observed ultra-rapid products of 24 hours excel in even shorter latency of only several hours, but their accuracy deteriorates and their clock sample interval is further enlarged to 15 minutes; finally, the predicted ultra-rapid products of 24 hours can apply to real-time applications and their orbits can achieve a sufficiently high accuracy of about 5 cm, but their clocks suffer from a rather poor accuracy of 3 ns.

In PPP, these satellite products need to be interpolated to coincide with the sample interval of the actual measurements. From Table 1.1, we can find that all orbit products are sampled every 15 minutes. Yousif and El-Rabbany (2007) illustrated that the interpolation accuracies for the

Table 1.1: Quality of IGS GPS satellite products[a]

Product types		Accuracy	Latency	Updates	Sample interval
Final	orbits	∼2.5 cm	12–18 days	every Thursday	15 minutes
	clocks	∼75 ps			30 s
Rapid	orbits	∼2.5 cm	17–41 hours	at 17 UTC daily	15 minutes
	clocks	∼75 ps			5 minutes
Ultra-rapid (observed half)	orbits	∼3 cm	3–9 hours	at 03, 09, 15, 21 UTC daily	15 minutes
	clocks	∼150 ps			15 minutes
Ultra-rapid (predicted half)	orbits	∼5 cm	real time	at 03, 09, 15, 21 UTC daily	15 minutes
	clocks	∼3 ns			15 minutes

[a] http://igscb.jpl.nasa.gov/components/prods.html visited on 28/08/2010

Lagrange, the Newton Divided Difference and the Trigonometric methods differ minimally and all achieve an accuracy of far better than 1 cm. On the other hand, linear interpolation between successive epochs is normally adopted for the precise clock products. Note that larger sample interval of satellite clocks leads to worse positioning quality of high-rate PPP (Hesselbarth and Wanninger 2008). In Table 1.1, the final products have the smallest sample interval of 30 s. Bock et al. (2009a) demonstrated that the epoch-wise positioning accuracy for 1-Hz data based on 1-second clocks is about 20% better than that based on 30-second clocks, but below 2% better than that based on 5-second clocks. Hence, since May 4th 2008, CODE has been providing precise GPS clocks of 5-second sample interval.

Furthermore, due to the poor accuracy of IGS predicted satellite clocks, they have to be re-estimated for real-time applications using a network of reference stations by fixing the corresponding IGS predicted satellite orbits (Hauschild and Montenbruck 2009). Since the accuracy of predicted orbits is degraded with the increasing interval to the end of the observed data arc, the latest products are used once they are available from the IGS (Douša 2010). Therefore, the predicted ultra-rapid orbits are used from their release epochs until the newer ones are available (Bock et al. 2009b; Geng 2009). Since June 26th 2007, the IGS has issued a call for participation for a real-time pilot project in which real-time clock generation and dissemination is one of the key objectives (see http://www.rtigs.net). Currently, JPL provides a Global Differential GPS (GDGPS) service where the real-time satellite clock accuracy is better than 0.7 ns with a latency of 4 to 6 s (see http://www.gdgps.net); BKG (Bundesamt für Kartographie und Geodäsie, Federal Agency for Cartography and Geodesy) provides GPS satellite clocks at a 5-second interval to support fully real-time kinematic PPP (Weber et al. 2007) (see IGS Mail-6081); DLR (Deutsches Zentrum für Luft- und Raumfahrt, German Aerospace Center) has issued their real-time GPS satellite clocks with an accuracy of better than 0.3 ns and a latency of about 7 s since April 19th 2010 (see IGS Mail-6133); ESOC (European Space Operations Center) has been submitting its real-time clocks with an accuracy of better than 0.2 ns to the IGS for test purposes since July 2008 (Agrotis et al. 2010b); moreover, some commercial real-time PPP services, such as the StarFire$^{\text{TM}}$ and the Starfix, are also available based on real-time satellite clocks that are generated with GIPSY (GPS-Inferred Positioning SYstem) (Dixon 2006; Melgard et al. 2010). It is worth indicating that none of these real-time clock products is used throughout this thesis.

Finally, PPP users cannot generate the satellite products themselves, but have to obtain them from a service provider. For post-processing users, the listed products in Table 1.1 can be easily accessed via the Internet. On the contrary, the dissemination of real-time satellite products

highly depends on the robustness of the communication link. Currently, these products reach the end users via geostationary satellites or the Internet (e.g. Dixon 2006; Kechine et al. 2004).

1.2.3 Multi-constellation and multi-frequency PPP

Due to the huge economic benefits of GNSS in the ongoing information revolution, the US government is modernizing GPS whilst the Russian government is restoring GLONASS (Global'naya Navigatsionnaya Sputnikovaya Sistema) (Revnivykh 2008). Meanwhile, the European and Chinese governments have also joined this race by independently building the Galileo and Compass systems (Cao 2009; Falcone 2008). Hence, PPP based on simulated or real multi-constellation and multi-frequency measurements has been reported in many publications. For the multi-constellation PPP, it is illustrated that adding GLONASS or Galileo measurements to GPS-based PPP can clearly improve the positioning quality in GPS-adverse environments where the number of GPS satellites significantly decreases and cycle slips frequently occur (Cai and Gao 2007; Cao et al. 2010; Gjevestad et al. 2007; Kjørsvik et al. 2007; Melgard et al. 2010). On the other hand, for multi-frequency measurements, most publications focus on the inter-frequency carrier-phase combinations to derive ionosphere-reduced low-noise long-wavelength measurements for efficient ambiguity resolution (e.g. Feng 2008; Hatch et al. 2000; Li et al. 2010). Henkel and Günther (2008) proposed an ionosphere-free mixed pseudorange-carrier combination which has a long wavelength of 3.215 m and a low noise level of 3.76 cm for multi-frequency PPP. Nevertheless, throughout this thesis, neither multi-constellation nor multi-frequency PPP is further discussed.

1.2.4 Advantages of PPP

PPP was first developed for highly efficient analysis of GPS measurements from huge networks (Zumberge et al. 1997). As demonstrated by Zumberge et al. (1997), PPP processing time linearly scales with the number of stations n, namely $O(n)$, but PPP closely reproduces an $O(n^3)$ full network solution which is normally achieved by double-difference data processing. Furthermore, in order to solve the problem of $O(n^4)$ computation burden after applying double-difference ambiguity resolution to a network solution by PPP, Blewitt (2008) chose an independent baseline set before fixing double-difference ambiguities, and consequently reduced the computation burden to $O(n)$ again. For example, a network analysis for 98 stations costs about 15 minutes for PPP whereas over 22 hours for double-difference data processing on a 3 GHz CPU (Blewitt 2008). In addition, Ge et al. (2006) improved the strategy of forming double-difference ambiguities with undifferenced ones, and thus considerably accelerate the network analysis.

On the other hand, PPP users do not need to establish any reference stations before they carry out surveying, which can significantly reduce the logistical expense and simplify the work (Bisnath and Gao 2009). This is because PPP does not require any raw measurements from a nearby receiver, but only the precise satellite products determined by a network of reference stations. Note that PPP users do not need to know the details of this reference network.

Moreover, PPP is a precise positioning technique working on a global scale in nature (Wübbena et al. 2005). Empirically, only a sparse reference network is needed to maintain a typical global PPP service. For example, a few tens of globally well distributed reference stations can lead to precise satellite products of comparable quality with the IGS rapid, or even final products (Geng et al. 2006; Hauschild and Montenbruck 2009), and PPP can be carried out even in open oceans where the nearest reference stations may be a few thousand kilometers

Table 1.2: RMS of the differences between PPP positions and ground truths

Measurements	Mode	RMS (cm)		
		East	North	Up
Dual-frequency	Daily static	<0.5	<0.5	<1.0
	Hourly static	∼4.0	∼2.0	∼3.0
	Post-processing kinematic	∼5.0	∼4.0	∼10.0
	Real-time kinematic	<10.0	<10.0	<20.0
Single-frequency	Post-processing kinematic	∼25.0	∼25.0	∼50.0
	Real-time kinematic	∼40.0	∼40.0	∼50.0

away (Geng et al. 2010c). In addition, Table 1.2 shows current GPS-based PPP performance under favorable conditions where carrier-phase measurements are continuous and the observation period is sufficiently long (e.g. Chen 2004; Chen and Gao 2005; Dixon 2006; Gao et al. 2006; Geng et al. 2010b; Héroux et al. 2004; Teferle et al. 2007; Tétreault et al. 2005).

Finally, for real-time applications, PPP requires only a limited transmission bandwidth compared with the NRTK services (Dixon 2006; Wübbena et al. 2005). This is because corrections from a PPP service provider mainly contain the orbits and clocks for all visible satellites of which the volume does not change with the number of reference stations. On the contrary, for FKP-based (Flächenkorrekturparameter, Area Correction Parameter) NRTK services, the number of reference stations defines the required transmission bandwidth; for VRS-based (Virtual Reference Station) services, the number of users decides the bandwidth; finally, for MAC-based (Master-Auxiliary-Concept) services, the number of auxiliary stations dominates the bandwidth (Wübbena et al. 2005). Hence, the transmission bandwidth of an NRTK service is increased when the system scale is enlarged.

Due to these advantages of PPP, it has been comprehensively applied to the geophysical analysis (e.g. Blewitt et al. 2006; Calais et al. 2006; Larson and Miyazaki 2008; Melbourne et al. 2002; Sato et al. 2008), meteorological studies (e.g. Iwabuchi et al. 2006; Leandro et al. 2010; Peng et al. 2008; Rocken et al. 2005; Skone et al. 2006), oceanographic research (e.g. King and Aoki 2003; King et al. 2005; Zhang and Andersen 2006), orbit determinations for low Earth orbiters (e.g. Hwang et al. 2009; Jäggi et al. 2007; Montenbruck et al. 2005) and industrial fields (e.g. Ebner and Featherstone 2008; Satirapod and Homniam 2006; Schweitzer et al. 2010; Yuan et al. 2009).

1.3 Problem statement: Deficiencies of PPP

Despite the above advantages, it is well-known that PPP still suffers from unresolved ambiguities and slow convergences (Bisnath and Gao 2007).

On the one hand, ambiguities at a single receiver are conventionally not fixed to integers. This is because the fractional-cycle biases (FCBs) in the GPS measurements are absorbed by the undifferenced ambiguity estimates and their integer properties are thus destroyed (Collins 2008; Ge et al. 2008; Mercier and Laurichesse 2008). In theory, these FCBs are presumed hardware-dependent and are present in all receivers and satellites (Teunissen and Kleusberg 1998). Hence, the FCBs cancel in double-difference data processing. Gabor and Nerem (1999) described the FCBs as the fractional-cycle part of the uncalibrated offsets in the frequency oscillators, uncalibrated delays from the transmitter and receiver hardware, or uncalibrated

offsets between the signal detection phase reference and the time-tag generation reference within a receiver. However, the temporal property of the FCBs is not exactly known. Blewitt (1989) empirically reported that they were stable to better than 1 ns, Gabor and Nerem (1999) simply assumed that they changed systematically with time and Wang and Gao (2007) found the high stability of the receiver-dependent FCBs during continuous observation periods. Despite this uncertainty, it is believed that the time-invariant parts of the FCBs cannot be separated from the undifferenced ambiguity estimates in the conventional PPP proposed by Zumberge et al. (1997), thus inhibiting integer ambiguity resolution at a single receiver.

On the other hand, the convergence in PPP means that the position or the ambiguity estimates steadily approach to a specific accuracy level and do not leave this level after reaching it. Typically, the convergence period is around 20 minutes before kinematic PPP can achieve a positioning accuracy of better than 20 cm (Bisnath and Gao 2007). Even worse, if continuous carrier-phase measurements cannot be guaranteed, i.e. when severe cycle slips or signal interruptions occur, a re-convergence may start. Compared with NRTK, such long convergence periods have significantly devalued PPP in many commercial real-time applications (Bisnath and Gao 2007). This slow convergence is largely attributed to the imprecise pseudorange measurements and the slow change of satellite geometry. For one thing, imprecise pseudorange measurements cannot effectively constrain the ambiguous carrier-phase measurements. Hence, the ambiguity estimates can hardly converge to sufficiently accurate values within a short observation period (Teunissen 1996). For another, slow geometry changes of visible satellites lead to a high correlation between the ambiguity and position parameters (Li and Shen 2010). As a result, a sufficient long period has to be spent before the satellite geometry sufficiently changes, as otherwise the position estimates can be significantly biased by inaccurate ambiguity estimates (Zhu et al. 2007).

1.4 Research objectives

Considering Section 1.3, this thesis concentrates on improving GPS-based PPP by resolving ambiguities for a single receiver and accelerating the convergence to ambiguity-fixed solutions in order to achieve centimeter-level positioning accuracy with only a few seconds of measurements. The key issues addressed in this thesis are as follows:

- What methods have been developed for integer ambiguity resolution at a single receiver and how do they differ in theory and practice?
- How do we implement a PPP-RTK service characterized by integer ambiguity resolution?
- How do the sub-daily static, post-processing kinematic and real-time kinematic PPP benefit from integer ambiguity resolution?
- What methods have been developed for rapid convergences to ambiguity-fixed solutions in the real-time PPP and are they realistic in practice?
- How can we significantly accelerate a re-convergence using precisely predicted ionospheric delays and the first convergence using a dense network of reference stations?
- How does the real-time PPP benefit from rapid re-convergences and what will affect the performance of rapid re-convergences?
- What are the prototype and the potential applications of a global PPP-RTK service based on rapid integer ambiguity resolution?

1.5 Thesis overview

This thesis is arranged into eight chapters which are outlined as follows. Following this chapter, Chapter 2 reviews the methods to date developed for integer ambiguity resolution at a single receiver and derives a theoretical proof for the equivalence between these methods. Then the improved methods developed in this thesis are presented.

Chapter 3 reviews and compares the attempts developed for rapid convergences in the real-time PPP. Of particular note, a method is originally developed in this thesis for the rapid re-convergences to ambiguity-fixed solutions and a potential strategy for accelerating the first convergence is proposed afterwards.

Chapter 4 introduces the software provided by Wuhan University for a research collaboration and then details the post-processing and real-time suites developed during this PhD research.

Chapter 5 presents and discusses the results for the sub-daily static, post-processing kinematic and real-time kinematic PPP after applying integer ambiguity resolution at a single receiver. The contribution of integer double-difference constraints to the positioning quality is highlighted. Then the comparison between the methods for integer ambiguity resolution is illustrated in detail.

Chapter 6 presents and discusses the results for rapid re-convergences to ambiguity-fixed solutions in PPP by applying the method developed in Chapter 3. The variation characteristics of ionospheric delays are investigated. Also, rapid convergences through interpolated ionospheric delays are briefly illustrated.

Chapter 7 proposes a prototype of a global PPP-RTK service and then compares it with NRTK services. Its potential applications are afterwards discussed and tested. The question that how many reference stations are sufficient to support this global service is also investigated.

Chapter 8 finally summarizes the main points and highlights the contributions of this thesis. Then the perspective of PPP with rapid integer ambiguity resolution is discussed.

Chapter 2

Integer Ambiguity Resolution

2.1 Introduction

Integer ambiguity resolution can significantly improve the positioning quality, especially in real time or when the observation period is short (e.g. Schwarz et al. 2009; Zumberge et al. 1997). Although ambiguity resolution has been routinely performed in relative positioning, it is only in recent years that ambiguity resolution at a single receiver has been preliminarily developed and implemented in PPP (e.g. Collins 2008; Ge et al. 2008; Laurichesse and Mercier 2007). Hence, this chapter first reviews the methods developed for ambiguity resolution at a single receiver, then proves the theoretical equivalence of the ambiguity-fixed position estimates derived from these methods and finally addresses the improved methods for ambiguity resolution developed in this thesis. In addition, the methods for ambiguity search and validation are discussed before ending this chapter.

2.2 Current advances

To date, the methods for ambiguity resolution at a single receiver can be categorized into two groups: One is based on the determination of FCBs and the other is based on the determination of integer-recovery clocks (IRCs). FCBs and IRCs have to be determined before they can be applied to a single-receiver solution in order to recover the integer properties of ambiguities. In this section, the fundamental measurement equations are first presented, and then the methods for ambiguity resolution at a single receiver are detailed through mathematical derivations.

2.2.1 Theoretical fundamentals of PPP

In general, undifferenced GPS pseudorange and carrier-phase measurements on frequency g ($g = 1, 2$) between receiver i and satellite k at a particular epoch can be respectively written as

$$\begin{cases} P_{gi}^k = \rho_i^k + ct_i^k + \dfrac{\mu_i^k}{f_g^2} + b_{gi}^k - e_{gi}^k \\ L_{gi}^k = \rho_i^k + ct_i^k - \dfrac{\mu_i^k}{f_g^2} + B_{gi}^k + \lambda_g N_{gi}^k - \varepsilon_{gi}^k \end{cases} \tag{2.1}$$

where ρ_i^k denotes the non-dispersive delay including the geometric distance, the tropospheric delay and the relativity effects; note that antenna phase center corrections have to be applied to P_{gi}^k and L_{gi}^k before ρ_i^k becomes unassociated with the frequency (refer to Section 1.2.1); c denotes the speed of light in vacuum, f_g denotes the signal frequency and λ_g denotes the wavelength; $t_i^k = t_i - t^k$ where t_i and t^k denote the receiver and satellite clocks, respectively; $\frac{\mu_i^k}{f_g^2}$ denotes the first-order ionospheric delay with the higher-order delays ignored; b_{gi}^k and B_{gi}^k respectively denote the pseudorange and carrier-phase hardware biases where $b_{gi}^k = b_{gi} - b_g^k$ and $B_{gi}^k = B_{gi} - B_g^k$ (Teunissen and Kleusberg 1998); b_{gi} and B_{gi} are for the receiver whereas b_g^k and B_g^k are for the satellite; N_{gi}^k denotes the integer ambiguity; finally, e_{gi}^k and ε_{gi}^k represent the residual or unmodeled errors, such as multipath effects (Dilssner et al. 2008), for the pseudorange and carrier-phase measurements, respectively. In addition, it should be emphasized that the hardware biases differ for different measurement types and signal frequencies. To date, the temporal property of these hardware biases has not been exactly known, and thus they are usually presumed to change slowly and minimally, or remain constant over time (e.g. Blewitt 1989; Dach et al. 2007; Gabor and Nerem 1999).

As introduced in Section 1.2.1, ionosphere-free combination observables are used in PPP to eliminate the first-order ionospheric delays in pseudorange and carrier-phase measurements (Dach et al. 2007; Hofmann-Wellenhof et al. 2001). Hence, the measurements used in the conventional PPP by Zumberge et al. (1997) are

$$\begin{cases} P_i^k = \rho_i^k + ct_i^k + b_i^k - e_i^k \\ \dfrac{f_1^2}{f_1^2 - f_2^2} L_{1i}^k - \dfrac{f_2^2}{f_1^2 - f_2^2} L_{2i}^k = \rho_i^k + ct_i^k + \left(\dfrac{f_1^2}{f_1^2 - f_2^2} B_{1i}^k - \dfrac{f_2^2}{f_1^2 - f_2^2} B_{2i}^k \right) + \\ \qquad\qquad \left(\dfrac{\lambda_1 f_1^2}{f_1^2 - f_2^2} N_{1i}^k - \dfrac{\lambda_2 f_2^2}{f_1^2 - f_2^2} N_{2i}^k \right) - \varepsilon_i^k \end{cases} \tag{2.2}$$

where the frequency notation g for the pseudorange observable is ignored to imply the quantities related to the ionosphere-free observables; $P_i^k = \dfrac{f_1^2}{f_1^2 - f_2^2} P_{1i}^k - \dfrac{f_2^2}{f_1^2 - f_2^2} P_{2i}^k$ and this relationship also holds for b_i^k, e_i^k and ε_i^k. According to the error propagation law (Wolf and Ghilani 1997), the noise of measurements in Equation 2.2 is about three times larger than that of the original measurements in Equation 2.1. Moreover, the nominal ambiguity term $\dfrac{\lambda_1 f_1^2}{f_1^2 - f_2^2} N_{1i}^k - \dfrac{\lambda_2 f_2^2}{f_1^2 - f_2^2} N_{2i}^k$ is no longer an integer times a specific wavelength, and a real ambiguity estimate is actually a combination of this ambiguity term and the hardware biases, i.e. $\dfrac{f_1^2}{f_1^2 - f_2^2} B_{1i}^k - \dfrac{f_2^2}{f_1^2 - f_2^2} B_{2i}^k$ and b_i^k (see Collins 2008; Zumberge et al. 1997). Furthermore, this nominal ambiguity term can be decomposed into a narrow-lane and a wide-lane term (Dach et al. 2007), namely

$$\frac{\lambda_1 f_1^2}{f_1^2 - f_2^2} N_{1i}^k - \frac{\lambda_2 f_2^2}{f_1^2 - f_2^2} N_{2i}^k = \lambda_n N_{1i}^k + \frac{f_2}{f_1 + f_2} \lambda_w N_{wi}^k \tag{2.3}$$

where $\lambda_n = \dfrac{c}{f_1 + f_2}$ and $\lambda_w = \dfrac{c}{f_1 - f_2}$ denote the narrow-lane and wide-lane wavelengths which are about 11 cm and 86 cm, respectively; $N_{wi}^k = N_{1i}^k - N_{2i}^k$ is called the wide-lane ambiguity whereas N_{1i}^k is correspondingly called the narrow-lane ambiguity.

Melbourne (1985) and Wübbena (1985) proposed a combination observable which is theo-

retically free from both the ionospheric delay and the non-dispersive delay, namely

$$L_{mi}^k = \lambda_w \left(\frac{L_{1i}^k}{\lambda_1} - \frac{L_{2i}^k}{\lambda_2} \right) - \frac{f_1 P_{1i}^k + f_2 P_{2i}^k}{f_1 + f_2} = \lambda_w \left(N_{wi}^k + \frac{B_{1i}^k}{\lambda_1} - \frac{B_{2i}^k}{\lambda_2} - \frac{\lambda_n}{\lambda_w} \left(\frac{b_{1i}^k}{\lambda_1} + \frac{b_{2i}^k}{\lambda_2} \right) \right) \quad (2.4)$$

where the residual errors e_{gi}^k and ε_{gi}^k are ignored. Hence, N_{wi}^k plus the hardware biases can be approximated with $\dfrac{L_{mi}^k}{\lambda_w}$. Multi-epoch averaging can smooth out the large pseudorange noise and thus lead to a more accurate estimate. Substituting N_{wi}^k in Equation 2.3 with Equation 2.4, we can obtain

$$\frac{\lambda_1 f_1^2}{f_1^2 - f_2^2} N_{1i}^k - \frac{\lambda_2 f_2^2}{f_1^2 - f_2^2} N_{2i}^k = \lambda_n N_{1i}^k + \frac{f_2 L_{mi}^k}{f_1 + f_2} - \frac{c f_2}{f_1^2 - f_2^2} \left(\frac{B_{1i}^k}{\lambda_1} - \frac{B_{2i}^k}{\lambda_2} - \frac{\lambda_n}{\lambda_w} \left(\frac{b_{1i}^k}{\lambda_1} + \frac{b_{2i}^k}{\lambda_2} \right) \right) \quad (2.5)$$

Finally, substituting the ambiguity term of Equation 2.2 with Equation 2.5, we can then obtain

$$\begin{cases} P_i^k = \rho_i^k + c t_i^k + b_i^k - e_i^k \\ L_i^k = \rho_i^k + c t_i^k + B_i^k + \lambda_n N_i^k - \varepsilon_i^k \end{cases} \quad (2.6)$$

where

$$\begin{cases} L_i^k = \dfrac{f_1^2}{f_1^2 - f_2^2} L_{1i}^k - \dfrac{f_2^2}{f_1^2 - f_2^2} L_{2i}^k - \dfrac{f_2}{f_1 + f_2} L_{mi}^k \\ B_i^k = \dfrac{f_1}{f_1 + f_2} B_{1i}^k + \dfrac{\lambda_n f_2}{f_1 + f_2} \left(\dfrac{b_{1i}^k}{\lambda_1} + \dfrac{b_{2i}^k}{\lambda_2} \right) \\ N_i^k = N_{1i}^k \end{cases} \quad (2.7)$$

Hence, the carrier-phase hardware bias in Equation 2.6 is a combination of the carrier-phase and pseudorange hardware biases in Equation 2.1. Of particular note, an ambiguity term with integer property is finally introduced into the ionosphere-free carrier-phase measurements, and thus ambiguity resolution becomes possible in theory. Nevertheless, as demonstrated in Section 1.3, the float ambiguity estimate based on Equation 2.6 contains not only $\lambda_n N_i^k$, but also b_i^k and B_i^k. This point will be detailed in Section 2.3. In addition, it is worth emphasizing that Equation 2.6 is fundamental to both following methods, i.e. the FCB-based and IRC-based methods. The derivation of Equation 2.6 also implies that ambiguity resolution at a single receiver can be implemented by sequentially performing wide-lane and narrow-lane ambiguity resolution.

2.2.2 Methods based on fractional-cycle biases (FCBs)

Here FCBs are deemed as the fractional-cycle part of hardware biases, i.e. b_i^k and B_i^k in Equation 2.6. The remaining integer-cycle parts do not affect the integer property of ambiguities. Satellite hardware biases b^k and B^k are presumed constant over the observation period for the FCB-based methods. In the following, the two FCB-based methods developed by Ge et al. (2008) and Bertiger et al. (2010) are introduced, respectively. For both methods, the FCB determination with a network of reference stations is addressed before a single-receiver solution augmented by the FCB estimates is presented. Finally, the key points for the FCB-based methods are summarized.

A Method by Ge et al. (2008)

The method developed by Ge et al. (2008) can be schematically illustrated with Figure 2.1. In general, this method consists of four sequential steps which are performed within the two modules, namely the network and single-receiver solutions. In the network solution, wide-lane

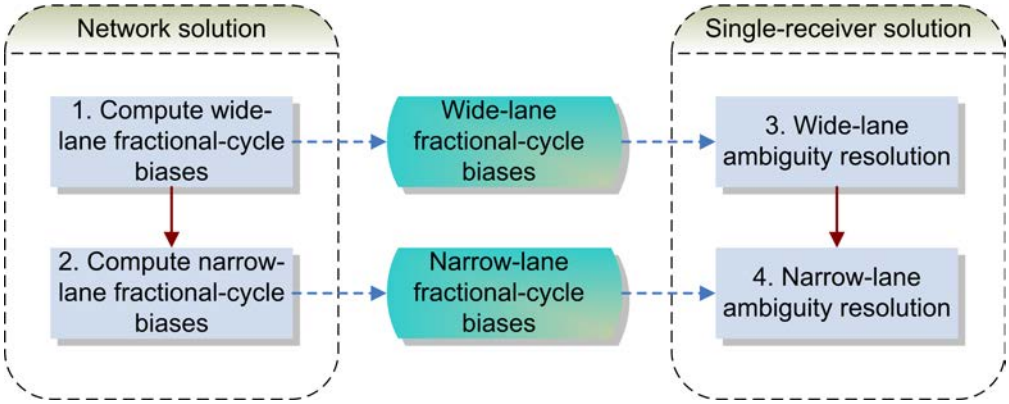

Figure 2.1: Procedure of FCB-based ambiguity resolution by Ge et al. (2008). The solid arrows represent the computation sequences while the dashed arrows represent the input/output operations

and narrow-lane FCBs are estimated. In the single-receiver solution, the FCB estimates are then used to retrieve the integer property of the wide-lane and narrow-lane ambiguity estimates.

For the network solution, wide-lane FCB estimates are derived from the Melbourne-Wübbena combination measurements (Equation 2.4). Specifically, a float estimate of a wide-lane ambiguity plus its pertinent hardware bias is

$$\hat{N}_{wi}^{k} = N_{wi}^{k} + \frac{B_{1i}^{k}}{\lambda_1} - \frac{B_{2i}^{k}}{\lambda_2} - \frac{\lambda_n}{\lambda_w}\left(\frac{b_{1i}^{k}}{\lambda_1} + \frac{b_{2i}^{k}}{\lambda_2}\right) = \left\langle \frac{L_{mi}^{k}}{\lambda_w} \right\rangle \tag{2.8}$$

where $< \cdot >$ here represents averaging over all involved epochs. In order to avoid the possibly varying receiver FCBs (Wang and Gao 2007), Ge et al. (2008) proposed the difference between satellites in order to eliminate the receiver FCBs. However, note that this difference applies to only ambiguity estimates, not the raw measurements. A difference between satellites k and l is

$$\hat{N}_{wi}^{kl} = N_{wi}^{kl} - \frac{B_{1}^{kl}}{\lambda_1} + \frac{B_{2}^{kl}}{\lambda_2} + \frac{\lambda_n}{\lambda_w}\left(\frac{b_{1}^{kl}}{\lambda_1} + \frac{b_{2}^{kl}}{\lambda_2}\right) = \left\langle \frac{L_{mi}^{k}}{\lambda_w} \right\rangle - \left\langle \frac{L_{mi}^{l}}{\lambda_w} \right\rangle \tag{2.9}$$

where the superscript "kl" denotes satellite k minus l; the subscript i disappears from the hardware-bias terms because the remaining FCBs are only satellite-dependent. In this case, the wide-lane FCB estimate for the satellite-pair k and l is

$$\phi_{w}^{kl} = \left\langle \hat{N}_{w}^{kl} - \left[\hat{N}_{w}^{kl}\right] \right\rangle \tag{2.10}$$

and its variance is

$$\sigma_{\phi_w^{kl}}^{2} = \frac{\left\langle \left(\hat{N}_{w}^{kl} - \left[\hat{N}_{w}^{kl}\right] - \phi_{w}^{kl}\right)^{2} \right\rangle}{R^{kl}} \tag{2.11}$$

where R^{kl} denotes the number of ambiguities pertinent to the satellite-pair k and l at all receivers; $[\cdot]$ represents rounding to the nearest integer; $< \cdot >$ represents averaging over all involved ambiguities. Note that the rounding to the nearest integer here is actually not a trivial operation (Gabor and Nerem 1999; Ge et al. 2008). ϕ_w^{kl} is cyclical in nature. This means that -0.5 cycles is actually identical to $+0.5$ cycles. For an FCB of which the true value is half a cycle, the measurement noise may cause a discrepancy of about 1 cycle between the fractional parts of some ambiguity estimates. Hence, Gabor and Nerem (1999) suggested an alternative strategy

to estimate FCBs, namely

$$\phi_w^{kl} = \frac{\arctan\left(\sum^{R^{kl}} \sin\left(2\pi \hat{N}_w^{kl}\right) \Big/ \sum^{R^{kl}} \cos\left(2\pi \hat{N}_w^{kl}\right)\right)}{2\pi} \tag{2.12}$$

It is worth indicating that $\left[\hat{N}_{wi}^{kl}\right]$ consists of N_{wi}^{kl} and the integer-cycle part of the hardware bias in Equation 2.9. However, in order to simplify the subsequent formula derivations, it is presumed that $\phi_w^{kl} = -\frac{B_1^{kl}}{\lambda_1} + \frac{B_2^{kl}}{\lambda_2} + \frac{\lambda_n}{\lambda_w}\left(\frac{b_1^{kl}}{\lambda_1} + \frac{b_2^{kl}}{\lambda_2}\right)$ which is fractional and thus $\left[\hat{N}_{wi}^{kl}\right] = N_{wi}^{kl}$. Note that this assumption will not affect the final solutions because the integer-cycle offset of the hardware bias is common for all ambiguities pertinent to the satellite-pair k and l at all receivers. Hence, this offset will finally cancel at single-receiver solutions.

Once the wide-lane FCBs ϕ_w^{kl} are obtained, the integer wide-lane ambiguities N_{wi}^{kl} at all involved receivers can also be obtained. In this case, the transformation from Equation 2.2 to 2.6 can be carried out. Furthermore, the float estimate of the narrow-lane ambiguity N_i^k in Equation 2.6 suffers from the hardware biases b_i^k and B_i^k and thus its integer property is destroyed after a least squares adjustment. Similar to Equation 2.10, the narrow-lane FCB estimate for the satellite-pair k and l can be obtained with

$$\phi_n^{kl} = \left\langle \hat{N}^{kl} - \left[\hat{N}^{kl}\right] \right\rangle \tag{2.13}$$

and its variance is

$$\sigma^2_{\phi_n^{kl}} = \frac{\left\langle \left(\hat{N}^{kl} - \left[\hat{N}^{kl}\right] - \phi_n^{kl}\right)^2 \right\rangle}{R^{kl}} \tag{2.14}$$

where $\hat{N}^{kl}$ denotes the float estimate of N^{kl} and other notations refer to Equation 2.10. Note that the difference between satellites is also applied to the narrow-lane ambiguities. In addition, $\left[\hat{N}_i^{kl}\right] = N_i^{kl}$ is assumed in order to simplify the subsequent formula derivations.

On the other hand, at a single receiver, the above FCBs ϕ_w^{kl} and ϕ_n^{kl} are used to respectively correct wide-lane and narrow-lane ambiguity estimates in order to retrieve their integer properties. Specifically, an integer wide-lane ambiguity at receiver i can be retrieved with

$$N_{wi}^{kl} = \hat{N}_{wi}^{kl} - \phi_w^{kl} \tag{2.15}$$

and its variance is

$$\sigma^2_{N_{wi}^{kl}} = \frac{\left\langle \left(\frac{L_{mi}^k}{\lambda_w} - \hat{N}_{wi}^k\right)^2 \right\rangle}{R_i^k} + \frac{\left\langle \left(\frac{L_{mi}^l}{\lambda_w} - \hat{N}_{wi}^l\right)^2 \right\rangle}{R_i^l} + \sigma^2_{\phi_w^{kl}} \tag{2.16}$$

where R_i^k and R_i^l are the number of epochs used for the averaging and other notations refer to Equation 2.8 and 2.9. If N_{wi}^{kl} can be successfully fixed to an integer, the corresponding narrow-lane ambiguity $\hat{N}_i^{kl}$ can then be obtained following the principle of Equation 2.3 to 2.5, and its integer property can be retrieved with

$$N_i^{kl} = \hat{N}_i^{kl} - \phi_n^{kl} \tag{2.17}$$

and its variance depends on the unit-weight variance and the inversed normal matrix (Wolf and Ghilani 1997). Finally, if both wide-lane and narrow-lane resolutions succeed, ambiguity-fixed solutions can be achieved by tightly constraining the ambiguity estimates derived from Equation 2.2 to $\lambda_n \left(N_i^{kl} + \phi_n^{kl}\right) + \dfrac{f_2}{f_1 + f_2}\lambda_w N_{wi}^{kl}$ (refer to Equation 2.3). Hence, the accuracy of narrow-lane FCBs ϕ_n^{kl}, other than the correctness of integer N_i^{kl} and N_{wi}^{kl}, affect the quality of the final ambiguity-fixed solutions. Comparatively, wide-lane FCBs ϕ_w^{kl} are used only for integer resolutions, and thus their accuracy requirement is not as high as that for ϕ_n^{kl}.

This FCB-based method was actually first developed by Gabor and Nerem (1999). The only difference is that $N_{wi}^{kl} + \phi_w^{kl}$ replaces N_{wi}^{kl} to derive the narrow-lane ambiguity $\hat{N}_i^{kl}$ in Equation 2.3. In this case, both accuracies of ϕ_w^{kl} and ϕ_n^{kl} affect the quality of the final ambiguity-fixed solutions. Unfortunately, highly accurate ϕ_w^{kl} cannot be guaranteed because of the noisy Melbourne-Wübbena combination measurements. Hence, the method by Ge et al. (2008) is advantageous and has thus been adopted and improved in this thesis. Moreover, Wang and Gao (2006) used simulated GPS measurements to verify this method, Henkel and Günther (2008) showed an application of this method to the multi-frequency PPP (see also Henkel et al. 2010) whereas El-Mowafy (2009) showed an alternative to this method when there is only one available reference station. Similar applications of this method can also be found in Mervart et al. (2008) for real-time scenarios and Rocken et al. (2008) for oceanic surveying. Specifically, Ge et al. (2008) reported that FCB-based ambiguity resolution can improve the RMS statistics of daily position estimates against the IGS weekly solutions (Altamimi and Collilieux 2009) from 4.1, 3.1 and 8.3 mm to 2.8, 3.0 and 7.8 mm for the East, North and Up components, respectively; El-Mowafy (2009) showed a few post-processing kinematic cases where centimeter-level positioning accuracy can be achieved at ambiguity-fixed epochs; finally, Rocken et al. (2008) presented a simulated real-time case study in which ambiguity-fixed PPP can reach a positioning accuracy of 1.8, 1.9 and 4.1 cm for the East, North and Up components, respectively. However, a comprehensive and close study on the potential performance of ambiguity-fixed PPP is still necessary.

B Method by Bertiger et al. (2010)

The method developed by Bertiger et al. (2010) can be schematically illustrated with Figure 2.2. Compared with the method by Ge et al. (2008), FCBs are not estimated in the network solution. Instead, the time spans and float estimates of undifferenced ambiguities are generated and then delivered to users for ambiguity resolution. This ambiguity product is used to form double-difference ambiguities with the undifferenced ambiguity estimates in a single-receiver solution. Hence, ambiguity resolution is actually performed on the double-difference ambiguities. However, note that only the raw measurements from user's receivers are needed for ambiguity resolution.

For the network solution, undifferenced wide-lane ambiguity estimates are also derived from the Melbourne-Wübbena combination measurements (Blewitt 1989). By forming double-difference wide-lane ambiguities between receivers i and j for the satellite-pair k and l, the hardware-bias terms in Equation 2.8 can be totally eliminated, namely

$$\hat{N}_{wij}^{kl} = N_{wi}^{k} - N_{wi}^{l} - N_{wj}^{k} + N_{wj}^{l} = \left\langle \frac{L_{mi}^{k}}{\lambda_w} \right\rangle - \left\langle \frac{L_{mi}^{l}}{\lambda_w} \right\rangle - \left\langle \frac{L_{mj}^{k}}{\lambda_w} \right\rangle + \left\langle \frac{L_{mj}^{l}}{\lambda_w} \right\rangle \tag{2.18}$$

Hence, double-difference wide-lane ambiguities preserve their integer properties and thus integer

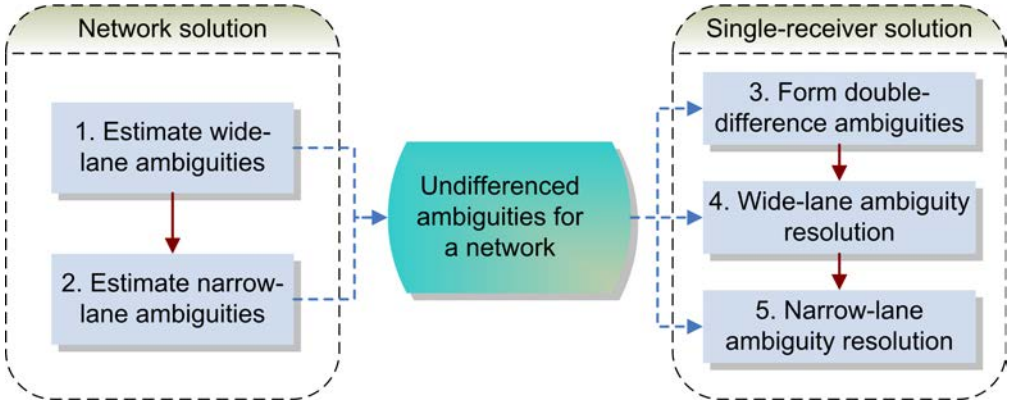

Figure 2.2: Procedure of FCB-based ambiguity resolution by Bertiger et al. (2010). Meanings of arrows refer to Figure 2.1

resolutions can be directly attempted without considering the wide-lane FCBs. In the next step, undifferenced ionosphere-free measurements are formed with Equation 2.2. Likewise, double differencing is applied to the resulting undifferenced ambiguity estimates in order to totally eliminate the hardware biases. In this case, the double-difference ambiguity estimate between receivers i and j for the satellite-pair k and l becomes $\frac{\lambda_1 f_1^2}{f_1^2 - f_2^2} N_{1ij}^{kl} - \frac{\lambda_2 f_2^2}{f_1^2 - f_2^2} N_{2ij}^{kl}$, and it can be further decomposed into

$$\frac{\lambda_1 f_1^2}{f_1^2 - f_2^2} N_{1ij}^{kl} - \frac{\lambda_2 f_2^2}{f_1^2 - f_2^2} N_{2ij}^{kl} = \lambda_n N_{1ij}^{kl} + \frac{f_2}{f_1 + f_2} \lambda_w N_{wij}^{kl} \tag{2.19}$$

which is actually similar to Equation 2.3. In this manner, the integer wide-lane ambiguity estimate in Equation 2.18 can be substituted into Equation 2.19 to obtain the double-difference narrow-lane ambiguity estimate N_{1ij}^{kl}. Note that this narrow-lane ambiguity estimate also preserves its integer property, and thus can also be directly fixed to an integer without considering any narrow-lane FCBs. Finally, once both wide-lane and narrow-lane resolutions succeed, a tight constraint based on Equation 2.19 can be imposed on the undifferenced ambiguities (Ge et al. 2005a, 2006). As a result, undifferenced ionosphere-free-observable ambiguity estimates are generated under the constraints of integer double-difference ambiguities.

In addition, it should be noted that the above processing strategy is part of the routine global network analysis by JPL using GIPSY-OASIS (Orbit Analysis SImulation Software) (Bertiger et al. 2010; Blewitt 1989, 2008; Webb and Zumberge 1997). After this network analysis, undifferenced wide-lane and ionosphere-free-observable ambiguity estimates are provided as an ambiguity product together with the satellite products for users. Also, the ambiguity time spans and the receiver knowledge are delivered for the convenience of forming double-difference ambiguities in a single-receiver solution (Bertiger et al. 2010).

On the other hand, at a single receiver, one first generates an ambiguity-float solution based on JPL's satellite products. Then the ambiguity product is searched for the most preferable undifferenced ambiguity estimates that can form double-difference ambiguities with the undifferenced ambiguity estimates at this receiver (Bertiger et al. 2010). The criteria for the preferable ambiguities are short baselines, long time of common view, etc. Once this formation is accomplished, integer resolutions of wide-lane and narrow-lane ambiguities can be sequentially attempted in terms of Equation 2.18 and 2.19. Finally, ambiguity-fixed solutions can be achieved only if both wide-lane and narrow-lane resolutions are successful.

In practice, Bertiger et al. (2010) improved the daily position repeatability from 2.9 to 1.9 mm for the East component by applying this single-receiver ambiguity resolution. Moreover, post-processing epoch-wise positioning using 30-hour GPS measurements at static stations showed an RMS reduction from 9.9, 9.2 and 13.6 mm to 7.7, 8.4 and 11.7 mm for the East, North and Up components, respectively, against the daily estimates.

In conclusion, this method can be considered an FCB-based method although FCBs are not explicitly determined. FCBs underlie the above ambiguity product. This can be understood by recognizing the ambiguity product as a sum of integer ambiguities and FCBs. Therefore, FCBs in a single-receiver solution can be corrected with the ambiguity product.

C Remarks on the FCB-based methods

According to the above discussions, the methods by Ge et al. (2008) and Bertiger et al. (2010) differ in the following three aspects:

- FCBs are explicitly separated from the integer ambiguities as an independent product in the method by Ge et al. (2008) whereas preserved in the float ambiguity estimates which finally form an ambiguity product in the method by Bertiger et al. (2010). Hence, dedicated algorithms and strategies have to be developed in the first method to accurately identify the FCBs;
- Furthermore, FCBs are presumed constant over the whole observation period in the method by Ge et al. (2008) whereas this assumption is not rigorously required in the method by Bertiger et al. (2010). Because FCBs are estimated by averaging the fractional parts of all involved ambiguity estimates for a satellite pair, varying FCBs over time and space will invalidate this averaging operation. Comparatively, FCBs are presumed constant in the second method only during the common-view period of a satellite pair by a number of receivers. Double-difference ambiguities can then have integer properties;
- Finally, the size of the satellite-pair FCB product solely depends on the number of satellites whereas the size of the ambiguity product primarily depends on the number of reference stations involved in a network solution. Hence, the size of the ambiguity product may become too large to be conveniently delivered to users. Usually, a dense network is required to achieve a high performance of ambiguity resolution, and consequently a huge ambiguity product seems unavoidable. This limitation prevents the real-time application of the method by Bertiger et al. (2010).

On the other hand, the FCB-based methods are characterized by three points:

- Undifferenced measurements from a single receiver are processed although it is the differential ambiguities that are fixed to integers. Differencing is performed on the undifferenced ambiguity estimates, rather than the raw measurements;
- FCBs are eliminated or separated from the integer ambiguities by directly processing the ambiguity estimates. This means that FCBs are not used to directly reduce the raw measurements;
- Because only the ambiguity estimates are used to preform ambiguity resolution, the FCB-based methods are totally compatible with the conventional PPP by Zumberge et al. (1997). Therefore, FCB-based ambiguity resolution can conveniently supplement the conventional PPP without causing considerable revisions of the classic algorithms.

Finally, for completeness, Gao and Shen (2001) proposed a pseudo-fixing strategy in which undifferenced ambiguity estimates are directly fixed to their nearest integers, regardless of the

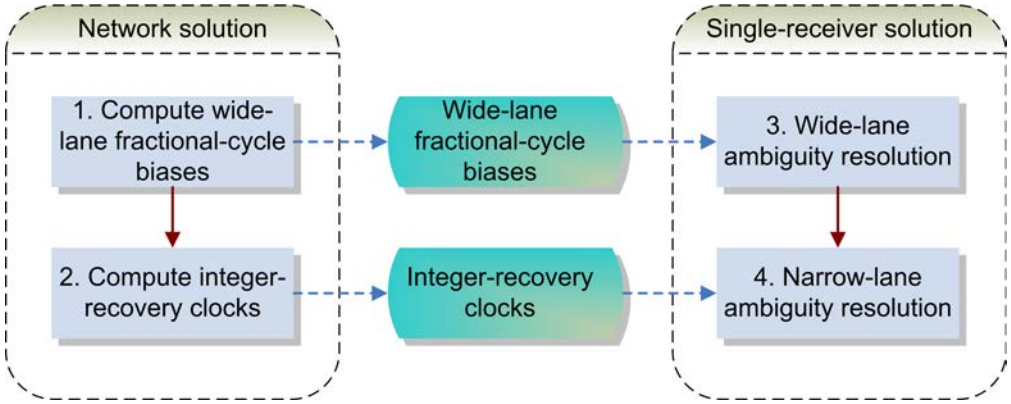

Figure 2.3: Procedure of IRC-based ambiguity resolution by Laurichesse et al. (2009c). Meaning of arrows refers to Figure 2.1

FCBs. Hence, no network solution is required to estimate FCBs. In fact, this strategy was used to accelerate the convergence of real-time PPP (Abdel-salam and Gao 2003). As reported by Gao and Shen (2001), successful pseudo-fixing can improve the positioning accuracy to better than 40 cm during the early convergence period. Nevertheless, pseudo-fixing is actually fixing ambiguities to erroneous values. To mitigate the resulting negative impacts, ambiguity-float solutions have to be kept at the same time (Abdel-salam 2004). Anyway, this method potentially jeopardizes the PPP performance, although it may slightly contribute to the rapid convergences in the real-time PPP.

2.2.3 Methods based on integer-recovery clocks (IRCs)

The IRCs are named as this because they are used in PPP to directly generate the ambiguity estimates that hold the integer properties, hence differing from the official clock products in Table 1.1. Unlike the FCB-based methods, the IRC-based methods do not require a rigorous assumption of constant satellite hardware biases. In the following, two methods developed by Laurichesse et al. (2009c) and Collins (2008) are introduced. For each method, the IRC determination with a network of reference stations is detailed before a single-receiver solution based on the IRCs is presented. Finally, the key points for the IRC-based methods are summarized.

A Method by Laurichesse et al. (2009c)

The method developed by Laurichesse et al. (2009c) can be schematically illustrated with Figure 2.3. Similar to the FCB-based methods, this method consists of the network solution and the single-receiver solution. In the network solution, wide-lane FCBs are determined before the IRCs are estimated. By utilizing the wide-lane FCB and IRC products, users can sequentially attempt the wide-lane and narrow-lane ambiguity resolution at a single receiver.

For the network solution, the estimates of wide-lane FCBs are also derived from the Melbourne-Wübbena combination measurements. However, unlike the FCB-based method by Ge et al. (2008) where single-difference FCBs between satellites are estimated, undifferenced wide-lane FCBs are determined directly from the undifferenced wide-lane ambiguity estimates. By reformulating Equation 2.8, we can obtain

$$\hat{N}_{wi}^{k} = N_{wi}^{k} + \phi_{wi} - \phi_{w}^{k} = \left\langle \frac{L_{mi}^{k}}{\lambda_{w}} \right\rangle \tag{2.20}$$

where

$$\begin{cases} \phi_{wi} = \dfrac{B_{1i}}{\lambda_1} - \dfrac{B_{2i}}{\lambda_2} - \dfrac{\lambda_n}{\lambda_w}\left(\dfrac{b_{1i}}{\lambda_1} + \dfrac{b_{2i}}{\lambda_2}\right) \\ \phi_w^k = \dfrac{B_1^k}{\lambda_1} - \dfrac{B_2^k}{\lambda_2} - \dfrac{\lambda_n}{\lambda_w}\left(\dfrac{b_1^k}{\lambda_1} + \dfrac{b_2^k}{\lambda_2}\right) \end{cases} \tag{2.21}$$

and ϕ_{wi} and ϕ_w^k represent the undifferenced receiver and satellite wide-lane FCBs, respectively. As demonstrated by Wang and Gao (2007), ϕ_{wi} might be a varying quantity. However, for continuously operating receivers at the IGS permanent stations, ϕ_{wi} can be quite stable (Laurichesse et al. 2009c). On the other hand, ϕ_w^k for most GPS satellites has been observed to be quite stable over a long time up to a few months and to change quite slowly at about 0.5 cycles/year (Gabor and Nerem 1999). If the variations of ϕ_{wi} and ϕ_w^k are sufficiently slow and small, the integer resolution of wide-lane ambiguities with a long wavelength of about 86 cm will hardly be impaired (Laurichesse et al. 2009c). Moreover, similar to the FCB-based methods, ϕ_w^k is used only for the wide-lane ambiguity resolution. Therefore, Laurichesse et al. (2009c) could safely presume constant values for both ϕ_{wi} and ϕ_w^k over 24 hours without affecting the final ambiguity-fixed solutions. Furthermore, N_{wi}^k can be identified by an integer rounding, and thus Equation 2.20 becomes

$$\hat{N}_{wi}^k - N_{wi}^k = \phi_{wi} - \phi_w^k \tag{2.22}$$

For all undifferenced wide-lane ambiguity estimates, Equation 2.22 can be superimposed as pseudo measurements to a normal equation in order to estimate the receiver-specific ϕ_{wi} and the satellite-specific ϕ_w^k. In addition, to keep consistency among all $\hat{N}_{wi}^k - N_{wi}^k$, some $\hat{N}_{wi}^k - N_{wi}^k$ might be shifted by a few integer cycles (Laurichesse and Mercier 2007). Note that the resulting normal matrix is rank deficiency, and thus a ϕ_{wi} or ϕ_w^k has to be assigned an arbitrary value, such as zero. In this manner, the undifferenced satellite wide-lane FCBs ϕ_w^k are obtained.

At the same time, integer wide-lane ambiguities N_{wi}^k at all involved receivers can also be obtained. We can then achieve Equation 2.6 by deriving the narrow-lane ambiguity N_i^k. Of important note, N_i^k is identified as an integer before estimating the final satellite clocks using a network of reference stations. Laurichesse et al. (2009c) first derived estimates of ρ_i^k and t_i^k through an ambiguity-float PPP. Then the carrier-phase measurement in Equation 2.6 can be re-written as

$$L_i^k - \rho_i^k = ct_i^k + B_i^k + \lambda_n N_i^k - \varepsilon_i^k \tag{2.23}$$

Similar to Equation 2.20, this equation can be reformulated as

$$L_i^k - \rho_i^k = \lambda_n N_i^k + (ct_i + B_i) - \left(ct^k + B^k\right) \tag{2.24}$$

where the residual error ε_i^k is ignored for brevity. N_i^k should be first fixed to the nearest integer of its float estimate. Note that a shift of a few integer cycles might be necessary to keep consistency among all N_i^k in the network solution. Hence, $(ct_i + B_i)$ and $\left(ct^k + B^k\right)$ can be identified following the strategy of deriving ϕ_{wi} or ϕ_w^k with Equation 2.22. Of particular note, $\left(t_i + \dfrac{B_i}{c}\right)$ and $\left(t^k + \dfrac{B^k}{c}\right)$ are the so-called IRCs defined in the IRC-based methods. We can find that narrow-lane FCBs are now absorbed by clocks, and $(ct_i + B_i)$ and $\left(ct^k + B^k\right)$ have to be estimated at each epoch, rather than only once per the whole observation period. This thus explains why an assumption of constant satellite hardware biases over the observation period is not rigorously required in the IRC-based methods. Moreover, instead of fixing a specific

$(ct_i + B_i)$ to zero to avoid the rank deficiency, this $(ct_i + B_i)$ should be fixed to the estimate of ct_i derived from the aforementioned ambiguity-float PPP. Finally, the satellite IRC $\left(t^k + \frac{B^k}{c}\right)$ is obtained.

On the other hand, at a single receiver, the above undifferenced wide-lane FCBs ϕ_w^k are used to correct the wide-lane ambiguity estimates in order to recover their integer properties, whereas the satellite IRCs $\left(t^k + \frac{B^k}{c}\right)$ replace the official satellite clock products in PPP data processing in order to directly obtain narrow-lane ambiguity estimates with integer properties. Specifically, a float wide-lane ambiguity estimate corrected by its corresponding undifferenced wide-lane FCB can be written as

$$N_{wi}^k + \phi_{wi} = \hat{N}_{wi}^k + \phi_w^k \tag{2.25}$$

and its variance is

$$\sigma^2_{N_{wi}^k} = \frac{\left\langle \left(\frac{L_{mi}^k}{\lambda_w} - \hat{N}_{wi}^k \right)^2 \right\rangle}{R_i^k} + \sigma^2_{\phi_w^k} \tag{2.26}$$

where $\sigma^2_{\phi_w^k}$ is the variance of ϕ_w^k and other notations refer to Equation 2.16. Note that ϕ_{wi} is identical for all satellites observed at a single receiver. Hence, a fractional value can be assigned to ϕ_{wi} in order to recover the integer property of N_{wi}^k, and integer resolutions are attempted for the resulting undifferenced wide-lane ambiguity estimates at receiver i. Note that the assigned value of ϕ_{wi} can cause an integer bias for all resulting integer wide-lane ambiguities, but this bias will not jeopardize the subsequent narrow-lane ambiguity resolution, because this bias is common for all satellites at receiver i and thus can be totally absorbed by receiver clocks.

Once wide-lane ambiguity resolution succeeds, narrow-lane ambiguities can be introduced into the measurement equations of PPP as demonstrated by Equation 2.6. Then the above satellite IRCs are introduced and fixed during the undifferenced data processing, namely

$$L_i^k + c\left(t^k + \frac{B^k}{c}\right) = \rho_i^k + c\left(t_i + \frac{B_i}{c}\right) + \lambda_n N_i^k - \varepsilon_i^k \tag{2.27}$$

In order to obtain the integer properties of narrow-lane ambiguity estimates, a narrow-lane ambiguity is arbitrarily fixed to an integer, and hence the receiver clock can be identified. As a result, all remaining narrow-lane ambiguities acquire integer properties (Laurichesse and Mercier 2007; Laurichesse et al. 2009c). Ambiguity resolution is then attempted. A successful narrow-lane ambiguity resolution will directly lead to the ambiguity-fixed solution at a single receiver.

This IRC-based method has been discussed in a number of publications and has been implemented for the routine GPS analysis at the French Space Geodesy Research Group since GPS week 1582 (see IGS Mail-6155 and http://www.igsac-cnes.cls.fr). Moreover, Laurichesse and Mercier (2007) reported that the post-processing horizontal accuracy of the epoch-wise position estimates at a static receiver was better than 2 cm; Delporte et al. (2008) applied this method to the time transfer based on PPP and achieved an agreement of about 0.3 ns with the BIPM (Bureau International des Poids et Mesures) two-way satellite time and frequency transfer; Laurichesse et al. (2008b) applied this method to the precise orbit determination of low Earth orbiters (LEOs) and reduced the RMS statistics of Satellite Laser Ranging (SLR) residuals by around 1.5 mm; Laurichesse et al. (2008a, 2009a) presented simulated real-time case studies in which IRC-based ambiguity resolution improves real-time GPS orbit quality and

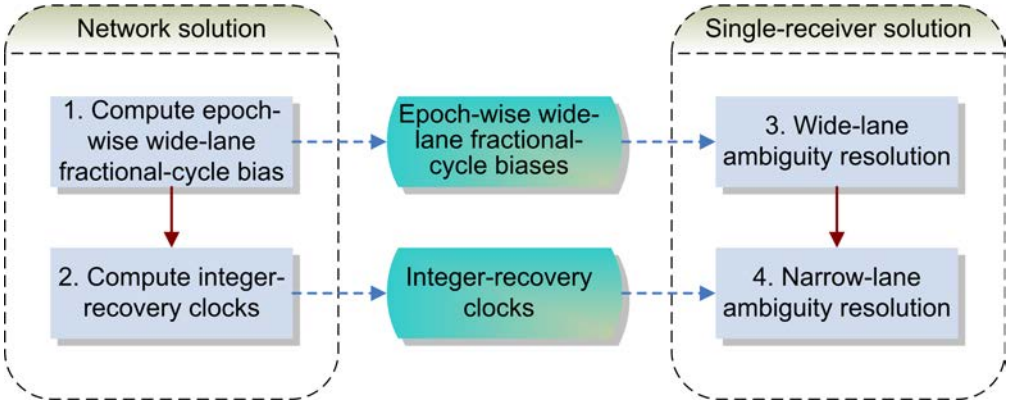

Figure 2.4: Procedure of IRC-based ambiguity resolution by Collins (2008). Meaning of arrows refers to Figure 2.1

leads to an epoch-wise positioning accuracy of better than 2 cm at a static receiver; finally, Laurichesse et al. (2009b) even attempted ambiguity resolution at single-frequency receivers by summing pseudorange measurements and carrier-phase measurements to mitigate ionospheric delays. However, all these studies showed only a limited number of cases to quantify the performance of IRC-based ambiguity resolution.

B Method by Collins (2008)

The method developed by Collins (2008) can be schematically illustrated with Figure 2.4. Compared with the method by Laurichesse et al. (2009c), wide-lane FCBs are not taken as constant values over the observation period, but are estimated at each epoch like the IRCs in the network solution. These clock-like wide-lane FCBs are then delivered together with the IRCs to a single receiver in order to sequentially fix the wide-lane and narrow-lane ambiguities to integers.

For the network solution, a wide-lane ambiguity estimate is decomposed like Equation 2.20. Nonetheless, both ϕ_{wi} and ϕ_w^k are not taken as constant parameters in a least squares adjustment. After identifying N_{wi}^k as an integer, the undifferenced satellite wide-lane FCB ϕ_w^k is estimated like clock parameters. In this manner, Collins (2008) avoided the issue of presuming the temporal and spatial properties of FCBs, because these properties have not been confirmed by the GPS community. However, the problem is that a large number of clock-like wide-lane FCBs have to be delivered to users, which will significantly increase the communication burden, especially in real-time applications.

Once these undifferenced wide-lane FCBs are obtained, integer wide-lane ambiguities at all reference receivers can also be obtained. IRCs can then be estimated following the methodology by Laurichesse et al. (2009c). Of particular note, Collins (2008) proposed a decoupled clock model where the IRCs derived from carrier-phase measurements differ from the clocks in pseudorange measurements. Specifically, similar to the derivation of Equation 2.24, the pseudorange measurement in Equation 2.6 can be reformulated as

$$P_i^k - \rho_i^k = (ct_i + b_i) - \left(ct^k + b^k\right) \tag{2.28}$$

where the residual error e_i^k is ignored for brevity. With Equation 2.28, the pseudorange clocks,

namely $\left(t_i + \frac{b_i}{c}\right)$ and $\left(t^k + \frac{b^k}{c}\right)$, can be determined following the methodology of estimating IRCs. However, it is worth indicating that these pseudorange clocks totally differ from the IRCs. According to this point, Collins (2008) argued that clock and clock-like products should be separately generated for each type of observables that are used in the undifferenced GPS data processing. In this manner, biases in pseudorange measurement residuals can be significantly reduced. More importantly, the data processing models are more rigorous in theory and can be potentially generalized for multi-frequency measurements.

On the other hand, at a single receiver, undifferenced wide-lane and narrow-lane ambiguity resolutions are performed by applying the above epoch-wise wide-lane FCBs and the IRCs. The ambiguity resolution refers to the method by Laurichesse et al. (2009c). Note that the satellite clocks applied to the pseudorange measurements should be $\left(t^k + \frac{b^k}{c}\right)$ instead of the satellite IRCs.

In practice, Collins et al. (2008) illustrated that the positioning accuracy for 90% of hourly position estimates was improved from around 10 cm to better than 2 cm after applying the decoupled clock model for ambiguity resolution at a single receiver. Moreover, Collins et al. (2009) showed that the epoch-wise positioning accuracy of horizontal components could be improved by about 30% after ambiguity resolution if daily GPS measurements at static receivers were used.

C Remarks on the IRC-based methods

According to the discussions above, Laurichesse et al. (2009c) and Collins (2008) adopted identical algorithms to determine the IRCs which is critical to the integer recovery of undifferenced ambiguities at a single receiver. Nonetheless, apart from these IRCs, Collins (2008) estimated the epoch-wise wide-lane FCBs and the pseudorange clocks which have to be delivered to users. Hence, compared with the method by Laurichesse et al. (2009c), the practicability of the method by Collins (2008) is significantly weakened. Furthermore, as illustrated by Gabor and Nerem (1999) and Ge et al. (2008), the wide-lane FCBs actually change minimally and slowly over time and space. If the wide-lane FCBs are used only for ambiguity resolution, an accuracy of better than $\frac{1}{4}\lambda_w$ is sufficient, which implies that the epoch-wise estimation of wide-lane FCBs is actually not necessary. Finally, as narrow-lane ambiguities are fixed to integers before estimating the clocks, pseudorange measurements actually lose their indispensable role of separating clocks from ambiguities (Collins 2008), implying that pseudorange measurements could be ignored in estimating the IRCs. In this case, pseudorange clocks generated with the method by Collins (2008) are actually not required by users and can be safely ignored.

In conclusion, the IRC-based methods are characterized by the three points:

- Undifferenced ambiguities are fixed to integers, and no differencing is imposed on raw measurements or undifferenced ambiguity estimates. In order to achieve this, an arbitrary fractional value has to be assigned to a receiver FCB in wide-lane ambiguity resolution or a receiver clock in narrow-lane ambiguity resolution.
- FCBs are separated from integer ambiguities when reducing the raw measurements with the IRCs. This means that the integer properties of undifferenced ambiguities have been preserved in the carrier-phase measurement modeling.
- Because the data processing strategy is considerably changed in the IRC-based methods, the resulting IRCs are not compatible with current official clock products issued by the

IGS (Kouba and Springer 2001). Hence, it is not an easy task to combine the IRCs with the official clock products.

2.3 Theoretical comparison between the two methods

By contrasting the FCB- and IRC-based methods introduced above, we can find that their key difference is the strategy of separating narrow-lane FCBs from integer ambiguities. Ge et al. (2008) estimated narrow-lane FCBs with float ambiguity estimates, whereas Laurichesse et al. (2009c) assimilated narrow-lane FCBs into clock estimates. From current publications, the positioning quality of the FCB-based method is close to that of the IRC-based method. In this case, of great interest is whether the ambiguity-fixed position estimates derived from these two methods coincide in theory and how they agree in practice.

This section therefore aims at comparing these two methods from a theoretical aspect and finally prove the equivalence between their ambiguity-fixed position estimates. In the following, Section 2.3.1 specifies the assumptions that the theoretical analysis is based on; Section 2.3.2 and 2.3.3 derive the theoretical compositions of the FCB and IRC estimates, and their corresponding ambiguity-fixed position estimates, respectively; finally, Section 2.3.4 concludes the equivalence of the theoretical ambiguity-fixed position estimates and highlights the differences between the FCB- and IRC-based methods. Note that how the ambiguity-fixed position estimates agree in practice will be illustrated in Section 5.8 using one year of GPS measurements.

2.3.1 Assumptions for the theoretical analysis

Due to the uncertainty of the temporal properties of hardware biases, they are divided into a time-invariant and a time-dependent part to rigorously model their physical properties. Hence, according to Equation 2.6, the linearized undifferenced measurement equations between receiver i and satellite k at a particular epoch are

$$\begin{cases} \Delta P_i^k = \mathbf{u}_i^k \Delta \mathbf{x}_i + c\Delta t_i^k + \lambda_n \left(\ell b_i^k + \delta b_i^k\right) - e_i^k \\ \Delta L_i^k = \mathbf{u}_i^k \Delta \mathbf{x}_i + c\Delta t_i^k + \lambda_n \left(\ell B_i^k + \delta B_i^k\right) + \lambda_n \Delta N_i^k - \varepsilon_i^k \end{cases} \tag{2.29}$$

where ΔP_i^k and ΔL_i^k denote the observed minus computed measurements for the pseudorange and carrier-phase, respectively; $\mathbf{u}_i^k$ contains the unit vector from the satellite to the receiver and the mapping function of ZTD; $\Delta \mathbf{x}_i^k$ contains the increments for the a priori receiver position vector and ZTD; $\Delta t_i^k = \Delta t_i - \Delta t^k$ where Δt_i and Δt^k denote the increments for the a priori receiver and satellite clocks, respectively; $\left(\ell B_i^k + \delta B_i^k\right)$ is the carrier-phase narrow-lane FCB where ℓB_i^k denotes the constant offset, i.e. the time-invariant part, whereas δB_i^k denotes the time-dependent deviation from ℓB_i^k; similarly, $\left(\ell b_i^k + \delta b_i^k\right)$ is the fractional-cycle part of the pseudorange bias which is hereafter called pseudorange FCB for convenience; ΔN_i^k denotes the integer increments of the a priori narrow-lane ambiguity (Teunissen and Kleusberg 1998). In addition, wide-lane FCBs are not discussed in Section 2.3 and thus all "FCBs" throughout this section represent "narrow-lane FCBs" for brevity except when otherwise noted.

From Equation 2.29, if receiver i observes m satellites at this epoch, we can obtain

$$\begin{bmatrix} e_i^1 \\ \vdots \\ e_i^m \\ \varepsilon_i^1 \\ \vdots \\ \varepsilon_i^m \end{bmatrix} = \begin{bmatrix} \mathbf{u}_i^1 & c\mathbf{I}^1 & \lambda_n\mathbf{I}^1 & \lambda_n\mathbf{I}^1 & \mathbf{0} & \mathbf{0} & \mathbf{0} \\ \vdots & \vdots & \vdots & \vdots & \vdots & \vdots & \vdots \\ \mathbf{u}_i^m & c\mathbf{I}^m & \lambda_n\mathbf{I}^m & \lambda_n\mathbf{I}^m & \mathbf{0} & \mathbf{0} & \mathbf{0} \\ \mathbf{u}_i^1 & c\mathbf{I}^1 & \mathbf{0} & \mathbf{0} & \lambda_n\mathbf{I}^1 & \lambda_n\mathbf{I}^1 & \lambda_n\mathbf{I}^1 \\ \vdots & \vdots & \vdots & \vdots & \vdots & \vdots & \vdots \\ \mathbf{u}_i^m & c\mathbf{I}^m & \mathbf{0} & \mathbf{0} & \lambda_n\mathbf{I}^m & \lambda_n\mathbf{I}^m & \lambda_n\mathbf{I}^m \end{bmatrix} \begin{bmatrix} \Delta\mathbf{x}_i \\ \Delta\mathbf{t}_i \\ \ell\mathbf{b}_i \\ \delta\mathbf{b}_i \\ \ell\mathbf{B}_i \\ \delta\mathbf{B}_i \\ \Delta\mathbf{N}_i \end{bmatrix} - \begin{bmatrix} \Delta P_i^1 \\ \vdots \\ \Delta P_i^m \\ \Delta L_i^1 \\ \vdots \\ \Delta L_i^m \end{bmatrix} \tag{2.30}$$

where $\mathbf{I}^h$ denotes an m-dimensional row-vector of which the h-th element is 1 while all others are 0 ($h = 1, \cdots m$); $\mathbf{0}$ denotes an m-dimensional row-vector with all elements as zero; finally, each of $\Delta\mathbf{t}_i$, $\ell\mathbf{b}_i$, $\delta\mathbf{b}_i$, $\ell\mathbf{B}_i$, $\delta\mathbf{B}_i$ and $\Delta\mathbf{N}_i$ denotes an m-dimensional column-vector corresponding to m satellites, $\Delta\mathbf{t}_i = \left[\Delta t_i^1, \cdots \Delta t_i^m\right]^{\mathrm{T}}$ for example. All unknown parameters except $\Delta\mathbf{x}_i$ are linearly correlated, hence preventing them from being simultaneously estimated in a least squares adjustment.

In fact, only $\Delta\mathbf{x}_i$, $\Delta\mathbf{t}_i$ and $\Delta\mathbf{N}_i$ are taken as to-be-estimated parameters in PPP. Hence, after a least squares adjustment, all $\ell\mathbf{b}_i$, $\delta\mathbf{b}_i$, $\ell\mathbf{B}_i$ and $\delta\mathbf{B}_i$ should finally be assimilated into $\Delta\mathbf{t}_i$ and $\Delta\mathbf{N}_i$, or otherwise into the residuals, namely the left side of Equation 2.30. Such an assimilation should rigorously satisfy the requirement of minimizing the weighted sum squares of residuals. Under the constraint of this rule, these assimilations are derived by applying elementary column transformations (Meyer 2000) to Equation 2.30 and conclude what the FCB and IRC estimates theoretically contain after a network solution. Note that the assumption for this theoretical analysis is that FCBs are hardware-dependent and only they are assimilated into the to-be-estimated parameters whilst all e_i^k and ε_i^k add to the residuals.

Then, these theoretical FCB and IRC estimates are applied to a single-receiver solution and finally achieve identical ambiguity-fixed position estimates for these two methods. To simplify the formula derivation, the difference between satellites is applied to Equation 2.30 to avoid considering the receiver clocks and the receiver-dependent FCBs. Note that this operation does not affect the estimates of $\Delta\mathbf{x}_i$. More importantly, in this case, the pseudorange measurements can be ignored because they are not needed to separate the clocks and the ambiguities. Moreover, satellite clocks are precisely known and thus should be moved to the observed minus computed measurements. Hence,

$$\begin{bmatrix} \varepsilon_i^{2,1} \\ \vdots \\ \varepsilon_i^{m,1} \end{bmatrix} = \begin{bmatrix} \mathbf{u}_i^{2,1} & -\lambda_n\mathbf{I}^1 & -\lambda_n\mathbf{I}^1 & \lambda_n\mathbf{I}^1 \\ \vdots & \vdots & \vdots & \vdots \\ \mathbf{u}_i^{m,1} & -\lambda_n\mathbf{I}^{m-1} & -\lambda_n\mathbf{I}^{m-1} & \lambda_n\mathbf{I}^{m-1} \end{bmatrix} \begin{bmatrix} \Delta\mathbf{x}_i \\ \ell\dot{\mathbf{B}} \\ \delta\dot{\mathbf{B}} \\ \Delta\dot{\mathbf{N}}_i \end{bmatrix} - \begin{bmatrix} \Delta L_i^{2,1} + c\Delta t^{2,1} \\ \vdots \\ \Delta L_i^{m,1} + c\Delta t^{m,1} \end{bmatrix} \tag{2.31}$$

where $\mathbf{I}^h$ is an $(m-1)$-dimensional row-vector; $\ell\dot{\mathbf{B}} = \left[\ell B^{2,1}, \cdots \ell B^{m,1}\right]^{\mathrm{T}}$, $\delta\dot{\mathbf{B}} = \left[\delta B^{2,1}, \cdots \delta B^{m,1}\right]^{\mathrm{T}}$ and $\Delta\dot{\mathbf{N}}_i = \left[\Delta N_i^{2,1}, \cdots \Delta N_i^{m,1}\right]^{\mathrm{T}}$ where the superscript for each vector element denotes the difference between satellites. In the following, the FCBs and IRCs are first derived using Equation 2.30 and then derive the ambiguity-fixed position estimates using Equation 2.31.

2.3.2 FCB determination and ambiguity-fixed position estimates

In order to determine FCBs, what a narrow-lane ambiguity estimate theoretically contains after a least squares adjustment has to be derived. As demonstrated by Defraigne and Bruyninx

(2007), biases in the pseudorange measurements govern the absolute clock offsets generated in the conventional PPP. Hence in Equation 2.30, the pseudorange time-invariant FCBs $\ell\mathbf{b}_i$ should be assimilated into the clocks. For the carrier-phase measurements, offsets of $\ell\mathbf{b}_i$ are thus introduced by the pseudorange-based clocks, and are finally assimilated into the integer ambiguities together with the carrier-phase time-invariant FCBs $\ell\mathbf{B}_i$, namely

$$\begin{bmatrix} e_i^1 \\ \vdots \\ e_i^m \\ \varepsilon_i^1 \\ \vdots \\ \varepsilon_i^m \end{bmatrix} = \begin{bmatrix} \mathbf{u}_i^1 & c\mathbf{I}^1 & \lambda_n\mathbf{I}^1 & \mathbf{0} & \mathbf{0} \\ \vdots & \vdots & \vdots & \vdots & \vdots \\ \mathbf{u}_i^m & c\mathbf{I}^m & \lambda_n\mathbf{I}^m & \mathbf{0} & \mathbf{0} \\ \mathbf{u}_i^1 & c\mathbf{I}^1 & \mathbf{0} & \lambda_n\mathbf{I}^1 & \lambda_n\mathbf{I}^1 \\ \vdots & \vdots & \vdots & \vdots & \vdots \\ \mathbf{u}_i^m & c\mathbf{I}^m & \mathbf{0} & \lambda_n\mathbf{I}^m & \lambda_n\mathbf{I}^m \end{bmatrix} \begin{bmatrix} \Delta\mathbf{x}_i \\ \Delta\mathbf{t}_i + \dfrac{\lambda_n}{c}\ell\mathbf{b}_i \\ \delta\mathbf{b}_i \\ \delta\mathbf{B}_i \\ \Delta\mathbf{N}_i + \ell\mathbf{B}_i - \ell\mathbf{b}_i \end{bmatrix} - \begin{bmatrix} \Delta P_i^1 \\ \vdots \\ \Delta P_i^m \\ \Delta L_i^1 \\ \vdots \\ \Delta L_i^m \end{bmatrix} \tag{2.32}$$

Note that the residuals are not changed. Conversely, if it is the carrier-phase time-invariant FCBs $\ell\mathbf{B}_i$ that are assimilated into the clocks, the resulting offsets $\ell\mathbf{B}_i$ in the pseudorange measurements then have to be assimilated into the pseudorange residuals, consequently enlarging the weighted sum squares of residuals. This apagogically proves the manner in which time-invariant FCBs are assimilated into the clocks and ambiguities, as illustrated by Equation 2.32.

On the other hand, time-dependent FCBs can be assimilated only into the clocks. However, the residuals have to be enlarged because the pseudorange and carrier-phase FCBs differ. Due to the far-weak weights imposed on pseudorange measurements, the carrier-phase FCBs $\delta\mathbf{B}_i$, rather than the pseudorange FCBs $\delta\mathbf{b}_i$, should be assimilated into the clocks and all remaining FCBs are assimilated into the pseudorange residuals, namely

$$\begin{bmatrix} e_i^1 - \lambda_n\delta b_i^1 + \lambda_n\delta B_i^1 \\ \vdots \\ e_i^m - \lambda_n\delta b_i^m + \lambda_n\delta B_i^m \\ \varepsilon_i^1 \\ \vdots \\ \varepsilon_i^m \end{bmatrix} = \begin{bmatrix} \mathbf{u}_i^1 & c\mathbf{I}^1 & \mathbf{0} \\ \vdots & \vdots & \vdots \\ \mathbf{u}_i^m & c\mathbf{I}^m & \mathbf{0} \\ \mathbf{u}_i^1 & c\mathbf{I}^1 & \lambda_n\mathbf{I}^1 \\ \vdots & \vdots & \vdots \\ \mathbf{u}_i^m & c\mathbf{I}^m & \lambda_n\mathbf{I}^m \end{bmatrix} \begin{bmatrix} \Delta\mathbf{x}_i \\ \Delta\mathbf{t}_i + \dfrac{\lambda_n}{c}\ell\mathbf{b}_i + \dfrac{\lambda_n}{c}\delta\mathbf{B}_i \\ \Delta\mathbf{N}_i + \ell\mathbf{B}_i - \ell\mathbf{b}_i \end{bmatrix} - \begin{bmatrix} \Delta P_i^1 \\ \vdots \\ \Delta P_i^m \\ \Delta L_i^1 \\ \vdots \\ \Delta L_i^m \end{bmatrix} \tag{2.33}$$

Conversely, if it is $\delta\mathbf{b}_i$ that are assimilated into the clocks, the resulting offsets $\delta\mathbf{b}_i$ in the carrier-phase measurements then have to be assimilated into the highly-weighted carrier-phase residuals, consequently enlarging the weighted sum squares of residuals more significantly than Equation 2.33. This again apagogically justifies the derivation of Equation 2.33. Note that the unknowns in Equation 2.33 should be estimated using a network of reference stations.

From Equation 2.33, it can be derived that $\Delta\mathbf{t}_i + \dfrac{\lambda_n}{c}\ell\mathbf{b}_i + \dfrac{\lambda_n}{c}\delta\mathbf{B}_i$ are the estimated increments for the a priori clocks, whereas $\Delta\mathbf{N}_i + \ell\mathbf{B}_i - \ell\mathbf{b}_i$ are the estimated float increments for the a priori integer ambiguities. The clock estimates should be divided into the receiver and satellite clocks by constraining a receiver clock to zero or the sum of a clock ensemble to zero. Hence, the clock estimate for a specific satellite k can be written as $\Delta t^k + \dfrac{\lambda_n}{c}\ell b^k + \dfrac{\lambda_n}{c}\delta B^k$. In practice, an unknown bias should be present in this satellite clock estimate, but fortunately this bias is identical for all satellite clocks and can be absorbed by the receiver clock in a single-receiver solution without impairing the position estimate. Furthermore, the ambiguity estimates are differenced between the k-th and the first satellites and obtain $\Delta N_i^{k,1} + \ell b^{k,1} - \ell B^{k,1}$ $(k = 2, \cdots m)$. For convenience, it is presumed that $\ell b^{k,1} - \ell B^{k,1}$ is still fractional. After removing

$\Delta N_i^{k,1}$ by an integer rounding, the FCB estimates for satellite pairs, namely $\phi_n^{k1} = \ell b^{k,1} - \ell B^{k,1}$, are finally obtained.

At a single receiver, the above satellite clock and satellite-pair FCB estimates are applied to Equation 2.31 in order to achieve ambiguity-fixed position estimates. Note that $\Delta t^{k,1}$ in Equation 2.31 should be replaced by $\Delta t^{k,1} + \frac{\lambda_n}{c}\ell b^{k,1} + \frac{\lambda_n}{c}\delta B^{k,1}$. As a result, $\delta\dot{\mathbf{B}}$ can be removed from the parameter vector in Equation 2.31 because they have been corrected by the satellite clocks, but $\ell\dot{\mathbf{b}}$ has to be inserted because the satellite clocks introduce additional errors of $\ell\dot{\mathbf{b}}$, namely

$$\begin{bmatrix} \varepsilon_i^{2,1} \\ \vdots \\ \varepsilon_i^{m,1} \end{bmatrix} = \begin{bmatrix} \mathbf{u}_i^{2,1} & \lambda_n\mathbf{I}^1 & -\lambda_n\mathbf{I}^1 & \lambda_n\mathbf{I}^1 \\ \vdots & \vdots & \vdots & \vdots \\ \mathbf{u}_i^{m,1} & \lambda_n\mathbf{I}^{m-1} & -\lambda_n\mathbf{I}^{m-1} & \lambda_n\mathbf{I}^{m-1} \end{bmatrix} \begin{bmatrix} \Delta\mathbf{x}_i \\ \ell\dot{\mathbf{b}} \\ \ell\dot{\mathbf{B}} \\ \Delta\dot{\mathbf{N}}_i \end{bmatrix} - \begin{bmatrix} \Delta L_i^{2,1} + c\Delta t^{2,1} + \lambda_n\ell b^{2,1} + \lambda_n\delta B^{2,1} \\ \vdots \\ \Delta L_i^{m,1} + c\Delta t^{m,1} + \lambda_n\ell b^{m,1} + \lambda_n\delta B^{m,1} \end{bmatrix} \tag{2.34}$$

where $\ell\dot{\mathbf{b}} = \left[\ell b^{2,1}, \cdots \ell b^{m,1}\right]^{\mathrm{T}}$. Furthermore, similar to Equation 2.32, Equation 2.34 actually becomes

$$\begin{bmatrix} \varepsilon_i^{2,1} \\ \vdots \\ \varepsilon_i^{m,1} \end{bmatrix} = \begin{bmatrix} \mathbf{u}_i^{2,1} & \lambda_n\mathbf{I}^1 \\ \vdots & \vdots \\ \mathbf{u}_i^{m,1} & \lambda_n\mathbf{I}^{m-1} \end{bmatrix} \begin{bmatrix} \Delta\mathbf{x}_i \\ \Delta\dot{\mathbf{N}}_i + \ell\dot{\mathbf{b}} - \ell\dot{\mathbf{B}} \end{bmatrix} - \begin{bmatrix} \Delta L_i^{2,1} + c\Delta t^{2,1} + \lambda_n\ell b^{2,1} + \lambda_n\delta B^{2,1} \\ \vdots \\ \Delta L_i^{m,1} + c\Delta t^{m,1} + \lambda_n\ell b^{m,1} + \lambda_n\delta B^{m,1} \end{bmatrix} \tag{2.35}$$

From Equation 2.35, if the resulting float ambiguity estimate $\Delta N_i^{k,1} + \ell b^{k,1} - \ell B^{k,1}$ is corrected by the satellite-pair FCB $\ell b^{k,1} - \ell B^{k,1}$, we can attempt to fix the resulting $\Delta N_i^{k,1}$ to an integer. If this integer resolution succeeds, the unknown parameters contain only $\Delta\mathbf{x}_i$ and hence the fixed ambiguities are deducted from the observed minus computed measurements, namely

$$\begin{bmatrix} \varepsilon_i^{2,1} \\ \vdots \\ \varepsilon_i^{m,1} \end{bmatrix} = \begin{bmatrix} \mathbf{u}_i^{2,1} \\ \vdots \\ \mathbf{u}_i^{m,1} \end{bmatrix} \begin{bmatrix} \Delta\mathbf{x}_i \end{bmatrix} - \begin{bmatrix} \Delta L_i^{2,1} - \lambda_n\Delta N_i^{2,1} + c\Delta t^{2,1} + \lambda_n\ell B^{2,1} + \lambda_n\delta B^{2,1} \\ \vdots \\ \Delta L_i^{m,1} - \lambda_n\Delta N_i^{m,1} + c\Delta t^{m,1} + \lambda_n\ell B^{m,1} + \lambda_n\delta B^{m,1} \end{bmatrix} \tag{2.36}$$

Equation 2.36 is then used to estimate the ambiguity-fixed $\Delta\mathbf{x}_i$ according to the theory of least squares adjustment. Note that Equation 2.36 is actually for epoch-wise positioning, but multi-epoch positioning can be easily derived by superimposing Equation 2.36.

2.3.3 IRC determination and ambiguity-fixed position estimates

In order to determine IRCs, the undifferenced ambiguities have to be first identified as integers in a network solution. In Equation 2.30, if $\Delta\mathbf{N}_i$ is successfully fixed to integers, $\Delta\mathbf{N}_i$ can then be removed from the parameter vector and deducted from the observed minus computed

measurements, namely

$$\begin{bmatrix} e_i^1 \\ \vdots \\ e_i^m \\ \varepsilon_i^1 \\ \vdots \\ \varepsilon_i^m \end{bmatrix} = \begin{bmatrix} \mathbf{u}_i^1 & c\mathbf{I}^1 & \lambda_n\mathbf{I}^1 & \lambda_n\mathbf{I}^1 & \mathbf{0} & \mathbf{0} \\ \vdots & \vdots & \vdots & \vdots & \vdots & \vdots \\ \mathbf{u}_i^m & c\mathbf{I}^m & \lambda_n\mathbf{I}^m & \lambda_n\mathbf{I}^m & \mathbf{0} & \mathbf{0} \\ \mathbf{u}_i^1 & c\mathbf{I}^1 & \mathbf{0} & \mathbf{0} & \lambda_n\mathbf{I}^1 & \lambda_n\mathbf{I}^1 \\ \vdots & \vdots & \vdots & \vdots & \vdots & \vdots \\ \mathbf{u}_i^m & c\mathbf{I}^m & \mathbf{0} & \mathbf{0} & \lambda_n\mathbf{I}^m & \lambda_n\mathbf{I}^m \end{bmatrix} \begin{bmatrix} \Delta\mathbf{x}_i \\ \Delta\mathbf{t}_i \\ \ell\mathbf{b}_i \\ \delta\mathbf{b}_i \\ \ell\mathbf{B}_i \\ \delta\mathbf{B}_i \end{bmatrix} - \begin{bmatrix} \Delta P_i^1 \\ \vdots \\ \Delta P_i^m \\ \Delta L_i^1 - \lambda_n \Delta N_i^1 \\ \vdots \\ \Delta L_i^m - \lambda_n \Delta N_i^m \end{bmatrix} \tag{2.37}$$

Then similar to Equation 2.33, the carrier-phase FCBs $\ell\mathbf{B}_i + \delta\mathbf{B}_i$, rather than the pseudorange FCBs $\ell\mathbf{b}_i + \delta\mathbf{b}_i$, are assimilated into the clocks. The resulting offsets $\ell\mathbf{B}_i + \delta\mathbf{B}_i$ in the pseudorange measurements have to be assimilated into the pseudorange residuals together with $\ell\mathbf{b}_i + \delta\mathbf{b}_i$. Hence, Equation 2.37 becomes

$$\begin{bmatrix} e_i^1 - \lambda_n \ell b_i^1 - \lambda_n \delta b_i^1 + \lambda_n \ell B_i^1 + \lambda_n \delta B_i^1 \\ \vdots \\ e_i^m - \lambda_n \ell b_i^m - \lambda_n \delta b_i^m + \lambda_n \ell B_i^m + \lambda_n \delta B_i^m \\ \varepsilon_i^1 \\ \vdots \\ \varepsilon_i^m \end{bmatrix} =$$

$$\begin{bmatrix} \mathbf{u}_i^1 & c\mathbf{I}^1 \\ \vdots & \vdots \\ \mathbf{u}_i^m & c\mathbf{I}^m \\ \mathbf{u}_i^1 & c\mathbf{I}^1 \\ \vdots & \vdots \\ \mathbf{u}_i^m & c\mathbf{I}^m \end{bmatrix} \begin{bmatrix} \Delta\mathbf{x}_i \\ \Delta\mathbf{t}_i + \frac{\lambda_n}{c}\ell\mathbf{B}_i + \frac{\lambda_n}{c}\delta\mathbf{B}_i \end{bmatrix} - \begin{bmatrix} \Delta P_i^1 \\ \vdots \\ \Delta P_i^m \\ \Delta L_i^1 - \lambda_n \Delta N_i^1 \\ \vdots \\ \Delta L_i^m - \lambda_n \Delta N_i^m \end{bmatrix} \tag{2.38}$$

Again, the unknowns in Equation 2.38 should be estimated with a network of reference stations. Hence, IRCs are equal to $\Delta\mathbf{t}_i + \frac{\lambda_n}{c}\ell\mathbf{B}_i + \frac{\lambda_n}{c}\delta\mathbf{B}_i$ plus the a priori clocks. The IRC for a specific satellite k can be written as $\Delta t^k + \frac{\lambda_n}{c}\ell B^k + \frac{\lambda_n}{c}\delta B^k$.

At a single receiver, the above satellite IRCs are applied to Equation 2.31 in order to achieve ambiguity-fixed position estimates. Note that $\Delta t^{k,1}$ in Equation 2.31 should be replaced by $\Delta t^{k,1} + \frac{\lambda_n}{c}\ell B^{k,1} + \frac{\lambda_n}{c}\delta B^{k,1}$. As a result, both $\ell\dot{\mathbf{B}}$ and $\delta\dot{\mathbf{B}}$ are removed from the parameter vector in Equation 2.31 because they have been corrected by the satellite clocks, namely

$$\begin{bmatrix} \varepsilon_i^{2,1} \\ \vdots \\ \varepsilon_i^{m,1} \end{bmatrix} = \begin{bmatrix} \mathbf{u}_i^{2,1} & \lambda_n\mathbf{I}^1 \\ \vdots & \vdots \\ \mathbf{u}_i^{m,1} & \lambda_n\mathbf{I}^{m-1} \end{bmatrix} \begin{bmatrix} \Delta\mathbf{x}_i \\ \Delta\dot{\mathbf{N}}_i \end{bmatrix} - \begin{bmatrix} \Delta L_i^{2,1} + c\Delta t^{2,1} + \lambda_n \ell B^{2,1} + \lambda_n \delta B^{2,1} \\ \vdots \\ \Delta L_i^{m,1} + c\Delta t^{m,1} + \lambda_n \ell B^{m,1} + \lambda_n \delta B^{m,1} \end{bmatrix} \tag{2.39}$$

Then, if $\Delta\dot{\mathbf{N}}_i$ can be successfully fixed to integers, they can be deducted from the observed minus computed measurements and Equation 2.39 becomes

$$\begin{bmatrix} \varepsilon_i^{2,1} \\ \vdots \\ \varepsilon_i^{m,1} \end{bmatrix} = \begin{bmatrix} \mathbf{u}_i^{2,1} \\ \vdots \\ \mathbf{u}_i^{m,1} \end{bmatrix} \begin{bmatrix} \Delta\mathbf{x}_i \end{bmatrix} - \begin{bmatrix} \Delta L_i^{2,1} - \lambda_n \Delta N_i^{2,1} + c\Delta t^{2,1} + \lambda_n \ell B^{2,1} + \lambda_n \delta B^{2,1} \\ \vdots \\ \Delta L_i^{m,1} - \lambda_n \Delta N_i^{m,1} + c\Delta t^{m,1} + \lambda_n \ell B^{m,1} + \lambda_n \delta B^{m,1} \end{bmatrix} \tag{2.40}$$

2.3.4 Remarks on the theoretical comparison

By contrasting Equation 2.36 and 2.40, it can be found that their design matrices and observed minus computed measurements are exactly the same, which demonstrates that the resulting estimates for $\Delta\mathbf{x}_i$ from the FCB- and IRC-based methods should also be identical. This equivalence implies that a systematic difference between the $\Delta\mathbf{x}_i$ estimates in practice, if existing, should not be caused by the differences of the two methods themselves. Ideally, the difference between the actual $\Delta\mathbf{x}_i$ estimates should be minimal and random in nature. In addition, in terms of Equation 2.29, $\Delta\mathbf{x}_i$ also contains ZTD. Hence, identical ZTD estimates can also be achieved using these two methods. Note that this theoretical equivalence is derived from Equation 2.30, namely the linearized measurement equation, thereby implying that identical models should be employed to reduce the raw measurements in order to achieve identical $\Delta\mathbf{x}_i$ estimates.

Nevertheless, this equivalence is largely based on the assumption that only the hardware-dependent FCBs are assimilated into the clock and undifferenced ambiguity estimates, which is not true in practice. Ge et al. (2008) illustrated that satellite-pair FCB estimates change temporally and spatially, and the fluctuation magnitude can reach up to 0.4 cycles, showing that these FCB estimates are contaminated by unknown temporally- and spatially-correlated errors, such as the inaccurate modeling of tropospheric delays. This explains why FCB estimates are not constant values in practice and thus Ge et al. (2008) proposed a 15-minute mean to achieve high-precision FCB estimates. Likewise, actual IRC estimates are likely to absorb not only the hardware-dependent FCBs, but also some unknown common errors among a network of stations. It should be stressed that these unknown redundant errors are not hardware-dependent, and thus they are likely to change under different distributions of reference stations. In the subsequent part of this thesis, "FCB estimates" thus also contain these redundant errors.

Furthermore, from the observed minus computed measurements in Equation 2.36 and 2.40, $\Delta t^{k,1} + \frac{\lambda_n}{c}\ell B^{k,1} + \frac{\lambda_n}{c}\delta B^{k,1}$ $(k = 2, \cdots m)$ can actually be taken as the satellite clock that can assist retrieving integer ambiguities. In the FCB-based method, this clock is finally achieved by combining the satellite clock estimate and the FCB estimate. Comparatively, this clock is exactly the IRC in the IRC-based method. This difference is attributed to the different strategies of separating FCBs from integer ambiguities in these two methods. Specifically, this separation is performed at the ambiguity-estimate level in the FCB-based method, whereas at the measurement-modeling level in the IRC-based method. As a result, the composition of redundant errors can be significantly different between the actual IRC estimates and the actual FCB estimates plus their corresponding satellite clock estimates, finally leading to different $\Delta\mathbf{x}_i$ estimates.

2.4 Method improvements made in this thesis

The FCB-based method by Ge et al. (2008) is adopted and improved for the PPP data analysis presented in this thesis. The IRC-based method by Laurichesse et al. (2009c) is also implemented and its results are compared with those by the FCB-based method. Method implementations will be addressed in Chapter 4. This section will introduce four improvements or developments that have been achieved in this thesis for the FCB-based method.

2.4.1 Derivation of undifferenced FCBs

Undifferenced FCBs are preferred to satellite-pair FCBs because the number of FCBs can be significantly reduced. For example, if m satellites are observed, $m(m-1)/2$ satellite-pair FCBs will be generated. By contrast, only m undifferenced FCBs are needed to express all these satellite-pair FCBs. A large number of FCBs cannot be conveniently transmitted, especially in real-time applications. Furthermore, because undifferenced FCBs are satellite-dependent, they can actually be combined with the epoch-wise satellite clocks (Mervart et al. 2008). Such combination can further reduce the data transmission bandwidth, hence potentially enhancing the competitiveness of the FCB-based method against the IRC-based method where only satellite orbits and IRCs are transmitted to users.

In fact, the derivation of undifferenced FCBs is only a trivial task. A satellite-pair FCB ϕ^{kl} can be expressed as a pseudo measurement like $\phi^{kl} = \phi^k - \phi^l$. All these pseudo measurements can be superimposed to a normal equation in order to estimate undifferenced FCBs. Note that an undifferenced FCB has to be fixed to an arbitrary value to avoid the rank deficiency of the normal matrix. In addition, the resulting residuals after this adjustment can be used to identify any possible blunders in the satellite-pair FCB estimates.

2.4.2 One FCB per satellite-pair pass over a regional area

Daily mean wide-lane FCBs can be precisely determined even on a global scale (Gabor and Nerem 1999; Ge et al. 2008; Laurichesse and Mercier 2007). However, due to the low precisions of daily mean narrow-lane FCBs, Ge et al. (2008) instead suggested a 15-minute mean.

In this thesis, it is proposed that the narrow-lane FCBs for a satellite pair can be precisely determined within each continuous tracking period by a regional network, namely each full pass by this satellite pair over a regional network. Therefore, the fractional parts of all involved narrow-lane ambiguity estimates for a satellite pair during one full pass are averaged to estimate one narrow-lane FCB. The key difference of this strategy from the 15-minute mean by Ge et al. (2008) consists in the satellite orbit arc length for one narrow-lane FCB estimate. Empirically, there are usually two narrow-lane FCB estimates per 24 hours which actually correspond to two full passes of a satellite pair over a regional network. Compared with the large number of 15-minute mean narrow-lane FCBs by Ge et al. (2008), this strategy can significantly reduce the dissemination burden of the FCB products, which is well suited for practical use in a regional network. The performance of these FCBs will be assessed in Section 5.2.

2.4.3 Implementation of real-time ambiguity resolution

To date, FCB-based methods are assessed primarily for post-processing applications. Mervart et al. (2008) reported some real-time results but few technical details are released due to commercial reasons. Hence, it is still necessary to propose a PPP-RTK model where PPP provides rapid convergence to a reliable centimeter-level positioning accuracy based on an RTK reference network (e.g. Bisnath and Gao 2007; Wübbena et al. 2005), which can improve on current real-time ambiguity-float PPP services (e.g. Dixon 2006).

Overall, a PPP-RTK model consists of a server module providing FCB products and a user module achieving ambiguity-fixed solutions. For the server module, wide-lane FCBs are generated according to the method by Ge et al. (2008) as addressed in Section 2.2.2. Ge et al.

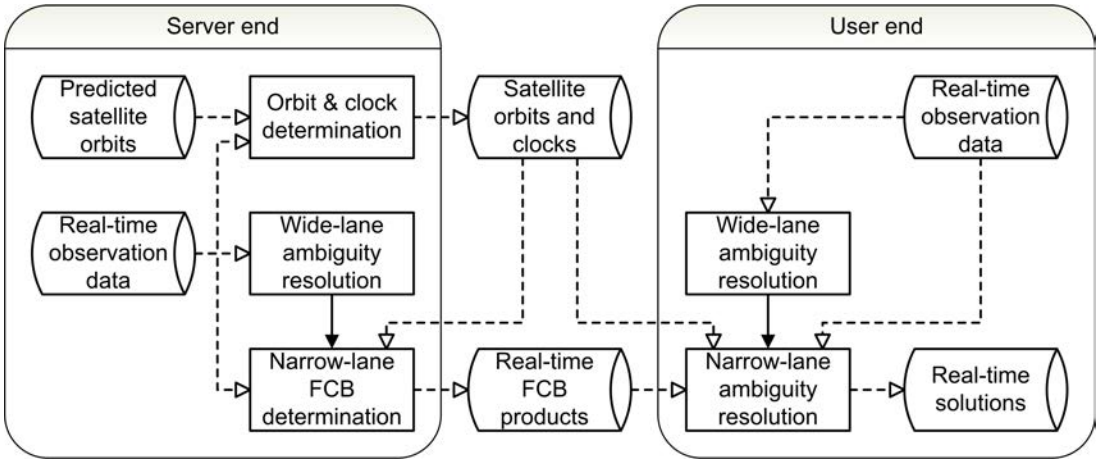

Figure 2.5: Data flowchart of a PPP-RTK model based on ambiguity resolution. Cylinders denote data storage and squares denote data-processing modules; dashed arrows denote data input or output; and solid arrows denote processing sequences

(2008) showed that wide-lane FCB estimates change within ±0.05 cycles within 2 weeks. Hence, wide-lane FCB products can be precisely predicted at an update rate of several days for real-time applications. However, narrow-lane FCBs have to be estimated at a sub-daily frequency in post-processing applications. Likewise, we have to frequently re-estimate and update the narrow-lane FCBs at the PPP-RTK server module. For the user module, wide-lane ambiguity resolution relies on the noisy Melbourne-Wübbena combination measurements. Hence, a sufficiently long time has to be spent before a wide-lane resolution can be reliably achieved. This time span is mainly subject to the pseudorange measurement noise, multipath effects and atmospheric delays. Afterwards, narrow-lane ambiguity resolution can be attempted according to the theories in Section 2.2.2. Note that the narrow-lane FCBs that are contributing to the achieved ambiguity-fixed solutions should be frequently updated because they are frequently re-estimated and re-disseminated at the server module (see Section 5.6.3 for detailed explanations).

Accordingly, Figure 2.5 presents the data flowchart at both the server and user modules for a conceptual PPP-RTK model. Compared with current real-time ambiguity-float PPP models, this model generates and disseminates not only the satellite orbits and clocks, but also the FCB products for users to achieve ambiguity-fixed solutions at a single receiver. Moreover, this model has to keep consistency among orbits, clocks and FCB products, rather than only between orbits and clocks (Geng et al. 2010c). In addition, in Figure 2.5, except the square denoting "orbit & clock determination", the other four squares exhibit three modules which are crucial to ambiguity resolution. It is presumed that wide-lane FCB products are easily known, and thus their determination module is ignored in Figure 2.5 for brevity. From the solid arrows in Figure 2.5, wide-lane ambiguity resolution is the prerequisite for both narrow-lane FCB determination and narrow-lane ambiguity resolution.

2.4.4 Constraints from integer double-difference ambiguities

As demonstrated in Section 2.2.2, FCBs are estimated by averaging the fractional parts of all involved ambiguity estimates at the reference stations. Nonetheless, due largely to the possible biases that are absorbed into the float ambiguity estimates, a sophisticated averaging technique, such as Equation 2.12, has to be adopted to achieve correct FCB estimates (see also Ge et al.

2008). Moreover, the temporal instability of narrow-lane FCBs (see Section 2.3.4) is likely to further complicate such averaging operations.

Fortunately, such averaging for narrow-lane FCBs can be avoided by applying tight constraints from integer double-difference ambiguities. In the FCB-based method by Bertiger et al. (2010), undifferenced ambiguity estimates can directly form double-difference ambiguities and integer resolutions can subsequently be attempted. This strategy was also discussed by Ge et al. (2005a, 2006). Successful ambiguity resolution will then improve the accuracy of undifferenced ambiguity estimates (Feng et al. 2007). Suppose we have two single-difference narrow-lane ambiguity estimates between satellites k and l at receiver i and j, namely $\hat{N}_i^{kl}$ and $\hat{N}_j^{kl}$, their difference $\hat{N}_i^{kl} - \hat{N}_j^{kl}$ should not be an integer after an initial PPP data processing. However, if double-difference ambiguity resolution is successfully performed on $\hat{N}_i^{kl} - \hat{N}_j^{kl}$, this difference can then be tightly constrained to an integer in a second PPP data processing. Hence, the fractional parts of the resulting estimates for $\hat{N}_i^{kl}$ and $\hat{N}_j^{kl}$ are identical. In this way, most fractional parts of single-difference ambiguity estimates for a satellite pair are identical if the fixing rate of double-difference ambiguities is sufficiently high. Fortunately, Ge et al. (2005a) suggested an innovative strategy and showed that a fixing rate of higher than 97% can be routinely achieved using daily GPS measurements on a global scale. Therefore, narrow-lane FCBs can then be easily identified from the identical fractional parts of narrow-lane ambiguity estimates for a satellite pair.

Finally, it is worth highlighting that narrow-lane FCBs determined through these integer double-difference constraints theoretically have higher accuracy than that determined without these constraints. This point will be empirically verified in Section 5.7.

2.5 Ambiguity search and validation

By the FCB- or IRC-based methods, the integer properties of ambiguities at a single receiver can be retrieved. However, integer resolutions are accomplished through the ambiguity search and validation. Ambiguity search means determining the range of integer candidates for a float ambiguity estimate. Theoretically, this range depends on the float ambiguity estimate and its stochastic statistics. On the other hand, ambiguity validation means deciding whether an integer candidate should be accepted as the correct integer under a given confidence level. The criteria for this validation depend on the presumed statistical distribution of the quadratic form of least-squares residuals (Teunissen and Kleusberg 1998). In the following, the sequential bias rounding by Dong and Bock (1989) and the LAMBDA (Least-squares AMBiguity Decorrelation Adjustment) by Teunissen (1994) for ambiguity resolution is briefly introduced.

2.5.1 Sequential bias rounding

Sequential bias rounding, or integer bias bootstrapping (Teunissen 1998), means that a chosen set of ambiguities are rounded to integers at a particular step, and the estimates and precisions of remaining ambiguities are hence improved for a new bias-rounding step. The rounding procedure is based on the assumption that if a float ambiguity estimate is close to an integer and has a high precision, this integer is highly likely to be the correct one (Dong and Bock 1989). The

fixing decision is made according to a probability value, namely

$$P_0 = 1 - \sum_{i=1}^{\infty} \left(\text{efrc}\left(\frac{i - \left|\hat{N} - N\right|}{\sqrt{2}\sigma} \right) - \text{efrc}\left(\frac{i + \left|\hat{N} - N\right|}{\sqrt{2}\sigma} \right) \right) \tag{2.41}$$

where $\text{efrc}(x)$ is the complementary error function

$$\text{efrc}(x) = \frac{2}{\sqrt{\pi}} \int_x^{\infty} e^{-t^2}\, dt \tag{2.42}$$

and $\hat{N}$ is the float ambiguity estimate; σ is the precision or the standard deviation of $\hat{N}$; N is the nearest integer to $\hat{N}$. For a given confidence level α, an ambiguity can be fixed to its nearest integer if its corresponding P_0 is larger than $1 - \alpha$, and otherwise not (Dong and Bock 1989; Ge et al. 2005a, 2008). During the initial stage of sequential bias rounding, there may be only a few ambiguities that can be successfully fixed to integers using the criterion above. Nonetheless, as ambiguity resolution progresses, more ambiguities will be improved and thus can be resolved.

Similarly, Blewitt (1989) proposed a sequential bias optimizing method where the cumulative probability for all correctly resolved ambiguities is calculated and another ambiguity is fixed only if the cumulative probability stays larger than 99%. In addition, based on the above sequential bias bounding, Ge et al. (2006) suggested an integer resolution of a float ambiguity estimate according to only its closeness to an integer without considering its standard deviation. As a result, the ambiguity validation is performed by testing whether the residuals of measurements led by each ambiguity are compatible before and afterwards. Note that this strategy is suggested mainly for speeding up a huge-network analysis.

2.5.2 LAMBDA

The LAMBDA method offers the highest probability of coming up with the correct integer candidates for ambiguities (Joosten and Tiberius 2002). Ambiguity resolution is actually based on the least squares principle (e.g. Hofmann-Wellenhof et al. 2001), namely

$$S = \left(\hat{\mathbf{N}} - \mathbf{N}\right)^{\mathrm{T}} \mathbf{Q}_{\hat{\mathbf{N}}}^{-1} \left(\hat{\mathbf{N}} - \mathbf{N}\right) = \text{minimum} \tag{2.43}$$

where $\hat{\mathbf{N}}$ is the m-dimensional vector of float ambiguity estimates and $\mathbf{N}$ is its corresponding integer vector; $\mathbf{Q}_{\hat{\mathbf{N}}}$ is the variance-covariance matrix of $\hat{\mathbf{N}}$. Hence, ambiguity resolution is achieved by identifying an $\mathbf{N}$ that minimizes the sum squares of the ambiguity residual vector $\hat{\mathbf{N}} - \mathbf{N}$ weighted by the inverse of $\mathbf{Q}_{\hat{\mathbf{N}}}$. Due to the integer constraints on the ambiguities, Equation 2.43 has to be solved by means of a search. However, this search is not an easy task because it is carried out over the whole m-dimensional space of integers. In order to simplify this problem, the whole integer space has to be replaced by a smaller set of integers, which is hereafter called the ambiguity search space. This space is located at $\hat{\mathbf{N}}$ and its shape and orientation are governed by $\mathbf{Q}_{\hat{\mathbf{N}}}$. It is in this local space that the search for the integer least-squares solution is performed (Teunissen 1998).

Teunissen (1994) defined the ambiguity search space as a set of grid points $\mathbf{N}$ that satisfies

$$S = \left(\hat{\mathbf{N}} - \mathbf{N}\right)^{\mathrm{T}} \mathbf{Q}_{\hat{\mathbf{N}}}^{-1} \left(\hat{\mathbf{N}} - \mathbf{N}\right) \leqslant \chi^2 \tag{2.44}$$

where the constant χ^2 guarantees that the search space contains the correct integer candidate. For details on how to determine χ^2 refer to de Jonge and Tiberius (1996). It is worth emphasizing that the volume of an ambiguity search space is governed by both χ^2 and $\mathbf{Q}_{\hat{\mathbf{N}}}$. Due to the high correlation between the float ambiguity estimates in the scenario of a very short observation period, the resulting search space is usually severely elongated and stretched over a considerable range of cycles (Joosten and Tiberius 2002). Consequently, a search over such space is extremely inefficient. Hence, Teunissen (1994) proposed an integer invertible volume-preserving matrix $\mathbf{Z}$ to transform the original search space into a sphere-like one, namely

$$\mathbf{N}' = \mathbf{Z}\mathbf{N},\ \hat{\mathbf{N}}' = \mathbf{Z}\hat{\mathbf{N}},\ \mathbf{Q}_{\hat{\mathbf{N}}'} = \mathbf{Z}\mathbf{Q}_{\hat{\mathbf{N}}}\mathbf{Z}^{\mathrm{T}} \tag{2.45}$$

The search is then performed in this transformed space and the results are finally transformed back (de Jonge and Tiberius 1996). This transformation can be recognized as a decorrelation of ambiguity estimates after which the corresponding variance-covariance matrix $\mathbf{Q}_{\hat{\mathbf{N}}}$ becomes more diagonal. Note that $\mathbf{Z}$ transforms only the shape and the orientation of the ambiguity search space, but not its volume. In addition, for completeness, latest developments on the LAMBDA method are given in Henkel et al. (2009), Henkel and Günther (2010) and Teunissen (2010).

On the other hand, the optimum integers identified by the above LAMBDA method should be validated before being accepted as correct values. As addressed by Teunissen and Kleusberg (1998), ambiguity validation includes an acceptance test and a discrimination test. The acceptance test can be recognized as the compatibility between the potential integer candidates and the associated GPS measurements (Wang et al. 1998). For example, one possible test is based on the compatibility between the unit variances of the ambiguity-fixed and ambiguity-float solutions (Han 1997b; Teunissen and Kleusberg 1998), namely

$$\frac{\sigma^2_{\text{fixed}}}{\sigma^2_{\text{float}}} < \frac{m}{r-t}\left(F_{m,r-t-m;\alpha} - 1\right) + 1 \tag{2.46}$$

where r is the number of measurements; m is the number of ambiguities; t is the number of remaining parameters; $F_{m,r-t-m;\alpha}$ denotes the F-distribution of a confidence level α with m and $r-t-m$ degrees of freedom. Furthermore,

$$\frac{\sigma^2_{\text{fixed}}}{\sigma^2_{\text{float}}} = \frac{r-t-m}{r-t} \cdot \frac{\Omega_{\text{float}} + S}{\Omega_{\text{float}}} \tag{2.47}$$

where Ω_{float} is the quadratic form of least-squares residuals in an ambiguity-float solution. A smaller $\dfrac{\sigma^2_{\text{fixed}}}{\sigma^2_{\text{float}}}$ indicates a more reliable integer resolution.

Moreover, the discrimination test is to confirm that the optimum integers are statistically significantly better than the second-optimum integers. This test is normally performed by quantifying the ratio between the second minimum and the minimum quadratic form of ambiguity residuals, which is hereafter called the ratio test (Euler and Schaffrin 1990), namely

$$\frac{S_{\text{opt2}}}{S_{\text{opt1}}} > \gamma \tag{2.48}$$

where S_{opt2} and S_{opt1} correspond to the second-optimum and optimum integers, respectively; γ is a critical threshold value. From statistical theories, γ should be selected according to

the statistical distribution of $\frac{S_{\text{opt2}}}{S_{\text{opt1}}}$ and a given confidence level. However, although a number of studies have been dedicated to deriving this statistical distribution (e.g. Wang et al. 1998; Teunissen and Verhagen 2009), the rigorous distribution cannot be exactly known (Teunissen and Kleusberg 1998; Verhagen 2004). Hence, throughout this thesis, a constant value such as 2 or 3 is simply assigned to γ. As shown by Han (1997b,a), 2 is usually used and 3 is deemed as a conservative threshold in the ratio test. Finally, the ratio value $\frac{S_{\text{opt2}}}{S_{\text{opt1}}}$ is usually recognized as an index of denoting the reliability of ambiguity resolution, and thus a larger ratio value indicates a more reliable ambiguity resolution.

2.6 Summary

This chapter reviews the up-to-date methods for ambiguity resolution at a single receiver, namely the FCB- and the IRC-based methods. Their respective characteristics are concluded and summarized. Moreover, a theoretical equivalence between the ambiguity-fixed position estimates derived from these two methods is proved and the differences between these two methods are also addressed. Finally, an improved FCB-based method developed in this thesis is introduced. A few points on ambiguity search and validation end this chapter. Chapter 5 will present empirical results to assess the improved FCB-based method.

Chapter 3

Rapid Convergences

3.1 Introduction

As introduced in Section 1.3, slow convergences to a decimeter- or centimeter-level positioning accuracy have long been a limiting factor for real-time PPP to be accepted in most commercial applications (Bisnath and Gao 2007). Although this issue is of great concern to the GPS community (e.g. Dixon 2006; Huber et al. 2010; Melgard et al. 2010), only a limited number of publications focus on this topic. This chapter thus first introduces the attempts on accelerating convergences in real-time PPP, and then compares these attempts. Finally, a novel method where ionospheric delays are precisely predicted to the succeeding epochs in order to significantly accelerate re-convergences to ambiguity-fixed solutions is originally developed, and a potential strategy of accelerating the first convergence by precisely interpolating ionospheric delays from a dense network of reference stations is discussed.

3.2 Current advances

To date, few authors have formally proposed effective methods of significantly accelerating convergences in real-time PPP. This is because the two limiting factors causing slow convergences, i.e. the imprecise pseudorange measurements and the slow satellite-geometry change, cannot be easily overcome (see Section 1.3). Since 1997 when PPP was first introduced by Zumberge et al. (1997), only a few attempts on accelerating convergences have been performed by estimating the pseudorange precision, constraining the position parameters, improving the ambiguity validation or applying the ambiguity resolution. These four attempts are respectively detailed in the following before a comparison between them ends this section.

3.2.1 Attempt by estimating the pseudorange precision

Highly precise pseudorange measurements, if available, can tightly constrain ambiguous carrier-phase measurements and thus speed up the convergence of ambiguity estimates to accurate values. In this case, position estimates can also rapidly converge to accurate values. This principle was adopted by Gao and Shen (2001) who proposed a new pseudorange combination observable and a pertinent stochastic estimation.

Disregarding the conventional ionosphere-free pseudorange combination observable in Equation

2.2, Gao and Shen (2001) developed an alternative in terms of Equation 2.1

$$\frac{1}{2}\left(P_{gi}^{k}+L_{gi}^{k}\right)=\rho_{i}^{k}+ct_{i}^{k}+\frac{1}{2}\left(b_{gi}^{k}+B_{gi}^{k}\right)+\frac{1}{2}\lambda_{g}N_{gi}^{k}-\frac{1}{2}\left(e_{gi}^{k}+\varepsilon_{gi}^{k}\right) \tag{3.1}$$

where the ionospheric delay is also removed but the measurement noise is only $\frac{1}{2}$ of the original pseudorange noise if the carrier-phase noise is sufficiently small and thus ignored. Hence, Equation 3.1 is then combined with the carrier-phase measurement in Equation 2.2 for PPP (Gao and Shen 2001). However, Equation 3.1 has two defects: On the one hand, Equation 3.1 is no longer a pseudorange but a noisy ambiguous measurement; consequently, it cannot effectively constrain carrier-phase measurements. On the other hand, Equation 3.1 is based on a carrier-phase measurement which is individually used for PPP; hence, Equation 3.1 and the carrier-phase measurement are actually correlated, and this correlation should not be simply ignored in theory. Nonetheless, these two points were ignored by Gao and Shen (2001).

Furthermore, Gao and Shen (2001) applied a stochastic estimation in order to faithfully quantify the pseudorange precision. Stochastic modeling relates to how measurements are weighted in a least squares adjustment (Amiri-Simkooei et al. 2009; Wolf and Ghilani 1997). Because pseudorange and carrier-phase measurements are used, their relative precision needs to be carefully adjusted, which is conventionally treated by simply presuming a very high precision for carrier-phase and a very low precision for pseudorange measurements. However, this stochastic modeling may underestimate the actual pseudorange precision, possibly leading to degraded solutions or even a divergence of position estimates (Bona 2000; Gao and Shen 2001). Hence, in this attempt, the stochastic estimation is performed in order to reproduce the actual precision of pseudorange measurements. Suppose the a priori unit-weight measurement variance as σ_0^2 and the a priori variance of ionosphere-free pseudorange measurement in Equation 2.2 as $\sigma_{P_{\mathrm{IF}}}^2$, if the posteriori unit-weight measurement variance is $\hat{\sigma}_0^2$, we can obtain an estimate of the pseudorange variance as

$$\hat{\sigma}_{P_{\mathrm{IF}}}^2=\sigma_{P_{\mathrm{IF}}}^2\cdot\frac{\hat{\sigma}_0^2}{\sigma_0^2} \tag{3.2}$$

If we further assume an identical precision for pseudorange measurements on both frequencies, according to the error propagation law (Wolf and Ghilani 1997), we can have

$$\begin{aligned}\sigma_{P_{\mathrm{IF}}}^2&=\left(\frac{f_1^2}{f_1^2-f_2^2}\right)^2\sigma_P^2+\left(\frac{f_2^2}{f_1^2-f_2^2}\right)^2\sigma_P^2\\&\approx 8.87\sigma_P^2\end{aligned} \tag{3.3}$$

Hence, an estimate of the variance of the measurement in Equation 3.1 is

$$\hat{\sigma}_{P+L}^2\approx\frac{1}{4}\hat{\sigma}_P^2=\frac{\sigma_{P_{\mathrm{IF}}}^2\hat{\sigma}_0^2}{35.5\sigma_0^2} \tag{3.4}$$

Equation 3.4 is then used to quantify the actual precision of Equation 3.1. Due to the development of GPS hardware, the precision of pseudorange measurements has been significantly improved during the past decade. The actual precision of Equation 3.1 may be better than the presumed precision in most GPS software packages. Hence, this stochastic estimation can potentially reproduce the actual pseudorange precision and accelerate the convergence of PPP.

In practice, Gao and Shen (2001) reported that the convergence period to a 3D positioning accuracy of better than 40 cm was reduced to less than 5 minutes after applying the above

technique. Compared with the conventional PPP, an improvement of about 20% was achieved. However, these results were not conclusive because measurements collected under preferable conditions were used. Moreover, Abdel-salam (2004) suggested applying the ambiguity pseudo-fixing strategy (see the end of Section 2.2.2) to the convergence of real-time PPP. The idea underlying this strategy is not to wait for the convergence of all ambiguities but only a few of them that are believed to be sufficiently close to accurate estimates. These relatively accurate ambiguities are then properly constrained in the estimation to accelerate the convergence. However, how to screen such accurate ambiguities and how to constrain them were not discussed by Abdel-salam (2004), although in a case study at a static receiver, they reported that a 3D positioning accuracy of better than 40 cm could be achieved within a few epochs of high-rate measurements.

3.2.2 Attempt by constraining the position parameters

The slowly changing geometry of satellites can cause a high correlation between ambiguity and position parameters, consequently leading to a long convergence period. Hence, a tight constraint imposed on the position parameters can strongly assist decorrelating the ambiguity and position parameters, finally accelerating the ambiguity convergence to accurate estimates and reducing the convergence period of real-time PPP. This is the strategy proposed by Colombo et al. (2001).

Kinematic GPS users normally simplify the vehicle dynamics because they are usually poorly known in reality (e.g. Yang et al. 2007). However, for a buoy floating on the sea, the running average of its vertical positions should approximate the wave-filtered, time-varying vertical positions measured with a tide gauge, which changes gradually and predictably over time. Hence,

$$H_{\text{est}} = H_{\text{model}} + \alpha + \nu \tag{3.5}$$

where H_{est} is the unknown vertical component of a buoy; H_{model} is the modeled value of the vertical component which is derived from a running average over several minutes; α is the model bias that can be described as a constant plus a random walk variable; finally, ν denotes the residual error. Note that ν actually decides the precision of Equation 3.5. This equation represents a pseudo measurement which can be introduced into the normal equation of real-time PPP, and its weight depends on ν. A smaller ν means a higher precision and thus a larger weight. In this case, the vertical position can be tightly constrained and its correlation with ambiguities can thus be reduced, finally leading to a shorter convergence period (Colombo 2004, 2009). However, it is worth indicating that such position constraints are available only under some special conditions.

In a typical experiment, all three components of a buoy could reach an accuracy of better than 20 cm within a few tens of minutes when Equation 3.5 was applied; however, nearly 2 hours were needed if Equation 3.5 was not applied (Colombo et al. 2001). In addition, it was proposed that an inertial navigation system (INS) could be combined with PPP to provide dynamic constraints like Equation 3.5, although significant reduction of the convergence periods was not observed (Le and Lorga 2006; Zhang and Gao 2008).

3.2.3 Attempt by improving the ambiguity validation

Ambiguity validation decides whether an integer candidate can be accepted with a high confidence level. The ratio test is deemed as a good validation procedure, but is not an easy task if a theoretically rigorous validation is required (refer to Section 2.5.2). As pointed out by Teunissen and Verhagen (2009), most existing software packages choose a fixed threshold for the ratio test, no matter the strength of the underlying GPS model. This is not reasonable in theory because with a varying strength of GPS model or varying degrees of freedom, certainly varying thresholds should be used. Considering Section 2.5.2, a fixed threshold can be understood in terms of a lack of a proper theory. A fixed threshold may cause a rejection of correct integer candidates, consequently prolonging the convergence period to an ambiguity-fixed solution. Hence, an improved validation test has the potential to accelerate the convergence to an ambiguity-fixed solution (Collins et al. 2009).

For example, Teunissen and Verhagen (2009) recommended a fixed failure-rate method. A user-defined fixed value for the failure rate is chosen and the corresponding threshold for the ratio test is derived. Unfortunately, this derivation is not easy and a look-up table is thus suggested. Similarly, a W-test is developed by Wang et al. (1998) to avoid the fixed threshold in the ratio test. Nevertheless, as pointed out by Verhagen (2004), ambiguity validation is not so easy a task. More importantly, it is still difficult to state that rapid convergences of only a few seconds can be achieved even if an ideal and perfect validation strategy is found.

3.2.4 Attempt by applying the ambiguity resolution

Ambiguity resolution removes the correlation between ambiguity and position parameters, which will significantly improve the positioning accuracy. Hence, it has been highly expected that ambiguity resolution is the most promising method that can be used to overcome slow convergences in real-time PPP (Bisnath and Gao 2007; Landau et al. 2007).

Wang and Gao (2006) used simulated GPS measurements, where no FCBs were present, to perform ambiguity resolution at a single receiver. They found that ambiguity resolution reduced the convergence period from about 1000 to 120 s in kinematic PPP. However, with real measurements, Laurichesse et al. (2008a) reported that only after about 15 minutes could ambiguity resolution be accomplished for about 61% of all test cases even in static PPP; moreover, this percentage significantly decreased to only about 17% in kinematic PPP. Likewise, Mervart et al. (2008) illustrated that 15- to 30-minute measurements were usually required before ambiguities at a single receiver could be reliably fixed to integers in real-time PPP.

So slow convergences to ambiguity-fixed solutions are attributed to two factors. On the one hand, a wide-lane ambiguity is estimated based on noisy Melbourne-Wübbena combination measurements, and thus a long observation period is required to sufficiently smooth the noise. On the other hand, rapid narrow-lane resolution is handicapped by imprecise pseudorange measurements which cannot sufficiently shrink the search space for integer ambiguities suffering from a short wavelength of only 11 cm (Teunissen 1996). Hence, a long observation period has to be used to average out sufficiently precise pseudorange measurements in order to derive accurate ambiguity estimates (Teunissen et al. 1997). To date, it is still extremely difficult to develop an effective method to accelerate the convergence.

3.2.5 Remarks on the above attempts

According to the above discussions, all four attempts were actually not successful and their effectiveness were not conclusive. Pseudorange precision can be precisely reproduced with a stochastic estimation, but its contribution to accelerating convergences depends on whether the actual precision is better than the presumed one. Moreover, additional constraints imposed on the position parameters are not always available for common users. On the other hand, these constraints can actually be recognized as pseudorange-like measurements, but with a much higher precision compared with that of GPS pseudorange measurements. This thus explains why these constraints can significantly contribute to shortening the convergence period. Finally, it is actually unrealistic to improve ambiguity validation techniques in order to accelerate convergences. Whether an ambiguity resolution can be reliably confirmed depends on the strength of the GPS model, but whether a sufficient strength can be achieved does not depend on whether the validation tests can be passed. In fact, achieving such a strength may require a long enough observation period, implying that ambiguity validation cannot effectively assist accelerating the convergences. This explanation also shows why ambiguity resolution cannot be rapidly achieved with only a few seconds of measurements.

In addition, of particular interest is how ambiguity resolution relates to the convergence. As addressed in Section 3.2.4, it has been highly expected that ambiguity resolution can significantly accelerate the convergences. However, a reliable ambiguity resolution cannot be achieved until a few tens of minutes later. This implies that the position and ambiguity estimates have to converge to an adequate accuracy level before an ambiguity resolution can be confirmed with a high confidence level. Afterwards, the positioning accuracy can be further improved by this ambiguity resolution. Therefore, a reliable ambiguity resolution is closely related to a sufficiently long convergence period.

However, a long convergence period to an ambiguity-fixed solution almost totally devalues the accuracy improvement contributed by ambiguity resolution. Since it is still quite difficult to accelerate convergences, real-time PPP can be robustly used only in the environments with uninterrupted satellite signal availability (Bisnath and Gao 2007). Any loss of signal lock for many satellites may require PPP to re-converge, hence again resulting in a few tens of minutes during which the positioning accuracy deteriorates to the sub-meter, or even meter level. Therefore, a rapid re-convergence can make real-time PPP more practical and be of great benefit and significance for many commercial applications. Section 3.3 introduces a method for rapid re-convergences by repairing cycle slips and Section 3.4 then introduces an originally developed method for rapid re-convergences to ambiguity-fixed solutions where ionospheric delays are precisely predicted over time in order to significantly accelerate both wide-lane and narrow-lane resolutions.

3.3 Rapid re-convergence by repairing cycle slips

When a re-convergence due to cycle slips for many satellites starts at a particular epoch, the differencing between this epoch and the previous epoch of carrier-phase measurements removes the FCBs and thus integer cycle slips are left as unknowns in these epoch-differenced measurements. Integer cycle slips can then be resolved following the methodology of ambiguity resolution. As a result, correctly repairing cycle slips recovers the continuousness of undifferenced

carrier-phase measurements and finally prevents a long convergence period in real-time PPP. This is the idea developed by Banville and Langley (2009).

According to Equation 2.1, epoch-differenced GPS measurements can be written as

$$\begin{cases} \delta P_{gi}^k = \delta\rho_i^k + c\delta t_i^k + \dfrac{\delta\mu_i^k}{f_g^2} - \delta e_{gi}^k \\ \delta L_{gi}^k = \delta\rho_i^k + c\delta t_i^k - \dfrac{\delta\mu_i^k}{f_g^2} + \lambda_g A_{gi}^k - \delta\varepsilon_{gi}^k \end{cases} \tag{3.6}$$

where δ denotes the epoch-differencing operation; A_{gi}^k denotes the integer cycle slips on frequency g and it disappears if no cycle slips occur. Note that the hardware biases b_{gi}^k and B_{gi}^k are totally eliminated, which is reasonable if the epoch-differencing is performed over two epochs with a gap of less than a few minutes (Banville and Langley 2009). Likewise, atmospheric delays at these two epochs are close to each other, and hence $\delta\mu_i^k$ can be presumed negligible (Dai et al. 2003; Kashani et al. 2007). This approximation also applies to the tropospheric delays in $\delta\rho_i^k$ (Kaplan and Hegarty 2006; Stoew et al. 2007). Moreover, satellite clocks here are known and the epoch-differenced receiver clock δt_i is deemed as a to-be-estimated parameter.

Note that $\delta\rho_i^k$ contains unknown positions at both epochs if PPP is performed for a mobile receiver. If a linearization like Equation 2.29 is applied, we can obtain

$$\mathbf{u}_i^k(\tau_2)\,\Delta\mathbf{x}_i(\tau_2) - \mathbf{u}_i^k(\tau_1)\,\Delta\mathbf{x}_i(\tau_1) = \left(\mathbf{u}_i^k(\tau_2) - \mathbf{u}_i^k(\tau_1)\right)\Delta\mathbf{x}_i(\tau_2) + \mathbf{u}_i^k(\tau_1)\left(\Delta\mathbf{x}_i(\tau_2) - \Delta\mathbf{x}_i(\tau_1)\right) \tag{3.7}$$

where $\mathbf{u}_i^k(\tau)$ and $\Delta\mathbf{x}_i(\tau)$ denote the unit vector from satellite k to receiver i and the increments for the a priori receiver position vector at epoch τ, respectively. Note that ZTD-related quantities have been removed from both $\mathbf{u}_i^k(\tau)$ and $\Delta\mathbf{x}_i(\tau)$. From the left side of this equation, due to the slowly changing geometry of visible satellites, $\mathbf{u}_i^k(\tau_2)$ should be quite close to $\mathbf{u}_i^k(\tau_1)$ if $\tau_2 - \tau_1$ is sufficiently small, e.g. a few minutes (e.g. Santerre 1991). As a result, simultaneous estimation of $\Delta\mathbf{x}_i(\tau_2)$ and $\Delta\mathbf{x}_i(\tau_1)$ is likely to lead to an ill-condition of the resulting normal equation. However, from the right side of this equation, $\mathbf{u}_i^k(\tau_2) - \mathbf{u}_i^k(\tau_1)$ is close to a zero vector. We can hence reasonably and safely presume that $\left(\mathbf{u}_i^k(\tau_2) - \mathbf{u}_i^k(\tau_1)\right)\Delta\mathbf{x}_i(\tau_2)$ is negligible if $\tau_2 - \tau_1$ is less than a few minutes and each element of $\Delta\mathbf{x}_i(\tau_2)$ is smaller than a few meters. Furthermore, if $\Delta\mathbf{x}_i(\tau_2) - \Delta\mathbf{x}_i(\tau_1)$ is deemed as one to-be-estimated parameter vector, the resulting normal equation will no longer suffer from the ill-condition. For more technical details about Equation 3.7 refer to van Graas and Soloviev (2004).

Therefore, Equation 3.6 is used to estimate $\Delta\mathbf{x}_i(\tau_2) - \Delta\mathbf{x}_i(\tau_1)$, δt_i and A_{gi}^k. A_{gi}^k is afterwards fixed to an integer. In this manner, carrier-phase cycle slips can be mitigated and the continuousness of undifferenced carrier-phase measurements retrieved. As a result, a possible time-consuming re-convergence is avoided and the already achieved positioning quality prior to this re-convergence continues.

In order to improve the success rate of integer cycle-slip resolution based on Equation 3.6, wide-lane carrier-phase measurements can be formed, namely

$$\begin{aligned} L_{wi}^k &= \frac{f_1}{f_1 - f_2}L_{1i}^k - \frac{f_2}{f_1 - f_2}L_{2i}^k \\ &= \rho_i^k + ct_i^k + \frac{\mu_i^k}{f_1 f_2} + B_{wi}^k + \lambda_w N_{wi}^k - \varepsilon_{wi}^k \end{aligned} \tag{3.8}$$

where

$$\begin{cases} B_{wi}^k = \dfrac{f_1}{f_1 - f_2} B_{1i}^k - \dfrac{f_2}{f_1 - f_2} B_{2i}^k \\ \varepsilon_{wi}^k = \dfrac{f_1}{f_1 - f_2} \varepsilon_{1i}^k - \dfrac{f_2}{f_1 - f_2} \varepsilon_{2i}^k \end{cases} \tag{3.9}$$

Then epoch-differencing is applied to Equation 3.8 like that of Equation 3.6, and a cycle slip $A_{wi}^k = A_{1i}^k - A_{2i}^k$ on this wide-lane carrier-phase measurement can be relatively easily identified because of its long wavelength of about 86 cm. Once A_{wi}^k is successfully fixed to an integer, geometry-free carrier-phase measurements can be formed as

$$L_{Ii}^k = L_{1i}^k - L_{2i}^k = -\frac{\mu_i^k}{f_1^2} + \frac{\mu_i^k}{f_2^2} + B_{Ii}^k + \lambda_1 N_{1i}^k - \lambda_2 N_{2i}^k - \varepsilon_{Ii}^k \tag{3.10}$$

where

$$\begin{cases} B_{Ii}^k = B_{1i}^k - B_{2i}^k \\ \varepsilon_{Ii}^k = \varepsilon_{1i}^k - \varepsilon_{2i}^k \end{cases} \tag{3.11}$$

and epoch-differencing is then applied to derive the corresponding cycle-slip estimate as

$$\hat{A}_{Ii}^k = \lambda_1 \hat{A}_{1i}^k - \lambda_2 \hat{A}_{2i}^k \tag{3.12}$$

Note that both $-\dfrac{\mu_i^k}{f_1^2} + \dfrac{\mu_i^k}{f_2^2}$ and B_{Ii}^k are presumed to be totally eliminated after this epoch-differencing. Hence, we can obtain an estimate of the cycle slip on $L1$, namely

$$\hat{A}_{1i}^k = \frac{\lambda_2 A_{wi}^k - \hat{A}_{Ii}^k}{\lambda_2 - \lambda_1} \tag{3.13}$$

Note that the accuracy of the estimate of $\hat{A}_{Ii}^k$ with Equation 3.12 depends on the magnitude of $-\dfrac{\mu_i^k}{f_1^2} + \dfrac{\mu_i^k}{f_2^2}$ which actually cannot be totally eliminated if the gap between the two epochs is over a few minutes. Moreover, the wavelength for the integer cycle slip in Equation 3.13 is $\lambda_2 - \lambda_1$, namely about 5.4 cm. This means that the residual errors in Equation 3.12 should not exceed approximately 1.4 cm if $\hat{A}_{1i}^k$ needs to be reliably fixed to an integer.

In practice, Banville and Langley (2009) carried out a few tests for this method. At a static receiver collecting 4-hour 1-Hz GPS measurements, the success rate of integer cycle-slip resolution reached 99.7% even when $\tau_2 - \tau_1$ was 10 s, but this success rate was reduced when $\tau_2 - \tau_1$ was enlarged further. Banville and Langley (2009) emphasized that a high success rate cannot be guaranteed when the ionosphere condition is active. Hence, this method should be carefully used if rapid ionosphere variation is anticipated. Furthermore, for a mobile vessel at a speed of 2 to 9 knots and a mobile car, the success rate was rapidly reduced to only 16.9% and 32.4%, respectively, even though $\tau_2 - \tau_1$ was only 20 s (Banville and Langley 2009).

3.4 Rapid re-convergence developed in this thesis

In terms of Section 3.2.4, the keys to accelerating convergences to ambiguity-fixed solutions consist in both avoiding Melbourne-Wübbena combination measurements and shrinking the search space for integer ambiguities. The volume of this search space is governed by the variance-covariance matrix of ambiguity estimates, and it approximately observes the following

rule (Teunissen 1996, 1997):

$$V \propto \frac{\sigma_P}{R\lambda} \tag{3.14}$$

where V is the volume of the search space; σ_P is the precision of pseudorange or unambiguous measurements; R is the number of epochs; λ is the wavelength of carrier-phase measurements; and $\propto$ denotes a proportional relationship. To achieve rapid convergences, increasing R is unrealistic, and thus the only choices are diminishing σ_P or enlarging λ. This section thereby derives how to precisely predict ionospheric delays and how to apply these delays to accelerate both wide-lane and narrow-lane ambiguity resolutions, and then discuss the implementation of this method.

3.4.1 Precisely predict ionospheric delays

Reformulating Equation 3.8, at a particular epoch, we can obtain

$$L_{wi}^k = \frac{\mu_i^k}{f_1 f_2} + \rho_i^k + ct_i^k + B_{wi}^k + \lambda_w N_{wi}^k - \varepsilon_{wi}^k \tag{3.15}$$

which is hereafter used to estimate the ionospheric delay, namely the term of $\frac{\mu_i^k}{f_1 f_2}$ in theory, at all ambiguity-fixed epochs. For a low-dynamic receiver, the ionospheric delays for each satellite normally manifest a strong temporal correlation over a few minutes, especially when the ionosphere condition is relatively quiet (Dai et al. 2003; Kashani et al. 2007). This principle is the foremost foundation of my method for rapid re-convergences.

Despite this favorable characteristic of ionospheric delays, it is necessary to further quantify the residual biases that are possibly assimilated into the estimate of $\frac{\mu_i^k}{f_1 f_2}$, and investigate their temporal characteristics. First, the receiver clock error seems an unstable quantity over time. Hence, a single difference between satellites k and l at this epoch can be formed, namely

$$L_{wi}^{kl} = \frac{\mu_i^{kl}}{f_1 f_2} + \rho_i^{kl} - ct^{kl} + B_w^{kl} + \lambda_w N_{wi}^{kl} - \varepsilon_{wi}^{kl} \tag{3.16}$$

where the receiver clock t_i and the receiver hardware bias B_{wi} are consequently eliminated.

Second, ρ_i^{kl} depends on the receiver and satellite positions, and the tropospheric delay. To date, predicted GPS satellite orbits over 24 hours have reached an accuracy of around 5 cm (see Table 1.1). Residual radial orbit errors can be mostly mitigated by satellite clocks (Senior et al. 2008), if a consistent yaw-attitude model is applied to GPS satellites (Kouba 2009a). Moreover, GPS satellite orbits are tightly constrained by dynamic force models (e.g. Steigenberger et al. 2009), and thus the residual orbit errors should theoretically change smoothly. Note that unannounced satellite maneuvers can significantly degrade the orbit accuracy. For the precise prediction of ionospheric delays, maneuvers can be a limiting factor, but are hereafter ignored because they are normally rare. On the other hand, the receiver position can be known to centimeter-level accuracy in the ambiguity-fixed solution at this epoch (Geng et al. 2010d). In addition, tropospheric delays can be mostly mitigated by estimating a ZTD. Residual tropospheric delays are only a few millimeters at high elevations, but can be up to several centimeters at an elevation of smaller than 10° (Stoew et al. 2007). However, the troposphere condition around a low-dynamic receiver normally changes very slightly over at least several minutes if neither rapid weather fronts nor large height variations occur for this receiver (Gregorius and

Blewitt 1999; Shan et al. 2007). Considering this similar temporal property to that of ionospheric delays, these two atmospheric delays can be alternatively combined and their sum is predicted over time. Note that this combination is not applied in this thesis.

Third, due to the high correlation between t^{kl} and the satellite orbits (Senior et al. 2008), favorable user range errors of centimeter level can be achieved (Hauschild and Montenbruck 2009). Nonetheless, this t^{kl} is normally a predicted value due to communication delays in real-time applications. Fortunately, Senior et al. (2008) reported that the Rubidium and Cesium clocks on GPS satellites can be precisely predicted to a precision of better than 0.1 ns up to a period of 40 s which covers typical communication delays. In addition, current satellite clock products are based on ionosphere-free measurements. Applying these clocks to wide-lane measurements in Equation 3.15 can potentially cause a bias. Fortunately, this bias seems quite stable over time (Collins et al. 2005). Hence, it is hereafter assumed that errors of satellite clocks are always smaller than 0.1 ns.

Fourth, N_{wi}^{kl} is firstly resolved using Melbourne-Wübbena combination measurements, rather than wide-lane measurements in Equation 3.15. As a result, a possible integer-cycle hardware bias originating from pseudorange measurements can be assimilated into N_{wi}^{kl}, finally leading to an integer bias in the ionospheric delays. Fortunately, from the observed high stability of wide-lane FCB estimates (Gabor and Nerem 1999; Ge et al. 2008; Laurichesse et al. 2009c), it can be inferred that these integer biases are normally constant over at least 24 hours. On the other hand, as B_w^{kl} is part of wide-lane FCBs in Equation 2.9, it can be also deemed rather stable over time. Note that the above pseudorange-related integer-cycle bias in the subsequent formula derivations are ignored for brevity.

Finally, ε_{wi}^{kl} is the most uncertain quantity and it is believed that the multipath effect dominates among all possible unmodeled errors (e.g. Bilich et al. 2008; King and Watson 2010; Ogaja and Satirapod 2007). Dilssner et al. (2008) showed that the carrier-phase biases caused by multipath effects stemming from solely radiating near fields can theoretically reach a few centimeters for low-elevation satellites. Although Han and Rizos (2000b) described the strong temporal correlation of the multipath signatures at static antennas, these signatures can be quite random and thus unpredictable at mobile receivers.

Therefore, at an ambiguity-fixed epoch, the precisely known quantities of ρ_i^{kl}, t^{kl} and N_{wi}^{kl} can be deducted from L_{wi}^{kl} and the ionospheric-delay estimate can be derived as

$$\begin{aligned} \hat{I}_w^{kl} &= L_{wi}^{kl} - \hat{\rho}_i^{kl} + ct^{kl} - N_{wi}^{kl} \\ &= \frac{\mu_i^{kl}}{f_1 f_2} + B_w^{kl} + \xi_{wi}^{kl} - \varepsilon_{wi}^{kl} \end{aligned} \tag{3.17}$$

where $\hat{\rho}_i^{kl}$ is the estimate of ρ_i^{kl} which is derived from the ambiguity-fixed solution of this epoch; ξ_{wi}^{kl} contains the errors of the satellite products and the tropospheric delays. According to the quantitative assessments above, it can be inferred that $\xi_{wi}^{kl} - \varepsilon_{wi}^{kl}$ can easily amount to over 10 cm for low-elevation satellites. Nonetheless, ξ_{wi}^{kl} changes slightly or predictably over a few minutes, and B_w^{kl} changes negligibly over a long time, thereby negligibly impairing the temporal-correlation characteristic of $\frac{\mu_i^{kl}}{f_1 f_2}$. Hence, $\hat{I}_w^{kl}$ can be precisely predicted to the succeeding epochs over a few minutes, especially at static stations where multipath effects in ε_{wi}^{kl} are also temporally correlated. Note that the error caused by the receiver position estimate is ignored in Equation 3.17 because this error will be absorbed by the position estimate where the predicted ionospheric

delays are applied (refer to the next section). In this study, $\hat{I}_w^{kl}$ is called "ionospheric delay" for brevity although it contains more than a true ionospheric delay.

For the predicting strategy, both the constant bias model and the linear fitting model are suggested (Dai et al. 2003). In the constant bias model, predicted ionospheric delays are equal to the previous estimated ionospheric delays; in the linear fitting model, however, previous estimated ionospheric delays within a sliding time window are used to fit a linear function, and predicted ionospheric delays are extrapolated using this function. In this study, the time span between a predicted and the latest estimated ionospheric delay is named as the latency of this predicted delay. This latency can be caused by data gaps, for example. The prediction error at an epoch is quantified by differencing the predicted and estimated ionospheric delays at this epoch. Furthermore, the prediction error is increased when the elevation angle is smaller and the latency is longer, and the increasing rate depends on the ionosphere condition. Therefore, an elevation-dependent and a latency-dependent weighting on the predicted ionospheric delays are required, such as

$$W(E) = \begin{cases} 1.0 & 30^\circ \leqslant E \leqslant 90^\circ \\ 2\sin E & 7^\circ < E < 30^\circ \end{cases} \tag{3.18}$$

and

$$W(\tau) = \begin{cases} 1.0 & \tau < 30\,\mathrm{s} \\ \tan\left(\dfrac{\pi}{4} \cdot \dfrac{30}{\tau}\right) & \tau \geqslant 30\,\mathrm{s} \end{cases} \tag{3.19}$$

where E denotes the elevation angle in degrees; τ here denotes the latency in seconds and the "30 s" will be illustrated in Section 6.2.3.

3.4.2 Rapidly retrieve integer ambiguities

Integer ambiguities can be rapidly retrieved by applying the precisely predicted ionospheric delays after a re-convergence occurs. This is achieved in two steps. First, at a particular epoch where the ambiguity-fixed solution has been lost, wide-lane measurements are formed using Equation 3.16 and are corrected with the known satellite products, the latest ZTD estimate, and the predicted ionospheric delays. If the latency is smaller than a few minutes, the errors caused by FCBs, satellite products and atmospheric delays can be canceled out or mostly mitigated by the counterparts in the predicted ionospheric delays (Dai et al. 2003; Kashani et al. 2007). Note that unmodeled errors are not easy to predict and are thereby supposed to be sufficiently small in this study. Finally, we can obtain

$$L_w^{kl} + ct^{kl} - \breve{I}_w^{kl} = \rho_i^{kl} + \lambda_w N_{wi}^{kl} + \zeta_{wi}^{kl} \tag{3.20}$$

where $\breve{I}_w^{kl}$ is the predicted ionospheric delay; ζ_{wi}^{kl} contains the unmodeled errors and the prediction error of ionospheric delays, and it actually quantifies the precision of Equation 3.20; only the positions and ambiguities are unknown. With the constraint from ionosphere-free pseudorange measurements, wide-lane ambiguity N_{wi}^{kl} can be resolved with Equation 3.20 if ζ_{wi}^{kl} is small enough (e.g. $< \dfrac{1}{4}\lambda_w$). In terms of Equation 3.14, thanks to the relatively long wavelength for wide-lane ambiguities, ionosphere-free pseudorange measurements can normally sufficiently shrink the search space to only a few integer candidates (Teunissen 1996, 1997), thereby improving the search efficiency and accelerating the identification of integer ambiguities.

Second, at this epoch, once the wide-lane ambiguity is successfully resolved, Equation 3.20 becomes a precise unambiguous measurement, namely

$$L_w^{kl} + ct^{kl} - \breve{I}_w^{kl} - \lambda_w N_{wi}^{kl} = \rho_i^{kl} + \zeta_{wi}^{kl} \tag{3.21}$$

In this study, it is Equation 3.21, rather than pseudorange measurements, that is introduced into the normal equation of PPP and thus constrains the integer identification of narrow-lane ambiguities during rapid re-convergences. In terms of Equation 3.14, if the magnitude of ζ_{wi}^{kl} is far smaller than a few centimeters, applying Equation 3.21 can considerably shrink the search space for narrow-lane ambiguities to a few integer candidates (Teunissen 1996, 1997). As a result, narrow-lane ambiguity resolution can be accelerated. Note that the prediction error of ionospheric delays dominates ζ_{wi}^{kl} if the latency is long. An imprecisely predicted ionospheric delay will weaken the constraint by Equation 3.21, possibly failing a rapid re-convergence.

Finally, it is worth emphasizing that both rapid resolutions above do not rely on satellite geometry changes, but on the sufficient shrink of the search space for integer candidates. Such shrinks are achieved by applying ionosphere-free pseudorange and ionosphere-corrected unambiguous wide-lane measurements which are precise enough relative to the wide-lane and narrow-lane wavelengths, respectively. Hence, float ambiguity estimates are close to correct integers and these integers can then be relatively easily identified, even though only one epoch of measurements are used.

3.4.3 Remarks on the method implementation

From the method description above, the prerequisite is how to precisely predict ionospheric delays, which depends on three aspects:

- Temporal properties of all errors in the ionospheric delay estimate according to Equation 3.17. Although the true ionospheric delay dominates its temporal variation, other errors including clock predictions and multipath effects should also be carefully regarded;
- Predicting strategy. Currently, it is not easy to precisely predict the ionosphere condition over a long time due to its complicated relationships with the geomagnetic field and the solar activity, especially during an ionospheric storm (e.g. van Barneveld et al. 2009). For example, sudden ionospheric disturbances and scintillations may occur during high ionosphere activities in polar and equatorial regions (Basu et al. 2002). As a result, temporal ionospheric irregularities cannot be precisely quantified beforehand in real-time applications. In this case, only the linear trend of the ionosphere change can usually be quantified with a relatively high confidence level (Dai et al. 2003). However, we should keep in mind that the residual variations can sometimes be very large and thus fail the precise prediction of ionospheric delays;
- Model consistency between the ionospheric delay estimation with Equation 3.17 and the wide-lane ambiguity resolution with Equation 3.20. Note that both models are derived from Equation 3.16. In this manner, their common biases can naturally cancel out without impairing the integer ambiguities, hence explaining why it is not the biases assimilated into the estimated ionospheric delays, but only their prediction errors, that are cared about in my method.

3.5 Comparison between rapid re-convergence methods

The two methods in Section 3.3 and 3.4 are used to improve real-time PPP during re-convergences based on the high temporal correlation of atmospheric delays and the negligible variation of hardware biases within a short period of up to a few minutes. There are five key differences between them that need to be highlighted:

- Banville and Langley (2009) repair cycle slips on L1 with the geometry-free measurements after the wide-lane cycle-slip repair. The wavelength of such L1-related cycle slips is only about 5.4 cm. Nonetheless, my method resolves integer ambiguities on L1 with the ionosphere-free measurements after wide-lane ambiguity resolution. The wavelength of these L1-related ambiguities is about 11 cm, approximately doubling the counterpart in the method by Banville and Langley (2009). In theory, the integer resolution for longer-wavelength ambiguities should be relatively easier.
- Banville and Langley (2009) do not need to estimate positions along with L1-related cycle slips. This avoids the high correlation between the ambiguity and position parameters in the estimation. Comparatively, my method has to simultaneously estimate the L1-related ambiguity and position parameters. They are decorrelated with the tight constraints imposed by ionosphere-corrected unambiguous wide-lane measurements.
- Banville and Langley (2009) simply presume that atmospheric delays totally cancel when differencing is performed over two epochs with a gap of less than a few minutes. Atmospheric delays are not estimated and hence the success rate of cycle-slip repair decreases when the gap is increased. Likewise, my method suffers from the degraded accuracy of predicted ionospheric delays when the time gap is increased. However, because ionospheric delays are estimated in my method, they can be potentially precisely modeled and predicted for a relatively longer period. In this way, the mitigation of ionospheric delays is somewhat controllable in my method and the mitigation efficiency can potentially outperform that of Banville and Langley (2009).
- Banville and Langley (2009) repair cycle slips to keep the continuousness of undifferenced carrier-phase measurements, and hence the convergence of ambiguity-float PPP is not interrupted by cycle slips. In this manner, a possible re-convergence can be avoided. On the contrary, my method rapidly resolves ambiguities during re-convergences in order to keep ambiguity-fixed solutions. In this case, users do not need to wait for a long period before they can again achieve ambiguity-fixed solutions.
- Banville and Langley (2009) do not need a number of epochs of measurements to repair cycle slips. Normally, only two epochs are used to repair the cycle slips between them. Conversely, a rapid re-convergence in my method is only possible when its previous solution is ambiguity-fixed. This means that the first ambiguity-fixed solutions have to be achieved before my method can be applied.

Finally, it should be noted that the method by Banville and Langley (2009) can complement my method. As demonstrated above, the first ambiguity-fixed solution is the prerequisite of my method. This solution cannot be achieved until a sufficiently long period of continuous carrier-phase measurements are guaranteed. In this case, the method by Banville and Langley (2009) can be used to keep the carrier-phase continuousness before the first ambiguity-fixed solution is achieved.

3.6 A strategy for accelerating the first convergence

As discussed in Section 3.4, re-convergences can be significantly accelerated by applying ionospheric delays precisely predicted by users themselves. We can imagine that the convergences, including the first one, can be significantly accelerated if these ionospheric delays are provided for users by a service provider with a precise ionosphere model. Note that this model should generate ionospheric delays at an accuracy of less than a few centimeters, i.e. $\leq$0.3 TECU for the L1 frequency. This section thus first introduces the advancement of current real-time ionosphere products, and then addresses a strategy for rapid convergences based on interpolated ionospheric delays from a dense network of reference stations.

3.6.1 Real-time ionosphere products

Precise ionosphere imaging in real time is a challenging issue in the Earth ionosphere community (Bust and Mitchell 2008). The ionosphere is characterized by a significant number of ionized neutral atoms, hence leading to a mixture of free electrons and ions. The ionization level is governed by solar extreme ultraviolet radiation and particle precipitation. Moreover, the ionosphere is embedded within the Earth's magnetic field and hence is constrained by the interactions of the ionized particles with the magnetic field. Consequently, ionosphere scintillations, large-scale TEC gradients and irregularities frequently occur, especially in low-latitude regions and during ionosphere storms (Skone 2000). Despite the complexity of the ionosphere physics, the most important quantity among all physical parameters is the electron density (Bust and Mitchell 2008). Ionosphere imaging of the electron density provides snapshots of the global ionosphere structure and its temporal evolution. Ionosphere imaging relates to using integrated measurements of electron density, known as TEC measurements, in order to generate 2-, 3- or 4-dimensional maps of electron density. Such imaging is extremely important because the electron density governs all effects on radio signals. Hence, in the following, current methods for real-time ionosphere imaging and their respective accuracy are briefly introduced.

A Klobuchar model

A straightforward method for the real-time mitigation of ionospheric delays is the Klobuchar model (Klobuchar 1986) which has been included in the GPS broadcast navigation message. The coefficients of this model are daily updated. However, only 50% of TEC can be eliminated by this model, which is far from sufficient for assisting wide-lane or narrow-lane ambiguity resolution.

B Ionosphere grid

An ionosphere grid is a thin shell at a specific height of 350–450 km above the Earth's surface. This shell is sampled on a regularly spaced grid along latitude and longitude. Vertical TEC at the grid points are estimated using GPS measurements from a network of reference stations. Users then interpolate their required slant TEC based on this grid model with a mapping function (El-Arini et al. 1995). However, an ionosphere grid has two defects (Liu 2003): On the one hand, a specific height for the ionosphere grid is presumed, which is only an approximation of the reality and is not physically true; on the other hand, a grid model is 2-dimensional and hence it cannot depict the vertical profile of the ionosphere structure. The global ionosphere maps by the IGS are grid-based, and currently the accuracy for the rapid products is between 2 and 9 TECU with

a latency of below 24 hours (see http://igscb.jpl.nasa.gov/components/prods.html). WAAS and EGNOS employ regional grids to quantify ionospheric delays, but the real-time accuracy can be up to 55 cm (∼3 TECU) (e.g. Jensen et al. 2007). Due to these poor accuracies, some authors are still trying to improve the ionosphere grid model (e.g. Yuan et al. 2008).

C Ionosphere tomography

An ionosphere tomography outperforms an ionosphere grid by its imaging of the ionosphere's vertical profile. Hence, an ionosphere tomography is a 3-dimensional model. It is constructed by a set of spherical harmonic functions and empirical orthogonal functions. The spherical harmonic functions describe the horizontal ionospheric characteristics whereas the empirical orthogonal functions depict the vertical ionosphere properties (Liu 2003; Bust and Mitchell 2008). Hernández-Pajares et al. (1999) reported that real-time tomography can provide an accuracy of better than 1 TECU for double-difference slant TEC based on a sparse network of up to 1300-kilometer inter-station distances under an active ionosphere condition. However, this conclusion has not been confirmed with extensive tests. Moreover, Liu and Gao (2004) assessed 5-minute TEC predictions over a regional reference network and achieved an accuracy of about 2.8 TECU in the vertical direction.

3.6.2 Accelerating convergences with a dense network

Considering the accuracy level of current real-time ionosphere products, unfortunately, it is still quite difficult to interpolate sufficiently precise ionospheric delays based on a quite sparse reference network at scales of many hundred kilometers. Nonetheless, if a dense network of reference stations at scales of several tens of kilometers is available, ionospheric delays can be estimated at the reference stations and then interpolated for single users to assist rapid convergences. In this case, the first ambiguity-fixed solutions can also be rapidly achieved.

Interpolated ionospheric delays are more reliable than those estimated and predicted by users themselves. As discussed in Section 3.4, the prerequisite for a rapid re-convergence is that the previous solution is correctly ambiguity-fixed. An incorrect ambiguity-fixed solution will fail the subsequent rapid re-convergences. Due to the precisely known positions and the good observation environments at reference stations, the generation of ionospheric delays becomes relatively easier and more reliable than that by users themselves. Normally, this generation is continuous and is independent of the users. Hence, users do not have to worry too much about the quality of interpolated ionospheric delays.

However, the deficiency of interpolated ionospheric delays is also obvious, i.e. a dense network of reference stations have to be used. This augmentation will significantly devalue the most attractive advantage of PPP, i.e. no need of any nearby reference stations. Moreover, even if such dense networks are available, the foremost question is then whether this augmented PPP can outperform the NRTK which has been well established in many areas.

Therefore, accelerating the first convergence to the ambiguity-fixed solution based on a dense network is feasible in theory, but its value in practice should be carefully assessed.

3.7 Summary

This chapter reviews the up-to-date attempts to achieve rapid convergences in real-time PPP. It is shown that these attempts are not sufficiently effective in speeding up convergences. On the other hand, in order to rapidly re-converge to ambiguity-fixed solutions, this thesis originally develops a novel method in which ionospheric delays estimated at previous ambiguity-fixed epochs are precisely predicted to the succeeding epochs in order to significantly accelerate ambiguity resolution in case of a re-convergence. Finally, a strategy for achieving the first ambiguity-fixed solution is suggested in which a dense network of reference stations is required. Chapter 6 will present empirical results to assess these methods for the rapid convergences to ambiguity-fixed solutions.

Chapter 4

PANDA Software

4.1 Introduction

PANDA (Positioning And Navigation Data Analyst) software was originally developed at Wuhan University in China (Liu and Ge 2003). It is a versatile tool for the scientific analysis of GPS positioning and navigation data, and currently serves as a fundamental platform for scientific studies in China. The University of Nottingham signed an agreement with Wuhan University for a free version of the Unix-based PANDA software package in 2007. This software package is capable of simultaneously processing various types of measurements from GNSS, SLR, KBR (K-Band Ranging) (Kang et al. 2003), star trackers and accelerometers in order to estimate ground station coordinates, ZTDs, ERPs (Earth Rotation Parameters) and orbits for GNSS satellites, LEOs and GEOs (Geosynchronous Earth Orbiters) (Geng et al. 2006; Li et al. 2008; Shi et al. 2006, 2008b).

Since 2003, PANDA software has been contributing to the Chinese GNSS research and applications. For example, it was extensively used in two key National High-Tech Research and Development Programs of China, i.e. Real-Time National PPP Service for Decimeter Positioning Accuracy (Geng et al. 2007b) and Near Real-Time Precise Orbit Determination of LEOs (Geng et al. 2007a). On the Wenchuan earthquake in 2008, the PANDA software generated one of the most excellent 1-Hz position time series with near-field GPS measurements (Shi et al. 2010).

The PANDA software is also used by a number of international renowned research institutes, such as DEOS (Delft–Institute of Earth-Oriented Space Research), NCTU (National Chiao Tung University) and IESSG (Insitute of Engineering Surveying and Space Geodesy). DEOS used PANDA software to determine precise orbits of CHAMP (CHAllenging Minisatellite Payload) and GRACE (GRAvity Climate Experiment) satellites in order to recover the time-varying Earth gravity (Liu et al. 2010). NCTU used PANDA software to determine the precise orbits of COSMIC (Constellation Observing System for Meteorology Ionosphere and Climate) satellites in order to validate their own results which were based on Bernese GPS software 5.0 (Dach et al. 2007; Hwang et al. 2009). IESSG used PANDA software for the research of rapid integer ambiguity resolution at a single receiver, and this thesis is mainly supported by this software (Geng et al. 2009).

This chapter first briefly exhibits the overall structure of PANDA software, and then details my adaptation and development of PANDA software. Note that the algorithm design and program development are also important contributions of this thesis. Finally, two software

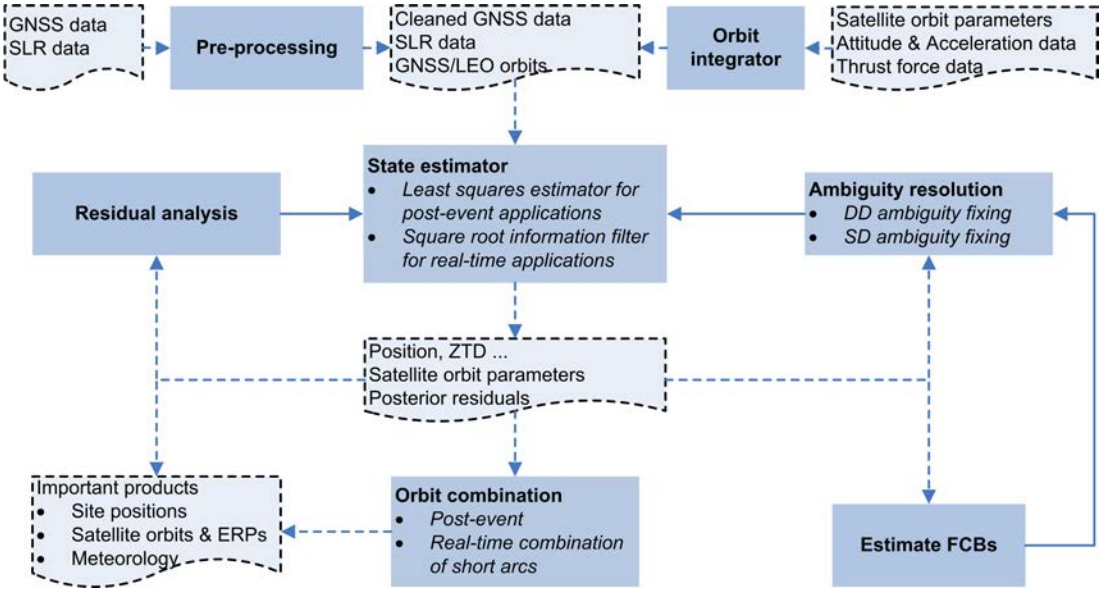

Figure 4.1: Brief structure of the PANDA software. The solid arrows denote processing sequences and the dashed arrows denote input/output. The squares represent the data processing modules while others represent the data and results (adapted based on Shi et al. (2008b))

suites, i.e. post-processing PPP and real-time PPP, are schematically introduced.

4.2 Software structure

Figure 4.1 describes the overall structure of the PANDA software. Its core modules are the orbit integrator and the state estimator. The orbit integrator is in charge of generating dynamic orbits based on the orbit parameters and force models, whereas the state estimator is responsible for all measurement models and statistical estimations, such as the least squares adjustment for post-processing tasks and the square root information filter for real-time applications (Bierman 1977).

Double-difference ambiguity resolution is performed directly using undifferenced ambiguity estimates generated by PPP (Ge et al. 2005a). Hence, the high flexibility and efficiency of PPP are exploited, but the benefits from ambiguity resolution are still achieved. Ge et al. (2005a) developed a new strategy where ambiguities are pre-eliminated once their last pertinent carrier-phase measurements are introduced into the normal equation, but ambiguity resolution is still achievable. This strategy can significantly improve the processing efficiency of a huge-network solution (Ge et al. 2006). Moreover, post-processing ambiguity resolution at a single receiver is also applied in the PANDA software package (Ge et al. 2008).

For real-time data processing, a new data screening method was developed in the PANDA software specifically for the square root information filter (Shi et al. 2008a). In this method, posterior residual vectors which are a byproduct of the filter are used to detect cycle slips or blunders. A sensitivity vector of each posterior residual with respect to cycle slips and blunders at a particular epoch can also be computed to assess the correlations between contaminated measurements and residuals. According to a quantitative correlation analysis, cycle slips and blunders can be identified and estimated in the filter to mitigate their detrimental impacts on navigation solutions. Since the algorithm takes the correlations between posterior residuals into

account, multiple cycle slips and blunders at an epoch can be effectively and reliably identified.

In addition, raw GPS measurements are pre-processed station by station based on an enhanced automatic editing strategy (Blewitt 1990). To detect remaining cycle slips and bad measurements, raw measurements are further cleaned by analyzing posterior residuals derived from the estimation. Thus least-squares estimation and residual analysis need to be iteratively carried out until neither cycle slips nor bad measurements can be identified.

Finally, the products by the PANDA software include post-processing and real-time ones. The post-processing products are mainly used for high-precision applications in scientific studies, such as crustal deformation, orbit determination for the Earth gravity recovery, meteorology and ERP time series analysis. The real-time products deliver kinematic positions, near real-time ZTDs and real-time GPS satellite orbits and clocks.

4.3 Software adaptation and development for this thesis

Since September of 2007, I have based my PhD study on the PANDA software and significantly improved it for my research. These improvements mainly include:

- Fixing software bugs, such as the filter divergence due to the incorrect understanding of the theory by Bierman (1977), and the UT1-UTC error;
- Enhancing software capabilities. For example, I applied the IERS (International Earth Rotation and Reference Systems Service) 2003 conventions (McCarthy and Petit 2004), the horizontal troposphere gradients (Bar-Sever et al. 1998), GPT/GMF (Global Pressure/Temperature & Global Mapping Function) (Boehm et al. 2006a, 2007) and VMF1 (Vienna Mapping Function 1) (Boehm et al. 2006b, 2009; Kouba 2008). Furthermore, I implemented piece-wise static PPP with continuous ambiguity and ZTD estimates for sub-daily crustal deformation monitoring (Melbourne et al. 2002; Teferle et al. 2008) and satellite clock determination based on the epoch-differencing for rapid high-rate clock products in real time (Ge et al. 2010);
- Improving ambiguity searching. Prior to the ambiguity search with the LAMBDA method, candidate ambiguities have to be carefully selected and permutated in order to maximize the success rate of ambiguity fixing. I select candidate ambiguities according to the fixing probability computed by Equation 2.41 and permutate them according to satellite elevations. Partial fixing of ambiguities is also implemented (Dai et al. 2007);
- Implementing the IRC-based method by Laurichesse et al. (2009c). IRCs are estimated by first fixing ambiguities to integers in a network solution (refer to Section 2.2.3);
- Implementing real-time ambiguity resolution at a single receiver. Narrow-lane FCBs are estimated and ambiguity resolution is performed in real time (refer to Section 2.4.3) (Geng et al. 2010d);
- Developing and implementing rapid re-convergences to ambiguity-fixed solutions by precisely predicting ionospheric delays. Two filters are embedded in this module: One is for wide-lane ambiguity resolution based on wide-lane carrier-phase measurements and the other is for narrow-lane ambiguity resolution based on ionosphere-free measurements (refer to Section 3.4) (Geng 2009).
- Developing and implementing rapid convergences with interpolated ionospheric delays from a dense network of reference stations. A dedicated module is designed and implemented

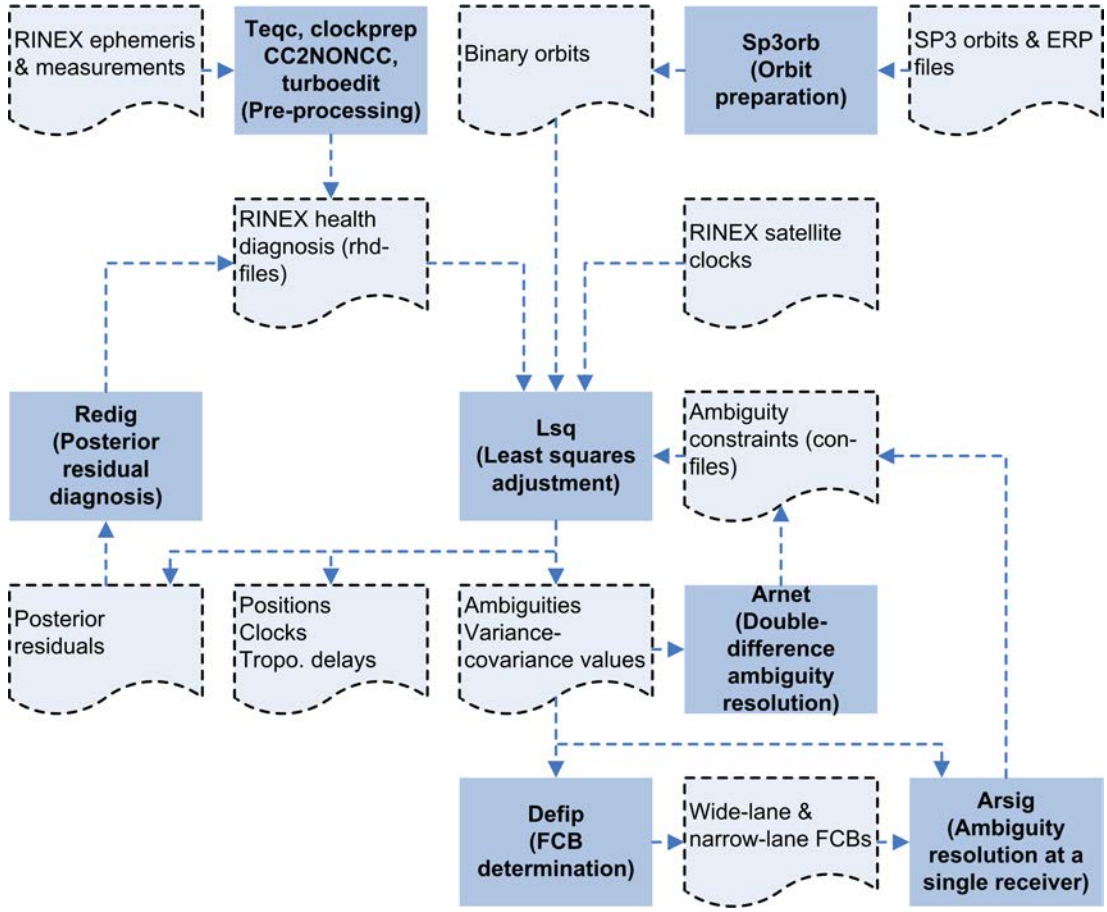

Figure 4.2: Structure of the post-processing PPP suite. The squares contain the names of the data processing modules while others list the data and results

in order to estimate and interpolate atmospheric delays at static or mobile receivers (refer to Section 3.4.2) (Geng et al. 2010a).

4.4 Post-processing PPP suite

This section focuses on the structure of post-processing PPP suite in the PANDA software and the data processing procedure for post-processing PPP.

4.4.1 Structure description

Figure 4.2 illustrates the structure of the post-processing PPP suite of the PANDA software. This figure is actually composed of only processing modules and data files. The processing modules include

- Pre-processing. This module includes the software packages **teqc** (translation, editing, and quality check) developed by UNAVCO (University NAVSTAR Consortium) (Estey and Meertens 1999), **clockprep** developed by Prof Freymueller at the University of Alaska Fairbanks, **cc2noncc** developed by Dr Ray at the US National Geodetic Survey (NGS), and **turboedit** which is based on the pre-processing algorithms by Blewitt (1990). In the PANDA software, **teqc** is used for RINEX (Receiver INdependent EXchange) formatting in order to avoid software abnormality due to format bugs; **clockprep** is used to convert

RINEX observation files of receiver time into those of GPS time in order to avoid pseudo cycle slips detected by **turboedit**; **cc2noncc** is used to convert pseudorange measurements from a cross-correlation receiver to those that are compatible with the modern Y-codeless pseudorange tracking (Dach et al. 2007) in order to keep consistency between clock products and pseudorange measurements; finally, **turboedit** is used to identify bad measurements and cycle slips in a RINEX observation file.

- Orbit preparation. The module is solely based on **sp3orb** which transforms SP3 (NGS Standard Product – 3) orbit files into a self-defined binary format. In this manner, the PANDA software can efficiently access the precise orbit products. In addition, the reference frame is changed from an Earth-fixed system into an inertial system through the ERP files.
- Least squares adjustment. The module **lsq** is used to reduce raw measurements and estimate unknown parameters.
- Posterior residual diagnosis. The module **redig** is to analyze posterior measurement residuals derived from **lsq** in order to identify remaining cycle slips and bad measurements.
- Double-difference ambiguity resolution. The module **arnet** is used for network solutions where double-difference ambiguities are formed based on undifferenced ambiguity estimates and ambiguity resolution is then attempted.
- FCB determination. The module **defip** is used to estimate wide-lane and narrow-lane FCBs based on ambiguity estimates derived from network solutions.
- Ambiguity resolution at a single receiver. The module **arsig** is used to form single-difference ambiguities between satellites based on undifferenced ambiguity estimates and then apply FCB products in order to recover the integer properties of these single-difference ambiguities.

Moreover, the data files include

- Input data. RINEX ephemerides and measurements, SP3 orbits and ERP files, and RINEX satellite clocks. Broadcast ephemerides are used by **turboedit**. SP3 orbits, RINEX clocks and ERP files can be freely obtained from the IGS.
- Binary orbits. Intermediate results which are generated by **sp3orb**.
- RINEX health diagnosis files. Each RINEX file corresponds to a health diagnosis file recording the locations of problematic measurements. It is initially generated by **turboedit** and subsequently updated by **redig**. RINEX health diagnosis files should accompany raw RINEX measurements as input files to **lsq**.
- Posterior residuals. These are generated by **lsq** and then input to **redig**. RINEX health diagnosis files are updated according to the analysis on these residuals.
- Positions, clocks and tropospheric delays. These are the output of **lsq**. Positions can be daily, sub-daily or epoch-wise estimates. Satellite clocks can also be estimated in a network solution by **lsq**. Tropospheric delays include ZTDs and horizontal gradients.
- Ambiguities and their optional variance-covariance statistics. These are generated by **lsq** and are the input of ambiguity resolution. If the variance-covariance statistics are available, ambiguity search by the LAMBDA method can be performed.
- Wide-lane and narrow-lane FCBs. These are estimated in **defip**. Wide-lane FCBs are daily estimated whereas narrow-lane FCBs can be estimated every 15 minutes or within each satellite-pair pass over a regional network.
- Ambiguity constraints. Double-difference and single-difference integer constraints. These files are the output of ambiguity resolution. They record the combinations of four or two undifferenced ambiguities. These combinations form integer constraints which are

subsequently imposed on the normal equation of **lsq** in order to achieve ambiguity-fixed solutions.

4.4.2 Processing procedure

This section addresses the processing procedures for post-processing PPP and ambiguity resolution at a single receiver. The satellite clock determination and double-difference ambiguity resolution are ignored for the brevity of this thesis.

A Post-processing PPP

Post-processing PPP in the PANDA software mainly relies on **lsq** and **redig**. Specifically, the procedure for a post-processing ambiguity-float PPP is divided into four steps, namely

1. Build a processing environment. All raw measurements should be put in an independent folder and a work folder has to be created for each project. Afterwards, a number of table files have to be copied into this work folder, mainly including antenna phase center offsets and variations, planetary ephemerides, leap seconds, coefficients for the ocean tide loading model, P1-C1 corrections and satellite states. Moreover, ERP files and satellite clocks need to be copied into the work folder. SP3 orbits can then be transformed into a binary format.
2. Pre-processing. **teqc** is first used to check the format of raw measurements. **clockprep** is then applied to all RINEX measurements. **cc2noncc** should be applied to only cross-correlation receivers and receivers without P1 measurements. Hence, such receivers must be identified before **cc2noncc** is run. Finally, **turboedit** is used to generate RINEX health diagnosis files.
3. Estimation. **lsq** is run at this step. Unknown parameters are estimated and posterior residuals are generated.
4. Residual editing. **redig** is applied to posterior residuals. Once new bad measurements or new cycle slips are identified, the third step has to be run again. Otherwise, final results can be collected.

B Ambiguity resolution at a single receiver

Ambiguity resolution at a single receiver is performed by running **defip** and **arsig**. The processing procedure is

1. A network solution where FCBs are estimated.
   (a) Ambiguity-float PPP for a network of reference stations (refer to Section A).
   (b) Estimate FCBs. **defip** is applied to all undifferenced ambiguity estimates generated in the network solution. We can ultimately obtain wide-lane and narrow-lane FCB estimates.
2. Resolve ambiguities at a single receiver by applying FCBs.
   (a) Ambiguity-float PPP for a single receiver (refer to Section A).
   (b) Ambiguity resolution. **arsig** employs FCBs to retrieve the integer properties of single-difference ambiguities between satellites at a single receiver. Ambiguity resolution can then be attempted.

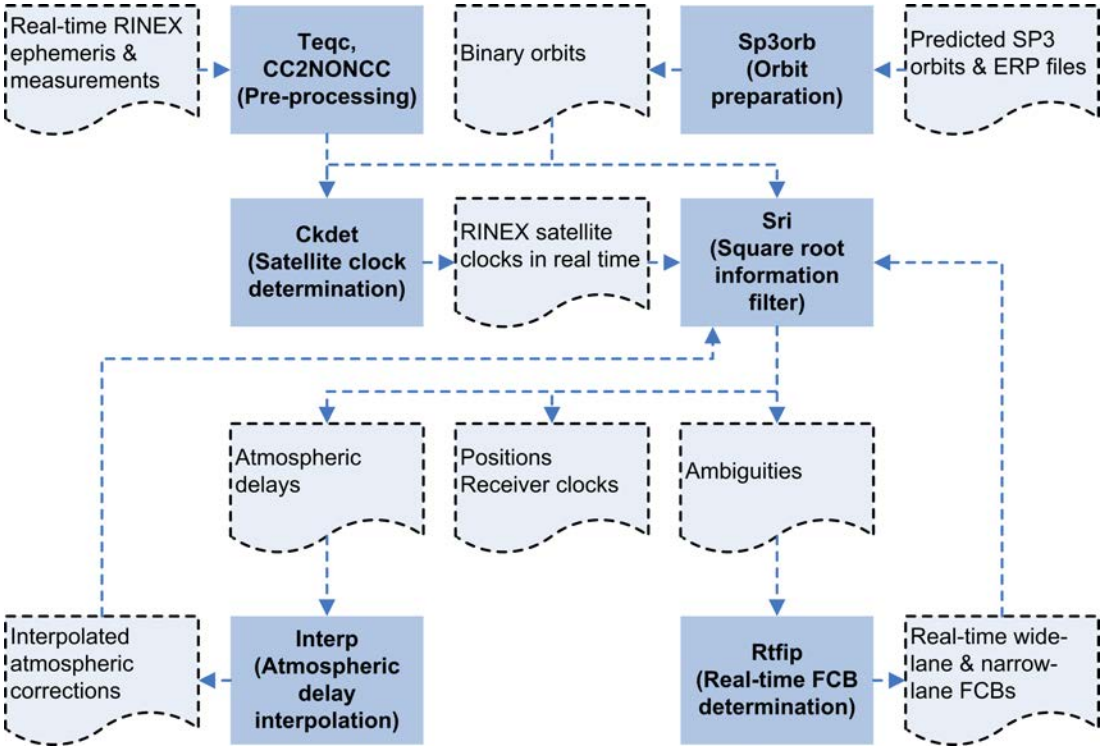

Figure 4.3: Structure of the real-time PPP suite. Meaning of symbols refer to Figure 4.2

(c) PPP by applying integer constraints. **lsq** is run again and integer-constraint files will be used automatically. Finally, ambiguity-fixed solutions can be achieved.

4.5 Real-time PPP suite

This section focuses on the structure of the real-time PPP suite in the PANDA software and the data processing procedure for real-time PPP.

4.5.1 Structure description

Figure 4.3 illustrates the structure of the real-time PPP suite of the PANDA software. This figure is also composed of only processing modules and data files. The processing modules include

- Pre-processing. Refer to Section 4.4.1. **teqc** and **cc2noncc** cannot be used in real time, but adapting them into real-time modules is not a complicated task. **turboedit** cannot be used and a real-time data screening is embedded into the filter **sri** (see Section 4.2). Finally, **clockprep** is not applied because it is not a real-time module. Fortunately, most receivers do not need this processing module.
- Orbit preparation. Refer to Section 4.4.1. Because only predicted satellite orbits are used, according to Table 1.1, we have to update the orbits and ERPs once newer ones are released by the IGS.
- Satellite clock determination. **ckdet** is based on epoch-differenced data processing, but undifferenced satellite clocks are generated at each epoch. Its efficiency has been illustrated by Ge et al. (2010).

- Square root information filter. This real-time filter is characterized by its high numerical stability (Bierman 1977). Data screening and quality control in real time are embedded into this filter to identify bad measurements and cycle slips. Moreover, real-time ambiguity resolution is also applied to this filter (Geng et al. 2010d). Note that backward smoothing is not allowed in this filter.
- Real-time FCB determination. **rtfip** is used to estimate only narrow-lane FCBs at a given update rate based on undifferenced ambiguity estimates from a network solution. Note that wide-lane FCBs can be precisely predicted over 24 hours due to their high temporal stability (Ge et al. 2008; Geng et al. 2010d), and hence they are not estimated in **rtfip**.
- Interpolation of atmospheric delays. **interp** is used to interpolate ionospheric and tropospheric delays for a single receiver from its surrounding reference stations. These interpolated atmospheric delays contribute to accelerating convergences to ambiguity-fixed solutions (refer to Section 3.6).

Moreover, the data files include

- Input data, including RINEX ephemerides and measurements, predicted SP3 orbits and ERP files (refer to Section 4.4.1 and Table 1.1).
- Binary orbits. Refer to Section 4.4.1.
- Real-time satellite clocks. As demonstrated in Section 1.2.2, satellite clocks have to be estimated in real time. It is worth stressing that we should keep consistency between the predicted orbits and the clocks.
- Positions and receiver clocks. These are the output of **sri**.
- Atmospheric delays. Slant ionospheric delays and tropospheric delays. According to Section 3.4.1, slant ionospheric delays can be estimated with wide-lane measurements (Equation 3.17) after a successful wide-lane ambiguity resolution. In addition, slant tropospheric delays are computed with ZTD estimates and posterior carrier-phase residuals.
- Interpolated atmospheric corrections. These corrections are generated by **interp**. If slant atmospheric delays are available at some reference stations, interpolated atmospheric delays can then be computed at a user receiver located inside the coverage of these reference stations. Interpolation methods refer to Dai et al. (2004).
- Ambiguities. At reference stations, undifferenced ambiguity estimates can be output at an interval of a few minutes, for example, rather than every epoch. This can significantly reduce the computation burden of **sri**.
- Real-time wide-lane and narrow-lane FCBs. Wide-lane FCBs are presumed known whereas narrow-lane FCBs are generated by **rtfip**. Because narrow-lane FCBs are normally stable over a few tens of minutes, an update rate of a few minutes is usually sufficient. Real-time FCBs are then input to **sri** for ambiguity resolution.

4.5.2 Processing procedure

This section addresses the processing procedures for real-time PPP, real-time ambiguity resolution at a single receiver and rapid ambiguity resolution with interpolated atmospheric delays. Satellite clock determination in real time by **ckdet** is ignored for the brevity of this thesis.

A Real-time PPP

Real-time PPP in the PANDA software mainly relies on **sri**. Specifically, the procedure for a real-time PPP is

1. Build a processing environment (refer to Section 4.4.2).
2. Satellite clock determination. If real-time satellite clocks are not available, a network of reference stations has to be used to estimate epoch-wise clocks in a real-time manner.
3. Estimation. **sri** is run for this step. Briefly, raw measurements are preliminarily cleaned using the Melbourne-Wübbena and the geometry-free combination measurements. Undifferenced ionosphere-free measurements are then reduced and the filtering is started. Posterior residuals are analyzed to further clean the measurements. Estimates are output at every epoch. Furthermore, ambiguity resolution will be attempted if FCB products are available and rapid re-convergences are started once cycle slips occur.

B Real-time ambiguity resolution

Real-time ambiguity resolution at a single receiver is based on both **rtfip** and **sri**. The processing procedure is

1. A network solution where real-time FCBs are estimated.
   (a) Satellite clock determination. Refer to Section A.
   (b) Real-time FCB determination. Ambiguity estimates at all reference stations are input to **rtfip**. Wide-lane FCBs are presumed known and narrow-lane FCBs are estimated.
2. Single-receiver solution. Refer to Section A.

C Rapid ambiguity resolution with interpolated atmospheric delays

Dense network has to be used if precise atmospheric delays are required. The processing procedure of rapid ambiguity resolution with interpolated atmospheric delays is

1. Determination of satellite clocks and FCBs. Refer to Section A and B.
2. Determination of atmospheric delays at reference stations. By applying known satellite products, slant ionospheric delays are estimated after wide-lane ambiguity resolution and slant tropospheric delays are estimated after narrow-lane ambiguity resolution.
3. Interpolation of atmospheric delays. This is performed by **interp**. Slant ionospheric and tropospheric delays are separately interpolated for an interested position.
4. Single-receiver solution. Note that ZTD parameters are no longer required and **sri** does not need to predict ionospheric delays itself.

4.6 Summary

This chapter introduces the PANDA software used and developed in this thesis. The structure, characteristics and capabilities of this software are briefly addressed. Then my contributions to this software are detailed and highlighted. Afterwards, the two software suites for post-processing and real-time PPP are introduced by illustrating their functional modules and processing procedures. These can be recognized as a brief manual for the PPP modules of the PANDA software. Most results shown in the subsequent chapters 5, 6 and 7 on ambiguity resolution and rapid convergences are achieved with this software.

Chapter 5

Results on Ambiguity Resolutions

5.1 Introduction

Chapter 2 has introduced the methods recently developed for integer ambiguity resolution at a single receiver, i.e. the FCB- and IRC-based methods (Collins 2008; Ge et al. 2008; Laurichesse et al. 2009c). This thesis adopts the FCB-based method and develops four improvements, i.e. the derivation of undifferenced FCBs, one FCB per satellite-pair pass over a regional area, implementation of real-time ambiguity resolution and constraints from integer double-difference ambiguities, in the PANDA software. This chapter thus assesses the "one FCB estimate per satellite-pair pass" in post-processing PPP with sub-daily and epoch-wise GPS measurements. Three crucial issues, i.e. the rapidity of wide-lane ambiguity resolution, the temporal stabilization of narrow-lane FCBs and the performance of narrow-lane ambiguity resolution, are closely investigated in order to assess real-time ambiguity-fixed PPP. Constraints from integer double-difference ambiguities is highlighted with their contribution to improving position quality of ambiguity-fixed PPP. Finally, a comparison study between the FCB- and IRC-based methods ends this chapter.

5.2 FCB determination with a regional network

Wide-lane FCBs are normally quite stable over a few days or even a few months, whereas narrow-lane FCB estimates are not so stable and have to be re-computed at a sub-daily frequency. Gabor and Nerem (1999) estimated single-difference wide-lane FCBs for 305 days in 1997. They showed that 73% of wide-lane FCBs slightly drifted by less than 0.5 cycles per year whilst only 8% drifted by more than 1.75 cycles per year. One possible reason for this drift was the bias divergence due to hardware aging, which meant that biases between different observables were present and these biases were time-dependent. Ge et al. (2008) exhibited typically 14 days of wide-lane FCBs and showed that these agreed with each other to better than 0.05 cycles. On the other hand, Ge et al. (2008) estimated narrow-lane FCBs every 15 minutes and reported that over 90% of narrow-lane ambiguities could be successfully fixed to integers. These narrow-lane FCBs were based on a global network of reference stations. Hence, this section applies the innovation of "one FCB estimate per satellite-pair pass" in Section 2.4.2 in order to assess the stability of narrow-lane FCBs that are estimated with a regional network.

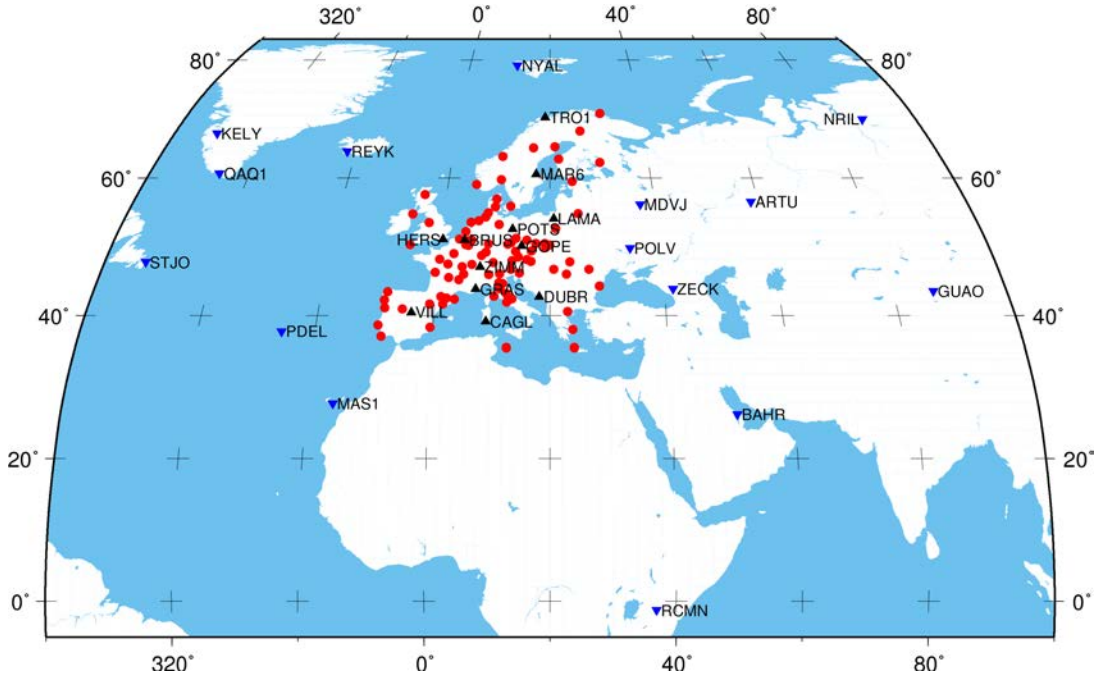

Figure 5.1: Distribution of stations used for static PPP. Red circles denote EPN stations used for the determination of FCBs and triangles denote IGS stations for testing ambiguity-fixed PPP. Black triangles denote stations inside the EPN and inverted blue triangles denote stations outside the EPN

5.2.1 Data and models

A regional network of about 80 stations from the EUREF (European Reference Frame) Permanent Network (EPN) (Figure 5.1) (Bruyninx et al. 2001) of which daily GPS measurements from day 245 to 251 in 2007 was used to estimate wide-lane and narrow-lane FCBs. The final satellite products, the ERPs and the DCBs provided by CODE (Dach et al. 2009) were used. The absolute antenna phase centers (Schmid et al. 2007), phase wind-up corrections (Wu et al. 1993) and station displacement corrections suggested in the IERS 2003 conventions (McCarthy and Petit 2004) were applied. The elevation cut-off angle was 7° and an elevation-dependent weighting strategy was applied to measurements at low elevations (Gendt et al. 2003). Receiver positions, receiver clocks, ZTDs, horizontal troposphere gradients and undifferenced ambiguities were estimated.

5.2.2 Wide-lane FCBs

Seven days' wide-lane FCBs for all satellites with respect to PRN01 (Pseudo-Random Noise) agree well to better than 0.06 cycles (3σ). If these wide-lane FCBs are applied to all EPN stations under a bias-rounding strategy with a round-off criterion of 0.2 cycles, the ambiguity fixing rate for each day ranges from 96% to 99% with an average of about 97.4%, hence verifying the high accuracy of these wide-lane FCB estimates.

5.2.3 Narrow-lane FCBs

In terms of Section 2.3.4, narrow-lane FCB estimates actually contain some unknown station-specific errors caused by the inaccurate modeling of tropospheric delays, etc. Discrepancies among these errors can thus be manifested for a global network with 24 hours of measurements,

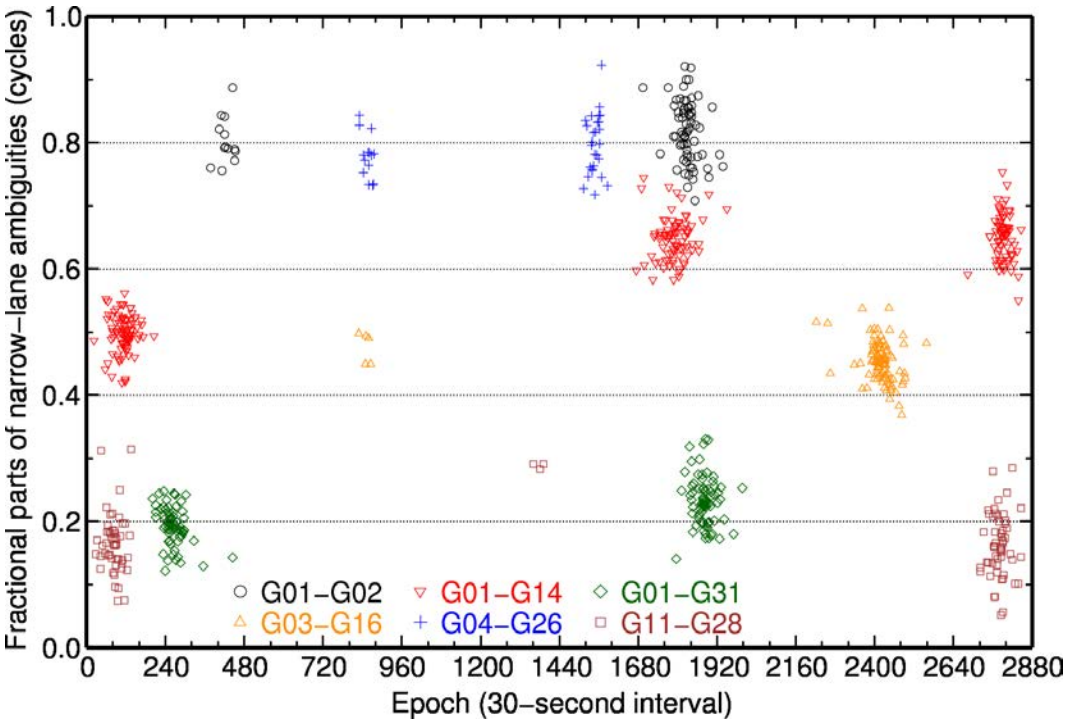

Figure 5.2: Fractional parts of all narrow-lane ambiguity estimates at all EPN stations on day 245. Each symbol denotes the fractional part of an ambiguity and each cluster of identical symbols corresponds to one pass of a satellite pair over the EPN. Note that each symbol is drawn at the central epoch of the ambiguity observation period. Only six representative satellite pairs are selected to avoid overlapping of different symbols and keep the figure clear to read

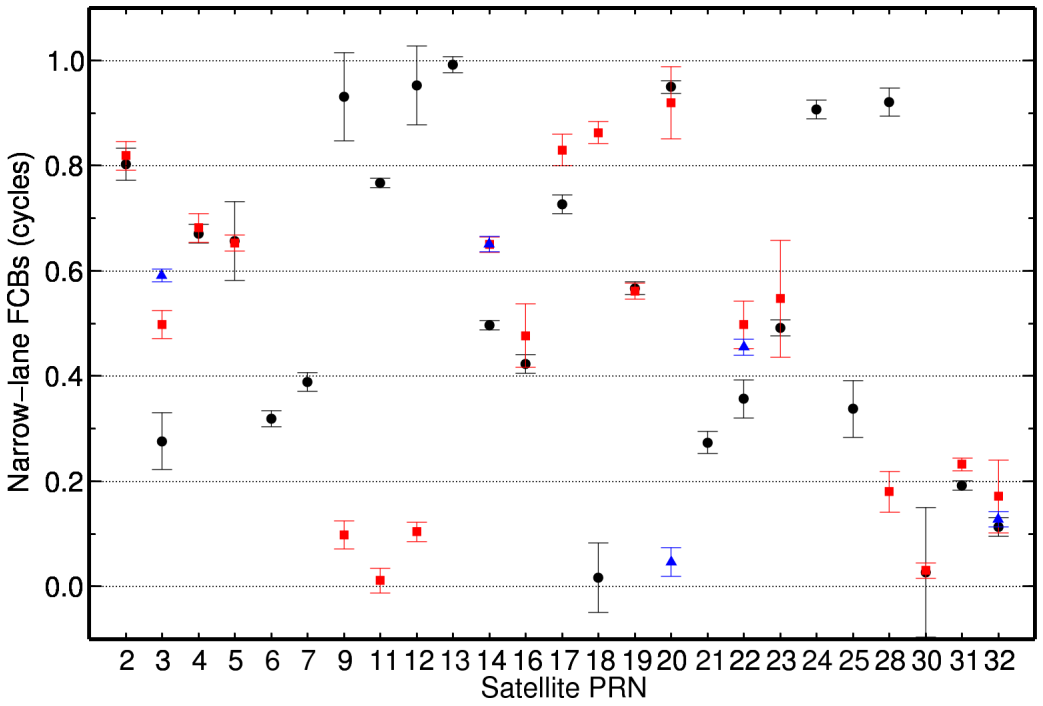

Figure 5.3: Narrow-lane FCB estimates for all satellites with respect to PRN01 over the EPN on day 245. Each estimate corresponds to one full pass over the EPN by a satellite pair. Solid black circles, red squares and blue triangles denote estimates for the first, second and third pass respectively. Error bars denote formal precisions of 3σ

thereby handicapping the precise determination of narrow-lane FCBs. However, for a regional network of stations among which the error correlation over time and space is relatively significant, narrow-lane FCB estimates might achieve good precisions even if these estimates are computed once per each satellite-pair pass over the regional network. Figure 5.2 shows the fractional parts of all narrow-lane ambiguities for six satellite pairs over 24 hours at all EPN stations on day 245. Each symbol denotes the fractional part of a narrow-lane ambiguity and each cluster of identical symbols corresponds to one pass of a satellite pair over the EPN. Within each pass, fractional parts change by less than 0.2 cycles, exhibiting a relatively high stability.

Moreover, Figure 5.3 shows the estimates and the formal precisions (3σ) of all narrow-lane FCBs with respect to satellite PRN01 on day 245. Each narrow-lane FCB estimate corresponds to one full pass of a satellite pair over the EPN. From Figure 5.3, it is apparent that estimates for the same satellite pair can differ significantly. Most formal precisions are less than 0.1 cycles. Considering the averaging over ambiguity fractional parts to estimate narrow-lane FCBs, these high formal precisions actually reflect the good stability of narrow-lane FCBs within each satellite-pair pass.

In addition, if these EPN-based narrow-lane FCBs are applied to the EPN stations to correct narrow-lane ambiguities, up to 97.1% of all residual fractional parts are within ± 0.15 cycles. These ambiguities can be reliably fixed to the nearest integers with the sequential bias rounding. Therefore, this fact further confirms the effectiveness of precisely estimating "one FCB estimate per satellite-pair pass" over a regional network.

Finally, if the 15-minute mean is applied for the narrow-lane FCB determination, the resulting formal precisions may be even smaller. However, much more narrow-lane FCB estimates will be generated and the FCB-dissemination burden is consequently increased. Hence, my innovation of "one FCB estimate per satellite-pair pass" excels in significantly reducing the number of narrow-lane FCB estimates.

5.3 Impact of ambiguity resolution on hourly PPP

Conventionally, it is a great challenge for hourly PPP to achieve a millimeter-level positioning accuracy. Ambiguity-float PPP can usually reach only sub-decimeter- to centimeter-level accuracy based on less than three hours of measurements (Ghoddousi-Fard and Dare 2006; Tétreault et al. 2005). Comparatively, static relative positioning with double-difference ambiguity resolution based on less than three hours of measurements is normally able to achieve sub-centimeter-level accuracy for the horizontal and about 2-centimeter accuracy for the vertical components on baselines of many tens to a few hundred kilometers (Creager and Maggio 1998; Eckl et al. 2001; Soler et al. 2006). In this thesis, it is expected that ambiguity resolution at a single receiver can significantly improve the positioning accuracy of hourly PPP, because PPP ambiguity resolution improved daily position estimates by 10.2% against the IGS weekly estimates (Ge et al. 2008). Note that the innovation of "one FCB estimate per satellite-pair pass" over a regional network is applied in this section.

5.3.1 Data, models and methods

In Figure 5.1, 27 test stations from the IGS network were used to perform hourly PPP for day 245 to 251 in 2007. Hence, 168 hourly solutions could be obtained for each station if there was

no large data loss. Solutions with measurements of less than 30 minutes or with less than five satellites for more than 30 minutes were removed as unreliable solutions. Among 27 stations, 12 were distributed evenly within the coverage of the EPN and were denoted as "inside-EPN" stations. Remaining 12 were scattered outside the EPN in roughly all directions and were denoted as "outside-EPN" stations. Note that FCB estimates were from Section 5.2 and all 27 stations were not involved in the FCB determination. Models adopted at test stations were the same as those at the EPN stations in Section 5.2.1, except for horizontal troposphere gradients which cannot be precisely estimated with only one hour of measurements. In order to assess the accuracy of hourly position and ZTD estimates, their daily estimates were used as truth benchmarks instead of the official EUREF estimates. In this manner, potential biases between my solutions and the EUREF ones can be avoided (Teferle et al. 2007).

Wide-lane ambiguity resolution followed the method of sequential bias rounding. Due to strong correlations among ambiguity estimates in hourly solutions, a search strategy based on the LAMBDA method was applied to perform narrow-lane ambiguity resolution. Moreover, GPS measurements at lower elevations were usually affected by higher noise levels and larger biases than those at higher elevations, and this can increase the likelihood of incorrect ambiguity resolution for low-elevation satellites. Hence, only the satellites at elevations of over 15° were used for ambiguity resolution. In addition, if a set of narrow-lane ambiguities cannot all be reliably fixed to integers, at most two of them could be excluded and the search was then repeated until the validation tests were passed, unless all possible integer candidates were rejected. The criterion for the ratio test is 3. Note that the acceptance test that was discussed in Section 2.5.2 often failed if Equation 2.46 was applied to this study, even when correct integers were found. This implies that the right side of Equation 2.46 might be too conservative. Hence, as a trade-off between maximizing the pass rate for ambiguity validation and minimizing the number of incorrectly fixed solutions, a criterion of 1.8, which was empirically determined in terms of all $\frac{\sigma^2_{\text{fixed}}}{\sigma^2_{\text{float}}}$ estimates derived from all solutions in this study, was used instead of the right side of Equation 2.46.

5.3.2 Performance of inside-EPN stations

For all inside-EPN stations, Table 5.1 shows the ambiguity fixing rates, the ratio values and the RMS (Root Mean Square) of all hourly position and ZTD estimates against the truth benchmarks. A fixing rate is the ratio between the number of fixed ambiguities and the number of all ambiguities during 7 days. A ratio value in this table is the mean of all ratio values in all ambiguity-fixed solutions.

From Table 5.1, the fixing rate for each station is larger than 96% and the mean fixing rate is larger than 98%. All ratio values are larger than 30 with an average of over 40 which is much larger than 3, i.e. the chosen criterion. Therefore, these statistics demonstrate that the EPN-based FCBs are effective for a reliable ambiguity resolution at the inside-EPN stations.

Moreover, Table 5.1 shows that the mean RMS is significantly reduced from 3.8, 1.5, 2.8 cm to 0.5, 0.5, 1.4 cm for the East, North and Up components respectively, with a mean reduction of 68.3% for the 3D position. The horizontal RMS statistics of all stations are at sub-centimeter level and most of them are smaller than 5 mm. The East RMS achieves the largest reduction of 86.7%. The Up RMS statistics of most stations are smaller than 1.5 cm with a mean reduction of 50.0%. This relatively smaller reduction, compared with the horizontal reduction, is associated

Table 5.1: Performance of hourly PPP ambiguity resolution at inside-EPN stations. Ambiguity fixing rates, ratio values, and RMS of the position and ZTD estimates in ambiguity-float and ambiguity-fixed hourly solutions against daily estimates are shown for all stations during 7 days

Station	Fixing rates	Ratio values	Ambiguity-float (cm)				Ambiguity-fixed (cm)			
			East	North	Up	ZTD	East	North	Up	ZTD
BRUS	98.4%	52.2	3.3	1.4	2.8	0.55	0.4	0.4	1.3	0.40
CAGL	96.2%	32.1	4.8	1.9	4.0	0.74	1.0	0.8	2.0	0.57
DUBR	98.2%	36.2	5.6	1.9	3.3	0.49	0.4	0.6	1.3	0.36
GOPE	97.1%	33.8	4.5	1.8	2.9	0.61	0.3	0.4	1.5	0.52
GRAS	98.9%	58.3	2.4	1.1	2.4	0.48	0.4	0.4	1.3	0.39
HERS	99.7%	61.4	4.1	1.3	2.4	0.49	0.3	0.4	1.2	0.35
LAMA	99.1%	40.1	3.8	1.5	2.6	0.56	0.7	0.6	1.4	0.46
MAR6	98.6%	32.9	3.3	1.6	2.3	0.49	0.7	0.7	1.5	0.42
POTS	99.0%	38.6	3.6	1.4	2.8	0.50	0.3	0.4	1.3	0.41
TRO1	98.4%	32.3	1.5	1.1	1.8	0.34	0.3	0.3	1.2	0.27
VILL	98.5%	33.5	4.1	1.5	3.4	0.70	0.4	0.5	1.5	0.49
ZIMM	98.8%	42.0	3.1	1.2	2.4	0.48	0.4	0.4	1.2	0.39
Mean	98.4%	41.1	3.8	1.5	2.8	0.54	0.5	0.5	1.4	0.42

with the relatively smaller correlation between the vertical component and the ambiguities (Blewitt 1989). In addition, the ZTD RMS is reduced by 22.2% on average after ambiguity resolution. From these statistics, it is demonstrated that ambiguity resolution at a single receiver significantly improves hourly position accuracy.

In order to analyze the efficiency of ambiguity resolution, integer ambiguities derived from daily data processing were used as the truth measure to identify the hourly solutions with incorrect ambiguity resolution. Hourly solutions without any ambiguities resolved were also identified. The percentages of these two types of solutions are 0.85% and 0.40%, respectively. These solutions may be failed due to the qualities of measurements and satellite products (e.g. severe multipath effect and satellite eclipse).

Table 5.2: Hourly solutions in which ambiguity resolution leads to degraded positioning accuracy. "Successful" denotes the number of Successful solutions, "Degraded" denotes the number of degraded solutions, "Mean" is the mean RMS increment and "Max" is the maximum RMS increment (cm)

Station	ZTD estimated				ZTD fixed			
	Successful	Degraded	Mean	Max	Successful	Degraded	Mean	Max
BRUS	166	1	2.7	2.7	166	0	0.0	0.0
CAGL	158	2	2.2	2.9	160	1	2.5	2.5
DUBR	158	1	1.5	1.5	160	1	2.5	2.5
GOPE	166	2	1.1	1.1	165	0	0.0	0.0
GRAS	156	1	1.3	1.3	158	0	0.0	0.0
HERS	168	0	0.0	0.0	168	0	0.0	0.0
LAMA	164	3	1.4	1.9	165	0	0.0	0.0
MAR6	154	1	1.3	1.3	153	1	1.6	1.6
POTS	160	1	1.6	1.6	163	0	0.0	0.0
TRO1	168	4	1.4	1.6	168	0	0.0	0.0
VILL	167	4	1.3	1.7	168	0	0.0	0.0
ZIMM	166	2	1.5	1.8	167	0	0.0	0.0
Total	1951	22	–	–	1961	3	–	–

In addition, there are a few solutions in which the position RMS statistics are enlarged, rather than reduced, after correct ambiguity resolution. These solutions are hereafter called degraded solutions. The 3D RMS increment may reach 3 cm at the inside-EPN stations. The percentage of degraded solutions in all successful ones is 1.13%. To investigate this issue, hourly PPP solutions with ZTDs fixed to precise estimates derived from daily PPP were also generated. Table 5.2 shows the number of successful and degraded solutions, the mean and maximum RMS increment when ZTDs are estimated or fixed for all inside-EPN stations. It can be found that all RMS increments are at centimeter level which is significant compared with the hourly position RMS shown in Table 5.1. Moreover, the percentage of degraded solutions in all successful ones is dramatically reduced to 0.15% if ZTDs are not estimated, but fixed to a priori precise values. This demonstrates that ZTD is a crucial factor affecting the occurrence of degraded solutions in hourly PPP. This will be further investigated in Section 5.4.5.

5.3.3 Performance of outside-EPN stations

For each outside-EPN station, Table 5.3 shows the distances to the nearest EPN stations which are denoted as "to-EPN" distances, ambiguity fixing rates, ratio values, and RMS of all hourly position estimates against the truth benchmarks. In Table 5.3, the outside-EPN stations are arranged according to their to-EPN distances, of which the average is approximately 2000 km.

Table 5.3 shows that the fixing rates at outside-EPN stations fall with the increase of their to-EPN distances. When these distances are less than 2000 km, almost all fixing rates are over 95%. When these distances increase up to 3000 km, the fixing rates are reduced to below 95% but still higher than 90%. However, when they are over 3000 km, the fixing rates fall to below 90%. This descent tendency is directly related to the reduced ambiguity fixing rates which are due to the unavailability of some narrow-lane FCBs at the outside-EPN stations. However,

Table 5.3: Performance of hourly PPP ambiguity resolution at outside-EPN stations. Distances to the nearest EPN stations, ambiguity fixing rates, ratio values, and RMS of the position estimates in ambiguity-float and ambiguity-fixed solutions against the daily estimates are shown for all stations during 7 days

Stations	Dist. (km)	Fixing rates	Ratio values	Ambiguity-float (cm)			Ambiguity-fixed (cm)		
				East	North	Up	East	North	Up
POLV	660.7	97.9%	21.6	4.0	1.9	3.0	0.4	0.5	1.7
MDVJ	769.9	93.5%	26.1	3.1	1.2	2.2	0.4	0.7	1.6
ZECK	1034.4	95.0%	14.7	5.3	1.9	4.5	0.7	1.0	2.5
NYAL	1100.6	97.0%	37.2	1.0	0.9	1.6	0.3	0.4	1.5
REYK	1208.4	97.0%	13.5	4.0	2.0	3.2	0.5	0.6	2.2
MAS1	1222.3	96.6%	19.9	5.4	1.4	4.6	0.5	0.6	2.5
PDEL	1421.6	98.5%	22.6	3.8	1.5	3.6	0.6	0.5	1.9
ARTU	1724.5	95.8%	20.8	3.7	2.0	3.2	0.5	0.6	1.6
NRIL	2116.4	93.7%	24.8	1.7	1.6	2.2	0.5	0.5	1.7
QAQ1	2368.2	93.4%	26.1	2.3	1.2	2.1	0.4	0.5	1.7
KELY	2554.2	94.5%	20.8	1.9	1.2	2.3	0.7	0.6	1.7
BAHR	2708.5	91.6%	17.3	4.5	1.3	4.7	0.9	0.6	2.5
STJO	3264.0	85.7%	22.5	3.8	1.9	3.1	0.8	0.8	2.1
GUAO	4116.3	84.3%	13.6	4.5	1.4	3.4	0.8	0.7	1.8
RCMN	4201.5	72.1%	21.9	3.7	1.1	3.1	0.7	0.7	2.4
Mean		92.4%	21.6	3.7	1.5	3.2	0.6	0.6	2.0

this tendency is not observed in the ratio values. It can be found that almost all ratio values are smaller than 30, with an average of about 20, which is almost half of that for the inside-EPN stations. This issue can be explained in terms of the degraded accuracies of EPN-based narrow-lane FCBs when they are applied to outside-EPN stations.

Furthermore, the improvement of positioning accuracy also slightly suffers from the accuracy degradation of narrow-lane FCBs. In Table 5.3, the mean position RMS for the East, North and Up components are significantly reduced from 3.7, 1.5, 3.2 cm in the ambiguity-float solutions to 0.6, 0.6, 2.0 cm in the ambiguity-fixed solutions, with a mean reduction of 57.9% for the 3D position which is roughly 10% smaller than that of Table 5.1. In comparison to the inside-EPN stations, the vertical RMS is affected more than the horizontal one by the accuracy degradation of narrow-lane FCBs. However, Table 5.3 still suggests that the EPN-based narrow-lane FCBs are sufficiently applicable to the outside-EPN stations even when their to-EPN distances are up to 4000 km.

In addition, Table 5.3 shows that the position RMS statistics in the ambiguity-fixed solutions stand at nearly the same level, despite their varying to-EPN distances. Considering the same narrow-lane FCBs used at these stations, this implies that the narrow-lane FCB accuracy does not rapidly deteriorate with the increased to-EPN distances. Therefore, it can be argued that narrow-lane FCBs should be quite stable within a region stretching several thousands of kilometers in both longitudinal and latitudinal directions.

Of particular interest is the question that over what regional extent narrow-lane FCBs are still sufficiently stable. This issue is related to the efficient determination of narrow-lane FCBs, and the positioning accuracy in ambiguity-fixed solutions. Clarifications may be made by investigating the relationship between the positioning accuracy in ambiguity-fixed solutions and the accuracy of narrow-lane FCB estimates.

5.3.4 Conclusions

The performance of hourly ambiguity-fixed PPP at the inside-EPN and outside-EPN stations demonstrates that narrow-lane FCBs can be accurately determined within each full pass of a satellite pair over a regional network. This study also demonstrates that ambiguity resolution at a single receiver can reduce the RMS of differences between hourly and daily position estimates to approximately 0.5 cm for the horizontal and about 1.5 cm for the vertical components even if only hourly measurements are used.

From the comparison between the inside-EPN and the outside-EPN stations, the accuracy of EPN-based narrow-lane FCBs is slightly degraded when they are applied to the outside-EPN stations. However, they are still sufficiently applicable to ambiguity resolution at the outside-EPN stations which are even up to 4000 km away, potentially showing a great advantage over current network-based GPS augmentation systems. The horizontal position RMS at the outside-EPN stations can still achieve the sub-centimeter level with significant improvement over ambiguity-float solutions. More importantly, it is demonstrated that narrow-lane FCBs are quite stable within a region stretching several thousands of kilometers in both longitudinal and latitudinal directions. This finding confirms that ambiguity resolution can be applied to a receiver which is outside an FCB-determination network, but within 4000 km.

5.4 Impact of observation period on ambiguity resolution

A static PPP solution with good positioning quality is more possible when a longer observation period is available. However, in practice, at most a few hours of observing work are likely to be carried out in a field survey (Creager and Maggio 1998; Eckl et al. 2001; Soler et al. 2006). In this case, the static positioning accuracy can hardly achieve millimeter level if PPP has to be applied to this field survey. For example, Ghoddousi-Fard and Dare (2006), and Tétreault et al. (2005) reported that hourly position estimates can achieve only sub-decimeter accuracy and 4-hourly estimates can achieve centimeter-level accuracy. From Section 5.3, ambiguity resolution can significantly improve the positioning accuracy of sub-daily PPP, but a reliable ambiguity resolution can hardly be achieved if measurements are insufficient. Therefore, this section assesses the performance of ambiguity-fixed static PPP with different short observation periods, i.e. one, two, three and four hours. Note that the innovation of "one FCB estimate per satellite-pair pass" over a regional network is also applied in this section.

5.4.1 Data, models and methods

The measurements at the inside-EPN stations from day 245 to 251 in 2007 were used (refer to Section 5.2.1 and 5.3.1). Hence, 168 hourly, 84 2-hourly, 56 3-hourly and 42 4-hourly solutions can be obtained for each station if there was no large data loss. Solutions with data of less than half of the required duration or with less than five satellites during most of the observation period were removed. Daily position estimates were again used as ground truths. RMS statistics of the differences between short-period and daily PPP position estimates are used to quantify the positioning quality of short-period static PPP. Moreover, models and methods for ambiguity resolution were the same as those in Section 5.3.1.

5.4.2 Efficiency of ambiguity resolution

Table 5.4 shows the number of all solutions, solutions with successful ambiguity resolution, solutions without any ambiguities fixed, solutions with incorrect ambiguity resolution and outlier solutions in PPP for different short observation periods at all test stations. In this study, successful ambiguity resolution implies not only correct integer resolution, but also a 3D position RMS of better than 10 cm in the ambiguity-float or ambiguity-fixed solution, or in both; incorrectly fixed ambiguities are identified using the integer ambiguities derived from daily PPP; and outlier solutions denote those in which ambiguities are correctly fixed, but the 3D position RMS statistics in both ambiguity-float and ambiguity-fixed solutions are larger than 10 cm. This threshold of 10 cm is chosen in terms of the normal 3D position RMS derived in hourly PPP (e.g. Ghoddousi-Fard and Dare 2006; Tétreault et al. 2005).

Table 5.4: Efficiency of short-period ambiguity resolution. Column 2–6 denote numbers of all solutions, solutions with successful ambiguity resolution, solutions without any ambiguities fixed, solutions with incorrect ambiguity resolution and outlier solutions

Observation period	Total	Successful	Unfixed	Incorrect	Outlier
One hour	1992	1951	8	17	16
Two hours	1001	997	0	2	2
Three hours	667	667	0	0	0
Four hours	501	501	0	0	0

In Table 5.4, when the observation period is increased from one hour to two, three and four hours, the percentage of solutions with successful ambiguity resolution is increased from 97.9% to 99.6%, 100.0% and 100.0%, respectively. The number of failed solutions, shown in the last three columns of Table 5.4, decreases to zero when the observation period is over three hours. Hence, it can be concluded that longer observation periods lead to higher success rates of ambiguity resolution in short-period static PPP, and a 100.0% success rate is achievable when over three hours of measurements are used.

5.4.3 Reliability of ambiguity resolution

Figure 5.4 shows the mean values of test statistics for ambiguity validation in all ambiguity-fixed solutions at all test stations when different short observation periods are used. Black bars denote the $\frac{\sigma^2_{\text{fixed}}}{\sigma^2_{\text{float}}}$ test statistic and gray bars denote the $\frac{S_{\text{opt2}}}{S_{\text{opt1}}}$ test statistic (refer to Section 2.5.2). With the gradual increase of the observation period from one to two, three and four hours, $\frac{\sigma^2_{\text{fixed}}}{\sigma^2_{\text{float}}}$ decreases from 1.19 to 1.15, 1.13 and 1.12, respectively. According to Equation 2.47, this descent tendency of $\frac{\sigma^2_{\text{fixed}}}{\sigma^2_{\text{float}}}$ suggests that the increase of the observation period contributes to more reliable ambiguity resolution in short-period static PPP. On the other hand, Figure 5.4 shows that all the $\frac{S_{\text{opt2}}}{S_{\text{opt1}}}$ test statistics are significantly larger than the chosen criterion of 3 for all observation periods. These results demonstrate that ambiguity resolution at the test stations within a short observation period is rather reliable. Nevertheless, $\frac{S_{\text{opt2}}}{S_{\text{opt1}}}$ increases first, but then decreases when the observation period is over two hours. It appears that ambiguity resolution with longer observation period is even less reliable than that with only two hours of measurements, which is not reasonable in theory. Actually, this issue can be explained in terms of the different degrees of freedom for the $\frac{S_{\text{opt2}}}{S_{\text{opt1}}}$ test statistics because different periods of measurements are used. Therefore, the statistical distributions of these $\frac{S_{\text{opt2}}}{S_{\text{opt1}}}$ test statistics are totally different from each other, leading to no comparability between them.

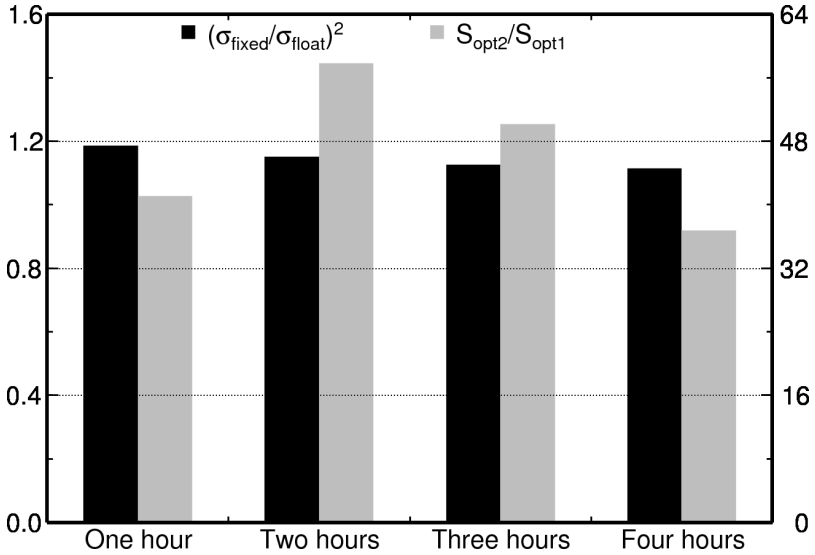

Figure 5.4: Reliability of short-period ambiguity resolution. Each bar denotes a mean value of test statistics in all ambiguity-fixed solutions (refer to Section 2.5.2). Black bars refer to the left axis and grey bars the right

Table 5.5: Positioning accuracy of short-period static PPP. Mean RMS statistics of differences between short-period and daily position estimates are shown for ambiguity-float and ambiguity-fixed solutions

Observation period	Ambiguity-float (cm)				Ambiguity-fixed (cm)			
	East	North	Up	3D	East	North	Up	3D
One hour	3.8	1.5	2.8	5.0	0.5	0.5	1.4	1.6
Two hours	2.0	0.9	1.8	2.9	0.4	0.4	1.0	1.2
Three hours	1.3	0.6	1.3	1.9	0.3	0.4	0.9	1.0
Four hours	0.9	0.5	1.0	1.4	0.3	0.4	0.8	0.9

5.4.4 Positioning accuracy

Table 5.5 shows the mean position RMS of all short-period PPP solutions at all test stations. Table 5.5 shows that, even in the 4-hourly PPP, the RMS of the East component is still significantly reduced by approximately 66.7% and the 3D reduction achieves 35.7% when ambiguity resolution is applied. These results confirm that the positioning accuracy of short-period static PPP, especially for the horizontal components, benefits significantly from ambiguity resolution.

In addition, it is clear in Table 5.5 that increasing the observation period significantly improves the positioning accuracy of ambiguity-float solutions. When the observation period increases from one hour to two, three and four hours, the 3D position RMS is markedly improved from 5.0 to 2.9, 1.9 and 1.4 cm, respectively. However, this tendency is not so evident in ambiguity-fixed solutions. Specifically, the RMS for each horizontal component remains around 4 mm for all short observation periods, and only the vertical component exhibits the tendency of RMS reduction with the increased observation period. Therefore, it is demonstrated that, for ambiguity-fixed solutions, the horizontal positioning accuracy can hardly be affected by the length of observation periods when they are over one hour, while the vertical one can be improved when the observation periods are increased from one to four hours.

5.4.5 Degraded solutions

As mentioned in Section 5.3.2, a correct ambiguity resolution does not always lead to an improved positioning accuracy when compared with the ambiguity-float ones. Table 5.6 shows the number of degraded solutions, their percentages in all solutions with successful ambiguity resolution, and the mean and maximum RMS increment for different short observation periods. In the hourly solutions, the percentage of degraded solutions is up to 1.1% and the maximum RMS increment is up to about 3 cm. When the observation period is increased to three hours, however, the percentage is decreased to 0.7% and the maximum RMS increment is reduced to 1.7 cm. As expected, the least percentage of 0.2% corresponds to the observation period of four hours. It

Table 5.6: Degraded solutions in short-period static PPP. Column 2–5 denote the number of degraded solutions, their percentages in all solutions with successful ambiguity resolution, mean RMS increment and maximum RMS increment

Observation period	Number	Percentage	Mean (cm)	Max (cm)
One hour	22	1.1%	1.5	2.9
Two hours	11	1.1%	1.5	2.7
Three hours	5	0.7%	1.3	1.7
Four hours	1	0.2%	1.2	1.2

Table 5.7: Occurrence rate and mean RMS increment for degraded solutions. Percentages of degraded solutions with RMS increment for the East, North or Up components and the corresponding mean increment for each component

Observation period	Percentage			Mean increment (cm)		
	East	North	Up	East	North	Up
One hour	45.5%	59.1%	100%	0.4	0.5	1.8
Two hours	45.5%	54.5%	100%	0.5	0.6	1.6
Three hours	40.0%	0	100%	0.7	0	1.9
Four hours	0	0	100%	0	0	1.8

has been demonstrated that degraded solutions are closely related to the estimation of ZTDs. A long observation period can contribute to highly accurate estimates of ZTDs. Hence, the occurrence of degraded solutions can be decreased by prolonging the observation period, rather than fixing ZTDs to precisely known values as discussed in Section 5.3.2.

Moreover, Table 5.7 shows the percentages of solutions with RMS increment for the East, North or Up components and the corresponding mean increment for each component. It can be found that all degraded solutions suffer the RMS increment for the Up component. Note that this component also exhibits the largest increment among all three components. Thus it is demonstrated that the RMS increment mainly occurs for the Up component. The Up component is strongly correlated with ZTD in estimation, thus explaining why degraded solutions are also closely associated with ZTD.

5.4.6 Conclusions

It is demonstrated that fairly reliable ambiguity resolution can be achieved when the observation period is over one hour. When the observation period is over three hours, the success rate of ambiguity resolution can even reach 100.0%.

In the ambiguity-fixed solutions of short-period static PPP, over one hour of measurements are sufficient for the horizontal position components to achieve an RMS of smaller than 1.0 cm against the daily estimates while over three hours of measurements are still required for the vertical component to achieve such an RMS level. Moreover, increasing the observation periods hardly reduces the horizontal RMS, but clearly reduces the vertical RMS in ambiguity-fixed solutions.

In addition, for degraded solutions, the RMS increment mainly occurs for the Up component. Increasing the observation periods to three hours can reduce the occurrence of degraded solutions to less than 1.0% of all solutions with successful ambiguity resolution.

5.5 Ambiguity resolution at a remote mobile receiver

Most offshore applications employ differential GPS positioning techniques, and thus relatively short baselines are preferable. Vessels used for seafloor geodesy are typically less than 500 km away from shores, and buoys supporting altimeter calibration are usually within 20 km of an onshore reference station (Chadwell and Bock 2001). Such baseline lengths can only cover a minimal margin of the vast oceanic areas, confining the oceanographic and geophysical research to inshore areas. Therefore, kinematic GPS positioning, providing an accuracy of a few centimeters for ultra long-range (e.g. >1000 km) marine platforms, is an indispensable prerequisite

for future oceanographic and geophysical applications in open oceans (Fell and Maul 2000). However, differential GPS positioning suffers from the so-called baseline length problem, i.e. the positioning accuracy deteriorates with the increased baseline length. The total decorrelation between the atmospheric delays at two ultra distant stations poses a great challenge for a reliable ambiguity resolution (e.g. Colombo et al. 2001). In this case, ambiguity resolution is sometimes ignored. Consequently, usually only decimeter-level kinematic positioning accuracy is achievable over ultra long baselines (Teunissen and Kleusberg 1998). In addition, due largely to logistical expenses, it is usually infeasible for ultra long-range differential positioning to employ multiple reference stations around a to-be-positioned station, although this can lead to more reliable and accurate positioning (Teunissen and Kleusberg 1998). Hence, in this section, differential positioning corresponds to only one reference station, except when otherwise noted.

By contrast, it is normally recognized that PPP is free from the constraint of baseline lengths, suggesting an efficient and cost-effective solution for highly precise kinematic positioning of marine platforms. Nevertheless, the satellite clocks supporting PPP have to be determined using a network of land-based reference stations, implying that PPP may also be subject to the distance between the network and the user station. This issue is critical for marine platforms located in central open oceans where the nearest reference station might be a few thousand kilometers away. Note that, due largely to the dynamic smoothing in the orbit determination, a homogeneous GPS orbit accuracy at centimeter level can be obtained within a continuous daily arc (Griffiths and Ray 2009), showing that the possible orbit accuracy deterioration over the vast oceanic areas is minimal and is thus ignored in this study.

Therefore, this section aims at assessing the accuracy of network-based satellite clock and FCB estimates when they are applied to the positioning of a remote marine platform. The kinematic PPP performance is compared with that of kinematic long-range differential positioning, when ambiguity resolution is applied to both techniques. Note that the innovation of "one FCB estimate per satellite-pair pass" over a regional network is again applied in this section.

5.5.1 Data, models and methods

A vessel-borne 1-Hz GPS data set was collected in the Bohai Sea of China on November 27th 2004, covering over six hours from about 1:37:00 am to around 7:53:00 am (UTC), during which the vessel sailed for more than 250 km at a mean velocity of approximately 10 m/s. Three 1-Hz reference stations, i.e. REF1, REF2 and REF3, were established around this vessel. Figure 5.5 shows the vessel trajectory and the baseline lengths between the 1-Hz reference stations.

The truth benchmark for the vessel-borne antenna positions is obtained by differential positioning with the three 1-Hz reference stations using Bernese GPS software 5.0 (Dach et al. 2007). An integrated adjustment of the three kinematic baselines was adopted and residual ZTDs were estimated. The horizontal and vertical accuracies of ambiguity-fixed position estimates were believed to be better than 5 cm and around 5 cm, respectively (see Grejner-Brzezinska et al. 2005). Moreover, 1-Hz data set were decimated every 5 s for efficiency.

Figure 5.6 shows the distribution of reference stations used for the satellite clock and FCB determination. The blue dots, brown triangles and black inverted triangles denote three rings of reference stations centered on the vessel with radii of roughly 900 km, 2000 km and 3600 km, respectively. For brevity, they are hereafter called the small-, medium-, and large-ring networks,

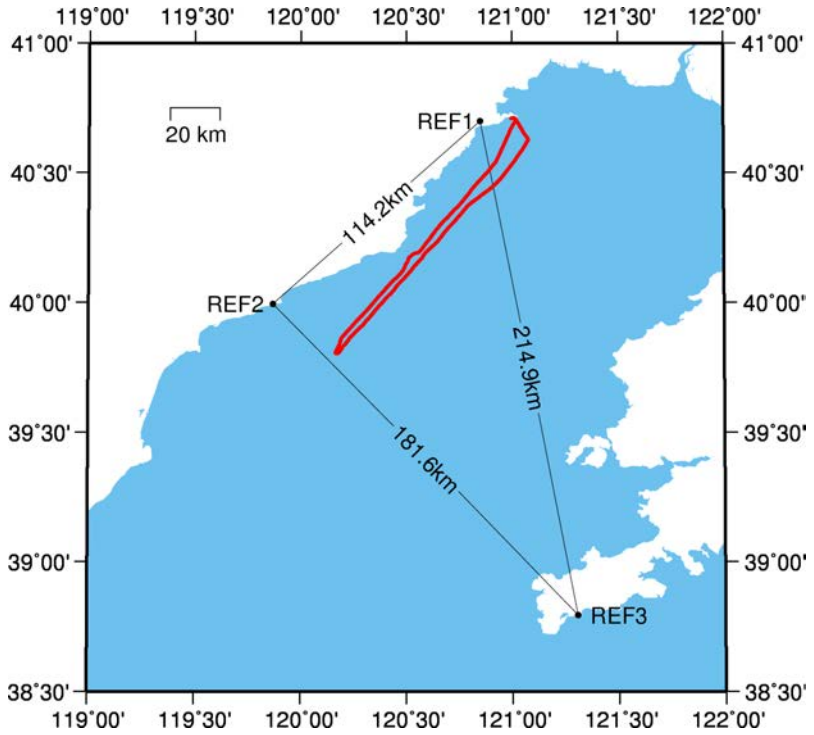

Figure 5.5: Vessel trajectory on the Bohai Sea of China (red line) and three 1-Hz reference stations (black dots) used to compute a reference vessel trajectory (truth benchmark)

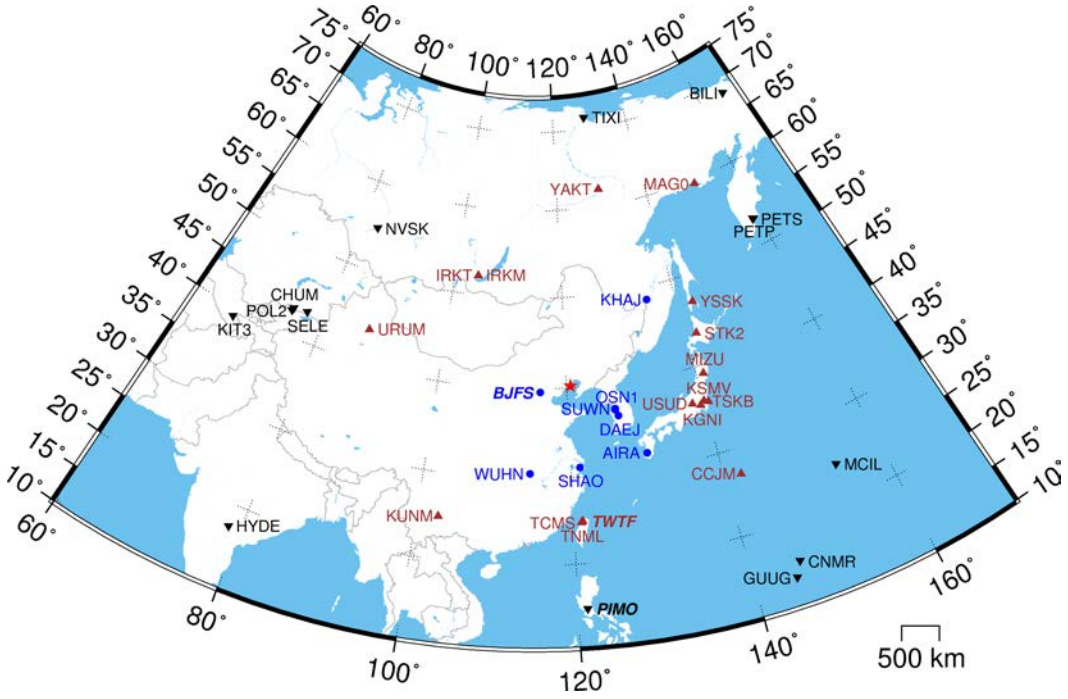

Figure 5.6: Three ring networks of reference stations used for the satellite clock and FCB determination. The red star denotes the approximate position of the vessel. Blue dots, brown triangles and black inverted triangles denote three rings of reference stations centered on the vessel with radii of about 900 km, 2000 km and 3600 km, respectively. For kinematic differential positioning, three stations with bold italic names, BJFS, TWTF and PIMO, are used as reference stations with distances to the vessel of about 400 km, 1700 km and 2800 km, respectively

which consist of 8, 17 and 14 stations, respectively. All reference stations are from the IGS permanent network with daily GPS measurements of 30-second interval. It is worth indicating that the three ring networks were used independently, and daily measurements were processed. In addition, the station BJFS, TWTF and PIMO are used as the reference stations in differential positioning, and their distances from the vessel are approximately 400 km, 1700 km and 2800 km, respectively (Figure 5.6). More than seven satellites per epoch were available on average at these three reference stations during the vessel-borne data collection.

Kinematic PPP and differential positioning use almost identical models. Satellite orbits, ERPs, and the P1-C1 DCBs from CODE were used. The relative antenna phase centers and the phase wind-up corrections were applied to keep consistency with the CODE products in 2004 (Gendt and Nischan 2005). A cut-off angle of 7° was set for usable measurements and an elevation-dependent weighting strategy was applied to measurements at low elevations (Gendt et al. 2003). For PPP, residual ZTDs were estimated every 60 minutes at the reference stations and every 10 minutes at the vessel. For differential positioning, however, they are estimated every 10 minutes at both the reference station and the vessel. In addition, due to the low data sampling rate at the reference stations in Figure 5.6, the 1-Hz vessel-borne GPS data were decimated into a 30-second interval.

For differential kinematic positioning, considering the decorrelation of atmospheric delays between two distant stations, ionosphere-free measurements were thus used to eliminate the first-order ionospheric delays, and the residual zenith tropospheric delays had to be estimated at both stations. In addition, using precise satellite orbits was also mandatory for ultra long baselines. Bernese GPS Software 5.0 was used for this study (Dach et al. 2007).

As recommended by (Dach et al. 2007), double-difference ambiguity resolution for ultra long baselines consists of two steps. First, wide-lane ambiguities are fixed to integers using Melbourne-Wübbena combination measurements. Second, narrow-lane ambiguities are computed using integer wide-lane ambiguities and ionosphere-free-observable ambiguity estimates. Narrow-lane ambiguity resolution is then attempted to generate ambiguity-fixed solutions. Thus this method actually highly resembles that for ambiguity resolution at a single receiver, except for the FCB determination. The sigma-dependent bias rounding strategy was adopted for ambiguity resolution of wide-lane and narrow-lane ambiguities.

5.5.2 Satellite clock estimates

Due to the different coverage and sky views of the three ring networks, it is unfair to assess the accuracy of all satellite clock estimates. Hence, only the estimates that are used at the vessel are compared with the truth benchmark, i.e. the CODE final clocks, of which the accuracy in 2004 was better than 0.1 ns (Gendt and Nischan 2005).

Before the comparison, the constellation and satellite-dependent offsets between the ring-network-based satellite clocks and the CODE final clocks were eliminated (Kouba and Héroux 2001). The constellation clock offset can be absorbed by receiver clocks, and the satellite-dependent clock offsets can be assimilated into ambiguity estimates (Rocken et al. 2006), thus hardly jeopardizing the PPP solution quality at the vessel. Constellation offsets are removed at each epoch by differencing between a reference clock and all other clocks, and a satellite-dependent offset is removed within each continuous observation session by deducting the mean clock bias. After the removal of both offsets, the RMS of the clock differences is used to quantify

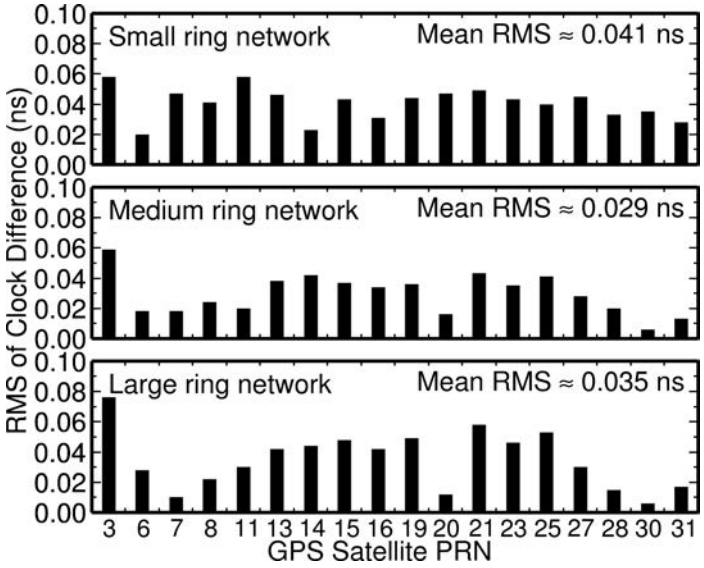

Figure 5.7: Clock comparison for three ring networks. RMS values of the satellite clock differences between the ring-network-based estimates and the CODE final products. Both the constellation and the satellite-dependent offsets have been removed

the clock accuracy.

For each satellite, all RMS values of the clock differences are better than 0.1 ns, and the three mean RMS values are only 0.041 ns, 0.029 ns and 0.035 ns respectively (Figure 5.7), indicating that the accuracy of ring-network-based clocks is very close to that of the CODE final clocks. Moreover, the differences between the three mean RMS values are within ± 0.02 ns, and we cannot see any pronounced RMS rise caused by the increasing ring-network radius. This might be because the CODE final clocks are not accurate enough to assess the actual accuracy of ring-network-based clock estimates. However, it can be demonstrated that the change of clock accuracy due to the increased ring-network radius up to a few thousand kilometers is smaller than 0.02 ns.

5.5.3 Narrow-lane FCB estimates

Narrow-lane FCB estimates that are used for the vessel are assessed in this section. Due to the lack of any external reference solutions, the relative accuracy between the three sets of estimates is assessed. Figure 5.8 shows the narrow-lane FCB estimates of all observed satellites with respect to PRN03 for the three ring networks. PRN03 is chosen as reference because it was constantly observed during the vessel-borne data collection. Each narrow-lane FCB estimate corresponds to one full pass over a ring network by a satellite pair. The mean formal precision (3σ) of all narrow-lane FCB estimates for each ring network is about 0.05 cycles. Note that the missing estimates for some ring networks, e.g. PRN20 for the small ring, are caused by the insufficient number of reference stations observing the corresponding satellite pair. From Figure 5.8, it can be found that, for a satellite pair within one pass, its three independent narrow-lane FCB estimates usually totally differ from each other. Overall, the RMS values of the narrow-lane FCB differences between the three sets of estimates reach up to 0.3 cycles. For this, one explanation is that different networks are used to determine satellite clocks, thus different clock offsets are introduced into ambiguity estimates, and thereby totally different narrow-lane FCB estimates are obtained.

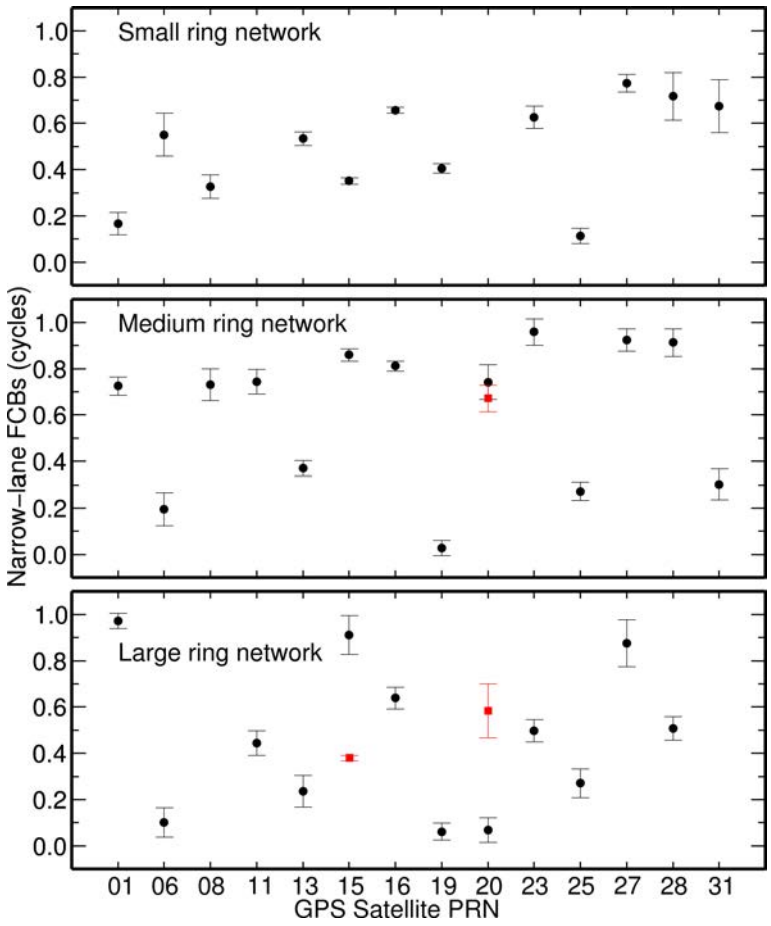

Figure 5.8: Narrow-lane FCBs of all observed satellites with respect to PRN03 for three ring networks. Each estimate corresponds to one full pass over a ring network by a satellite pair. Solid black circles and red squares denote the estimates for the first and second pass respectively, whereas error bars denote the formal precisions of 3σ

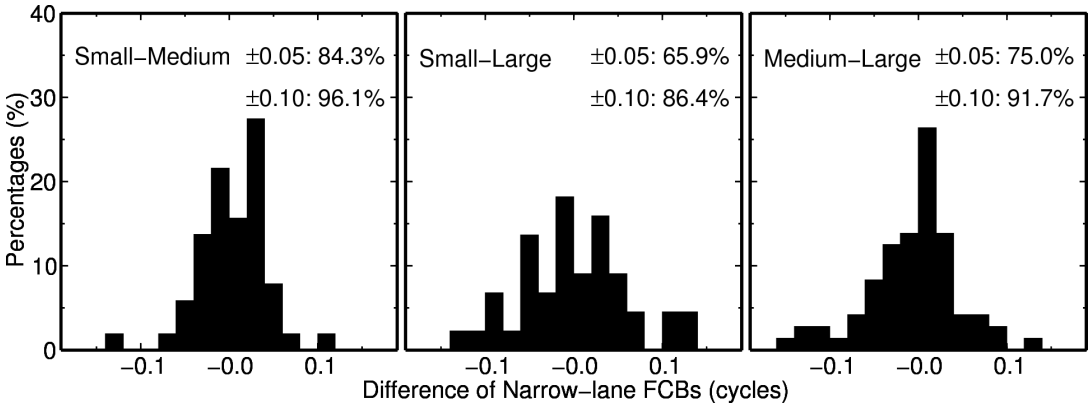

Figure 5.9: Distribution of narrow-lane FCB differences between the three ring networks. Note that satellite clocks based on the large ring-network are used in all three ring-network solutions

In this case, the large-ring-network-based satellite clocks are applied to both the small- and medium- ring networks to determine their narrow-lane FCBs again. Figure 5.9 shows the distribution of the new narrow-lane FCB differences between the three sets of estimates. For the three comparisons between the small and the medium, the small and the large, and the medium and the large ring networks, about 84.3%, 65.9% and 75.0% of all narrow-lane FCB differences are within ±0.05 cycles, and about 96.1%, 86.4% and 91.7% are within ±0.1 cycles, respectively (Figure 5.9). Correspondingly, the RMS values of the new narrow-lane FCB differences are significantly reduced to 0.04 cycles, 0.06 cycles and 0.05 cycles with a mean of only 0.05 cycles, thus confirming the above explanation. More importantly, from Figure 5.9, the narrow-lane FCB differences between the small and the large rings are clearly larger than those from the other two comparisons, and the differences between the medium and the large ring networks are clearly larger than those between the small and the medium ones. Considering the different coverage of the three ring networks, it is demonstrated that the narrow-lane FCB estimates that are used at the vessel are clearly affected by the increased ring-network radius.

5.5.4 Comparison between kinematic PPP and differential positioning

Firstly, the positioning accuracies that are achieved by kinematic PPP and differential positioning are compared. Table 5.8 shows the RMS values of the position differences between the truth benchmark and the estimates from kinematic PPP solutions. It can be clearly seen that ambiguity resolution reduces the horizontal RMS values to 1-cm level. The East components show larger reductions of 64.7%, 66.7% and 57.9%, whereas the North components of only 37.5%, 36.4% and 23.1% for the three ring networks respectively. By contrast, the vertical RMS values are around 3 cm after ambiguity resolution. Vertical RMS reductions due to ambiguity resolution are discernible for the medium- and large-ring networks, but not for the small one, which needs more investigation. Considering the actual accuracy of the truth benchmark, it can be inferred that the actual ambiguity-fixed horizontal accuracy for the vessel-borne antenna is at the centimeter level and the vertical at the sub-decimeter level in kinematic PPP. Furthermore, the RMS values are enlarged with the increasing ring-network radius. This issue is more pronounced when ambiguities are not fixed, showing that increasing the ring-network radius affects the positioning accuracy at the vessel.

For comparison, Table 5.9 shows the RMS values of the position differences between the truth benchmark and the estimates in kinematic differential solutions. It can be seen that ambiguity resolution does not reduce the RMS values for the TWTF- and PIMO-based differential positioning. As expected, the RMS values are enlarged with the increasing baseline length, but this enlarging rate is faster than that in Table 5.8 when ambiguities are fixed. Furthermore, after ambiguity resolution, the RMS values for PPP are smaller than those for the differential

Table 5.8: Position accuracy of kinematic PPP for a vessel. RMS statistics of the position differences between the truth benchmark and the estimates from ambiguity-float and ambiguity-fixed kinematic PPP solutions

Reference network	Ring radius (km)	Ambiguity-float (cm)			Ambiguity-fixed (cm)		
		East	North	Up	East	North	Up
Small ring	900	1.7	0.8	1.8	0.6	0.5	2.6
Medium ring	2000	1.5	1.1	3.5	0.5	0.7	2.8
Large ring	3600	1.9	1.3	5.0	0.8	1.0	3.2

Table 5.9: Position accuracy of kinematic differential positioning for a vessel. RMS statistics of the position differences between the truth benchmark and the estimates from ambiguity-float and ambiguity-fixed kinematic differential solutions

Reference station	Baseline length (km)	Ambiguity-float (cm)			Ambiguity-fixed (cm)		
		East	North	Up	East	North	Up
BJFS	400	0.7	0.9	2.0	0.5	0.5	1.9
TWTF	1700	0.8	1.5	2.9	0.9	1.7	3.4
PIMO	2800	1.4	2.2	3.5	1.8	2.3	3.7

positioning when the vessel is over a few thousand kilometers away from a reference station. For instance, the RMS values for large-ring-network-based PPP are 55.6%, 56.5% and 13.5% smaller in East, North and Up, respectively, than those for the PIMO-based differential positioning. Considering the use of multiple reference stations and the relatively short baseline lengths for the truth benchmark determination, the actual accuracy of this benchmark is believed to be better than that derived from the BJFS-, TWTF- or PIMO-based differential positioning. Hence, it is demonstrated that ambiguity-fixed PPP achieves better positioning accuracy than that of differential positioning when the vessel is over a few thousand kilometers away.

In addition, for the vessel-borne data, 1-Hz position estimates are of more interest. In this case, differential positioning requires 1-Hz data from reference stations. However, for all three ring networks, we can interpolate the above satellite clock estimates at a 1-second interval, and obtain ambiguity-fixed position estimates every 1 s. In this study, even if positions are estimated every 5 s in PPP, the resulting RMS values are very close to those in Table 5.8, and the largest difference is only 0.1 cm.

Secondly, the efficiencies of ambiguity resolution between kinematic PPP and differential positioning are compared. Table 5.10 shows the number of fixed ambiguities and the number of all ambiguities in PPP and differential positioning. Due to the different definitions for single-difference and double-difference ambiguities, it is not reasonable to directly compare the number of fixed ambiguities or the fixing rates between PPP and differential positioning. Hence, only the change rates of the number of fixed ambiguities relative to the increasing network radius or baseline length are compared. Irrespective of the ring-network radius, the number of fixed ambiguities for PPP is almost the same, whereas the number for differential positioning is sharply reduced from 13 to 7 with the increasing baseline length. Hence, it is demonstrated that, for ultra long-range kinematic positioning up to a few thousand kilometers, the efficiency of ambiguity resolution for PPP is higher than that for differential positioning.

Finally, it is worth indicating that the better performance of PPP than that of differential positioning is attributed to using a ring reference network around the vessel, rather than a single reference station. As a result, more observation information is used in PPP than that

Table 5.10: Efficiency of ambiguity resolution for kinematic PPP and differential positioning. Number of fixed ambiguities (before slash) and number of all ambiguities (behind slash) in kinematic PPP and differential positioning

Reference network	PPP	Reference station	Differential positioning
Small ring	14/16	BJFS	13/19
Medium ring	16/16	TWTF	13/21
Large ring	16/16	PIMO	7/16

in differential positioning. For instance, more than eight carrier phase observations per epoch are available on average at the vessel for all ring networks, whereas only seven are available for BJFS- and TWTF-based differential positioning, and fewer than six for PIMO.

5.5.5 Conclusions

For the satellite clocks that are used at the vessel, their accuracy change due to the increased ring-network radius to a few thousand kilometers is smaller than 0.02 ns. Moreover, a high relative accuracy between the three sets of narrow-lane FCB estimates can be achieved if the biases between their corresponding satellite clocks are removed, suggesting that narrow-lane FCBs are closely related to the satellite clocks. More importantly, the narrow-lane FCBs that are used at the vessel are clearly affected by the increasing ring-network radius, but the RMS values of the differences between the three sets of estimates are around 0.05 cycles only.

Ambiguity-fixed PPP can achieve a kinematic positioning accuracy of several centimeters at a remote marine platform. From the comparison between kinematic PPP and differential positioning, it is demonstrated that PPP can achieve both better accuracy of position estimates and higher efficiency of ambiguity resolution when a to-be-positioned marine platform is over a few thousand kilometers away from the reference stations. Moreover, the positioning accuracy of PPP at the vessel is affected by the increasing ring-network radius, but the change rate of accuracy is smaller for PPP than that for differential positioning.

Therefore, for the precise positioning of remote marine platforms, ambiguity-fixed PPP can achieve an accuracy of several centimeters, even if the distance between the reference network and the platform is up to a few thousand kilometers.

5.6 Real-time ambiguity resolution in PPP

Based on the results in sections 5.4 and 5.5 about post-processing ambiguity-fixed PPP, it can be reasonably expected that real-time PPP can also be improved by applying ambiguity resolution. This can potentially lead to an innovative PPP-RTK model where PPP provides rapid convergence of a few seconds to a reliable centimeter-level positioning accuracy based on an RTK reference network (e.g. Bisnath and Gao 2007; Wübbena et al. 2005). In order to verify this concept, Laurichesse et al. (2008a) and Mervart et al. (2008) reported that ambiguity resolution could improve the positioning accuracy of real-time PPP, but the convergence period to an ambiguity-fixed solution was usually over several tens of minutes at a mobile receiver. One reason for this long period is that smoothing noisy pseudorange measurements for reliable wide-lane ambiguity resolution usually requires a few tens of minutes; and the other is that the slowly changing geometry of visible satellites leads to an even longer period before narrow-lane ambiguity resolution can be attempted (Laurichesse et al. 2008a).

Hence, before implementing the PPP-RTK model above, at least three technical issues should be carefully investigated:

- Can wide-lane ambiguity resolution be performed not only reliably, but also rapidly? This issue is critical to both narrow-lane FCB determination at the server end and narrow-lane ambiguity resolution at users;
- Can narrow-lane FCB estimates rapidly stabilize to accurate values? To my knowledge, this issue has not been discussed in depth in recent publications, but it critically relates to

how to rapidly provide usable narrow-lane FCB products for users;

- How does ambiguity resolution affect the positioning quality of real-time PPP? This issue has been preliminarily reported before, but more investigations over a relatively large spatio-temporal scale are necessary.

Note that other technical issues, such as the stochastic modeling (e.g. Jin et al. 2005) and the quality control (e.g. Han 1997b), are also important, but are hereafter ignored because they are beyond the scope of this thesis.

This section therefore discusses the technical factors that affect the rapidity of both wide-lane ambiguity resolution and stabilization of narrow-lane FCB estimates, and then investigates the performance of narrow-lane ambiguity resolution in real-time PPP. Note that the innovation of real-time ambiguity resolution at a single receiver in Section 2.4.3 is applied in this study.

5.6.1 Data and models

For this study, 24-hour 1-Hz GPS measurements at 91 stations from the EUREF–Internet Protocol project (EUREF-IP) (Bruyninx 2004) and the Ordnance Survey of Great Britain (OSGB) real-time network (Figure 5.10) were used. These data covered seven days from July 6th to 12th 2008. Note that EUREF-IP data bore the gaps caused by communication or power interruptions. (http://www.epncb.oma.be/). At these stations, five receiver types including 9 Ashtech, 27 Javad, 21 Leica, 7 Topcon and 26 Trimble receivers were studied. Type 1, 2, 3, 4 and 5 are hereafter used to represent them, but their order is changed. Type-5 receivers contain six cross-correlation receivers and six receivers without choke-ring antennas.

For data modeling, the predicted parts of IGS ultra-rapid satellite orbits and ERPs were used from their release epochs until newer products were available. The P1-C1 DCBs, the absolute antenna phase centers, the phase wind-up corrections and the station displacement from the IERS conventions 2003 (McCarthy and Petit 2004) were applied. A cut-off angle of 7° for usable measurements and an elevation-dependent weighting strategy to measurements at low

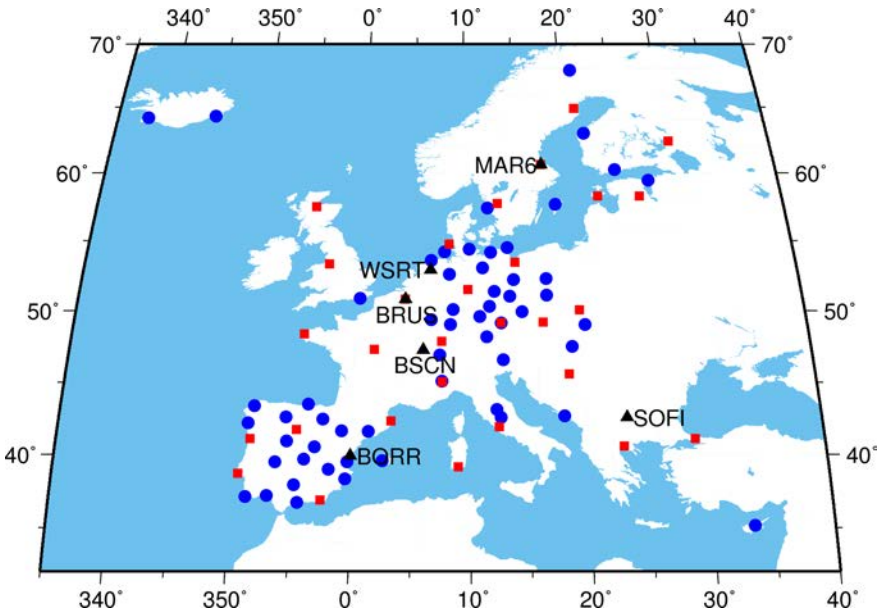

Figure 5.10: Distribution of 1-Hz stations for real-time PPP. Red squares denote stations for satellite clock determination; black annotated triangles denote simulated mobile stations; and all symbols denote stations for FCB determination

elevations were used (Gendt et al. 2003). Horizontal tropospheric gradients were estimated every 12 hours at the reference stations, whereas residual ZTDs every 3 hours. Satellite clocks were estimated by fixing predicted orbits and station positions, whereas narrow-lane FCBs by fixing satellite orbits and clocks. No communication delays of satellite clocks was simulated. About 30 stations were used to determine the satellite clocks, but all stations were used to determine FCBs, and finally six stations were used to simulate mobile users (Figure 5.10).

5.6.2 Rapidity of wide-lane ambiguity resolution

The rapidity of wide-lane ambiguity resolution is affected mainly by pseudorange measurement noise, multipath effects and atmospheric conditions. Empirically, the measurement noise is receiver-dependent, and the multipath effects and the atmospheric delays are very significant for satellites at low elevations. Hence, ambiguities were divided in terms of receiver types and an elevation angle of 15° to illustrate the impacts of these factors on wide-lane ambiguity resolution. Note that 15° was chosen because cut-off angles are normally set below it to remove low-elevation measurements which can degrade ambiguity estimates. In addition, six points are needed to be clarified:

- For a satellite, its elevation angles are averaged over its observation periods to obtain time-mean values, each of which actually corresponds to an undifferenced ambiguity;
- For a being-observed satellite pair, its later-observed satellite, rather than the earlier-observed one, decides the starting time of forming a single-difference ambiguity between this satellite pair;
- A round-off criterion of 0.25 cycles is applied to the bias-rounding strategy by Ge et al. (2005a);
- If a wide-lane ambiguity can be reliably fixed to an integer at a particular epoch, this actually mean that it can be fixed to the same integer at all subsequent epochs;
- The reliability of wide-lane ambiguity resolution is quantified by the ratio of reliably-fixed ambiguities to all ambiguities;
- Integer values of fixed wide-lane ambiguities in post-processing mode were used as the truth benchmarks.

A Ambiguities corresponding to high elevations

In this study, ambiguities corresponding to high elevations are those derived from only the measurements over an elevation angle of 15°. For each receiver type, Table 5.11 shows the mean time spent on wide-lane ambiguity resolution and the distribution of all times. Each receiver type spends a mean time of between 100 s and 360 s. On average, about 89.3% of all times are shorter than 600 s, and about 95.7% shorter than 1200 s. However, only 34.3% of all times are shorter than 20 s for all receiver types excluding Type 3. These statistics suggest that 600 s of measurements are required for most receiver types to reliably fix about 90% of wide-lane ambiguities that correspond to elevations of over 15°.

Interestingly, Type-3 receivers show the shortest mean time of only 105 s that is almost over two times shorter than those of other receiver types; and even 86.4% of all times are shorter than 20 s. This superiority might be related to the pseudorange smoothing strategies or the high-quality clocks applied within the Type-3 receivers. Hence, rapid wide-lane ambiguity resolution within only several seconds can be potentially feasible for the Type-3 receivers.

Table 5.11: Rapidity of wide-lane ambiguity resolution corresponding to high elevations. The number of wide-lane ambiguities, the mean time spent on the wide-lane ambiguity resolution, and the distribution of all times

Receiver types	Number of ambiguities[a]	Mean time (s)	Distribution of all times		
			<20 s	<600 s	<1200 s
1	28848	224	33.4	89.9%	96.4%
2	66359	360	28.4	82.1%	92.2%
3	49003	105	86.4	94.5%	97.5%
4	18489	262	27.5	88.1%	95.6%
5	106440	182	47.8	92.0%	96.8%
5[b]	81816	156	53.5	93.8%	97.3%
5[c]	67049	124	55.0	95.3%	98.3%

[a] all of which are computed using the measurements over an elevation angle of 15°
[b] excluding receivers of cross-correlation type from Type-5 receivers
[c] excluding receivers of cross-correlation type, and receivers without choke-ring antennas from Type-5 receivers

In addition, the impact of cross-correlation receivers and choke-ring antennas is investigated. In general, cross-correlation receivers suffer from relatively poor pseudorange quality and choke-ring antennas are useful in rejecting multipath-contaminated measurements. In Table 5.11, the mean time is significantly reduced from 182 to 156 s by the exclusion of cross-correlation receivers (Type 5[b]), and to 124 s by further exclusion of receivers without choke-ring antennas (Type 5[c]). Moreover, due to these exclusions, the percentages of times that are shorter than 20, 600 and 1200 s are steadily increased. Hence, these statistics demonstrate that cross-correlation receivers and the disuse of choke-ring antennas will prolong the time spent on the wide-lane ambiguity resolution.

B Ambiguities corresponding to low elevations

Due to a small number of measurements below an elevation angle of 15°, it is not appropriate to use only these measurements to compute ambiguities corresponding to low elevations. Instead, they are represented by the wide-lane ambiguities of which the later-observed satellites rise from below an elevation angle of 15°. For each receiver type, Table 5.12 shows the mean time spent on wide-lane ambiguity resolution, the distribution of all times and the distribution of time-mean elevation angles for the later-observed satellites.

In Table 5.12, except Type-3 receivers, each receiver type spends a mean time of between 400 and 700 s. On average, only 73.0% of all times are shorter than 600 s, and 87.6% shorter than 1200 s. Compared with the statistics in Table 1, these worse results can be attributed to the more severe multipath effects and the more turbulent atmospheric conditions at low elevations. Overall, over 1200 s of measurements are needed before fixing about 90% of wide-lane ambiguities of which the later-observed satellites rise from below an elevation angle of 15°.

Alternatively, it is proposed to use the time-mean elevation angles of the later-observed satellites to decide when a wide-lane ambiguity can be reliably fixed. In Table 5.12, when wide-lane ambiguities are fixed, over 90% of time-mean elevation angles are smaller than 15°, and almost 100% smaller than 20° for each receiver type. In practice, ambiguities corresponding to high elevations are preferred for integer resolutions, and the remnant ambiguities are usually left as float in order to avoid risky fixing until their corresponding satellites rise above a specific elevation angle, such as 15°. Hence, the time-mean elevation angle is believed to be a more

Table 5.12: Rapidity of wide-lane ambiguity resolution corresponding to low elevations. The number of wide-lane ambiguities, the mean time spent on wide-lane ambiguity resolution, the distribution of all times, and the distribution of time-mean elevation angles for the later-observed satellites when wide-lane ambiguities are fixed

Receiver types	Number of ambiguities[a]	Mean time (s)	Distribution of all times		Distribution of time-mean elevation angles	
			<600 s	<1200 s	⩽15°	⩽20°
1	17314	518	72.3%	88.9%	92.3%	99.1%
2	74252	690	61.8%	81.9%	94.2%	98.9%
3	47694	236	87.7%	94.4%	97.1%	99.4%
4	14316	487	74.5%	87.7%	94.0%	99.4%
5	44283	573	68.5%	85.3%	93.2%	98.7%
5^b	39115	551	70.7%	85.9%	94.6%	98.7%
5^c	25664	495	71.0%	88.0%	95.4%	99.2%

[a] of which the later-observed satellites rise from below an elevation angle of 15°
[b,c] see footnotes of Table 5.11

realistic threshold than the time span in fixing ambiguities corresponding to low elevations.

In addition, from Table 5.12, the exclusion of cross-correlation receivers (Type 5^b) reduces the mean time by 22 s, whereas the further exclusion of receivers without choke-ring antennas (Type 5^c) by 56 s, suggesting the significant contribution of choke-ring antennas to mitigating multipath effects.

C High rapidity or high reliability?

Disappointingly, the results above demonstrate that the high rapidity of a few seconds for wide-lane ambiguity resolution cannot be normally achieved in the PPP-RTK model in Section 2.4.3 if high reliability of over 90% is required. In this case, the high reliability is preferred to the risky high-rapidity. Then the thresholds for both the time span and the time-mean elevation angle should be carefully selected to decide when a wide-lane ambiguity can be reliably fixed. In Table 5.13, for a threshold combination of 600 s and 15°, 99.86% of all wide-lane ambiguities can be reliably fixed. Both longer time and larger elevation angle can improve this rate, but very slightly by not more than 0.05%. Hence, 600 s and 15° are finally chosen as thresholds throughout this thesis.

Furthermore, considering the practicability of a PPP-RTK service, three points need to be highlighted:

- A time requirement of 600 s before a reliable wide-lane ambiguity resolution can be accepted at the server end, but is unacceptable at the user end if instantaneous precise positions are always required. For this problem, the results here suggest that improving the pseudorange quality might be a solution, as demonstrated by Type-3 receivers;
- A time-mean elevation angle requirement of 15° before a reliable wide-lane ambiguity

Table 5.13: Rate of reliably fixed ambiguities in all wide-lane ambiguities under different thresholds

Time-mean elevation angle	Time span	
	600 s	1200 s
15°	99.86%	99.90%
20°	99.88%	99.91%

resolution can be accepted at both the sever and the user ends. Ambiguities corresponding to low elevations are seldom selected for narrow-lane ambiguity resolution in practice, due to their high possibility of incorrect fixing. Hence, wide-lane resolutions for these ambiguities are actually not urgent in real time;

- Pseudorange multipath effects can be much more complicated at a moving antenna, and thus the above thresholds should be carefully regarded in a kinematic environment.

5.6.3 Temporal stabilization of narrow-lane FCBs

Narrow-lane FCBs can be estimated once wide-lane ambiguity resolution is achieved at the reference stations. Section 5.2.3 reported that a narrow-lane FCB can be precisely determined for each full pass of a satellite pair over a regional network. In a real-time scenario, only up-to-present measurements, rather than all measurements during a full pass, can be used to estimate narrow-lane FCBs. As a result, narrow-lane FCB estimates may need some time to stabilize to accurate values. In this study, if the peak-to-peak amplitude during this stabilization decreases to smaller than 0.1 cycles, the narrow-lane FCB estimates are considered sufficiently stable. Note that this threshold coincides with the accuracy requirement for narrow-lane FCB estimates by Ge et al. (2008).

A Fluctuant fractional parts

Typically, Figure 5.11 shows the fractional parts of a narrow-lane ambiguity estimate and the two corresponding satellites' time-mean elevation angles every 100 s. It can be seen that the fractional parts gradually stabilize to relatively stable values after a fluctuation during the initial phase. This initial phase lasts for a few tens of minutes, during which the peak-to-peak amplitude of the fractional parts is up to 0.2 cycles. Considering the elevation angles in Figure 5.11, I argue that this fluctuation is related to the small elevation angles of the lower satellite during the initial phase.

In order to illustrate this argument, for all satellite pairs at all stations, Figure 5.12 shows the fractional-part peak-to-peak amplitudes against the time-mean elevation angles of the lower satellites. Note that such an elevation angle is computed at only the epoch when the corresponding satellite pair has been observed for 10 or 30 minutes and wide-lane ambiguity resolution has been achieved; moreover, the fractional-part estimates after only this epoch are used to compute the peak-to-peak amplitude and the narrow-lane FCB estimates. The blanks below 15° in Figure 5.12 are caused by the threshold of the time-mean elevation angle. In both Figure 5.12(a) and 5.12(b), about 70% of all peak-to-peak amplitudes are smaller than 0.1 cycles, and over 90% smaller than 0.25 cycles. Moreover, peak-to-peak amplitudes of larger than 0.5 cycles gather primarily below a time-mean elevation angle of 30°. Larger time-mean elevation angles lead to fewer peak-to-peak amplitudes that are larger than 0.1 cycles. Furthermore, prolonging the time span from 10 to 30 minutes significantly reduces the percentage of the peak-to-peak amplitudes of larger than 0.5 cycles from 0.8% to 0.4%. Therefore, it is demonstrated that large fractional-part fluctuations are closely related to small elevation angles, and usually occur during the initial observing phase of a satellite pair; in addition, the peak-to-peak amplitude is reduced when a satellite pair begins to be observed at a high elevation. These findings are likely related to carrier-phase multipath effects, imprecise satellite clock estimates, and residual tropospheric delays at low elevations.

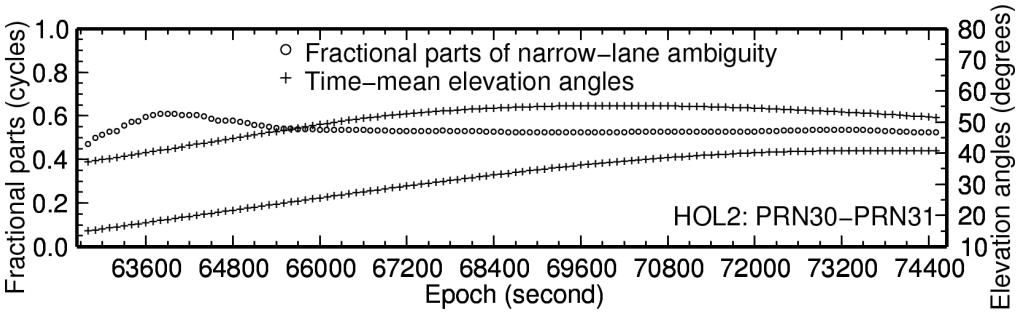

Figure 5.11: Fractional parts of a narrow-lane ambiguity between PRN30 and PRN31 at station HOL2 with the two satellites' time-mean elevation angles

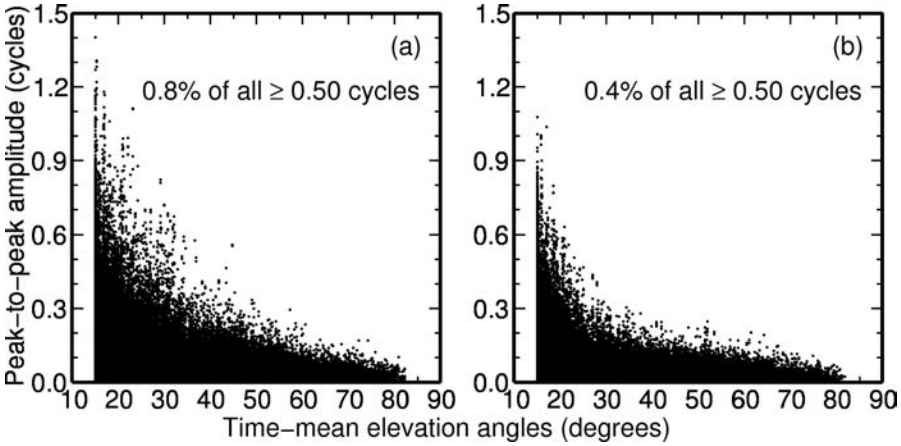

Figure 5.12: The peak-to-peak amplitudes of narrow-lane fractional parts against time-mean elevation angles. Note that all satellite pairs have been observed for 10 (a) and 30 minutes (b)

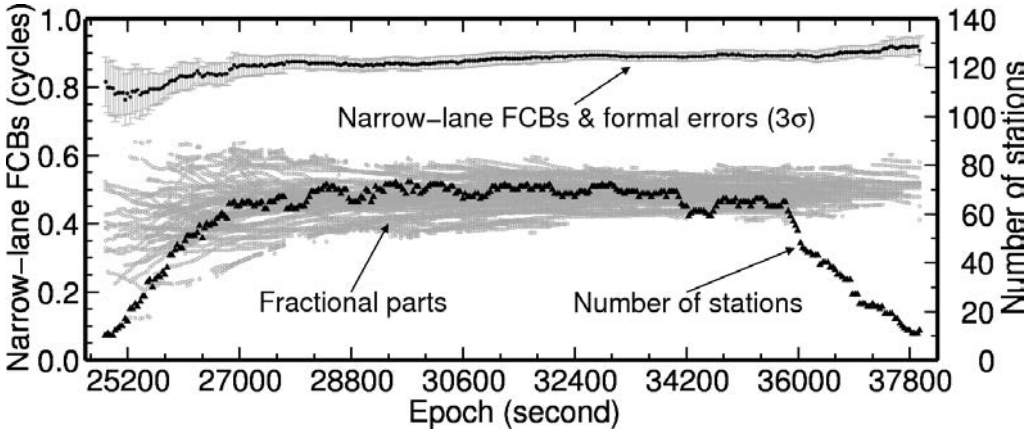

Figure 5.13: Variation of narrow-lane fractional parts and resulting FCBs over a regional network. The narrow-lane fractional parts for a satellite pair PRN02 and PRN04, the number of involved stations, and the narrow-lane FCB estimates and their formal errors of 3σ. Note that the FCB estimates are offset by 0.4 cycles, and the fractional parts refer to the left axis

B Fluctuant narrow-lane FCB estimates

Large fractional-part fluctuations can degrade the performance of averaging fractional parts. For a being-observed satellite pair, different stations generate different fractional-part fluctuations, and thus we may have to average very different fractional parts to estimate a narrow-lane FCB. As a result, both the estimate's precision and accuracy can be degraded, compared with those when fractional parts have sufficiently stabilized. Hence, we need to use a robust averaging technique (e.g. Xu 2005), and involve as many stations as possible for this averaging. In this study, at least 10 stations are required.

For instance, Figure 5.13 shows the fractional parts for a satellite pair, the number of involved stations, and the narrow-lane FCB estimates and their formal errors of 3σ every 40 s. During the initial phase, due to a satellite's rise from a low elevation with respect to my regional network, only a few stations observed this satellite pair. Consequently, large fractional-part fluctuations occur at many stations, leading to fluctuant narrow-lane FCB estimates of which the peak-to-peak amplitude is over 0.1 cycles. During the intermediate phase when several tens of stations observe this satellite pair and most fractional parts have sufficiently stabilized, highly precise and very stable narrow-lane FCB estimates can be obtained of which the peak-to-peak amplitude drops to smaller than 0.05 cycles. During the final phase, however, due to a satellite's gradual fall to a low elevation, the number of stations observing this satellite pair decreases, and thus the narrow-lane FCB estimates show slightly worse precisions and a slight fluctuation, but still within 0.05 cycles. Of particular note, large fluctuations of narrow-lane FCB estimates are mainly caused by satellites' rise from a low elevation with respect to my regional network. Hence, it is believed that a globally well-distributed network can reduce the fluctuation magnitudes.

Furthermore, if narrow-lane FCBs begin to be estimated when satellite pairs have been observed for at least 10 minutes, 69.0% of all estimates' peak-to-peak amplitudes are larger than 0.1 cycles. If the first 20-minute or 50-minute estimates are removed, this percentage will drop to 38.2% or 15.1%, respectively. Hence, for the regional network in Figure 5.10, over several tens of minutes are normally required before a narrow-lane FCB estimate stabilizes to an accuracy of far better than 0.1 cycles. Note that such high accuracy is required because narrow-lane FCBs are crucial to the ambiguity-fixed positioning accuracy. However, for ambiguity resolution only, this accuracy requirement can be relaxed to 0.25 cycles, for example. Actually, 87.9% of all peak-to-peak amplitudes are smaller than 0.25 cycles if narrow-lane FCBs begin to be estimated when satellite pairs have been observed for 10 minutes. In this case, narrow-lane FCB products can be generated and disseminated once wide-lane ambiguity resolution has been achieved. On the other hand, potential positioning biases caused by inaccurate narrow-lane FCB estimates can be mitigated in subsequent epochs by updating these estimates in ambiguity-fixed solutions. In this study, an update rate of 5 s is chosen due to the relatively rapid variation of narrow-lane FCB estimates during the initial phases.

5.6.4 Performance of narrow-lane ambiguity resolution

Once narrow-lane FCB estimates are obtained and wide-lane ambiguity resolution is achieved, narrow-lane ambiguity resolution can be attempted to achieve ambiguity-fixed solutions in real-time PPP. Considering the time spent on the narrow-lane FCB determination, the first 30 minutes of measurements are ignored at all six test stations, and the remaining data are divided into hourly files. Hence, there are about 161 hourly solutions at each test station during seven

Table 5.14: Position quality of real-time ambiguity-fixed PPP. The mean time spent on achieving ambiguity-fixed solutions, and the RMS of epoch-wise position estimates against the daily estimates for the ambiguity-float and ambiguity-fixed solutions

Station	Mean time (s)	Ambiguity-float (cm)			Ambiguity-fixed (cm)		
		East	North	Up	East	North	Up
BORR	1109	14.7	6.3	12.0	0.8	1.1	2.9
BRUS	940	12.7	7.1	11.7	0.6	0.7	1.9
BSCN	1002	17.3	7.8	12.9	0.8	0.9	2.6
MAR6	1140	10.7	8.2	9.9	0.8	0.9	2.4
SOFI	1197	16.7	6.7	11.4	0.9	0.9	2.8
WSRT	932	10.3	6.5	10.7	0.6	0.8	2.5

days. Daily position estimates are used as the ground truth to assess the accuracy of epoch-wise estimates.

Table 5.14 shows the overall statistics about the solution performance after narrow-lane ambiguity resolution at each test station. All mean times that are spent on achieving ambiguity-fixed solutions are more than 900 s, even up to 1200 s, thus confirming the results reported by Laurichesse et al. (2008a) and Mervart et al. (2008). Compared with the required 600-second period spent on wide-lane ambiguity resolution, narrow-lane ambiguity resolution significantly prolongs this period before ambiguity-fixed solutions can be achieved.

However, epoch-wise positioning accuracy is significantly improved after narrow-lane ambiguity resolution. In Table 5.14, the RMS statistics against the ground truth for the East, North and Up components are reduced on average by 94.5%, 87.6% and 78.0% from 13.7, 7.1 and 11.4 cm to 0.8, 0.9 and 2.5 cm, respectively. Moreover, Figure 5.14 shows the 1-hour differences of epoch-wise position estimates against the ground truth for the East, North and Up components in both ambiguity-float and ambiguity-fixed solutions at station BSCN. We can see that ambiguity-float positions do not converge to centimeter-level accuracy within one hour, but

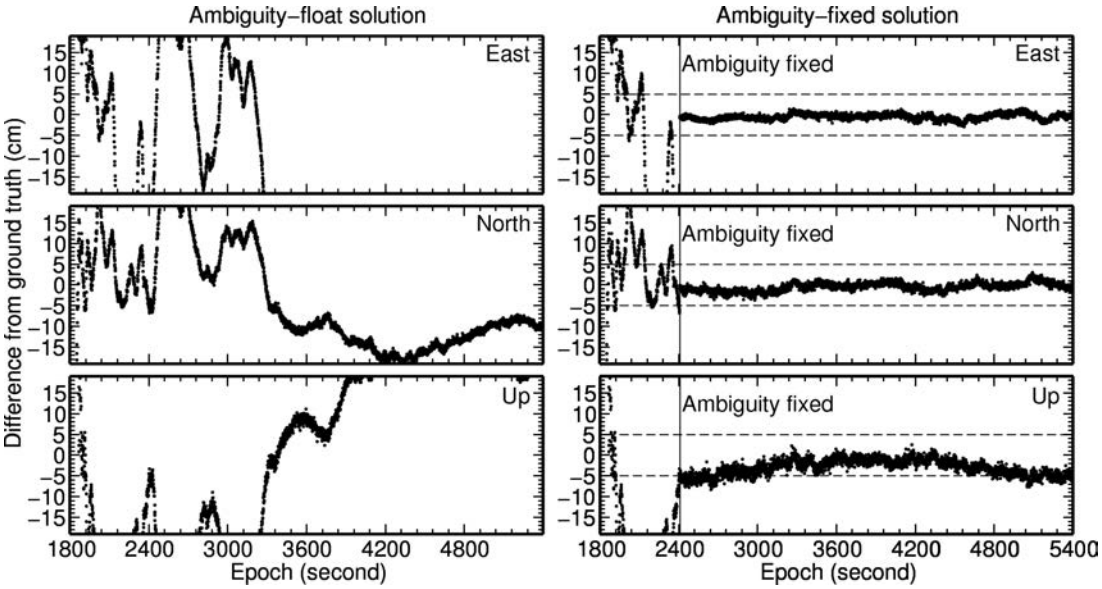

Figure 5.14: Position accuracy of real-time ambiguity-fixed PPP at station BSCN. Differences of epoch-wise position estimates against the daily estimates for the East, North and Up components in both ambiguity-float and ambiguity-fixed solutions. Note that estimates outside ±20 cm are not shown, and the three vertical lines denote the time when ambiguities are fixed

the ambiguity-fixed ones achieve this after about 600 s. Hence, according to the statistics above, it is demonstrated that ambiguity resolution can speed up the convergence to centimeter-level accuracy of epoch-wise position estimates within a few tens of minutes.

5.6.5 Conclusions

First, it is concluded that at least 10 minutes of observations are required for most receiver types to reliably fix about 90% of wide-lane ambiguities corresponding to elevations of over 15°, and over 20 minutes to fix about 90% of those corresponding to elevations of below 15°. Moreover, receivers of cross-correlation types or without choke-ring antennas require longer periods than those of others. Two thresholds, namely 10 minutes for the time span and 15° for the time-mean elevation angle, are proposed to decide when a wide-lane ambiguity can be reliably fixed.

Second, it is concluded that several tens of minutes are usually required for a regional network before a narrow-lane FCB estimate stabilizes to an accuracy of far better than 0.1 cycles. Large fluctuations of narrow-lane FCB estimates are mainly caused by satellites' rise from a low elevation with respect to a regional network. However, we can still generate and disseminate narrow-lane FCB products once wide-lane ambiguity resolution is achieved. These products are usable for ambiguity resolution, but we have to update them, every 5 s for example, in ambiguity-fixed solutions in order to achieve highly accurate position estimates.

Finally, ambiguity-fixed solutions with centimeter-level positioning accuracy can be achieved within a few tens of minutes. For hourly measurements, ambiguity resolution significantly reduces the RMS statistics of differences between the epoch-wise and daily position estimates from 13.7, 7.1 and 11.4 cm to 0.8, 0.9 and 2.5 cm on average for the East, North and Up components, respectively.

For the PPP-RTK model in Section 2.4.3, 10 minutes for wide-lane resolution of high-elevation ambiguities, 10 minutes for narrow-lane FCB generation and 5-second update rate are all acceptable at the server end. However, 10 minutes for wide-lane ambiguity resolution and even longer period for narrow-lane ambiguity resolution constitute the technical bottleneck which prohibits many real-time users who require instantaneous precise positioning from applying this PPP-RTK model. However, this model is still useful in some remote sensing applications where the timeliness requirement on the first ambiguity-fixed solution is not as critical as that in the instantaneous positioning, such as the near-real-time GPS meteorology. For future technical development, rapid ambiguity resolution at a single receiver will be the key problem to be resolved before we can implement an instantaneous PPP-RTK model where ambiguity-fixed solutions can be achieved using a few seconds or even one second of measurements.

5.7 Impact of integer double-difference constraints

As suggested in Section 2.4.4, hard constraints from integer double-difference ambiguities in a network solution can improve the accuracy of narrow-lane FCB estimates, which is beneficial for the positioning accuracy of ambiguity-fixed PPP. This section thus aims at quantifying the impacts of such constraints.

5.7.1 Data, models and methods

One year of daily GPS data at about 350 globally-distributed reference stations from the IGS permanent network in 2008 were used (Dow et al. 2009). Data files covering less than 6 hours of measurements were removed. Moreover, CODE final satellite orbits, 30-s satellite clocks, ERPs and P1-C1 DCBs were used (Dach et al. 2009). Note that using CODE satellite products, rather than IGS ones, is to avoid the possible inhomogeneities of the IGS final products which can degrade the positioning quality of PPP (Teferle et al. 2007).

For data modeling, the absolute phase centers (Schmid et al. 2007), phase-wind up effects (Wu et al. 1993) and station displacement models proposed by IERS conventions 2003 (McCarthy and Petit 2004) were applied. A cut-off angle of 7° was set for usable measurements and an elevation-dependent weighting strategy was applied to measurements at low elevations (Gendt et al. 2003). Moreover, ZTDs were estimated every one hour by applying the global pressure/temperature model and the global mapping function (Kouba 2009b), while horizontal tropospheric gradients every 12 hours (Bar-Sever et al. 1998).

CODE satellite products and ERPs were fixed during the data processing and about 180 globally-distributed stations were selected to estimate FCBs. According to Ge et al. (2008), narrow-lane FCBs were computed every 15 minutes. Then these FCBs were applied to all 350 stations in order to achieve ambiguity-fixed daily solutions. In this section, the narrow-lane FCBs that are derived by applying the double-difference ambiguity resolution are named as improved narrow-lane FCBs, and those otherwise as original narrow-lane FCBs.

5.7.2 Results

The original and improved narrow-lane FCB estimates are first compared. Daily RMS statistics of narrow-lane FCB differences for all satellite pairs at all 15-minute time spans are computed. All daily RMS statistics range from 0.021 to 0.089 cycles and the mean RMS of one year is about 0.035 cycles. These small differences are due to the highly-accurate daily ambiguity estimates even if double-difference ambiguity resolution is not applied.

Moreover, the daily position estimates based on the original and improved narrow-lane FCBs are also compared. Figure 5.15 shows the magnitude distribution of all these position

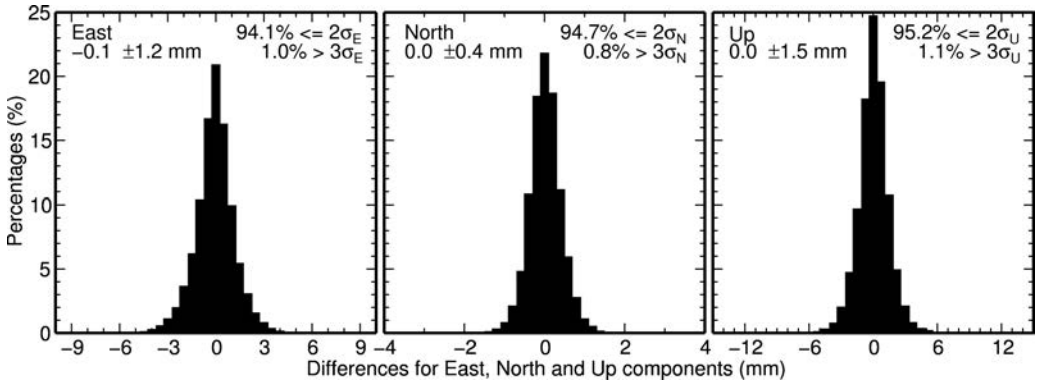

Figure 5.15: Magnitude distribution of all differences between the position estimates based on the original and improved narrow-lane FCBs for the East, North and Up components. The top-left corner of each subfigure shows the bias and the standard deviation (σ), whereas the top-right corner shows the percentages of deviations that are within 2σ, or larger than 3σ (σ_E=1.2 mm, σ_N=0.4 mm and σ_U=1.5 mm). Note that the three subfigures have different horizontal scales

Table 5.15: Mean RMS of transformed residuals of the daily position estimates against the IGS weekly solutions in 2008

Solution types	East	North	Up
Ambiguity-float	3.6	2.3	6.4
Ambiguity-fixed by original narrow-lane FCBs	2.6	2.2	6.1
Ambiguity-fixed by improved narrow-lane FCBs	2.2	2.2	6.1

differences for the East, North and Up components. We can see that the absolute biases of these position differences are not larger than 0.1 mm for all three components. Correspondingly, the standard deviations are 1.2, 0.4 and 1.5 mm for the East, North and Up components, respectively. Furthermore, 94.1%, 94.7% and 95.2% of all position differences are within two times the standard deviations for the three components, and minimally 1.0%, 0.8% and 1.1% of all are larger than three times the standard deviations. These statistics illustrate the small difference between the daily ambiguity-fixed position estimates based on the original and improved narrow-lane FCBs.

Nevertheless, the improvement of the positioning quality based on the improved narrow-lane FCBs can be identified when these daily position estimates are compared with the IGS weekly solutions. Seven-parameter Helmert transformations are applied during these daily comparisons. Table 5.15 shows the mean RMS statistics of the transformed residuals of the daily position estimates against the IGS weekly solutions in 2008. We can see that ambiguity resolution significantly reduces the RMS statistics, especially for the East component by 27.8%, hence confirming the results by Ge et al. (2008). After double-difference ambiguity resolution is applied to the network solution, the resulting narrow-lane FCB estimates contribute to a further reduction of the RMS statistics for the East component by 0.4 mm, although the RMS statistics for the North and Up components remain the same.

In addition, Figure 5.16 shows the RMS of the transformed residuals of the daily position estimates against the IGS weekly solutions for the East component. We can clearly find the RMS reduction led to by ambiguity resolution at a single receiver. Moreover, we can also easily identify the smaller further RMS reduction due to the improved narrow-lane FCBs. Specifically, almost on each day of the year, the RMS based on the improved narrow-lane FCBs is smaller than that based on the original narrow-lane FCBs. This result clearly demonstrates the improvement

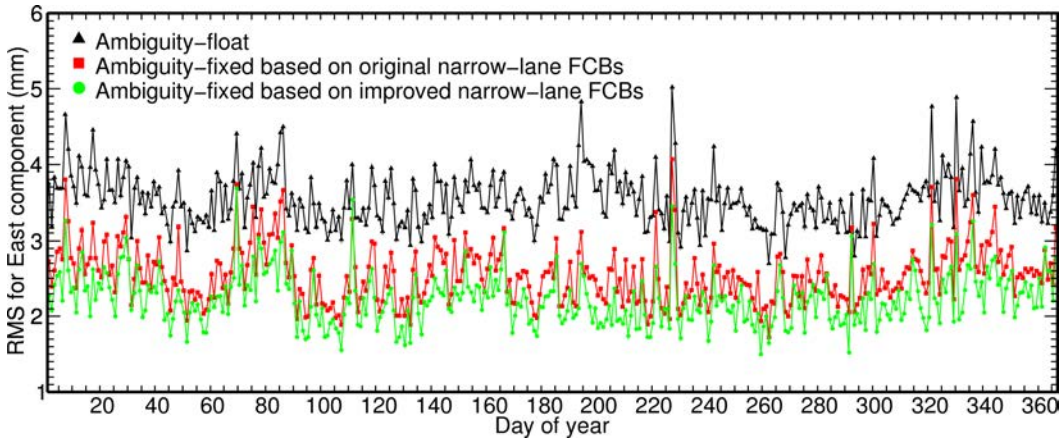

Figure 5.16: Daily RMS of transformed residuals of the position estimates against the IGS weekly solutions for the East component in 2008

of the positioning quality contributed by applying double-difference ambiguity resolution to narrow-lane FCB determination.

5.8 Comparison between FCB- and IRC-based methods

As discussed in Section 2.3, the ambiguity-fixed position estimates from the FCB- and IRC-based methods are theoretically identical. However, pronounced differences, especially in how to separate FCBs from integer ambiguities in a network solution, are still present between the two methods (refer to Section 2.3.4). Hence, this section compares the daily position estimates derived from these two methods in order to investigate how the two methods agree or differ in their ambiguity-fixed solutions. Note that the innovation of integer double-difference constraints in Section 2.4.4 has been applied to the FCB-based method.

5.8.1 Data, models and methods

Data and models refer to Section 5.7.1. For data processing, ambiguity-float daily position estimates were first obtained by fixing the CODE products. To keep consistency between the CODE products and the PANDA software, the satellite clocks were re-estimated in the FCB-based method by fixing the satellite orbits, the ERPs and the CODE-based ambiguity-float positions. These new satellite clocks were then fixed along with the satellite orbits and the ERPs to estimate the 15-minute mean narrow-lane FCBs using a global network of about 180 stations, most of which were located in Europe and North America. Finally, these FCB estimates were used at all 350 stations to fix ambiguities between satellites to integers. On the other hand, in the IRC-based method, the positions of the above 180 stations were fixed to the CODE-based ambiguity-float estimates in order to keep consistency between the reference frames of the FCB-based and IRC-based methods. Based on this, the IRCs were estimated after fixing ambiguities to integers. Finally, these IRC estimates were used at all 350 stations to perform the ambiguity resolution. Note that ambiguity resolution were based on the bias-rounding strategy by Ge et al. (2005a) under a round-off criterion of 0.2 cycles.

5.8.2 Position differences

Assessing the differences between the position estimates can directly illustrate to what extent these two methods agree in their positioning results. For each station, ambiguity-fixed position differences were computed between the two methods over one year, and outliers were removed with a threshold of five times the standard deviations. Finally, less than 0.1% of daily estimates were removed. The RMS statistics of all position differences for all stations are only 1.3, 0.8 and 2.0 mm for the East, North and Up components, respectively. These statistics are well below the formal precisions of 1.8–2.0 mm for the horizontal components and 5.0 mm for the vertical component which were reported for the IGS weekly solutions (Altamimi and Collilieux 2009), implying that the position differences are actually minimal. Furthermore, Figure 5.17 shows the magnitude distribution of more than 100,000 position differences for all stations on all days. The biases are only 0.2, 0.1 and 0.0 mm, whereas the standard deviations are 1.3, 0.8 and 2.0 mm for the East, North and Up components, respectively. Hence, the systematic biases between the daily position estimates of these two methods are actually minimal, or even negligible. In addition, about 94.7% in the East, 94.7% in the North and 95.2% in the Up components of all

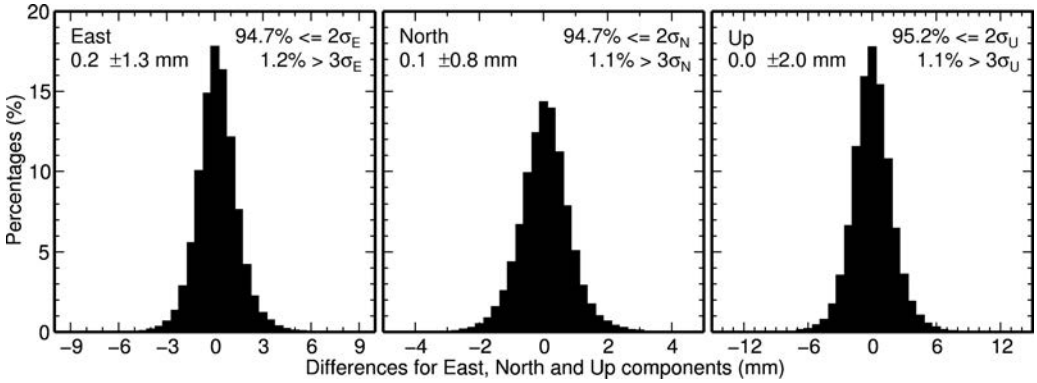

Figure 5.17: Magnitude distribution of all position differences between the FCB-based and the IRC-based methods for the East, North and Up components. The top-left corner of each subfigure shows the bias and the standard deviation (σ), whereas the top-right corner shows the percentages of deviations that are within 2σ, or larger than 3σ (σ_E=1.3 mm, σ_N=0.8 mm and σ_U=2.0 mm). Note that the three subfigures have different horizontal scales

deviations in Figure 5.17 are within two times the standard deviations. Therefore, these overall good agreements verify the theoretical equivalence of the ambiguity-fixed position estimates derived from the two methods.

Nonetheless, large position differences are still present at some stations. For instance, the absolute differences can be up to 10 mm for the East, 6 mm for the North and 20 mm for the Up components. Moreover, 1.2% in the East, 1.1% in the North and 1.1% in the Up components of all differences exceed three times the standard deviations as shown in Figure 5.17. Those stations with large position differences are usually located at oceanic islands like Hawaii and Tahiti. Hence, the RMS statistics of the position differences over one year are shown for the East component at each station using color scales on a global map (Figure 5.18). We can see that, in Europe and North America with relatively-dense networks of reference stations, the

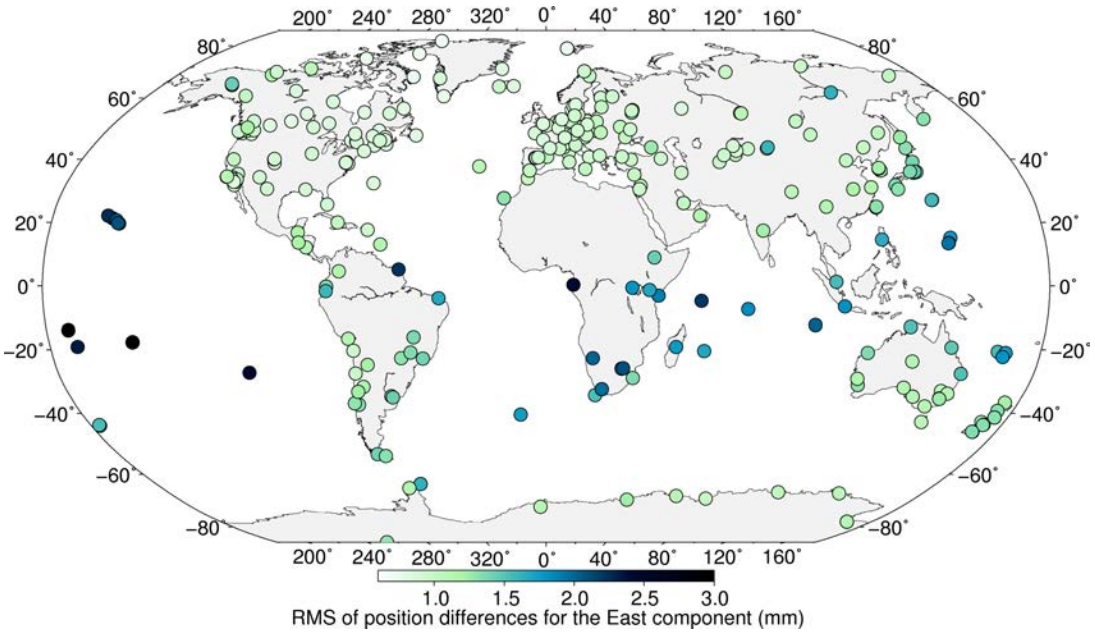

Figure 5.18: Geographical distribution of the station-specific RMS statistics of the position differences over one year between the FCB- and IRC-based methods for the East component

RMS statistics are well below 1.5 mm, whereas in oceanic areas and Africa with very sparse networks, the RMS statistics are usually over 2.0 mm. This geographical-distribution pattern can also be observed for the North and Up components (see Figure A.1 and A.2 in Appendix "Method Comparison"). This finding can be attributed to two aspects. On the one hand, the narrow-lane FCBs cannot be precisely determined or assimilated into clocks over a sparse network because the spatial correlation of errors among the reference stations is very weak. In this case, the difference of separating narrow-lane FCBs from integer ambiguities may amplify the position differences between these two methods. On the other hand, compared with the epoch-wise IRCs, 15-minute mean estimates may lead to degraded accuracies of narrow-lane FCBs.

5.8.3 Position repeatability

Position repeatability can quantitatively reflect the intrinsic positioning quality of these two methods. The position repeatability was generated by deducting a linear model from each station-specific positions over one year and then computing the RMS statistics of the resulting residuals. Outlier rejection was performed by a threshold of five times the standard deviations. Overall, the mean repeatability of all stations is 2.4, 2.2 and 7.7 mm for the FCB-based method, and 2.2, 2.3 and 7.6 mm for the IRC-based method for the East, North and Up components respectively. Hence, the repeatability differences are within only 0.2 mm for all three components which is minimal compared with the repeatability statistics themselves, further verifying the theoretical equivalence of the ambiguity-fixed position estimates derived from these two methods.

Nonetheless, these two methods perform geographically differently for the East repeatability. Figure 5.19 exhibits the East repeatability of the FCB-based method minus that of the IRC-based method for all stations. Hence, positive values in Figure 5.19 mean that the IRC-based method outperforms the FCB-based method. We can see that the FCB-based method performs relatively better in Europe, whereas the IRC-based method performs better in oceanic areas

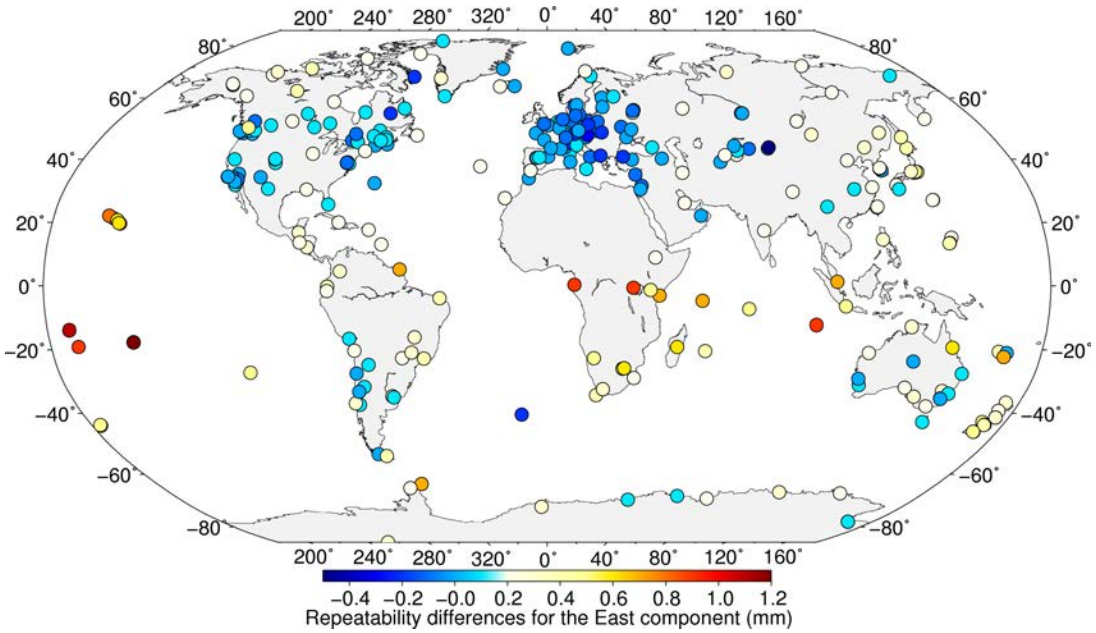

Figure 5.19: Geographical distribution of the station-specific position repeatability of the FCB-based method minus that of the IRC-based method for the East component over one year

like the Pacific and the Indian Ocean. Considering the same models used in both methods, this geography-related performance can be attributed to the reference network density which affects the performance of separating the FCBs from integer ambiguities. In other words, the FCB-based method performs better over a relatively dense network whereas the IRC-based method performs better over a sparse network. However, the IRC-based method can usually perform better by over 0.5 mm, whereas the FCB-based method performs better by less than 0.5 mm, explaining why the IRC-based method overall slightly outperforms the FCB-based method for the East repeatability.

Of particular note, the geographical-distribution pattern of the repeatability differences cannot be observed for the North and Up components (see Figure A.3 and A.4 in Appendix "Method Comparison"). Normally, the positioning qualities of the North and Up components are less affected by ambiguity resolution than that of the East component (e.g. Blewitt 1989; Ge et al. 2008), which might explain why similar geographical distributions cannot be easily observed for the North and Up components.

5.8.4 Comparison with the IGS weekly solutions

In this study, my daily position estimates were compared with the IGS weekly solutions through a 7-parameter Helmert transformation. The position estimates of which the transformed residuals are larger than 15 mm for the horizontal, 30 mm for the vertical components, or five times the standard deviations were removed. RMS statistics of the transformed residuals are used to quantitatively assess the extrinsic positioning quality. Table 5.16 shows the mean RMS statistics of all days for the ambiguity-float and ambiguity-fixed solutions. In this table, ambiguity resolution with the FCB-based method significantly improves the RMS statistics from 3.4, 2.2 and 6.2 mm to 2.0, 2.1 and 5.9 mm for the East, North and Up components respectively, thereby confirming the results reported by Ge et al. (2008). Likewise, ambiguity resolution with the IRC-based method improves the RMS statistics from 3.5, 2.3 and 6.3 mm to 1.9, 2.1 and 5.8 mm. Hence, the RMS difference for the ambiguity-fixed position estimates is within only 0.1 mm for each component which is negligible compared with the RMS statistics themselves, again verifying the theoretical equivalence of the ambiguity-fixed position estimates derived from these two methods.

Nonetheless, the IRC-based method performs slightly better for the East component. Figure 5.20 shows the daily RMS statistics for the East component of the ambiguity-fixed position estimates. Although the RMS statistics of the two methods are close, it is still discernible that the IRC-based statistics are slightly smaller than the FCB-based statistics on most days. Furthermore, the RMS statistics of the transformed ambiguity-fixed residuals are computed over all days at each station. Figure 5.21 exhibits the East RMS statistics of the FCB-based method minus those of the IRC-based method for each station. We can see that the FCB-

Table 5.16: Mean RMS statistics of the transformed residuals of the daily ambiguity-float and ambiguity-fixed position estimates against the IGS weekly solutions in 2008

Methods	Ambiguity-float (mm)			Ambiguity-fixed (mm)		
	East	North	Up	East	North	Up
FCB-based	3.4	2.2	6.2	2.0	2.1	5.9
IRC-based	3.5	2.3	6.3	1.9	2.1	5.8

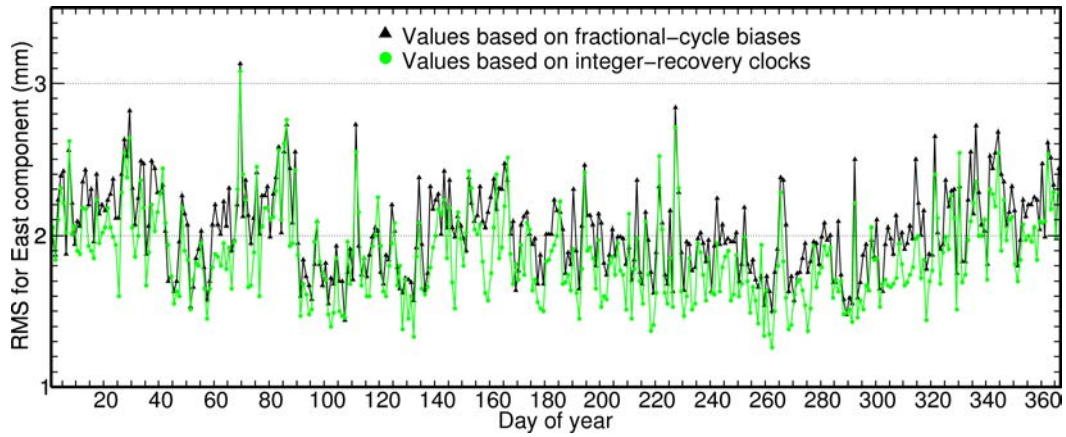

Figure 5.20: Daily RMS of the transformed residuals of the ambiguity-fixed position estimates against the IGS weekly solutions for the East component in 2008

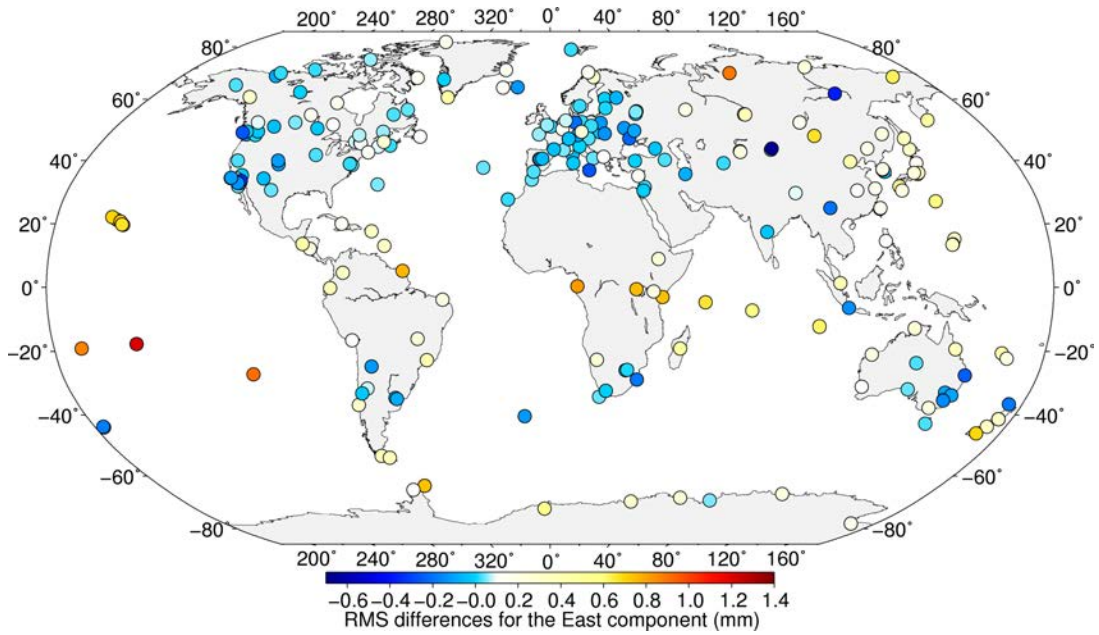

Figure 5.21: Geographical distribution of the station-specific East RMS for the FCB-based method minus that for the IRC-based method. An RMS is computed over the residuals of ambiguity-fixed position estimates against the IGS weekly solutions for the East component over one year

based method performs relatively better in Europe and North America, whereas the IRC-based method performs better in oceanic areas and Africa. However, the IRC-based method can usually perform better by up to 1.4 mm, whereas the FCB-based method performs better by less than 0.7 mm. Hence, the IRC-based method overall slightly outperforms the FCB-based method in the East RMS against the IGS weekly solutions. In addition, similar to Figure 5.19, this geographical-distribution pattern cannot be observed for the North and Up components (see Figure A.5 and A.6 in Appendix "Method Comparison").

5.8.5 Conclusions and suggestions

In order to verify the equivalence between the ambiguity-fixed position estimates derived from the two methods, ambiguity-fixed daily position estimates were computed using both methods with the data from a global network of about 350 reference stations over the whole year 2008. The biases between all position estimates are only 0.2, 0.1 and 0.0 mm, whereas the standard deviations of all position differences are only 1.3, 0.8 and 2.0 mm for the East, North and Up components, respectively. Moreover, the differences of position repeatabilities are within only 0.2 mm on average for all three components. The RMS of the position estimates minus those from the IGS weekly solutions for the FCB-based method differs by below 0.1 mm on average for each component from that for the IRC-based method. Hence, the systematic biases between the daily position estimates are actually minimal, or even negligible, and the closeness of the position estimates, repeatabilities and RMS statistics against the IGS weekly solutions overall verify the equivalence of the ambiguity-fixed position estimates derived from the FCB-based and IRC-based methods.

Nonetheless, the different strategies of separating the narrow-lane FCBs from integer ambiguities in these two methods lead to the geographical-distribution patterns of their positioning discrepancy. For instance, for the East component, the station-specific RMS statistics of the position differences are well below 1.5 mm in Europe and North America with relatively-dense networks, whereas usually over 2.0 mm in oceanic areas and Africa with very sparse networks. Moreover, in terms of the East position repeatability and the East RMS statistics against the IGS weekly solutions, the FCB-based method performs slightly better over dense networks, whereas the IRC-based method performs a little better over sparse networks. Overall, the IRC-based method overall slightly outperforms the FCB-based method for the East component.

Finally, I propose that these two methods should be used in terms of different task constraints. The FCB-based method can conveniently supplement current network solutions as an additional software module, and its narrow-lane FCB determination is compatible with current official clock-generation methods. By contrast, the IRC-based method employs IRCs which are incompatible with current clock products. However, using IRCs is straightforward for ambiguity resolution at a single receiver and the IRC-based method can potentially perform slightly better in practice.

5.9 Summary

This chapter quantitatively assesses the positioning quality of post-processing and real-time PPP enhanced by ambiguity resolution at a single receiver. Based on a regional network in Europe, ambiguity resolution clearly improves the positioning qualities of sub-daily and kinematic PPP.

Ambiguity resolution can be performed even at a remote receiver that is far from the FCB-determination network. Moreover, narrow-lane FCBs are strongly correlated with satellite clocks, and hence they should be kept compatible before they are used together for ambiguity resolution. On the other hand, real-time PPP also benefits from ambiguity resolution because its positioning accuracy can be significantly improved. However, its practicability is devalued by its slow convergence to ambiguity-fixed solutions. Finally, the theoretical equivalence between the ambiguity-fixed position estimates derived from the FCB- and IRC-based methods was verified by processing one year of GPS data, with the IRC-based method shown to lead to a better positioning quality over sparse networks.

Chapter 6

Results on Rapid Convergences

6.1 Introduction

Chapter 3 has summarized the previous published attempts for accelerating convergences in real-time PPP. Due to the difficulty of achieving the first ambiguity-fixed solution with only a few seconds of GPS measurements, in this thesis, a method for rapidly accelerating re-convergences to ambiguity-fixed solutions by precisely predicting ionospheric delays that are estimated in all ambiguity-fixed epochs is originally developed. The effectiveness of this novel method consists in two aspects: On the one hand, wide-lane ambiguities can be rapidly resolved with the ionosphere-corrected wide-lane measurements, instead of the noisy Melbourne-Wübbena combination measurements; on the other hand, narrow-lane ambiguity resolution can be accelerated significantly under the tight constraints derived from ionosphere-corrected unambiguous wide-lane measurements. This chapter thus assesses this method with 1-Hz measurements from static and mobile receivers. In addition, rapid convergence by interpolating ionospheric delays from a dense network of reference stations is also assessed before ending this chapter. Note that a "convergence" in this chapter implies a "convergence to an ambiguity-fixed solution".

6.2 Prediction error of ionospheric delays

As discussed in Section 3.4, the accuracy of predicted ionospheric delays is crucial to rapid re-convergences. This section thus assesses the prediction error of ionospheric delays in Europe typically when the ionosphere condition is relatively quiet.

6.2.1 Data, models and methods

One-Hz GPS measurements from stations BSCN (47.25°N, 5.99°E) and ACOR (43.36°N, 8.40°W) on July 6th 2008 and from station MUEJ (48.15°N, 11.57°E) on October 11th 2008 were used. These stations were chosen as representatives of stations located in Europe. The Kp index, which quantifies the ionosphere activity level, was below 4 on July 6th, showing a moderate ionosphere condition, and about 4 on October 11th, showing a relatively active ionosphere condition. In addition, predicted satellite orbits and ERPs by the IGS were fixed when estimating real-time satellite clocks.

Ionospheric delays were estimated with single-difference wide-lane measurements in Equation 3.17. Station positions were corrected for displacements suggested in IERS conventions 2003

(McCarthy and Petit 2004). Absolute antenna phase centers were also applied. Wide-lane ambiguities were estimated with Melbourne-Wübbena combination measurements and resolved with bias rounding under a round-off criterion of 0.25 cycles. Ambiguity-fixed PPP was carried out in order to mitigate tropospheric delays in wide-lane measurements. Note that such ionospheric delays contain not only the real delays caused by ionosphere, but also some residual errors associated with hardware biases, tropospheric delays, multipath effects, etc. These residual errors are ignored in this section due to their relatively negligible variation characteristics compared with those of ionosphere (refer to Section 3.4.1).

6.2.2 Variation characteristics of ionospheric delays

The prediction error of an ionospheric delay is subject to both the latency and the elevation angle. Note that the latency of a predicted ionospheric delay is the time span between this predicted delay and the latest estimated delay, and the prediction error of a predicted delay is its difference from the estimated delay at this epoch. Figure 6.1 shows the prediction errors of ionospheric delays under different latencies, i.e. 20, 60 and 120 s. Elevation angles for four satellite pairs at station BSCN, five at station MUEJ, and the planetary 3-hourly Kp indices on July 6th and October 11th are also shown. Here, the elevation angle of a satellite pair is defined as the elevation angle of the lower satellite. Stations BSCN and MUEJ are chosen as representatives due to both stations being located in central Europe. Note that these prediction errors here are actually the differences of estimated ionospheric delays at two epochs.

In Figure 6.1a, the prediction errors for the 60-second latency are somewhat noisier than those for the 20-second one. When the latency is increased to 120 s, oscillations, bending and biasing of the error time series are apparent which can be attributed to the irregularities of temporal ionospheric variations. Such an increase of prediction errors is more obvious in Figure 6.1b when the ionosphere condition is relatively more active. It is evident that prediction errors become larger and larger when latency is increased from 20 to 120 s. Hence, Dai et al. (2003) and Kashani et al. (2007) suggested that the weight of a predicted ionospheric delay should be inversely proportional to its latency.

Moreover, in Figures 6.1a and 6.1b, the prediction errors of ionospheric delays are larger when elevation angles are smaller, as the predicted ionospheric delays vary more irregularly and rapidly at low elevations. Consequently, neither the constant bias model nor the linear bias model (refer to Section 3.4.1) can sufficiently precisely predict ionospheric delays, and thus the weights at low elevations have to be reduced. Therefore, Equation 3.18 is adopted in this thesis.

6.2.3 Constant bias or linear fitting model?

Figure 6.2 exhibits the ionospheric delays at a typical station ACOR on July 6th. These delays are divided into two groups with an elevation angle of 30°, and the RMS of their prediction errors for all satellite pairs during 24 hours is plotted against both the latency and the time window width for the linear fitting model. As expected, the RMS is increased when the latency is prolonged. However, enlarging the time window width can slow down this increasing rate. As a large window width will lower the computation efficiency, a width of 120 s is finally chosen as a trade-off for ionospheric delays above 30°, and 240 s for those below 30° in this study. Specifically, 5-minute prediction can reach an accuracy of 3.7 cm for the ionospheric delays over 30° and 7.3 cm for those below 30°. Furthermore, in this study, the prediction error remains

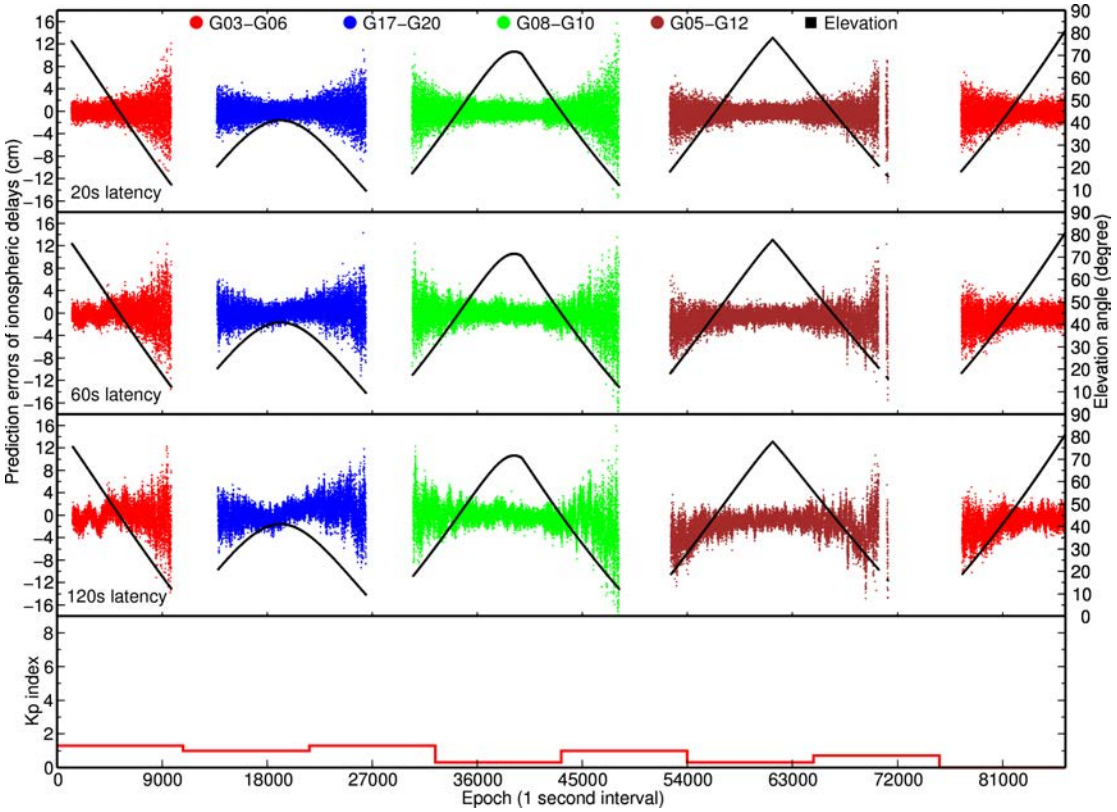

(a) Station BSCN on 06/07/2008. Note that the satellite-pair G03-G06 passed BSCN twice

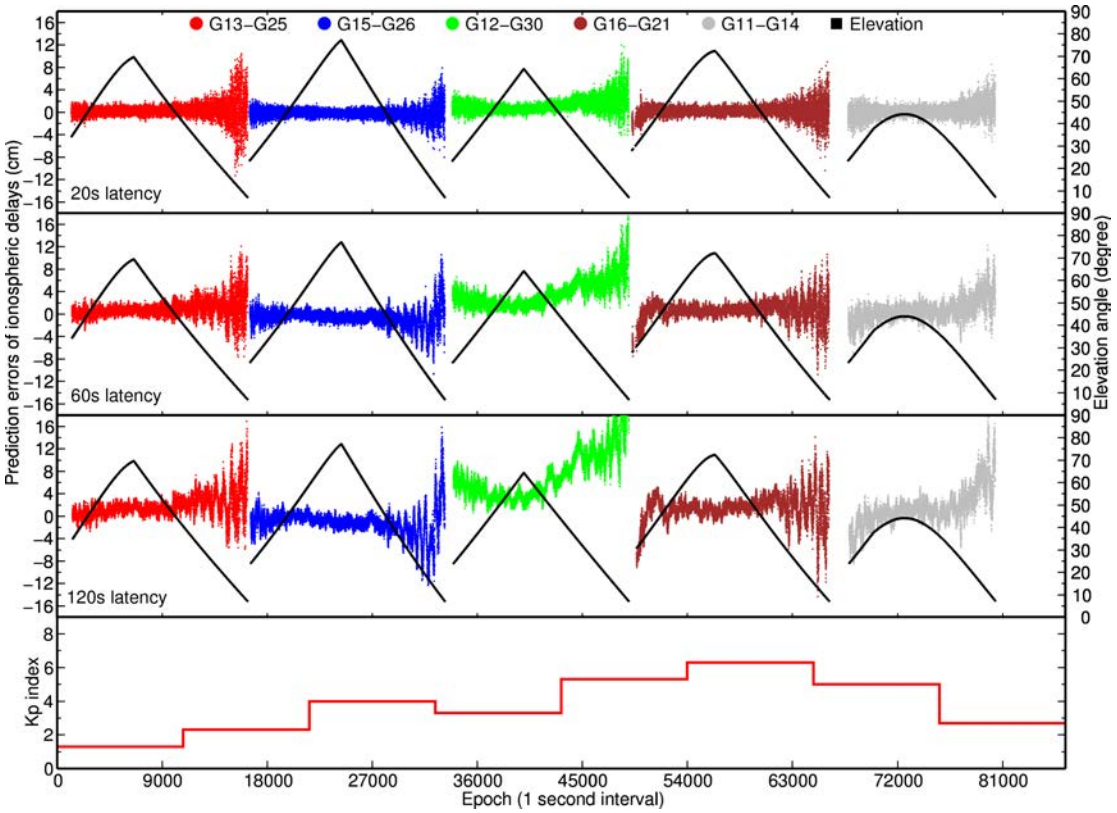

(b) Station MUEJ on 11/10/2008

Figure 6.1: Variation characteristics of ionospheric delays over Europe when ionosphere condition is relatively quiet. Prediction errors of ionospheric delays under different time latencies (20, 60 and 120 s) and different elevation angles. Planetary Kp index is shown every three hours. Note that these errors are actually the differences of estimated ionospheric delays at two epochs. The gap between these two epochs is named as latency

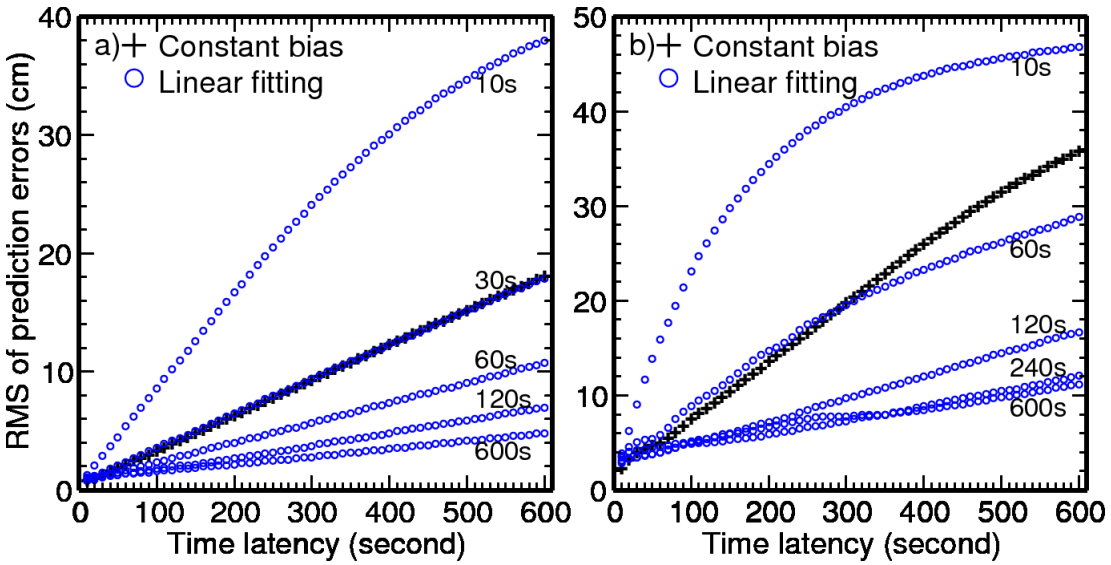

Figure 6.2: RMS of prediction errors of the ionospheric delays under different time window widths, latencies and elevation angles. Time window widths are plotted alongside the open circles. Subfigure a) shows ionospheric delays at elevation angles of $>30°$ and b) $\leqslant 30°$. Two predicting strategies are shown, i.e. the constant bias model (black crosses) and the linear fitting model (blue circles). Note the overlap between the prediction errors by the constant bias model and the linear fitting model with a 30-second window in the left subfigure

steady when the latency is below 30 s, hence explaining why identical weights are posed within 30 s in Equation 3.19. Finally, Figure 6.2 also presents the prediction error by the constant bias model. Surprisingly, the linear fitting model does not always outperform the constant bias model. For example, a 10-second window leads to larger prediction errors than those by the constant bias model for all time latencies that are up to 10 minutes. One possible reason for this is that a window of only a few tens of seconds cannot precisely image the overall tendency of the ionospheric delays. In this study, when the window width covers only the latest 30 or fewer seconds of ionospheric delays, the constant bias model is preferred to the linear fitting model.

6.3 Test rapid re-convergences with static stations

This section assesses the method for rapid re-convergences developed in Section 3.4. Static receivers were used to simulate mobile ones in order to quantify the impacts of latency on the method performance, e.g. the success rate of rapid re-convergences and the time spent on re-achieving ambiguity-fixed solutions.

6.3.1 Data, models and methods

Seven days of 24-hour 1-Hz GPS data from July 6th to 12th and on October 11th 2008 at about 90 stations across Europe were collected from the EUREF-IP project and the OSGB real-time network (Figure 5.10). These data bear the gaps caused by communication or power interruptions. Predicted satellite orbits and ERPs by the IGS were fixed during the real-time satellite clock determination. Communication delays of satellite clocks were presumed nonexistent in this simulated real-time test.

Moreover, P1-C1 DCBs, absolute antenna phase centers, phase wind-up corrections and

station displacements from the IERS conventions 2003 (McCarthy and Petit 2004) were applied. A cut-off angle of 7° for usable measurements was used (Gendt et al. 2003). For ambiguity resolution, the LAMBDA method was used to search for integer candidates. All available satellites above an elevation angle of 7° were used for wide-lane ambiguity resolution, and the satellites above 15° for narrow-lane ambiguity resolution. A partial search technique was also applied to avoid biased ambiguity estimates due to measurements from low-elevation satellites, for example (Dai et al. 2007), but at least four ambiguities should be fixed after an ambiguity search.

For all stations, positions were estimated as white noise at each epoch, and ZTDs were estimated every three hours. In order to test my method for rapid re-convergences, a total signal interruption was introduced 20 minutes after each successful convergence, and thus each station suffered from about 70 re-convergences per day, if there were no large data gaps. After each total signal interruption, a number of epochs of measurements were removed to simulate a latency for predicted ionospheric delays. This data set was quite representative for mid-latitude regions during moderate ionosphere conditions because it covered 24 hours per day and contained stations working in different environments.

6.3.2 Performance of rapid re-convergences

This section shows the impacts of precisely predicted ionospheric delays on the success rate of rapid re-convergences and the time spent on these re-convergences. Table 6.1 shows the statistics about rapid re-convergences achieved within five epochs of 1-Hz measurements under different latencies. When the latency is 10 s, 99.4% and 98.7% of re-convergences to wide-lane and narrow-lane ambiguity resolutions can be rapidly achieved, respectively. Even when the latency is up to 180 s, these two percentages can still reach 93.3% and 95.0%. For comparison, if precisely predicted ionospheric delays are not applied, only 78.9% of all re-convergences can be achieved within 20 minutes with a mean time of 694 s. Hence, the improvement on the re-convergence efficiency by my method is encouragingly significant.

However, when the latency is up to 300 s, the above two percentages steadily fall to 85.8% and 89.4%. This deterioration can be understood in terms of the amplified prediction error

Table 6.1: Performance of rapid re-convergences within five epochs of 1-Hz measurements under different latencies (s). A "success rate" is the ratio (within parentheses) between the number (before slashes) of rapid resolutions and the total number (behind slashes) of resolutions for wide-lane or narrow-lane ambiguities. A "time to fix" is the real-valued mean of all times (s) spent on resolving wide-lane or narrow-lane ambiguities. Note that one second here represents one epoch of measurements, and the time to fix a narrow-lane ambiguity begins to be measured when the corresponding wide-lane ambiguity is successfully resolved

Latency	Wide-lane resolution		Narrow-lane resolution	
	Success rate (%)	Time to fix	Success rate (%)	Time to fix
10	36459/36665 (99.4)	1.00	36159/36618 (98.7)	0.02
30	35236/35822 (98.4)	1.01	35223/35720 (98.6)	0.02
60	33782/34632 (97.5)	1.02	33860/34472 (98.2)	0.03
120	31003/32333 (95.9)	1.03	31011/32060 (96.7)	0.05
180	28060/30070 (93.3)	1.05	28024/29500 (95.0)	0.09
240	25134/28024 (89.7)	1.10	25058/27088 (92.5)	0.12
300	22417/26137 (85.8)	1.17	21875/24465 (89.4)	0.15

of ionospheric delays. From Equation 3.20, ionospheric delays of large prediction errors will enlarge the magnitude of ζ_{wi}^{kl}, hence possibly biasing the corresponding wide-lane ambiguity estimates and degrading the reliability of ambiguity resolution. Furthermore, even if a rapid wide-lane ambiguity resolution can be achieved, a large ζ_{wi}^{kl} will lead to a poor precision of an unambiguous wide-lane measurement (see Equation 3.21), hence weakening the resulting constraint on subsequent narrow-lane ambiguity resolution. Finally, when the latency is only 10 s, the failure rates for wide-lane and narrow-lane resolutions account for 0.6% and 1.3% respectively, most of which are caused by low satellite availability and poor satellite geometry.

On the other hand, Table 6.1 also shows the mean times to resolve wide-lane and narrow-lane ambiguities. When the latency is 10 s, only one epoch of measurements is required to resolve wide-lane ambiguities, whereas almost no more epochs are required to resolve narrow-lane ambiguities. Overall, increasing the latency will lead to longer time spent on achieving an ambiguity-fixed solution. However, these times are increased moderately or even minimally, implying that most rapid re-convergences are achieved with only one epoch of measurements, even though the latency is up to 300 s. In fact, this finding demonstrates that the contribution of satellite-geometry change to rapid re-convergences is minimal, or even negligible, in this study.

In order to further demonstrate the performance of rapid re-convergences, Figure 6.3 shows the epoch-wise position differences from the daily estimates for the East, North and Up components at station ACOR on July 6th. For clarity, only the first six hours of differences are presented. In this figure, three sub-figures show the position differences for the ambiguity-float solutions, ambiguity-fixed solutions without rapid re-convergences and ambiguity-fixed solutions with rapid re-convergences. At the beginning of this data set, a large gap occurs, which fails

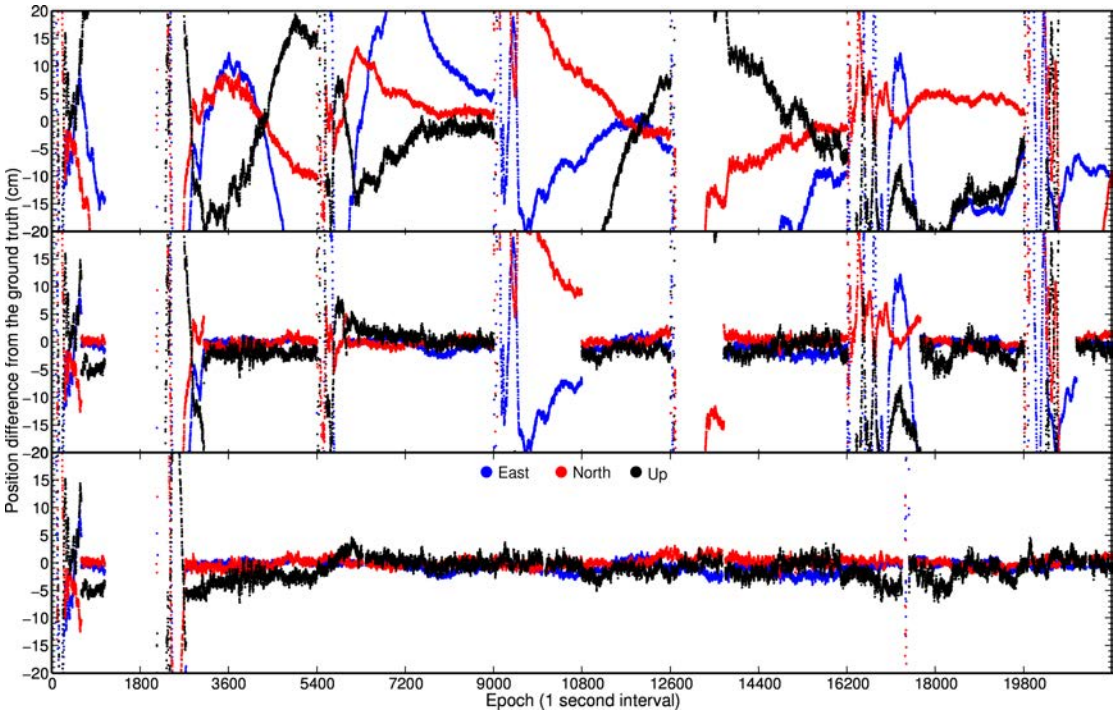

Figure 6.3: Six hours of position differences between the real-time epoch-wise and the daily estimates at station ACOR for the East, North and Up components. The top sub-figure shows the ambiguity-float solutions, the middle sub-figure shows the ambiguity-fixed solutions without rapid re-convergences and the bottom sub-figure shows the ambiguity-fixed solutions with rapid re-convergences enabled by my method

the corresponding rapid re-convergence. Total signal interruptions are introduced at the end of each hour of measurements. We can see that these simulated interruptions totally ruin the positioning quality of the ambiguity-float solutions as large undulations occur in the time series of position difference. By contrast, ambiguity resolution contributes significantly to improving the positioning accuracy, but re-convergence periods are still as long as several hundred seconds. When my method for rapid re-convergences is applied, the ambiguity-fixed solutions can normally be rapidly achieved with only a few epochs of measurements, although sometimes such a rapid re-convergence cannot be achieved until a few tens of epochs of measurements are used (see the case between Epoch 16200 and 18000).

6.3.3 Is single-epoch ambiguity resolution possible?

Single-epoch or instantaneous precise positioning has long been studied in real-time relative positioning (e.g. Han and Rizos 1996; Morujão and Mendes 2008; Pratt et al. 1997). For single-epoch precise positioning, carrier-phase cycle slips do not need to be identified, because ambiguity resolution is attempted independently for each epoch. Hence, single-epoch precise positioning is an appealing technique for GPS-adverse environments where signal obstructions frequently occur.

According to Table 6.1, most rapid re-convergences are achieved with only one epoch of 1-Hz measurements. We can thus expect that single-epoch precise positioning can be implemented after the first ambiguity-fixed solution has been achieved in real-time PPP. At an ambiguity-fixed epoch, ionospheric delays can be estimated and predicted to succeeding epochs. At each succeeding epoch, GPS measurements are independently processed and rapid ambiguity resolution is attempted by applying the predicted ionospheric delays. In this manner, single-epoch precise positioning can be implemented.

However, this single-epoch precise positioning cannot be maintained for a long observation period. Section 3.4.1 has demonstrated that ionospheric delays for accelerating re-convergences can be obtained only when wide-lane ambiguities are successfully fixed to integers. For newly-observed satellites, wide-lane ambiguities have to be first resolved with multi-epoch Melbourne-Wübbena combination measurements, and single-epoch measurements cannot guarantee a cor-

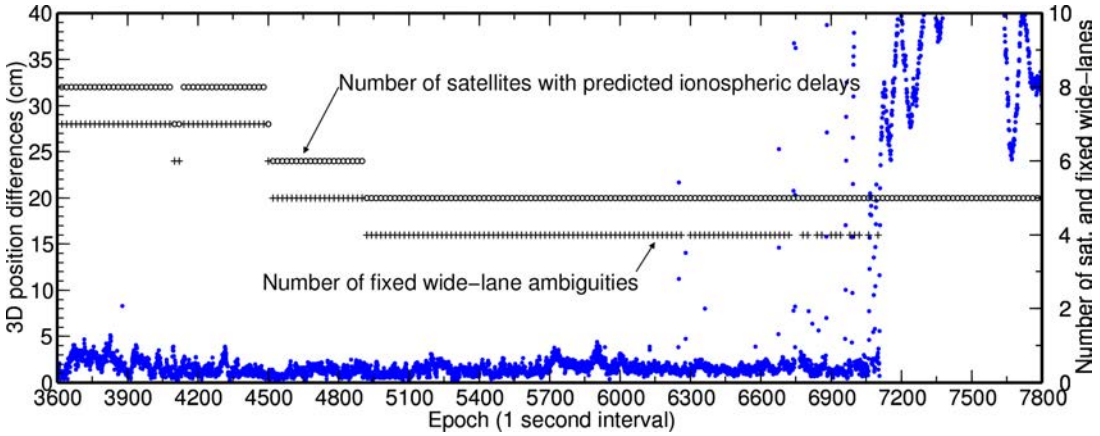

Figure 6.4: Performance of single-epoch precise positioning at station ACOR supported by rapid re-convergences. Solid blue circles denote the 3D positioning difference and thus refer to the left axis. The number of satellites with predicted ionospheric delays (open circles) and the number of fixed wide-lane ambiguities (crosses) refer to the right axis

rect resolution. As a result, wide-lane ambiguities for those newly-observed satellites cannot be fixed to integers during the single-epoch precise positioning. With the fall of the old satellites for which ionospheric delays are available, fewer and fewer satellites are eligible for a single-epoch ambiguity resolution, and hence ambiguity-fixed solutions can no longer be achieved. Figure 6.4 verifies this point by showing the performance of the single-epoch precise positioning at station ACOR on July 6th. The first hour of measurements were used to achieve the first ambiguity-fixed solution. Then single-epoch positioning started from the epoch of 3600 s. During the whole period of 4200 s, the number of satellites for which ionospheric delays were available decreased from eight to five, and correspondingly the number of fixed wide-lane ambiguities also decreased from seven to four, and finally zero. When over four ambiguities were resolved, the 3D position difference from the daily estimate was better than 5 cm. However, from the epoch of around 6300 s, fixing at least four ambiguities cannot be achieved at some epochs, and the resulting 3D position accuracy became significantly worse than 5 cm. Finally, after the epoch of about 7050 s, it became impossible to successfully fix four ambiguities at any epoch because old satellites were falling and wide-lane ambiguities for new satellites cannot be fixed to integers. Therefore, single-epoch precise positioning supported by rapid re-convergences is possible, but only within a short observation period.

6.4 Test rapid re-convergences with a mobile van

In this section, the method for rapid re-convergences is assessed for a van moving in a GPS-adverse environment, then ionospheric delays are interpolated over a dense reference network and finally the results are compared with those from a commercial NRTK service.

6.4.1 Data, models and methods

A van-borne 1-Hz GPS data set was collected in the city of Nottingham on May 11th 2009, covering about 2.5 hours from 11:30 to 14:04 (Local time). The Kp index was around 1 during this period, showing a quiet ionosphere condition. As shown in Figure 6.5, the van stopped or moved in four phases: 1) it stopped from 11:40 to 12:27 on a car park with an open sky view; 2) it moved from 12:27 to 13:12 along the red routes escorted by tall buildings, large trucks and thick trees; 3) it stopped again from 13:12 to 13:44 on the car park; 4) finally, it moved again from 13:44 to 14:04 along the blue routes on the car park with a few thick trees around. A reference station was located on top of the IESSG building which was within 2 km from the van at all times. This reference station was surrounded by another six reference stations within a distance from about 50 to 100 km (upper inset). They were used to interpolate ionospheric and tropospheric delays. In addition, the lower inset shows the satellite number which kept steady during the stopping phases, but changed dramatically during the moving phases due to signal obstructions.

For this van, because the antenna's attitudes during the moving phases were unknown, phase wind-up corrections were applied by assuming that the antenna's rotation was always around its boresight. In this case, the phase wind-up effects caused by this rotation can be fully assimilated into the receiver clock without affecting the correction proposed by Wu et al. (1993) (Kim et al. 2006; Banville and Langley 2009). Moreover, no antenna phase center corrections were applied in PPP solutions. Only one ZTD was estimated during this experiment because the time span

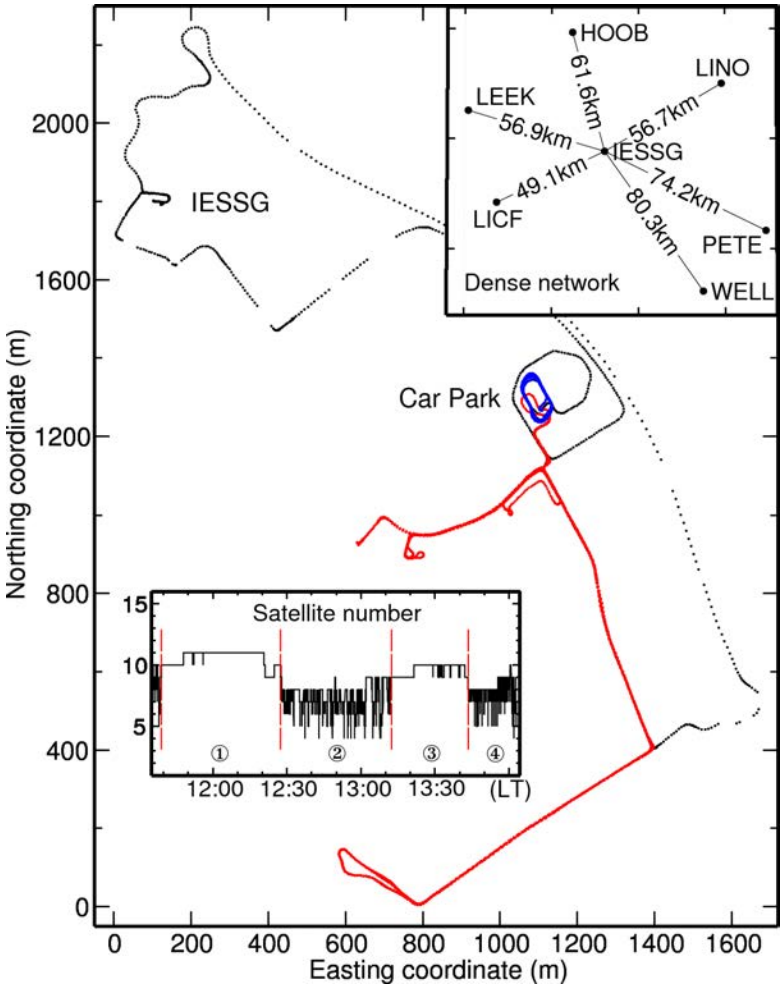

Figure 6.5: A mobile van used to test the method for rapid re-convergences developed in this thesis. The van trajectory consists of four phases: 1) it stopped on the car park with an open sky view; 2) it moved along the red routes escorted by tall buildings, large trucks and thick trees; 3) it stopped again on the car park; 4) it moved along the blue routes on the car park with a few thick trees around. A reference station was located at IESSG. The upper inset shows the distances between six reference stations and IESSG, and the lower inset shows the satellite number and the time spans for the four phases. "LT" denotes local time

was short and the area was small. A ground truth was computed using the Leica Geo Office software version 3.0[1] and the IESSG station was used as reference. Note that antenna phase center corrections were not applied for this ground truth. Hence this ground truth is actually for the true position of antenna phase center, and its 3D accuracy is believed to be better than a few centimeters. Moreover, an NRTK solution provided by the Leica SmartNet service (Aponte et al. 2009) was also collected for comparison. Antenna phase center corrections might be applied to this NRTK solution, but the details cannot be obtained for a real-time system.

6.4.2 Rapid convergences in a GPS-adverse environment

In a GPS-adverse environment, frequent and severe signal obstructions can jeopardize the performance of precise positioning and ambiguity resolution. In Figure 6.6, for the ambiguity-float solutions, a clear trend is present for the East component and a bias is present for the

[1] http://www.leica-geosystems.co.uk/en/Leica-Geo-Office_4611.htm

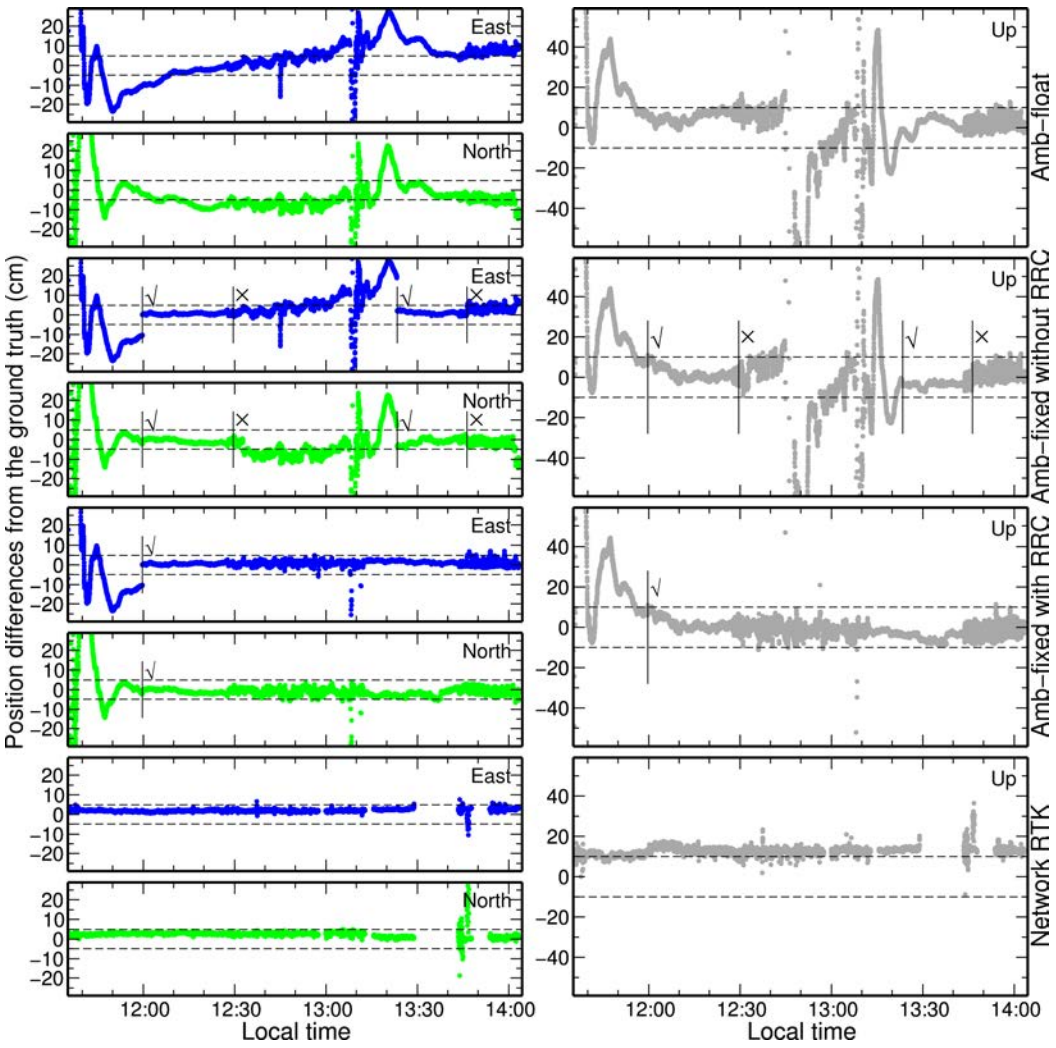

Figure 6.6: Differences between a mobile van's real-time position estimates and the ground truth for the East, North and Up components. From top to bottom show the ambiguity-float solutions, ambiguity-fixed solutions without and with rapid re-convergences (RRC), and NRTK solutions. The symbol "√" denotes the time when ambiguity-fixed solutions are achieved, whereas "×" denotes the time when ambiguity-fixed solutions are totally lost

North component. During the first moving phase when signals were frequently obstructed, all three components, especially the vertical, experience large position errors of over a few decimeters. If ambiguities are resolved, the positioning accuracy can be clearly improved for all three components, but this improvement only appears during the stopping phases as shown in Figure 6.6. Ambiguity-fixed solutions were quickly and totally lost after the moving phases began. This is because re-convergences occurred due to signal obstructions. Overall, the rate of ambiguity-fixed epochs is only 7.7% of all epochs during the moving phases.

However, by further applying my method for rapid re-convergences, ambiguity-fixed solutions can be well maintained during the moving phases. From Figure 6.6, the accuracies of both horizontal components during the moving phases are better than 5 cm, whereas that of vertical is better than 10 cm almost at all times. Large position errors are present at only a few epochs where ambiguity-fixed solutions cannot be achieved. More encouragingly, the rate of ambiguity-fixed epochs is increased to 93.6% of all epochs during the moving phases, showing a significant improvement over the ambiguity-fixed solutions without rapid re-convergences.

Table 6.2: Statistics of the position quality for both the ambiguity-fixed solution with rapid re-convergences and the NRTK solution for a van during its moving phases. "RRC" denotes "rapid re-convergence". The unit of all numerals is centimeter

Solutions	Bias[a]			Standard deviation			RMS		
	East	North	Up	East	North	Up	East	North	Up
Amb-fixed with RRC	0.7	−0.8	−0.8	1.0	1.3	2.7	1.2	1.6	2.8
Network RTK	2.0	2.4	12.6	0.6	1.0	1.4	2.1	2.5	12.6

[a] Antenna phase center corrections were not applied to the ambiguity-fixed solution with rapid re-convergences and the ground truth, but might be applied to the NRTK solution although relevant details cannot be obtained for a real-time system. This might explain why large biases occur in the NRTK solution

6.4.3 Comparisons with an NRTK solution

Normally, an NRTK service can provide centimeter-level positioning accuracy with double-difference measurements based on an RTK network. At the bottom of Figure 6.6, the position differences of an NRTK solution against the ground truth is presented. Note that the gaps are caused by the unavailability of NRTK correction messages. Following this, large positioning errors occur from 13:40 to 13:50, and thus are excluded from the following statistics (see Table 6.2). From Table 6.2, it can be clearly seen that biases are present in all three components of the NRTK solution. In terms of Section 6.4.1, I guess that these biases are largely caused by antenna phase center corrections applied to the NRTK solution. The largest bias appears for the Up component, and normally the height component for an antenna phase center offset is also the largest one. This coincidence may thus confirm my guess above. Disregarding these discrepancies, it can be found that the ambiguity-fixed solutions enhanced by rapid re-convergences perform comparably with the NRTK solution. Specifically, the standard deviations of the differences for the East, North and Up components during the moving phases are 1.0, 1.3 and 2.7 cm for the ambiguity-fixed solutions with rapid re-convergences respectively, whereas 0.6, 1.0 and 1.4 cm for the NRTK solution.

However, from Figure 6.6, the position differences during the moving phases for the NRTK solution clearly scatter less than those of the ambiguity-fixed PPP solutions enhanced by rapid convergences. On the contrary, the position differences during the stopping phases for all these solutions scatter comparably. This demonstrates that the internal consistency between the ground truth and the NRTK solution due to the software similarity cannot adequately explain the distinct scatters during the moving phases. Therefore, I argue that this issue might be because phase wind-up corrections for PPP cannot be precisely computed during the moving phases, since the antenna's true attitudes were unknown (Kim et al. 2006).

6.5 Conclusion on performance of rapid re-convergences

In this thesis, a novel method in which ionospheric delays are predicted to succeeding epochs to rapidly accelerate ambiguity resolution in the case of re-convergences is originally developed. In theory, the effectiveness of this method consists in two aspects: First, wide-lane ambiguities can be rapidly resolved with ionosphere-corrected wide-lane measurements, rather than noisy Melbourne-Wübbena combination measurements; second, narrow-lane ambiguities can be rapidly resolved under the tight constraints derived from ionosphere-corrected unambiguous wide-lane measurements.

This method is verified using two tests under moderate ionosphere conditions. At static

stations suffering from simulated total losses of tracking locks, even if the latency for predicted ionospheric delays is up to 180 s, 93.3% and 95.0% of re-convergences to wide-lane and narrow-lane ambiguity resolutions can be achieved within five epochs of 1-Hz measurements, respectively. If this latency is prolonged, the prediction error of ionospheric delays is increased, consequently reducing both percentages above. On the other hand, for most rapid re-convergences, only one epoch of measurements is needed, implying that the contribution of satellite-geometry changes to these rapid re-convergences is minimal in this study. At a mobile van moving in a GPS-adverse environment, ambiguity-fixed solutions can be well maintained when rapid re-convergences are applied. The rate of ambiguity-fixed epochs is significantly improved from 7.7% to 93.6% of all epochs during the moving phases. In addition, the RMS of position differences from the ground truth that is derived from a post-processed short-baseline solution are 1.0, 1.3 and 2.7 cm for the East, North and Up components respectively, which are slightly larger than but comparable with those of an NRTK solution.

6.6 Rapid convergence by interpolating ionospheric delays

Firstly, I need to state that my method can be applied to only re-convergences because ionospheric delays are required and they can be estimated only at ambiguity-fixed epochs. However, if a dense network of reference stations is available, ionospheric delays can also be estimated at the reference stations and then interpolated for single users to assist rapid convergences. If this is the case, then, in principle, the first ambiguity-fixed solution could also be rapidly achieved.

In this section, the van-borne data in Figure 6.5 are again used. From Section 6.4.2, the first ambiguity-fixed solution is achieved after a few tens of minutes. To overcome this slow convergence, the six surrounding reference stations were used to interpolate ionospheric delays for this van. As a result, only five epochs of 1-Hz measurements were needed to achieve the first ambiguity-fixed solution. Moreover, the epochs with large position errors become much fewer. The rate of ambiguity-fixed epochs reaches up to 97.2% of all epochs during the moving phases.

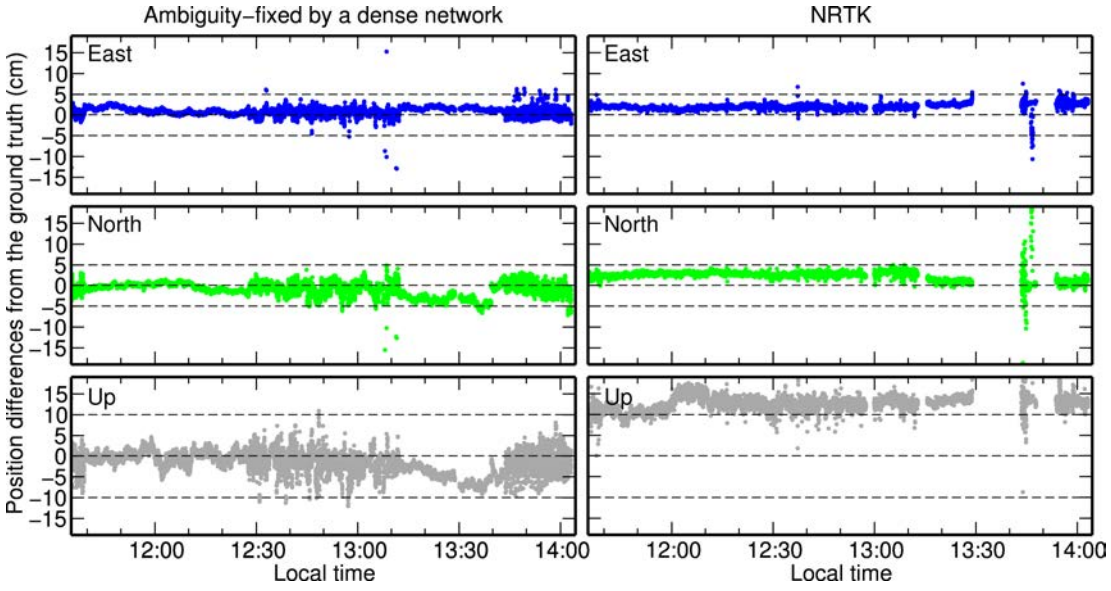

Figure 6.7: Differences between the ground truth and the position estimates of the ambiguity-fixed PPP solution supported by a dense network. The NRTK solution is shown here for comparison

This further improvement is largely attributed to the interpolated ionospheric delays which are more reliable than the predicted ones. Figure 6.7 shows the differences between the ground truth and the position estimates of the ambiguity-fixed PPP solution supported by a dense network. The NRTK solution is again here shown for comparison.

The results above rely on the ionospheric delays being interpolated from a dense network of reference stations, but such networks are normally not available for PPP. However, we can envisage that if precise ionospheric delays can be derived from a sparse network at scales of several hundred kilometers using an ionospheric tomography technique (Hernández-Pajares et al. 2000), a PPP-RTK service (Geng et al. 2010d) that can instantaneously provide ambiguity-fixed solutions may potentially prevail against current RTK positioning services based on dense networks.

6.7 Summary

This chapter quantitatively assesses the performance of the novel method originally developed rapid convergences and re-convergences in real-time PPP. Single PPP users can estimate and predict ionospheric delays themselves in order to accelerate ambiguity resolution in the case of re-convergences. Not only can the ambiguity-fixed solutions be rapidly achieved, but the rate of ambiguity-fixed epochs in all epochs can also be significantly improved. On the other hand, if a dense network of reference stations is available, ionospheric delays can be interpolated, and hence the first ambiguity-fixed solution can also be rapidly achieved. However, in principle, this negates the advantages of PPP in not requiring a dense network of reference stations, but in practice precise ionosphere tomography may be a solution for this problem in future.

Chapter 7

Global PPP-RTK

7.1 Introduction

In terms of the results in chapters 5 and 6, the performance and practicability of real-time PPP can be improved significantly by ambiguity resolution and rapid re-convergences. It is demonstrated in Section 1.2.4 that PPP is a global precise positioning technique in nature for which only a sparse global reference network is required. In this case, considering the deficiencies of NRTK services based on dense networks, this chapter thus proposes a prototype for a global PPP-RTK service enhanced by rapid ambiguity resolution at a single receiver, then investigates an important question, i.e. how many reference stations are sufficient to support this global PPP-RTK, and finally illustrate a potential application of global PPP-RTK in geohazard early warning with GPS measurements collected for the April 6th 2009 L'Aquila earthquake.

7.2 A prototype of global PPP-RTK

A prototype for a global PPP-RTK service is illustrated in Figure 7.1. Global service providers collect real-time GPS measurements from a sparse global network. These measurements are then processed to produce precise satellite orbits and high-rate satellite clocks in real time. Note that ambiguity resolution based on the FCB- or IRC-based methods is applied. The resulting ambiguity-fixed satellite products are then transmitted to GEO or the Internet and afterwards broadcast to global users. These users can be divided into two categories. For single users augmented by a dense network of reference stations, atmospheric delays can be interpolated and further sent to these users to assist them in achieving rapid centimeter-level positioning. Note that this dense network should also receive real-time satellite products from GEO. On the other hand, for single users without any assistance from such regional dense networks, it is still possible for them to accelerate re-convergences to ambiguity-fixed solutions, but there will be a long period for the first convergence. In the following, the three modules of global PPP-RTK, i.e. global service providers, augmentation service providers and single users are detailed before a brief comparison between global PPP-RTK and NRTK is made.

7.2.1 Global service providers

Global service providers have to first build a globally distributed real-time network of reference stations. High-rate measurements (e.g. 1-Hz) must be immediately transmitted to a processing

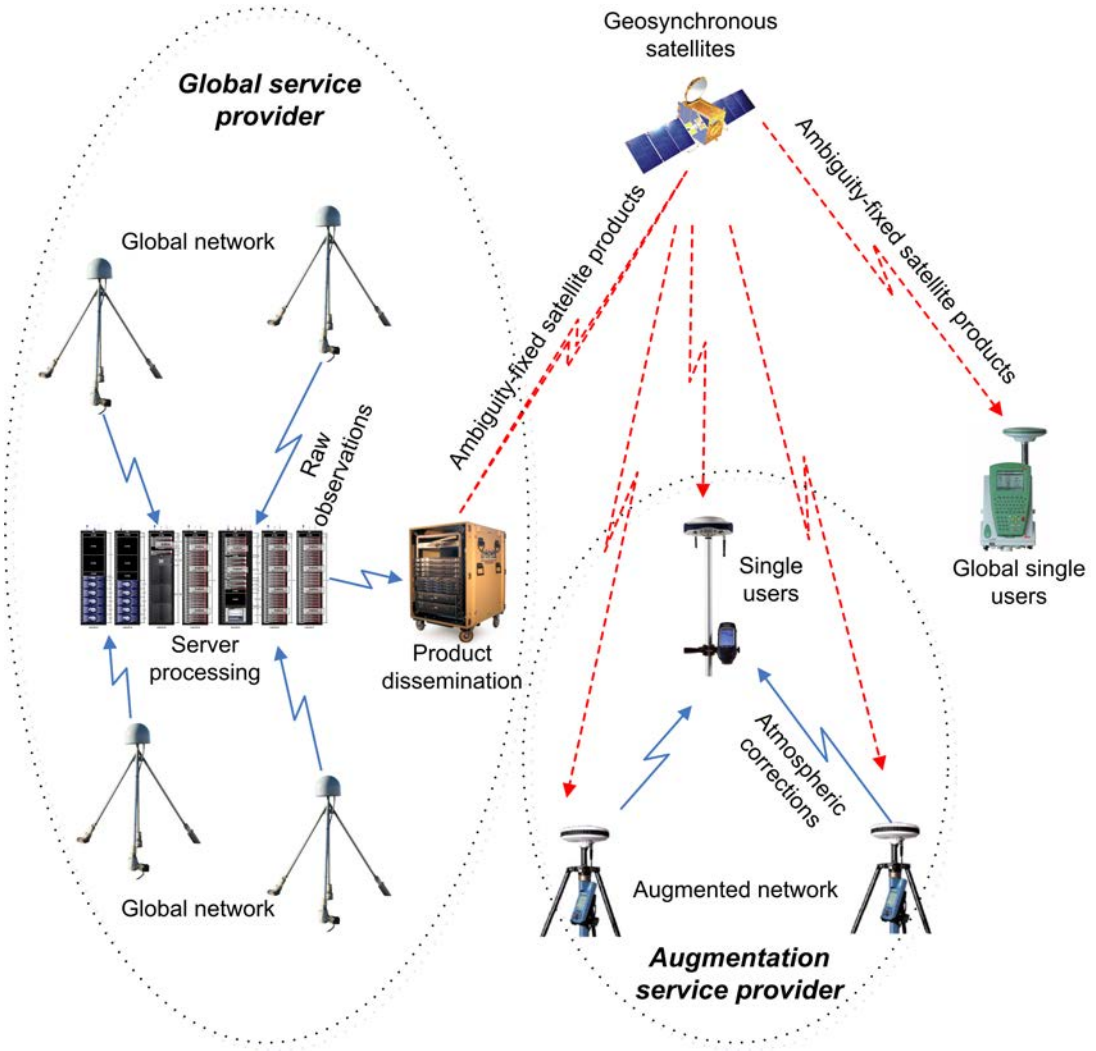

Figure 7.1: A prototype of a global PPP-RTK service based on rapid ambiguity resolution at a single receiver. Global service providers are to provide globally-applicable real-time satellite products that enable ambiguity resolution in PPP. An augmentation service provider usees a dense regional network to provide atmospheric delays for rapid convergences. "Ambiguity-fixed satellite products" denote those that enable ambiguity resolution at a single receiver

center through the Internet, for example. In theory, more reference stations can more reliably guarantee a robust service which provides high-quality satellite products. This issue will be further discussed in Section 7.3. In addition, a product dissemination facility has to be established in order to transmit real-time satellite products to global single users through GEO or the Internet.

In the processing center, raw GNSS measurements are used to estimate dynamic satellite orbits (Geng et al. 2006) and these orbits are then predicted over a short period, e.g. a few tens of minutes. Satellite maneuvers should be carefully regarded although they are normally rare. The quality control of these predicted orbits is thus essential. Moreover, satellite clocks have to be estimated with high-rate measurements by fixing the predicted satellite orbits. These real-time clocks need to be predicted over a few seconds considering inevitable communication delays for satellite clocks. Over how long these clocks can be predicted depends on the clock quality of GPS satellites (Senior et al. 2008). Finally, for ambiguity resolution, FCBs are estimated by fixing the predicted orbits and the real-time clocks (refer to Figure 2.5). However, the transmission

of FCBs as additional products will significantly enlarge the data bandwidth and increase the expense. In this case, combining FCBs and satellite clocks becomes a good alternative for the global PPP-RTK (refer to Section 2.4.1).

Therefore, ambiguity-fixed satellite orbits and clocks are the primary products generated by global service providers. Other products like integrity messages (e.g. Ziebart et al. 2007) are also required but beyond the scope of this thesis and thus ignored throughout.

7.2.2 Augmentation service providers

An augmentation service for the above global service is established by building a dense network of reference stations covering a relatively small area. Note that these stations have to receive the satellite products transmitted by the global service.

Unlike the global service where all raw GNSS measurements should be sent to the processing center, within an augmentation service, each reference station can independently generate and disseminate its own atmospheric corrections after it has performed ambiguity resolution. The method for this correction generation refers to Section 3.4 and 3.6. Hence, no processing center is required for such an augmentation services and thus each reference station is actually independent. In this manner, an augmentation service can be easily established and is quite flexible and somewhat cost-effective, compared with current NRTK services.

In addition, slant ionospheric and tropospheric delays are the primary products at each reference station in an augmentation service. Normally, these two products are generated separately on account of their different properties. Note that a prediction of these atmospheric delays over a short time is necessary considering communication delays.

7.2.3 Global single users

For global single users without any assistance from an augmentation service above, they need to first achieve ambiguity-fixed solutions in an environment of open sky view, and then begin to estimate ionospheric delays at all ambiguity-fixed epochs to allow for rapid re-convergences in the case of GPS-adverse environments (refer to Section 3.4 and 6.4). Hence, for these users, they benefit from the advantage of PPP, i.e. no need of any synchronous GPS measurements from a nearby reference station, and can still achieve ambiguity-fixed solutions that are greatly enhanced by rapid re-convergences developed in this thesis. However, as demonstrated in Section 3.4.3 and 6.3.3, neither ionospheric delays can be precisely predicted over a rather long period nor the preferable single-epoch precise positioning can be maintained for a long period. As a result, ambiguity-fixed solutions at these single users are still somewhat vulnerable and thus can be relatively easily lost.

On the other hand, for global single users with full assistance from an augmentation service, they can use the products of atmospheric delays from several reference stations and precisely interpolate the delays for their positions. These interpolated atmospheric delays are then used to rapidly achieve ambiguity-fixed solutions. Hence, the first ambiguity-fixed solution can be rapidly achieved and the single-epoch precise positioning can also be implemented. Moreover, ZTDs are no longer estimated at these single users. Note that these users can still generate their own atmospheric delays in case of any interrupted transmissions of atmospheric delays by reference stations. However, as indicated in Section 3.6.2, a dense network of reference stations for an augmentation service will totally devalue the advantages of PPP-RTK over NRTK.

7.2.4 Comparison with NRTK

GPS-based NRTK has been a very popular precise positioning service in many countries. The comparisons between the global PPP-RTK and NRTK are briefly summarized as follows:

- Global PPP-RTK is a precise positioning service on a global scale whereas NRTK is a regional service. Hence, global PPP-RTK can be used in oceanic or desert areas.
- Ambiguity resolution in global PPP-RTK is only achieved by first wide-lane and then narrow-lane resolutions. However, ambiguity resolution in NRTK is rather flexible and more robust. Specifically, ambiguity resolution can be directly performed on L1 or L2 measurements, other than wide-lane or narrow-lane measurements.
- Without an augmentation service, global PPP-RTK needs a few tens of minutes to achieve the first ambiguity-fixed solution. However, NRTK can normally provide instantaneous ambiguity-fixed solutions.
- The transmission bandwidth for satellite products of the global PPP-RTK depends only on the satellite number, whereas that for the corrections of NRTK depends on the number of reference stations and the technique applied (refer to Section 1.2.4). Hence, the scale expansion of an NRTK service is handicapped by this bandwidth limit.

7.2.5 Potential application: Geohazard early warning

Devastating natural hazards like earthquakes and tsunamis expose the deficiencies of human ability in mitigating these catastrophes. For example, without any early warning, the 2004 Sumatra-Andaman tsunami, the 2008 Wenchuan earthquake and the 2010 Haiti earthquake caused a total loss of about 0.53 million fatalities and 50 billion sterling. For earthquakes of large magnitude, seismometers suffer from saturations; and for tsunamis in open oceans, tide gauges are confined within coastal areas, cabled seafloor pressure sensors are very expensive to deploy and inland seismometers cannot directly measure the tsunami waves. In this case, one tool of great promise is the high-rate continuous GPS stations which can be relatively cheaply and flexibly established both inland and offshore. Currently, high-rate GPS has the potential of directly measuring displacements at millimeter level at a rate of 1 Hz up to 50 Hz (Bock et al. 2004; Genrich and Bock 2006). More importantly, GPS is characterized as a global and all-weather system. Therefore, high-rate GPS can potentially provide valuable input to early warning systems for earthquakes and tsunamis around the globe (Allen et al. 2009).

A Earthquake

Precise GPS positioning has been used to determine accurate ground motions over a wide range of frequencies and amplitudes (Anzidei et al. 2009; Larson 2009). High-rate GPS is a valuable tool in studying the earthquake process, and supplementing seismometers by enlarging the range of dynamic deformation and frequency spectrum (e.g. Banerjee et al. 2007; Larson et al. 2003; Miyazaki et al. 2004). Langbein and Bock (2004) reported that 1-Hz GPS positioning could provide a horizontal accuracy of better than 6 mm with a confidence level of 99%. Elósegui et al. (2006) found that the RMS error of 1-Hz GPS positions over a 15-minute duration of a simulated seismic event was 2.5 mm and about 96% of all position errors were smaller than 5 mm.

However, all these results focus on post-event studies, whereas earthquake early warnings require real-time GPS positioning in order to rapidly respond to devastating catastrophes (Allen

et al. 2009). In recent years, high-rate GPS has been preliminarily assessed for the earthquake early warning in California (Crowell et al. 2009). A network data processing technique was used and thus raw GPS measurements had to be transferred in real time to a central processing facility (Bock et al. 2000). Obviously, this transfer of huge data will delay the issue of a potential alert. Even worse, a specific station has to be presumed stable in this network processing, which is often not achievable during an earthquake of large magnitude. In this case, PPP is preferred because it is an onsite data processing technique in nature. No raw measurements have to be transferred. More importantly, PPP is three orders of magnitude faster than the network processing (Blewitt 2008). Furthermore, the developments in rapid ambiguity resolution improve the efficiency of achieving the centimeter- or even millimeter-level positioning accuracy. Therefore, the global PPP-RTK proposed in this thesis is of great potential for the earthquake early warnings.

B Tsunami

To date, a good number of studies have proposed that high-rate GPS should be included in tsunami early warning systems (e.g. Blewitt et al. 2006, 2009; Sobolev et al. 2007). Blewitt et al. (2006) suggested tracking the mean displacement of the Earth's surface related to the arrival of seismic waves by determining the earthquake's true size and the tsunami potential with up to 15-minute GPS measurements; moreover, Blewitt et al. (2009) demonstrated that the spatial pattern, magnitude and timing of GPS stations' displacement can be inverted to quantitatively derive the earthquake source and thus predict the displacement field of the ocean bottom, ultimately providing initial conditions for tsunami models; finally, Sobolev et al. (2007) proposed a near-field GPS array to measure both vertical and horizontal displacements and resolve higher-order features of the slip distribution on the fault. However, all these suggested approaches employ land-based GPS positioning at permanent stations to identify the earthquakes that result in tsunamis. As a result, the only official information forecasted at present by a typical tsunami early warning system is the tsunami arrival time. Titov et al. (2005) pointed out that the next-generation tsunami forecast should provide estimates of all critical tsunami parameters including amplitudes, inundation distances and current velocities with direct tsunami measurements. It can be found that measuring earthquakes with inland and onshore GPS stations is actually an indirect approach of identifying the possibly resulting tsunamis.

Buoy-borne GPS positioning can directly measure the tsunami evolution. Kato et al. (2005) used an offshore buoy, which is only 13 km away from the coastal reference station, to measure the amplitude of the tsunami waveforms to an accuracy at the centimeter level. Falck et al. (2010) also deployed buoys along the coastal line of Indonesia, on the basis that these buoy-borne GPS receivers cannot be far from the onshore reference stations if the centimeter-level positioning accuracy is required. Although buoy-borne GPS receivers can directly record the tsunami evolution, they cannot be located in the open ocean if relative positioning is adopted. However, successfully identifying a devastating tsunami in the open ocean will provide sufficient valuable time for the people to evacuate from coastal areas. In this case, the global PPP-RTK proposed in this thesis becomes a good choice which can achieve centimeter- or even millimeter-level positioning accuracy even if no nearby reference stations are available (refer to Section 5.5).

7.3 How many reference stations for this global PPP-RTK?

Deploying and maintaining a global network of reference stations is quite costly and complicated. Hence, reducing the number of reference stations, but still achieving a satisfactory positioning quality is of great concern before a global PPP-RTK service discussed in Section 7.2 can be implemented. In this section, three global networks are used to generate the GPS satellite orbits, clocks and FCBs. Then another global network is used to quantify the performance of real-time PPP with ambiguity resolution in order to illustrate how many reference stations are sufficient to support a relatively robust global PPP-RTK service.

7.3.1 Data and models

Daily GPS measurements on December 30th 2009 were collected from three networks that were composed of 58, 38 and 18 IGS globally distributed reference stations (Figure 7.2a, 7.2b and 7.2c). The data sampling interval is 30 s. These networks were already used by ESOC to estimate real-time satellite orbits and clocks (Agrotis et al. 2010b), and here they were further used for the FCB determination. Note that ESOC orbits and clocks were therefore used in this section. The orbit quality was comparable with that of the IGS ultra-rapid products and the clock accuracy was around 0.2 ns (Agrotis et al. 2010a,b). Moreover, a global network of 59 reference stations (Figure 7.3) was used to test real-time PPP by applying the orbits, clocks and FCBs generated from these three networks.

For data modeling, absolute phase centers (Schmid et al. 2007), phase-wind up effects (Wu et al. 1993) and station displacements proposed in IERS conventions 2003 (McCarthy and Petit 2004) were applied. A cut-off angle of 7° was set for usable measurements and an elevation-dependent weighting strategy was applied to measurements at low elevations (Gendt et al. 2003). Moreover, ZTDs were estimated every one hour by applying the global pressure/temperature model and the global mapping function (Boehm et al. 2006a), while horizontal tropospheric gradients every 12 hours (Bar-Sever et al. 1998). In addition, daily position estimates were used as ground truths to assess the accuracy of real-time epoch-wise position estimates.

7.3.2 Results

Table 7.1, 7.2 and 7.3 respectively present the performance of real-time PPP with ambiguity resolution at 59 simulated mobile stations when the 58-station, 38-station and 18-station global networks are used for the satellite orbit, clock and FCB determination. Overall, the performance for the 58-station network is the best among the three. Specifically, for the 58-station network, a mean observation period of about 1028 s is required before ambiguity-fixed solutions can be achieved. During 24 hours, ambiguity-fixed solutions are achieved at 97.1% of all epochs on average and the mean RMS statistics of differences between the epochs-wise and daily position estimates reach 0.9, 1.0 and 3.7 cm for the East, North and Up components, respectively. When the 38-station network is used, the mean time to fix ambiguities is slightly increased to 1101 s. The rate of ambiguity-fixed epochs is slightly reduced to 96.4% of all epochs and the RMS statistics slightly rise to 1.0, 1.1 and 4.0 cm. However, when the 18-station network is used, ambiguity-fixed solutions cannot be achieved at all 59 test stations; on average, the time to fix ambiguities dramatically increases to 13165 s and the rate of ambiguity-fixed epochs significantly decreases to 30.1%. The RMS statistics are also increased to 1.6, 1.5 and 5.1 cm.

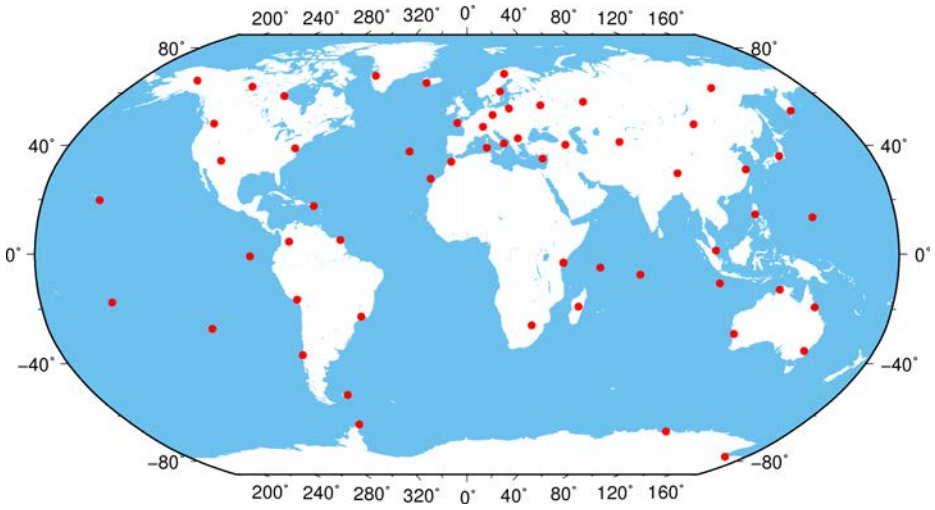

(a) 58 stations

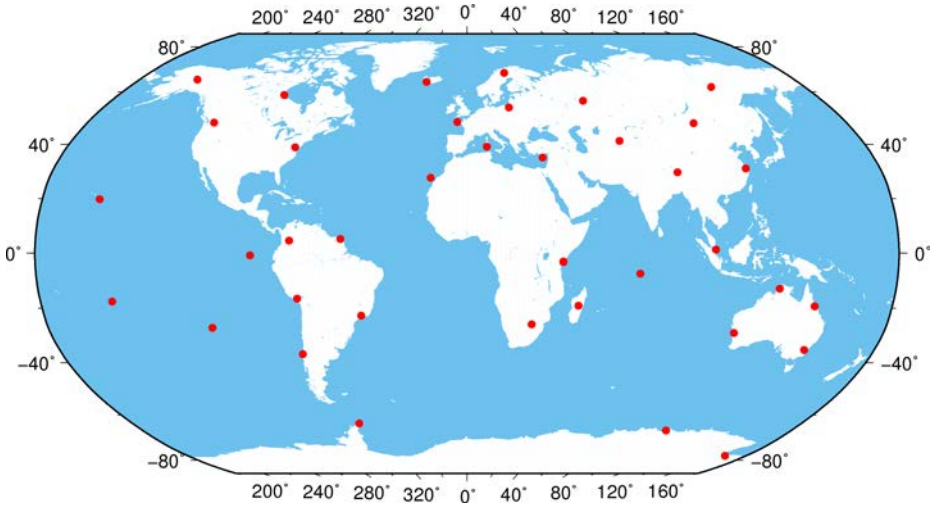

(b) 38 stations

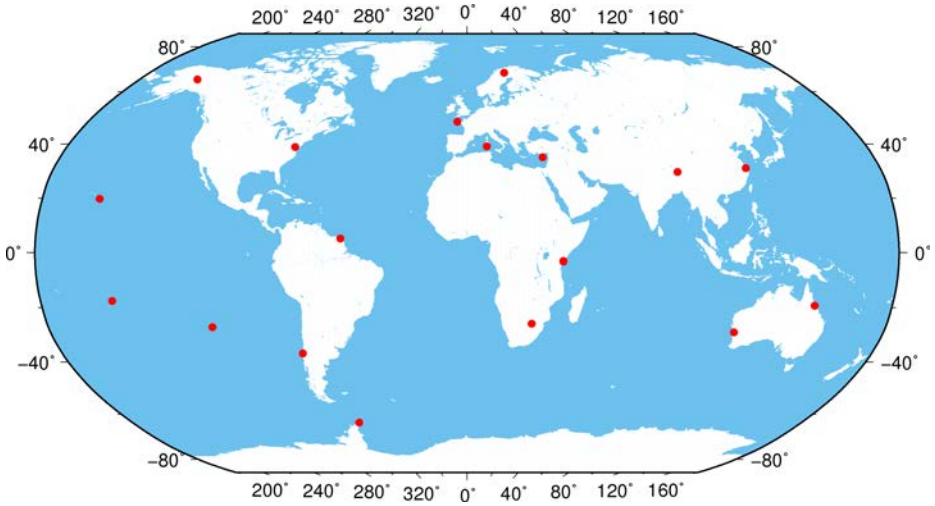

(c) 18 stations

Figure 7.2: Three global networks of reference stations for the determination of GPS satellite orbits, clocks and FCBs

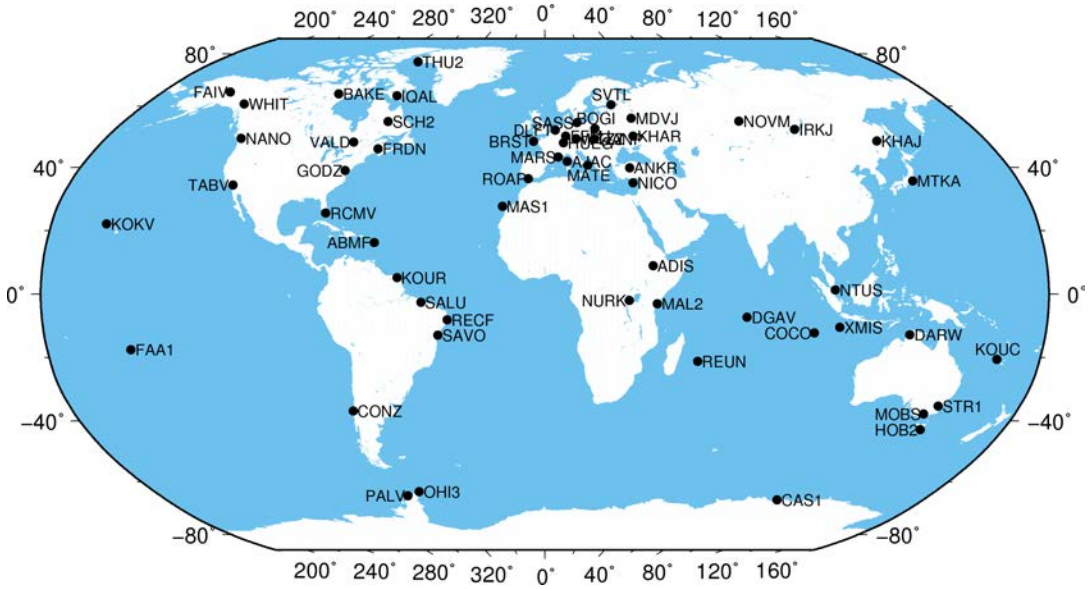

Figure 7.3: A global network of 59 reference stations used to assess real-time PPP with ambiguity resolution

From these statistics, the relatively long observation period before an ambiguity-fixed solution can be achieved coincide with the conclusion in Section 5.6.4. It is possible to achieve a high rate of ambiguity-fixed epochs among all epochs when only 38 globally distributed reference stations are employed. Increasing this number of reference stations up to 58 only minimally improves the performance, but decreasing this number to only 18 significantly degrades the performance.

Furthermore, from Table 7.1 and 7.2, most times to fix ambiguities at 59 test stations are smaller than 1800 s. However, in Table 7.3, many times can be as large as ten thousand seconds. This is actually because narrow-lane FCBs for some satellite pairs are not always obtainable during 24 hours. As discussed in Section 2.2.2, narrow-lane FCBs are estimated by averaging the fractional parts of ambiguity estimates at all involved stations. If the number of these involved stations is smaller than five, the resulting narrow-lane FCB estimates are deemed not reliable and removed in this thesis. As a result, ambiguity resolution is not always possible at all test stations. This also explains why the rate of ambiguity-fixed epochs among all epochs is so small at most test stations in Table 7.3.

Therefore, according to the statistics in these three tables, a global network of about 38 stations distributed like Figure 7.2b can lead to a global PPP-RTK service which can guarantee a rate of over 95% for ambiguity-fixed epochs among all epochs.

Table 7.1: Performance of real-time PPP with ambiguity resolution when the 58-station global network is used (see Figure 7.2a). "Time" means the time (s) used to achieve the ambiguity-fixed solution. "Rate" means the rate (%) of ambiguity-fixed epochs in all epochs. "East", "North" and "Up" denote the RMS (cm) of position differences from the daily position estimates for the East, North and Up components, respectively

Station	Time	Rate	East	North	Up	Station	Time	Rate	East	North	Up
ABMF	630	99.2	1.2	1.4	6.7	MAS1	780	97.0	0.7	0.7	3.6
ADIS	720	99.0	1.0	0.9	3.7	MATE	720	97.6	0.6	0.7	2.7
AJAC	630	97.8	0.9	1.0	3.5	MDVJ	1440	96.9	0.8	0.9	2.8
ANKR	810	97.5	0.6	0.6	2.3	MOBS	630	99.3	1.1	2.7	5.5

continued on next page

continued from previous page

Station	Time	Rate	East	North	Up	Station	Time	Rate	East	North	Up
BAKE	630	99.3	0.4	0.7	2.4	MTKA	1200	94.6	0.9	1.2	2.7
BOGI	1800	86.8	0.7	0.9	3.0	NANO	630	99.3	0.5	0.8	2.5
BRST	780	97.5	0.6	0.9	3.0	NICO	1770	96.6	0.6	0.7	3.2
CAS1	690	99.2	0.6	0.9	3.6	NOVM	1650	92.6	0.7	0.9	2.9
COCO	660	98.2	1.2	0.9	4.3	NTUS	1740	96.1	1.0	1.0	3.9
CONZ	630	85.8	0.7	0.8	2.6	NURK	1410	95.5	1.9	0.9	4.5
DARW	960	86.7	2.5	2.0	7.4	OHI3	630	98.5	0.5	0.8	2.8
DGAV	630	99.3	0.8	0.9	2.9	PALV	630	99.3	0.6	0.8	2.4
DLFT	660	97.7	0.6	0.9	3.0	RCMV	1080	97.6	1.8	1.3	8.5
FAA1	3120	96.0	1.5	1.5	6.8	RECF	690	99.2	1.3	1.5	4.4
FAIV	930	99.0	0.6	1.0	3.0	REUN	4320	94.9	1.4	1.5	6.8
FFMJ	690	97.5	0.6	0.9	2.8	ROAP	3630	90.8	1.5	2.0	6.0
FRDN	630	99.3	0.6	0.8	2.4	SALU	630	99.3	1.4	1.2	5.7
GANP	720	97.6	0.7	0.9	3.1	SASS	720	97.7	0.5	0.8	2.8
GODZ	1020	98.9	0.6	0.7	2.7	SAVO	630	99.3	1.1	0.8	4.0
HOB2	1530	98.3	1.0	1.0	3.1	SCH2	630	99.3	0.8	0.9	2.2
HUEG	690	97.7	0.5	0.9	2.7	STR1	780	99.1	1.0	1.7	6.0
IQAL	630	99.3	0.5	0.7	2.3	SVTL	960	97.8	0.8	0.8	2.8
IRKJ	2820	96.0	0.7	0.7	2.4	TABV	630	99.3	0.7	0.9	3.5
KHAJ	630	94.0	0.7	0.9	3.1	THU2	630	99.3	0.5	0.6	3.0
KHAR	990	97.2	0.6	0.8	2.8	VALD	630	97.2	0.6	0.7	1.9
KOKV	900	97.7	2.5	2.9	7.7	WHIT	810	99.1	0.4	0.6	1.7
KOUC	960	97.7	1.2	1.5	6.0	WTZJ	690	97.3	1.1	1.0	3.3
KOUR	630	99.3	1.1	0.8	3.4	WTZZ	630	97.8	0.7	0.8	2.7
MAL2	660	98.9	0.9	0.6	2.8	XMIS	780	98.0	1.2	0.8	3.9
MARS	750	97.0	0.7	0.9	3.5	Mean	1028	97.1	0.9	1.0	3.7

Table 7.2: Performance of real-time PPP with ambiguity resolution when the 38-station global network is used (see Figure 7.2b). Meanings of columns refer to Table 7.1

Station	Time	Rate	East	North	Up	Station	Time	Rate	East	North	Up
ABMF	630	99.2	1.1	1.3	6.7	MAS1	630	92.6	2.1	1.0	7.0
ADIS	660	99.2	1.0	0.9	3.6	MATE	870	97.4	0.7	0.8	3.1
AJAC	630	97.8	1.0	1.1	3.9	MDVJ	1380	96.9	0.9	0.9	3.1
ANKR	2010	96.1	0.8	0.7	2.5	MOBS	630	99.3	1.4	1.9	6.9
BAKE	630	99.3	0.7	1.0	3.6	MTKA	1260	94.0	1.1	1.3	5.0
BOGI	4860	81.2	0.9	1.0	3.1	NANO	690	99.2	0.7	1.0	3.7
BRST	960	97.2	0.6	1.0	3.4	NICO	1590	96.8	0.7	0.8	3.4
CAS1	690	99.2	0.7	1.0	3.5	NOVM	750	93.6	0.9	0.9	4.2
COCO	630	98.2	1.1	0.9	4.6	NTUS	1740	96.6	1.1	1.1	4.3
CONZ	690	86.5	0.7	0.8	2.5	NURK	690	95.9	0.9	0.8	3.8
DARW	750	93.8	2.3	2.2	7.5	OHI3	630	98.5	0.5	0.9	2.6
DGAV	840	99.0	0.8	0.9	2.7	PALV	690	99.2	0.6	0.9	2.5
DLFT	630	97.7	0.7	1.0	3.2	RCMV	1050	77.4	1.9	1.5	8.4
FAA1	1110	95.7	1.2	1.8	6.4	RECF	750	99.2	1.3	1.2	4.2
FAIV	630	99.3	0.8	1.1	3.0	REUN	3180	94.8	1.4	1.4	6.1
FFMJ	1110	96.9	0.9	1.0	3.3	ROAP	3450	89.6	1.7	2.7	6.5
FRDN	630	99.3	0.6	0.9	2.6	SALU	690	99.2	1.4	1.2	6.1

continued on next page

continued from previous page

Station	Time	Rate	East	North	Up	Station	Time	Rate	East	North	Up
GANP	1200	96.9	0.9	1.6	3.9	SASS	1350	97.0	0.6	0.8	2.6
GODZ	960	98.9	0.6	0.8	3.5	SAVO	780	99.1	0.9	0.8	3.9
HOB2	1530	98.2	1.0	1.1	3.8	SCH2	630	99.3	0.8	1.0	2.2
HUEG	1110	96.9	0.7	1.0	3.3	STR1	870	99.0	1.0	1.2	4.9
IQAL	630	99.3	0.6	0.7	3.0	SVTL	1110	97.5	0.9	0.9	2.7
IRKJ	780	98.4	0.7	0.9	2.3	TABV	630	99.3	0.9	1.1	4.6
KHAJ	690	93.4	0.8	1.1	4.0	THU2	630	99.3	0.6	0.6	3.8
KHAR	1320	96.9	0.8	0.9	3.2	VALD	630	97.2	0.6	0.8	2.4
KOKV	630	98.4	1.5	1.8	6.3	WHIT	630	99.3	0.7	0.9	2.5
KOUC	3120	85.5	3.5	3.1	6.2	WTZJ	1680	96.0	1.1	1.0	4.0
KOUR	690	99.2	1.1	0.8	3.6	WTZZ	1530	96.8	0.8	0.8	2.9
MAL2	1140	98.5	0.8	0.6	2.6	XMIS	1110	97.6	1.3	0.9	4.4
MARS	810	96.8	0.8	1.0	4.0	Mean	1101	96.4	1.0	1.1	4.0

Table 7.3: Performance of real-time PPP with ambiguity resolution when the 18-station global network is used (see Figure 7.2c). Meanings of columns refer to Table 7.1

Station	Time	Rate	East	North	Up	Station	Time	Rate	East	North	Up
ABMF	3540	56.7	1.1	1.1	7.1	MAS1	8070	17.4	0.9	1.4	4.3
ADIS	15150	47.1	1.3	0.9	5.7	MATE	8220	37.8	1.0	1.4	4.1
AJAC	8220	35.7	1.4	1.9	6.0	MDVJ	8160	27.5	3.1	2.2	3.9
ANKR	8220	49.7	2.1	1.5	7.7	MOBS	–	0.0	–	–	–
BAKE	3360	12.1	2.1	1.2	3.6	MTKA	29850	8.2	1.3	0.8	2.9
BOGI	8070	29.4	0.9	2.6	3.2	NANO	3360	15.9	1.8	1.4	2.9
BRST	8070	31.6	1.0	1.1	3.1	NICO	8220	54.0	1.0	1.0	2.7
CAS1	–	0.0	–	–	–	NOVM	14340	22.0	1.7	1.0	3.2
COCO	35580	9.5	2.1	0.5	6.4	NTUS	20220	49.8	1.6	1.3	5.3
CONZ	26010	44.2	1.1	1.3	4.5	NURK	14340	43.5	1.5	1.0	3.6
DARW	–	0.0	–	–	–	OHI3	39390	16.7	0.7	1.1	3.9
DGAV	26490	20.7	2.1	1.1	3.6	PALV	6870	10.2	0.8	1.6	9.0
DLFT	6960	27.2	0.8	1.9	6.9	RCMV	26100	9.5	0.8	1.1	5.0
FAA1	57300	20.1	1.3	0.7	4.1	RECF	4230	63.2	1.4	1.6	4.7
FAIV	4710	13.4	0.8	2.0	5.9	REUN	–	0.0	–	–	–
FFMJ	6960	28.0	1.0	2.2	7.2	ROAP	13890	12.1	2.5	1.6	9.9
FRDN	3540	28.5	1.2	2.9	2.9	SALU	16350	60.4	2.0	1.6	5.9
GANP	13890	16.4	3.0	1.4	8.6	SASS	8070	26.1	2.1	3.0	10.4
GODZ	3540	32.9	1.0	1.7	3.4	SAVO	15120	52.1	1.0	1.4	4.5
HOB2	–	0.0	–	–	–	SCH2	6960	18.8	2.2	2.3	2.5
HUEG	6960	28.0	1.0	1.7	6.8	STR1	–	0.0	–	–	–
IQAL	3540	15.7	2.2	1.9	3.5	SVTL	11940	10.9	3.9	3.1	7.9
IRKJ	8220	24.1	2.1	2.5	6.1	TABV	3540	14.8	2.5	1.3	5.5
KHAJ	54540	5.9	1.9	2.1	5.0	THU2	–	0.0	–	–	–
KHAR	8070	51.4	1.1	1.2	3.3	VALD	3540	34.3	1.2	2.1	2.5
KOKV	4710	15.3	1.8	1.6	7.7	WHIT	3540	18.1	1.6	1.1	4.9
KOUC	–	0.0	–	–	–	WTZJ	8220	32.3	2.6	1.3	5.4
KOUR	4230	86.4	1.1	0.8	4.4	WTZZ	8220	29.7	1.3	1.7	7.1
MAL2	14340	69.3	0.7	0.5	2.7	XMIS	28350	19.4	1.8	1.1	6.3
MARS	8070	31.5	1.4	1.4	4.8	Mean	13165	30.1	1.6	1.5	5.1

7.4 A case study on the 2009 L'Aquila earthquake

The global PPP-RTK can achieve centimeter- or even millimeter-level positioning accuracy even if no nearby reference stations are available (refer to Section 5.6 and 7.3). This section will show a case study on monitoring the April 6th 2009 L'Aquila earthquake with this PPP-RTK.

7.4.1 Data, models and methods

A M_w 6.3 earthquake struck the city of L'Aquila, Italy on April 6th 2009, resulting in hundreds of deaths and severe damage. To test the PPP-RTK, 18 1-Hz stations across Europe were selected from the EUREF-IP project (Figure 7.4) to estimate satellite clocks and FCBs by fixing predicted satellite orbits and ERPs from the IGS in a simulated real-time manner (i.e. forward data filtering without backward smoothing), but ignoring communication delays which usually occur in practice. A station M0SE at Rome was chosen as a GPS seismometer (Figure 7.4). It was about 85 km from the epicenter. Meanwhile, absolute antenna phase centers (Schmid et al. 2007), phase wind-up corrections (Wu et al. 1993) and station displacements according to the IERS 2003 conventions (McCarthy and Petit 2004) were applied. Ambiguity resolution at a single receiver was also applied in real time.

High-rate epoch-wise position estimates are significantly affected by multipath effects (e.g. Bilich et al. 2008; Larson et al. 2007). Hence, the GPS measurements at M0SE on April 5th were also processed in order to perform sidereal filtering at the coordinate level to mitigate the multipath effects (Ragheb et al. 2007).

7.4.2 Results

Figure 7.5 shows the displacements at M0SE for the East and North components. A period of 360 s is presented and the mean of epoch-wise position estimates during this period has been removed. The range of $\pm 2\sigma$ for each component is shown in order to attempt to distinguish the spurious and true movement of M0SE. In Figure 7.5, the time when the earthquake occurred is denoted by the left vertical line whilst the approximate time when the earthquake waveform reached M0SE by the right vertical line. Note that the waveform speed is presumed to be about 3 km/s. Hence, the duration for the waveform reaching M0SE is about $\frac{85}{3} \approx 28$ s. As shown in Figure 7.5, after the earthquake waveform reached M0SE, the scatter of the epoch-wise estimates for the horizontal components becomes a little greater. From this scatter, it can be inferred that the shake of M0SE due to this earthquake lasted for about 30 to 40 s.

In order to clearly describe the shake of M0SE during the earthquake, Figure 7.6 shows the estimated horizontal movement of M0SE before, during and after the earthquake. Corresponding to Figure 7.5, the left, middle and right subfigures of Figure 7.6 show the shake from 5510 to 5590 s, from 5590 to 5670 s and from 5670 to 5750 s, respectively. These three subfigures correspond to the aseismic, co-seismic and post-seismic periods. It can be easily found that the scatter of horizontal positions during the earthquake is much more pronounced than those before and after the earthquake, clearly demonstrating the shake of M0SE due to the L'Aquila earthquake.

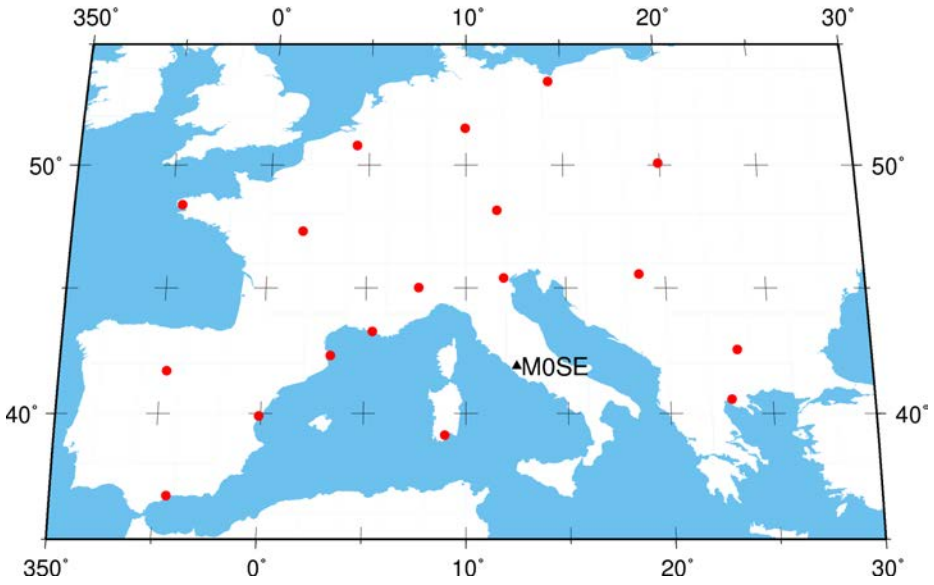

Figure 7.4: GPS stations for monitoring the 6th April 2009 L'Aquila earthquake. Red solid circles denote reference stations used for the satellite clock and FCB determination and the black triangle with name aside denotes the station used as a GPS seismometer

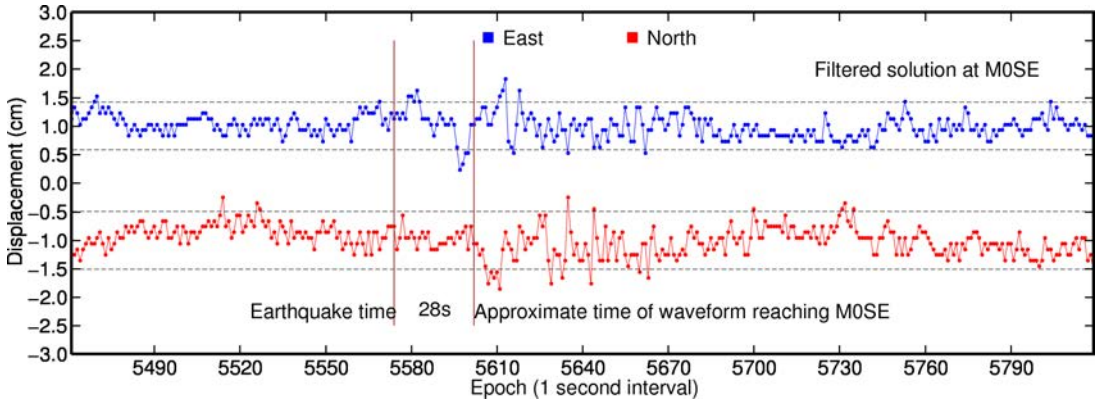

Figure 7.5: Displacements for the East and North components at M0SE due to the L'Aquila earthquake. The horizontal dashed lines denote two times the formal errors of the East and North components. The East component is offset by 1 cm whereas the North component by -1 cm for clarity

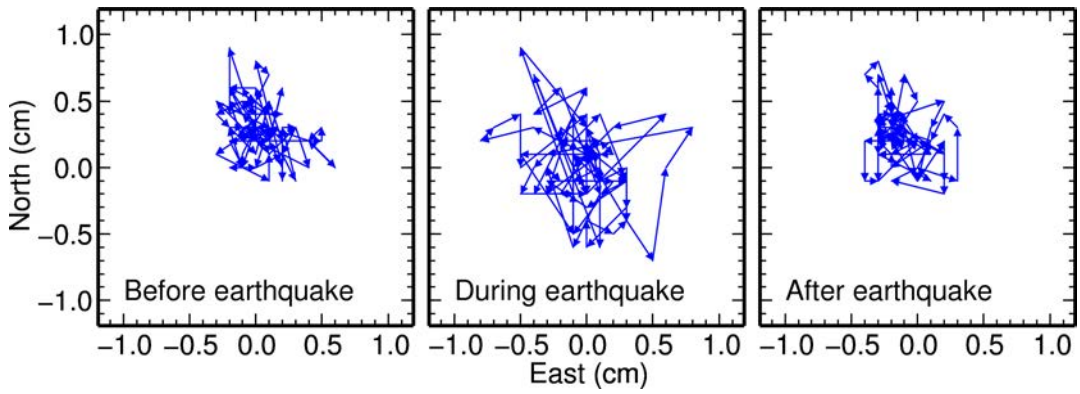

Figure 7.6: Estimated horizontal movement of M0SE before, during and after the L'Aquila earthquake

7.5 Summary

This chapter is based on the theories and results presented in Chapters 2, 3, 5 and 6, and suggests a prototype of a global PPP-RTK service which relies on real-time PPP that is greatly enhanced by ambiguity resolution and rapid convergences or re-convergences. The potential application of this PPP-RTK service to geohazard early warnings is also discussed. Then the interesting question that how many reference stations are sufficient to support such a global PPP-RTK service is preliminarily discussed by comparing three typical network distributions. Finally, a case study on the April 6th 2009 L'Aquila earthquake is presented.

Chapter 8

Conclusions and Perspectives

8.1 Summary

Over the past decade, PPP has been widely applied to many scientific and commercial fields due to its high computational efficiency, no need for any synchronous measurements from a nearby reference station and homogeneous positioning quality on a global scale. However, it is well-known that PPP suffers from unresolved ambiguities and slow convergences to ambiguity-fixed solutions. Hence, this thesis aims at improving PPP by resolving ambiguities for a single receiver and accelerating convergences to ambiguity-fixed solutions in order to achieve centimeter-level positioning accuracy with only a few seconds of measurements.

In this thesis, ambiguity resolution is primarily based on the method by Ge et al. (2008), but four improvements, i.e. the derivation of undifferenced FCBs, one FCB per satellite-pair pass over a regional area, implementation of real-time ambiguity resolution and constraints from integer double-difference ambiguities, are developed in this thesis. These improvements are quantitatively assessed in post-processing and real-time PPP. In addition, one of the main contributions of this thesis is the theoretical proof and empirical verification for the equivalence of ambiguity-fixed position estimates derived from the two recognized methods for PPP ambiguity resolution, i.e. the FCB- and IRC-based methods.

On the other hand, for the first time, a method for effectively re-achieving ambiguity-fixed solutions in real-time PPP with only a few seconds of measurements is originally developed and quantitatively assessed in this thesis. This method is based on the precisely predicted ionospheric delays generated by PPP users themselves, and hence the advantage of no need for any raw measurements from a nearby reference station is preserved and the practicability of real-time PPP is greatly improved. In addition, a strategy for achieving the first ambiguity-fixed solution is also proposed in this thesis. This strategy relies on a dense network of reference stations from which ionospheric delays can be precisely interpolated for PPP users.

Finally, a global PPP-RTK prototype is suggested in this thesis based on the above methods. The question that how many reference stations are sufficient to support this global PPP-RTK and its potential application in geohazard early warnings are discussed. In this chapter, the conclusions of this thesis are highlighted from two aspects, i.e. the theoretical analysis and the data analysis. The contributions and perspectives of this thesis then end this chapter.

8.2 Conclusions on the theoretical analysis

8.2.1 Integer ambiguity resolution

Methods for ambiguity resolution at a single receiver have two categories, i.e. the FCB- and IRC-based methods. The FCB-based methods perform ambiguity resolution on differential ambiguity estimates by correcting the FCBs assimilated into these ambiguity estimates. Note that FCBs do not apply to measurement modeling. This is because FCBs are derived from the undifferenced ambiguity estimates for a network of reference stations. An assumption of constant FCBs over the observation period is required in the theoretical derivation of the FCB-based methods. The FCB-based methods are compatible with the conventional PPP proposed by Zumberge et al. (1997) and thus can easily supplement the generation of IGS satellite products.

On the other hand, the IRC-based methods perform ambiguity resolution on undifferenced ambiguity estimates by applying the IRCs to the measurement modeling. Note that the integer property of an undifferenced ambiguity is preserved in the estimation. This is because the IRCs are estimated in a network solution by first fixing undifferenced ambiguities to integers. No assumption on FCBs' temporal or spatial properties is required. The IRC-based methods are not compatible with the conventional PPP and consequently the IRCs cannot be combined with the IGS satellite clocks.

8.2.2 Method comparison

The ambiguity-fixed position estimates of the FCB- and IRC-based methods are theoretically identical. This implies that a systematic difference between the ambiguity-fixed position estimates in practice, if existing, should not be caused by the differences between the two methods themselves. Ideally, the difference between the actual estimates should be minimal and random in nature. However, we have to keep in mind that this theoretical equivalence is rigorously based on the assumption that FCBs are hardware-dependent and only they are assimilated into the to-be-estimated parameters of PPP after a least squares adjustment.

8.2.3 Attempts for rapid convergences

To date, few feasible or effective methods have been developed to significantly accelerate convergences to ambiguity-fixed solutions in real-time PPP. To my knowledge, four attempts have been performed by: estimating the pseudorange precision; constraining the position parameters; improving the ambiguity validation; or applying the ambiguity resolution. Although the results of all four attempts are inconclusive, they at least confirm that the precision of pseudorange or unambiguous measurements is critical to the convergence speed, and demonstrate that neither ambiguity resolution nor improved ambiguity validation can effectively lead to a convergence period of less than a few seconds.

8.2.4 Rapid re-convergences to ambiguity-fixed solutions

Rapid re-convergences can be achieved by exploiting the high temporal correlation of ionospheric delays within a short period of up to a few minutes. In this thesis, ionospheric delays at all ambiguity-fixed epochs are estimated and precisely predicted to succeeding epochs in the case of re-convergences. These predicted ionospheric delays are first used to correct wide-lane

measurements in order to rapidly resolve wide-lane ambiguities. Then the resulting precise ionosphere-corrected unambiguous wide-lane measurements are used to tightly constrain and thus significantly accelerate subsequent narrow-lane ambiguity resolution. This method does not rely on the satellite-geometry change, but on the sufficient shrink of the search space for integer candidates. Key issues for this method include the temporal properties of all errors assimilated into ionospheric delay estimates, the predicting strategy for these delays, and the model consistency between estimating ionospheric delays and resolving wide-lane ambiguities.

8.3 Conclusions on the data analysis

8.3.1 One FCB per satellite-pair pass over a regional area

For ambiguity resolution, FCBs are divided into wide-lane and narrow-lane ones. Wide-lane FCBs have good stability over at least several days, even if they are estimated with a global network. However, narrow-lane FCB estimates manifest instability even within 24 hours. This instability is caused by non-hardware-dependent errors, e.g. tropospheric delays, that are assimilated into narrow-lane FCB estimates. Therefore, a narrow-lane FCB estimate contains more than a real hardware bias.

For a global network, Ge et al. (2008) suggested a 15-minute mean to estimate narrow-lane FCBs of high precisions. On the other hand, for a regional network like the EPN, this thesis suggests that narrow-lane FCBs can be precisely estimated once per satellite-pair pass over this network. Tests in this thesis demonstrate that most narrow-lane FCB estimates achieve high precisions of better than 0.1 cycles (3σ). Note that this strategy is developed not because it can outperform the 15-minute mean in the precisions of narrow-lane FCB estimates, but because it produces much fewer, but still sufficiently precise, narrow-lane FCBs for a regional network, thereby improving the efficiency of disseminating FCBs to users.

8.3.2 Post-processing PPP with ambiguity resolution

Ambiguity resolution can significantly improve the positioning quality of sub-daily PPP. Tests on the EPN demonstrate that ambiguity resolution reduces the RMS of differences between hourly and daily position estimates from 3.8, 1.5 and 2.8 cm to 0.5, 0.5 and 1.4 cm for the East, North and Up components for the inside-EPN stations, respectively. The success rate of ambiguity resolution is up to 98.75%. Surprisingly, EPN-based FCB estimates are applicable to ambiguity resolution for outside-EPN stations which can be up to 4000 km away. The RMS statistics are also reduced from 3.7, 1.5 and 3.2 cm in ambiguity-float solutions to 0.6, 0.6 and 2.0 cm in ambiguity-fixed solutions. This finding thus suggests a great advantage of ambiguity-fixed PPP over NRTK.

Note that correct ambiguity resolution does not always lead to an improved positioning accuracy. However, for hourly PPP at inside-EPN stations, the rate of these problematic solutions is greatly reduced from 1.13% to only 0.15% if tropospheric delays are mitigated with accurate a priori values, hence demonstrating that estimating ZTDs is a crucial factor for the occurrence of these problematic solutions.

Sub-daily PPP with more than one hour of measurements can further improve on the hourly PPP. Specifically, the success rate of ambiguity resolution reaches 100.0% and the rate of problematic solutions above falls to 0.7% if three hours of measurements are used. Note that

increasing the observation period from one to three hours minimally reduces the horizontal RMS, but clearly improves the vertical RMS in the ambiguity-fixed solutions.

In addition, the radius of a ring reference network centered on a remote user receiver can affect the performance of ambiguity-fixed kinematic PPP. When the radius is enlarged from 900, 2000 to 3600 km, the RMS statistics of epoch-wise position differences from ground truths are slightly increased from 0.6, 0.5 and 2.6 cm, 0.5, 0.7 and 2.8 cm to 0.8, 1.0 and 3.2 cm for the East, North and Up components respectively. However, the efficiency of ambiguity resolution is negligibly affected by this radius increase.

8.3.3 Real-time PPP with ambiguity resolution

Ambiguity resolution has the potential of leading to PPP-RTK in which PPP provides rapid convergences to the reliable centimeter-level positioning accuracy. It is illustrated that at least 10 minutes of measurements are required for most receiver types to reliably fix about 90% of wide-lane ambiguities corresponding to elevations of $\geqslant 30°$, and over 20 minutes to fix about 90% of those corresponding to elevations of $<30°$. Moreover, several tens of minutes are usually required for a regional network to stabilize a narrow-lane FCB estimate to an accuracy of far better than 0.1 cycles. Within one hour, ambiguity resolution can significantly reduce the RMS of differences between epoch-wise and daily position estimates by an order of magnitude from 13.7, 7.1 and 11.4 cm to 0.8, 0.9 and 2.5 cm for the East, North and Up components respectively, but a few tens of minutes is required to achieve the first ambiguity-fixed solution. In addition, a globally distributed network of 38 stations can lead to a global PPP-RTK which can guarantee a success rate of over 95% for the ambiguity-fixed epochs.

Therefore, PPP-RTK currently cannot satisfy the critical requirement of instantaneous precise positioning where ambiguity-fixed solutions have to be achieved with at most a few seconds of measurements. However, this PPP-RTK can still be applied to some near-real-time remote sensing applications, such as GPS meteorology and geohazard early warnings.

8.3.4 Integer constraints from double-difference ambiguities

Applying double-difference ambiguity resolution to a PPP-based network solution can improve the accuracy of narrow-lane FCB estimates. In a global network analysis over one year, the RMS of differences for the East component between the daily and IGS weekly estimates is reduced from 2.6 mm in solutions based on original narrow-lane FCBs to 2.2 mm in solutions based on improved narrow-lane FCBs.

8.3.5 Method comparison

Ambiguity-fixed position estimates derived from the FCB- and IRC-based methods are identical in theory. To verify this equivalence, one year of GPS data from a global network of about 350 stations were processed. The mean biases between all daily position estimates derived from these two methods are only 0.2, 0.1 and 0.0 mm, whereas the standard deviations of all position differences are only 1.3, 0.8 and 2.0 mm for the East, North and Up components, respectively. Moreover, the differences of the position repeatabilities are below 0.2 mm on average for all three components. The RMS of the position estimates minus those from the IGS weekly solutions for the FCB-based method differs by below 0.1 mm on average for each component from that for the

IRC-based method. Therefore, considering the recognized millimeter-level precision of current GPS-derived daily positions, these statistics empirically demonstrate the theoretical equivalence of the ambiguity-fixed position estimates derived from these two methods.

However, the different strategies of separating the FCBs from integer ambiguities in these two methods lead to geographical-distribution patterns of their positioning discrepancy. For instance, for the East component, the station-specific RMS statistics of the position differences are well below 1.5 mm in Europe and North America with relatively dense networks, whereas usually over 2.0 mm in oceanic areas and Africa with very sparse networks. Moreover, in terms of the East position repeatability and the East RMS statistics against the IGS weekly solutions, the FCB-based method performs slightly better over dense networks, whereas the IRC-based method performs a little better over sparse networks.

Overall, the IRC-based method slightly outperforms the FCB-based method for the East component. However, in practice, the FCB-based method is compatible with current IGS clock-generation methods, whereas the IRC-based method is not, but can potentially lead to slightly better positioning quality.

8.3.6 Rapid re-convergences to ambiguity-fixed solutions

In the case of re-convergences, ionospheric delays are precisely predicted to significantly accelerate ambiguity resolution. In a test for 90 static stations suffering from simulated total loss of tracking, 93.3% and 95.0% of re-convergences to wide-lane and narrow-lane ambiguity resolutions were achieved within five epochs of 1-Hz measurements respectively, even though the latency for predicted ionospheric delays was up to 180 s. If this latency is prolonged, the prediction error of ionospheric delays is increased, consequently reducing both percentages above. On the other hand, for most rapid re-convergences, only one epoch of measurements is needed, implying that the contribution of satellite-geometry changes to these rapid re-convergences is negligible.

In a test for a mobile van moving in a GPS-adverse environment where satellite number significantly decreases and cycle slips frequently occur, only when the predicted ionospheric delays are applied can the rate of ambiguity-fixed epochs be dramatically improved from 7.7% to 93.6% of all epochs. Moreover, the RMS of position differences from the ground truth derived from a post-processed short-baseline solution are 1.0, 1.3 and 2.7 cm for the East, North and Up components respectively, which are slightly larger than but comparable with those of an NRTK solution.

Therefore, my method for rapid re-convergences can potentially relieve the unrealistic requirement of a continuous open sky view by most PPP applications and improve the practicability of real-time PPP. Note that the effectiveness of this method is subject to the ionosphere condition. A high ionosphere activity may fail a rapid re-convergence, even if the latency is less than a few minutes.

8.4 Main contributions to knowledge

The foremost contributions of this thesis to the new knowledge are summarized as follows:

1. **Theoretical proof for the equivalence of ambiguity-fixed position estimates between the FCB- and IRC-based methods.** For the first time, the controversy on how to assess the methods for PPP ambiguity resolution, i.e. the FCB- and IRC-based

methods, is concluded by proving the theoretical equivalence between their individual ambiguity-fixed position estimates. Furthermore, through a substantial and representative data processing, the actual performance of these methods on a global scale is quantified and compared, consequently demonstrating the advantages and disadvantages of these methods in practice. This empirical analysis can be a guidance for the future implementation of these methods.

2. **Real-time implementation of the FCB-based method.** For the first time, a real-time model for the FCB-based method is developed by carefully investigating the temporal property of narrow-lane FCBs in a real-time scenario. Real-time PPP is of great interest, especially to the engineering community, and hence a real-time implementation of ambiguity-fixed PPP is essential and important.

3. **Rapid re-convergences to ambiguity-fixed solutions.** For the first time, a method for rapid re-convergences of only a few seconds to ambiguity-fixed solutions in real-time PPP is developed. This method can potentially relieve the unrealistic requirement of a continuous open sky view by most PPP applications and improve the practicability of real-time PPP, thus greatly enhancing its competitiveness against NRTK.

4. **A prototype of global PPP-RTK service.** This prototype design is based on all techniques introduced or developed in this thesis. Current global real-time PPP services cannot provide ambiguity-fixed solutions whereas NRTK services can hardly extend to a global scale. However, this global PPP-RTK combines the merits of both global real-time PPP and NRTK, i.e. providing ambiguity-fixed solutions as soon as possible on a global scale.

8.5 Recommendations and Perspectives

The recommendations and perspectives of this thesis are presented as follows:

1. **Quality control of the integer ambiguity resolution in real-time PPP.** Narrow-lane ambiguities suffer from a rather short wavelength of about 11 cm. Hence, narrow-lane ambiguities risk a greater possibility of an incorrect integer resolution. In this case, a good quality-control technique is required in order to reduce the risk of incorrect ambiguity resolution and recover from an incorrect resolution (Han 1997b).

2. **Wide-area ionospheric tomography.** As demonstrated in Section 3.6 and 6.6, interpolated precise ionospheric delays can be used to significantly accelerate the first convergence to ambiguity-fixed solution in real-time PPP. Although a sufficiently precise ionospheric tomography based on a sparse network at scales of several hundred kilometers is still under development, it is the most promising technique for providing far better than 1-TECU-level ionospheric delays in real time (Hernández-Pajares et al. 2000). If this ionospheric tomography is available, a PPP-RTK service (Geng et al. 2010d; Wübbena et al. 2005) that can rapidly provide ambiguity-fixed solutions may prevail against current RTK positioning services based on dense networks.

3. **Multi-frequency PPP.** Future multi-frequency GNSS data will lead to the possibility of forming ionosphere-reduced, low-noise and long-wavelength inter-frequency combina-

tion observables (Feng 2008). Hence, we can reasonably envisage that rapid ambiguity resolution may be achieved using an innovative dedicated combination observable.

4. **FCBs or IRCs?** The IRC-based methods can potentially produce better positioning quality than that of the FCB-based methods. Moreover, FCBs have to be combined with satellite clocks in order to relieve the transmission-bandwidth requirement, whereas IRCs do not suffer from this processing. However, IRCs are not compatible with the clock-generation strategy currently adopted by most research institutes and commercial firms. Hence, of great concern is whether the IRCs will finally be recognized and accepted as new standards for the next-generation PPP.

References

Abdel-salam M (2004) A hybrid solution to reduce the long convergence time in precise point positioning. In: Proceedings of ION GNSS 17th International Technical Meeting of the Satellite Division, Long Beach, US, pp 2555–2562

Abdel-salam M, Gao Y (2003) Ambiguity resolution in precise point positioning: Preliminary results. In: Proceedings of ION GNSS 16th International Technical Meeting of the Satellite Division, Portland, US, pp 1222–1228

Agrotis L, Sanz PA, Dow J, Zandbergen R, Švehla D, Ballereau A (2010a) ESOC's RETINA system and the generation of the IGS RT combination. Presented at IGS Workshop 2010, Newcastle upon Tyne, UK

Agrotis L, Sanz PA, Švehla D, Dow J, Zandbergen R (2010b) RTPP analysis results: Achievements and challenges. Abstracts for European Geosciences Union General Assembly, Vienna, Austria

Alkan RM (2001) GPS-single point positioning without selective availability. In: Proceedings of US Hydrographic Conference, Norfold, US

Allen RM, Gasparini P, Kamigaichi O, Böse M (2009) The status of earthquake early warning around the world: An introductory overview. Seismol Res Lett 80(5):682–693

Altamimi Z, Collilieux X (2009) IGS contribution to the ITRF. J Geod 83(3-4):375–383

Amiri-Simkooei AR, Teunissen PJG, Tiberius C (2009) Application of least-squares variance component estimation to GPS observables. J Surv Eng-ASCE 135(4):149–160

Anzidei M, Boschi E, Cannelli V, Devoti R, Esposito A, Galvani A, Melini D, Pietrantonio G, Riguzzi F, Sepe V, Serpelloni E (2009) Coseismic deformation of the destructive April 6, 2009 L'Aquila earthquake (central Italy) from GPS data. Geophys Res Lett 36:L17307. doi:10.1029/2009GL039145

Aponte J, Meng X, Hill C, Moore T, Burbidge M, Dodson AH (2009) Quality assessment of a network-based RTK GPS service in the UK. J Appl Geod 3(1):25–34

Banerjee P, Pollitz F, Nagarajan B, Burgmann R (2007) Coseismic slip distributions of the 26 December 2004 Sumatra-Andaman and 28 March 2005 earthquakes from GPS static offsets. Bull Seismol Soc Am 97(1A):S86–S102

Banville S, Langley RB (2009) Improving real-time kinematic PPP with instantaneous cycle-slip correction. In: Proceedings of ION GNSS 22nd International Technical Meeting of the Satellite Division, Savannah, US, pp 2470–2478

Bar-Sever YE (1996) A new model for GPS yaw attitude. J Geod 70(11):714–723

Bar-Sever YE, Kroger PM, Borjesson JA (1998) Estimating horizontal gradients of tropospheric path delay with a single GPS receiver. J Geophys Res 103(B3):5019–5035

van Barneveld PWL, Montenbruck O, Visser PNAM (2009) Epochwise prediction of GPS single differenced ionospheric delays of formation flying spacecraft. Adv Space Res 44(9):987–1001

Basu S, Groves KM, Basu Su, Sultan PJ (2002) Specification and forecasting of scintillations in communication/navigation links: Current status and future plans. J Atmos Sol-Terr Phy 64(16):1745–1754

Bertiger W, Desai SD, Haines B, Harvey N, Moore AW, Owen S, Weiss JP (2010) Single receiver phase ambiguity resolution with GPS data. J Geod 84(5):327–337

Beutler G, Schildknecht T, Hugentobler U, Gurtner W (2003) Orbit determination in satellite geodesy. Adv Space Res 31(8):1853–1868

Bierman GJ (1977) Factorization methods for discrete sequential estimation. Academic press Inc, Florida. pp 241

Bilich A, Larson KM, Axelrad P (2008) Modeling GPS phase multipath with SNR: Case study from the Salar de Uyuni, Boliva. J Geophys Res 113:B04401. doi:10.1029/2007JB005194

Bisnath S, Gao Y (2007) Current state of precise point positioning and future prospects and limitations. In: Sideris MG (ed) Observing our changing Earth, Springer-Verlag, Berlin Heidelberg, pp 615–623

Bisnath S, Gao Y (2009) Precise point positioning: A powerful technique with a promising future. GPS World 20(4):43–50

Blewitt G (1989) Carrier phase ambiguity resolution for the global positioning system applied to geodetic baselines up to 2000 km. J Geophys Res 94(B8):10187–10203

Blewitt G (1990) An automatic editing algorithm for GPS data. Geophys Res Lett 17(3):199–202

Blewitt G (2008) Fixed point theorems of GPS carrier phase ambiguity resolution and their application to massive network processing: Ambizap. J Geophys Res 113(B12):B12410. doi:10.1029/2008JB005736

Blewitt G, Kreemer C, Hammond WC, Plag HP, Stein S, Okal E (2006) Rapid determination of earthquake magnitude using GPS for tsunami warning systems. Geophys Res Lett 33:L11309. doi:10.1029/2006GL026145

Blewitt G, Hammond WC, Kreemer C, Plag HP, Stein S, Okal E (2009) GPS for real-time earthquake source determination and tsunami warning systems. J Geod 83(3-4):335–343

Bock H, Dach R, Jäggi A, Beutler G (2009a) High-rate GPS clock corrections from CODE: Support of 1 Hz applications. J Geod 83(11):1083–1094

Bock H, Dach R, Yoon Y, Montenbruck O (2009b) GPS clock correction estimation for near real-time orbit determination applications. Aerosp Sci Technol 13(7):415–422

Bock O, Tarniewicz J, Thom C, Pelon J, Kasser M (2001) Study of external path delay correction techniques for high accuracy height determination with GPS. Phys Chem Earth 26:165–171

Bock Y, Nikolaidis RM, de Jonge P, Bevis M (2000) Instantaneous geodetic positioning at medium distances with the Global Positioning System. J Geophys Res 105(B12):28223–28253

Bock Y, Prawirodirdjo L, Melbourne TI (2004) Detection of arbitrarily large dynamic ground motions with a dense high-rate GPS network. Geophys Res Lett 31:L06604. doi:10.1029/2003GL019150

Boehm J, Niell AE, Tregoning P, Schuh H (2006a) The Global Mapping Function (GMF): A new empirical mapping function based on data from numerical weather model data. Geophys

Res Lett 33:L07304. doi:10.1029/2005GL025546

Boehm J, Werl B, Schuh H (2006b) Troposphere mapping functions for GPS and very long baseline interferometry from European Centre for Medium-Range Weather Forecasts operational analysis data. J Geophys Res 111:B02406. doi:10.1029/2005JB003629

Boehm J, Heinkelmann R, Schuh H (2007) Short note: A global model of pressure and temperature for geodetic applications. J Geod 81(10):679–683

Boehm J, Kouba J, Schuh H (2009) Forecast Vienna Mapping Functions 1 for real-time analysis of space geodetic observations. J Geod 83(5):397–401

Bona P (2000) Precision, cross correlation, and time correlation of GPS phase and code observations. GPS Solut 4(2):3–13

Bosser P, Bock O, Thom C, Pelon J, Willis P (2010) A case study of using Raman lidar measurements in high-accuracy GPS applications. J Geod 84(4):251–265

Bouin MN, Ballu V, Calmant S, Boré JM, Folcher E, Ammann J (2009) A kinematic GPS methodology for sea surface mapping, Vanuatu. J Geod 83(12):1203–1217

Bruyninx C (2004) The EUREF permanent network: A multi-disciplinary network serving surveyors as well as scientists. GeoInformatics 7:32–35

Bruyninx C, Becker M, Stangl G (2001) Regional densification of the IGS in Europe using the EUREF permanent GPS network (EPN). Phys Chem Earth Pt A 26(6-8):531–538

Bust GS, Mitchell CN (2008) History, current state, and future directions of ionospheric imaging. Rev Geophys 46:RG1003. doi:10.1029/2006RG000212

Cai C, Gao Y (2007) Performance analysis of precise point positioning based on combined GPS and GLONASS. In: Proceedings of ION GNSS 20th International Technical Meeting of the Satellite Division, Fort Worth, US, pp 858–865

Calais E, Han JY, DeMets C, Nocquet JM (2006) Deformation of the North America plate interior from a decade of continuous GPS measurements. J Geophys Res 111:B06402. doi: 10.1029/2005JB004253

Cao C (2009) Status of COMPASS/BeiDou development. Presented at Stanford's PNT Challenges and Opportunities Symposium, Stanford, US

Cao W, Hauschild A, Steigenberger P, Langley RB, Urquhart L, Santos M, Montenbruck O (2010) Performance evaluation of integrated GPS/GIOVE precise point positioning. In: Proceedings of ION International Technical Meeting, San Diego, US, pp 540–552

Cardellach E, Elósegui P, Davis JL (2007) Global distortion of GPS networks associated with satellite antenna model errors. J Geophys Res 112:B07405. doi:10.1029/2006JB004675

Chadwell CD, Bock Y (2001) Direct estimation of absolute precipitable water in oceanic regions by GPS tracking of a coastal buoy. Geophys Res Lett 28(19):3701–3704

Chadwell CD, Spiess FN (2008) Plate motion at the ridge-transform boundary of the south Cleft Segment of the Juan de Fuca Ridge from GPS-acoustic data. J Geophys Res 113:B04415. doi: 10.1029/2007JB004936

Chen K (2004) Real-time precise point positioning and its potential applications. In: Proceedings of ION GNSS 17th International Technical Meeting of the Satellite Division, Long Beach, US, pp 1844–1854

Chen K, Gao Y (2005) Real-time precise point positioning using single frequency data. In:

Proceedings of ION GNSS 18th International Technical Meeting of the Satellite Division, Long Beach, US, pp 1514–1523

Collins P (2008) Isolating and estimating undifferenced GPS integer ambiguities. In: Proceedings of ION National Technical Meeting, San Diego, US, pp 720–732

Collins P, Gao Y, Lahaye F, Héroux P, MacLeod K, Chen K (2005) Accessing and processing real-time GPS corrections for precise point positioning – some user considerations. In: Proceedings of ION GNSS 18th International Technical Meeting of the Satellite Division, Long Beach, US, pp 1483–1491

Collins P, Lahaye F, Héroux P, Bisnath S (2008) Precise point positioning with ambiguity resolution using the decoupled clock model. In: Proceedings of ION GNSS 21st International Technical Meeting of the Satellite Division, Savannah, US, pp 1315–1322

Collins P, Henton J, Mireault Y, Héroux P, Schmidt M, Dragert H, Bisnath S (2009) Precise point positioning for real-time determination of co-seismic crustal motion. In: Proceedings of ION GNSS 22nd International Technical Meeting of the Satellite Division, Savannah, US, pp 2479–2488

Colombo OL (2004) Evaluation of precise, kinematic GPS point positioning. In: Proceedings of ION GNSS 17th International Technical Meeting of the Satellite Division, Long Beach, US, pp 1423–1430

Colombo OL (2006) A zenith delay model for precise kinematic aircraft navigation. In: Proceedings of ION GNSS 19th International Technical Meeting of the Satellite Division, Fort Worth, US, pp 68–76

Colombo OL (2009) Shortening the convergence time of wide-area real-time kinematic solutions. In: Proceedings of ION GNSS 22nd International Technical Meeting of the Satellite Division, Savannah, US, pp 2425–2436

Colombo OL, Evans AG, Ando M, Tadokoro K, Sato K, Yamada T (2001) Speeding up the estimation of floated ambiguities for sub-decimeter kinematic positioning at sea. In: Proceedings of ION GPS 14th International Technical Meeting of the Satellite Division, Salt Lake, US, pp 2980–2989

Creager GJ, Maggio RC (1998) How long must we wait? Duration of GPS observations for long GPS baselines. In: Proceedings of 54th Annual Meeting of the Institute of Navigation, Denver, US, pp 467–475

Crowell BW, Bock Y, Squibb MB (2009) Demonstration of earthquake early warning using total displacement waveforms from real-time GPS networks. Seismol Res Lett 80(5):772–782

Dach R, Hugentobler U, Fridez P, Meindl M (eds) (2007) Bernese GPS software Version 5.0. Astronomical Institute, University of Bern, Bern. pp 612

Dach R, Brockman E, Schaer S, Beutler G, Meindl M, Prange L, Bock H, Jäggi A, Ostini L (2009) GNSS processing at CODE: Status report. J Geod 83(3-4):353–365

Dai L (2000) Dual-frequency GPS/GLONASS real-time ambiguity resolution for medium-range kinematic positioning. In: Proceedings of ION GPS 13th International Technical Meeting of the Satellite Division, Salt Lake City, US, pp 1071–1079

Dai L, Wang J, Rizos C, Han S (2003) Predicting atmospheric biases for real-time ambiguity resolution in GPS/GLONASS reference station networks. J Geod 76(11-12):617–628

Dai L, Han S, Wang J, Rizos C (2004) Comparison of interpolation algorithms in network-based

GPS techniques. Navigation: Journal of the Institute of Navigation 50(4):277–293

Dai L, Eslinger D, Sharpe T (2007) Innovative algorithms to improve long range RTK reliability and availability. In: Proceedings of ION National Technical Meeting, San Diego, US, pp 860–872

van Dam T, Wahr J, Milly PCD, Shmakin AB, Blewitt G, Lavallée D, Larson KM (2001) Crustal displacements due to continental water loading. Geophys Res Lett 28(4):651–654

Defraigne P, Bruyninx C (2007) On the link between GPS pseudorange noise and day-boundary discontinuities in geodetic time transfer solutions. GPS Solut 11(4):239–249

Defraigne P, Guyennon N, Bruyninx C (2008) GPS time and frequency transfer: PPP and phase-only analysis. International Journal of Navigation and Observation 2008:175468. doi: 10.1155/2008/175468

Delporte J, Mercier F, Laurichesse D, Galy O (2008) GPS carrier-phase time transfer using single-difference integer ambiguity resolution. International Journal of Navigation and Observation 2008:273785. doi:10.1155/2008/273785

Dilssner F, Seeber G, Wübbena G, Schmitz M (2008) Impact of near-field effects on the GNSS position solution. In: Proceedings of ION GNSS 21st International Technical Meeting of the Satellite Division, Savannah, US, pp 612–624

Dilssner F, Springer T, Flohrer C, Dow J (2010) Estimation of phase center corrections for GLONASS-M satellite antennas. J Geod 84(8):467–480. doi:10.1007/s00190-010-0381-7

Dixon K (2006) Starfire$^{\mathrm{TM}}$: A global SBAS for sub-decimeter precise point positioning. In: Proceedings of ION GNSS 19th International Technical Meeting of the Satellite Division, Fort Worth, US, pp 2286–2296

Dong D, Bock Y (1989) Global positioning system network analysis with phase ambiguity resolution applied to crustal deformation studies in California. J Geophys Res 94(B4):3949–3966

Douša J (2010) The impact of errors in predicted GPS orbits on zenith troposphere delay estimation. GPS Solut 14(3):229–239

Dow JM, Neilan RE, Rizos C (2009) The International GNSS Service in a changing landscape of Global Navigation Satellite Systems. J Geod 83(3-4):191–198

Ebner R, Featherstone WE (2008) How well can online GPS PPP post-processing services be used to establish geodetic survey control networks? Journal of Applied Geodesy 2(3):149–157

Eckl MC, Snay RA, Soler T, Cline MW, Mader GL (2001) Accuracy of GPS-derived relative positions as a function of interstation distance and observing-session duration. J Geod 75(12):633–640

El-Arini MB, Conker R, Albertson T, Reegan JK, Klobuchar JA, Doherty P (1995) Comparison of real-time ionospheric algorithms for a GPS wide-area augmentation system (WAAS). Navigation: Journal of the Institute of Navigation 41(4):393–413

El-Mowafy A (2009) Alternative postprocessing relative positioning approach based on precise point positioning. J Surv Eng-ASCE 135(2):56–65

Elósegui P, Davis JL, Oberlander D, Baena R, Ekström G (2006) Accuracy of high-rate GPS for seismology. Geophys Res Lett 33:L11308. doi:10.1029/2006GL026065

Estey LH, Meertens CM (1999) Teqc: The multi-purpose toolkit for GPS/GLONASS data. GPS Solut 3(1):42–49

Euler HJ, Schaffrin B (1990) On a measure of the discernibility between different ambiguity solutions in the static-kinematic GPS mode. In: Schwarz KP, Lachapelle G (eds) Kinematic Systems in Geodesy, Surveying and Remote Sensing, Springer-Verlag, New York, pp 285–295

Falck C, Ramatschi M, Subarya C, Bartsch M, Merx A, Hoeberechts J, Schmidt G (2010) Near real-time GPS applications for tsunami early warning systems. Nat Hazards Earth Syst Sci 10:181–189

Falcone M (2008) Galileo programme status. In: Proceedings of ION GNSS 21st International Technical Meeting of the Satellite Division, Savannah, GA, pp 453–492

Fell P, Maul GA (2000) Marine positioning: State of technology. In: Proceedings of Oceans 2000 MTS/IEEE Conference and Exhibition, Providence, US

Feng Y (2008) GNSS three carrier ambiguity resolution using ionosphere-reduced virtual signals. J Geod 82(12):847–862

Feng Y, Rizos C, Higgins M (2007) Multiple carrier ambiguity resolution and performance benefits for RTK and PPP positioning services in regional areas. In: Proceedings of ION GNSS 20th International Technical Meeting of the Satellite Division, Fort Worth, US, pp 668–678

Fotopoulos G, Cannon ME (2001) An overview of multi-reference station methods for cm-level positioning. GPS Solut 4(3):1–10

Fund F, Morel L, Mocquet A, Boehm J (2010) Assessment of ECMWF-derived tropospheric delay models within the EUREF permanent network. GPS Solut doi:10.1007/s10291-010-0166-8

Gabor MJ, Nerem RS (1999) GPS carrier phase ambiguity resolution using satellite-satellite single difference. In: Proceedings of ION GNSS 12th International Technical Meeting of the Satellite Division, Nashville, US, pp 1569–1578

Ortiz de Galisteo JP, Toledano C, Cachorro V, Torres B (2010) Improvement in PWV estimation from GPS due to the absolute calibration of antenna phase center variations. GPS Solut doi: 10.1007/s10291-010-0163-y

Gao Y, Shen X (2001) Improving ambiguity convergence in carrier phase-based precise point positioning. In: Proceedings of ION GNSS 14th International Technical Meeting of the Satellite Division, Salt Lake City, US, pp 1532–1539

Gao Y, Zhang Y, Chen K (2006) Development of a real-time single-frequency precise point positioning system and test results. In: Proceedings of ION GNSS 19th International Technical Meeting of the Satellite Division, Fort Worth, US, pp 2297–2303

García-Fernández M, Markgraf M, Montenbruck O (2008) Spin rate estimation of sounding rockets using GPS wind-up. GPS Solut 12(3):155–161

Ge M, Gendt G, Dick G, Zhang FP (2005a) Improving carrier-phase ambiguity resolution in global GPS network solutions. J Geod 79(1-3):103–110

Ge M, Gendt G, Dick G, Zhang FP, Reigber C (2005b) Impact of GPS satellite antenna offsets on scale changes in global network solutions. Geophys Res Lett 32(6):L06310. doi:10.1029/2004GL022224

Ge M, Gendt G, Dick G, Zhang FP, Rothacher M (2006) A new data processing strategy for huge GNSS global networks. J Geod 80(4):199–203

Ge M, Gendt G, Rothacher M, Shi C, Liu J (2008) Resolution of GPS carrier-phase ambiguities in precise point positioning (PPP) with daily observations. J Geod 82(7):389–399

Ge M, Chen J, Douša J, Gendt G, Ramatschi M, Wickert J (2010) A new approach for estimating satellite clocks from large GNSS reference networks in real-time. Presented at IGS Workshop 2010, Newcastle upon Tyne, UK

Gendt G, Nischan T (2005) 2003/2004 analysis coordinator report. IGS Central Bureau, Pasadena, US

Gendt G, Dick G, Reigber CH, Tomassini M, Liu Y, Ramatschi M (2003) Demonstration of NRT GPS water vapor monitoring for numerical weather prediction in Germany. J Meteo Societ Jap 82(1B):360–370

Geng J (2009) Rapid re-convergence in real-time precise point positioning with ambiguity resolution. In: Proceedings of ION GNSS 22nd International Technical Meeting of the Satellite Division, Savannah, US, pp 2437–2448

Geng J, Shi C, Zhao Q, Liu J (2006) Integrated adjustment of LEO and GPS in precision orbit determination. In: Xu P, Liu J, Dermanis A (eds) Proceedings of VI Hotine-Marussi Symposium on Theoretical and Computational Geodesy, Springer-Verlag, Berlin Heidelberg, pp 133–137

Geng J, Shi C, Zhao Q, Liu J (2007a) GPS precision orbit determination from combined ground and space-borne data. Geomatics and Information Science of Wuhan University 32(10):906–909. (*in Chinese*)

Geng J, Teferle FN, Shi C, Meng X, Dodson AH, Liu J (2009) Ambiguity resolution in precise point positioning with hourly data. GPS Solut 13(4):263–270

Geng J, Meng X, Dodson AH, Ge M, Teferle FN (2010a) Rapid re-convergences to ambiguity-fixed solutions in precise point positioning. J Geod doi:10.1007/s00190-010-0404-4

Geng J, Meng X, Teferle FN, Dodson AH (2010b) Performance of precise point positioning with ambiguity resolution for 1- to 4-hour observation periods. Surv Rev 42(316):155–165

Geng J, Teferle FN, Meng X, Dodson AH (2010c) Kinematic precise point positioning at remote marine platforms. GPS Solut doi:10.1007/s10291-009-0157-9

Geng J, Teferle FN, Meng X, Dodson AH (2010d) Towards PPP-RTK: Ambiguity resolution in real-time precise point positioning. Adv Space Res doi:10.1016/j.asr.2010.03.030

Geng T, Zhao Q, Liu J, Du R (2007b) Real-time precise point positioning based on PANDA software. Geomatics and Information Science of Wuhan University 32(4):312–315. (*in Chinese*)

Genrich JF, Bock Y (2006) Instantaneous geodetic positioning with 10-50 Hz GPS measurements: Noise characteristics and implications for monitoring networks. J Geophys Res 111:B03403. doi:10.1029/2005JB003617

Ghoddousi-Fard R, Dare P (2006) Online GPS processing services: An initial study. GPS Solut 10(1):12–20

Gjevestad JGO, Øvstedal O, Kjørsvik NS (2007) The contribution of GLONASS and Galileo to kinematic GPS precise point positioning. In: Proceedings of ION GNSS 20th International Technical Meeting of the Satellite Division, Fort Worth, US, pp 876–882

van Graas F, Soloviev A (2004) Precise velocity estimation using a stand-alone GPS receiver. Navigation: Journal of the Institute of Navigation 51(4):283–292

Gregorius TLH, Blewitt G (1999) Modeling weather fronts to improve GPS heights: A new tool for GPS meteorology? J Geophys Res 104(B7):15261–15279

Grejner-Brzezinska DA, Kashani I, Wielgosz P (2005) On accuracy and reliability of instanta-

neous network RTK as a function of network geometry, station separation, and data processing strategy. GPS Solut 9(3):212–225

Grejner-Brzezinska DA, Arslan N, Wielgosz P, Hong CK (2009) Network calibration for unfavorable reference-rover geometry in network-based RTK: Ohio CORS case study. J Surv Eng-ASCE 135(3):90–100

Griffiths J, Ray JR (2009) On the precision and accuracy of IGS orbits. J Geod 83(3-4):277–287

Guida U, Vritschan M, Westbrook J (2007) The qualification of EGNOS, the final step to the operational service. In: Proceedings of ION GNSS 20th International Technical Meeting of the Satellite Division, Fort Worth, US, pp 900–906

Guo J, Langley RB (2003) A new tropospheric propagation delay mapping function for elevation angles down to 2°. In: Proceedings of ION GNSS 16th International Technical Meeting of the Satellite Division, Portland, US, pp 368–376

Han S (1997a) Ambiguity recovery for long-range GPS kinematic positioning. Navigation: Journal of the Institute of Navigation 44(2):257–266

Han S (1997b) Quality-control issues relating to instantaneous ambiguity resolution for real-time GPS kinematic positioning. J Geod 71(6):351–361

Han S, Rizos C (1996) Integrated method for instantaneous ambiguity resolution using new generation GPS receivers. In: Proceedings of IEEE Position, Location and Navigation Symposium, Atlanta, US, pp 254–261

Han S, Rizos C (2000a) Airborne GPS kinematic positioning and its application to oceanographic mapping. Earth Planets Space 52(10):819–824

Han S, Rizos C (2000b) GPS multipath mitigation using FIR filters. Surv Rev 35(277):487–498

Hatch R (1982) The synergism of GPS code and carrier measurements. In: Proceedings of the 3rd International Geodetic Symposium on Satellite Doppler Positioning, Las Cruces, US, pp 1213–1231

Hatch R, Jung J, Enge P, Pervan B (2000) Civilian GPS: The benefits of three frequencies. GPS Solut 3(4):1–9

Hauschild A, Montenbruck O (2009) Kalman-filter-based GPS clock estimation for near real-time positioning. GPS Solut 13(3):173–182

Henkel P, Günther C (2008) Precise point positioning with multiple Galileo frequencies. In: Proceedings of IEEE/ION Position, Location and Navigation Symposium, Monterey, US, pp 592–599

Henkel P, Günther C (2010) Partial integer decorrelation: Optimum trade-off between variance reduction and bias amplification. J Geod 84(1):51–63

Henkel P, Gomez V, Günther C (2009) Modified LAMBDA for absolute carrier phase positioning in the presence of biases. In: Proceedings of ION International Technical Meeting, Anaheim, US, pp 642–651

Henkel P, Wen Z, Günther C (2010) Estimation of satellite and receiver biases on multiple Galileo frequencies with a Kalman filter. In: Proceedings of ION International Technical Meeting, San Diego, US, pp 1067–1074

Hernández-Pajares M, Juan JM, Sanz J, Colombo OL (1999) Precise ionospheric determination and its application to real-time GPS ambiguity resolution. In: Proceedings of ION GNSS 12th International Technical Meeting of the Satellite Division, Nashville, US, pp 1409–1417

Hernández-Pajares M, Juan JM, Sanz J, Colombo OL (2000) Application of ionospheric tomography to real-time GPS carrier-phase ambiguities resolution, at scales of 400-1000 km and with high geomagnetic activity. Geophys Res Lett 27(13):2009–2012

Hernández-Pajares M, Juan JM, Sanz J, Orús R (2007) Second-order ionospheric term in GPS: Implementation and impact on geodetic estimates. J Geophys Res 112:B08417. doi:10.1029/2006JB004707

Hernández-Pajares M, Juan JM, Sanz J, Orús R, Garcia-Rigo A, Feltens J, Komjathy A, Schaer SC, Krankowski A (2009) The IGS VTEC maps: A reliable source of ionospheric information since 1998. J Geod 83(3-4):263–275

Héroux P, Gao Y, Kouba J, Lahaye F, Mireault Y, Collins P, Macleod K, Tétreault P, Chen K (2004) Products and applications for precise point positioning – moving towards real-time. In: Proceedings of ION GNSS 17th International Technical Meeting of the Satellite Division, Long Beach, US, pp 1832–1843

Hesselbarth A, Wanninger L (2008) Short-term stability of GNSS satellite clocks and its effects on precise point positioning. In: Proceedings of ION GNSS 21st International Technical Meeting of the Satellite Division, Savannah, US, pp 1855–1863

Hill EM, Davis JL, Elósegui P, Wernicke BP, Malikowski E, Niemi NA (2009) Characterization of site-specific GPS errors using a short-baseline network of braced monuments at Yucca Mountain, southern Nevada. J Geophys Res 114:B11402. doi:10.1029/2008JB006027

Hobiger T, Ichikawa R, Takasu T, Koyama Y, Kondo T (2008) Ray-traced troposphere slant delays for precise point positioning. Earth Planets Space 60(5):e1–e4

Hofmann-Wellenhof B, Lichtenegger H, Collins J (2001) GPS theory and practice, 5th edn. Springer-Verlag, Wien New York. pp 382

Hopfield HS (1969) Two-quadratic tropospheric refractivity profile for correction satellite data. J Geophys Res 74(18):4487–4499

Huber K, Heuberger F, Abart C, Karabatic A, Weber R, Berglez P (2010) PPP: Precise point positioning - constraints and opportunities. In: Proceedings of XXIV FIG International Congress, Sydney, Australia

Hwang C, Tseng TP, Lin T, Švehla D, Bill S (2009) Precise orbit determination for the FORMOSAT-3/COSMIC satellite mission using GPS. J Geod 83(5):477–489

Iwabuchi T, Rocken C, Lukes Z, Mervart L, Johnson J, Kanzaki M (2006) PPP and network true real-time 30 sec estimation of ZTD in dense and giant regional GPS network and the application of ZTD for nowcasting of heavy rainfall. In: Proceedings of ION GNSS 19th International Technical Meeting of the Satellite Division, Fort Worth, US, pp 1902–1909

Jäggi A, Hugentobler U, Bock H, Beutler G (2007) Precise orbit determination for GRACE using undifferenced or doubly differenced GPS data. Adv Space Res 39(10):1612–1619

Jefferson DC, Heflin MB, Muellerschoen RJ (2001) Examining the C1-P1 pseudorange bias. GPS Solut 4(4):25–30

Jensen ABO, Øvstedal O (2008) The effect of different tropospheric models on precise point positioning in kinematic mode. Surv Rev 40(308):173–187

Jensen ABO, Øvstedal O, Grinde G (2007) Development of a regional ionosphere model for Norway. In: Proceedings of ION GNSS 20th International Technical Meeting of the Satellite Division, Fort Worth, US, pp 2880–2889

Jin SG, Wang J, Park PH (2005) An improvement of GPS height estimates: Stochastic modeling. Earth Planets Space 57(4):253–259

de Jonge PJ, Tiberius CCJM (1996) The LAMBDA method for integer ambiguity estimation: Implementation aspects. Delft Geodetic Computing Center, Delft, Netherlands. pp 49

Joosten P, Tiberius C (2002) LAMBDA: FAQs. GPS Solut 6(1-2):109–114

Kang Z, Nagel P, Pastor R (2003) Precise orbit determination for GRACE. Adv Space Res 31(8):1875–1881

Kaplan ED, Hegarty CJ (eds) (2006) Understanding GPS principles and applications, 2nd edn. Artech House, Norwood, MA. pp 381–391

Kashani I, Wielgosz P, Grejner-Brzezinska D (2007) The impact of the ionospheric correction latency on long-baseline instantaneous kinematic GPS positioning. Surv Rev 39(305):238–251

Kato T, Terada Y, Ito K, Hattori R, Abe T, Miyake T, Koshimura S, Nagai T (2005) Tsunami due to the 2004 September 5th off the Kii peninsula earthquake, Japan, recorded by a new GPS buoy. Earth Planets Space 57(4):297–301

Kechine MO, Tiberius C, van der Marel H (2004) An experimental performance analysis of real-time kinematic positioning with NASA's internet-based global differential GPS. GPS Solut 8(1):9–22

Kee C, Parkinson BW, Axelrad P (1991) Wide area differential GPS. Navigation: Journal of the Institute of Navigation 38(2):123–145

Kim BC, Tinin MV (2007) Contribution of ionospheric irregularities to the error of dual-frequency GNSS positioning. J Geod 81(3):189–199

Kim D, Serrano L, Langley R (2006) Phase wind-up analysis: Assessing real-time kinematic performance. GPS World 17(9):58–64

King M, Aoki S (2003) Tidal observations on floating ice using a single GPS receiver. Geophys Res Lett 30(3):1138. doi:10.1029/2002GL016182

King MA (2009) The GPS contribution to the error budget of surface elevations derived from airborne LIDAR. IEEE T Geosci and Remote 47(3):874–883

King MA, Watson CS (2010) Long GPS coordinate time series: Multipath and geometry effects. J Geophys Res 115:B04403. doi:10.1029/2009JB006543

King MA, Williams SDP (2009) Apparent stability of GPS monumentation from short-baseline time series. J Geophys Res 114:B10403. doi:10.1029/2009JB006319

King MA, Colemar R, Nguyen LN (2003) Spurious periodic horizontal signals in sub-daily GPS position estimates. J Geod 77(1-2):15–21

King MA, Penna NT, Clarke PJ (2005) Validation of ocean tide models around Antarctica using onshore GPS and gravity data. J Geophys Res 110:B08401. doi:10.1029/2004JB003390

Kjørsvik NS, Øvstedal O, Gjevestad JGO (2007) Kinematic precise point positioning during marginal satellite availability. In: Sideris MG (ed) Observing our changing Earth, Springer-Verlag, Berlin Heidelberg, pp 691–699

Klobuchar JA (1986) Design and characteristics of the GPS ionospheric time delay algorithm for single-frequency users. In: Proceedings of PLANS-86 Conference, Las Vegas, US, pp 280–286

Kouba J (2008) Implementation and testing of the gridded Vienna Mapping Function 1 (VMF1). J Geod 82(4-5):193–205

Kouba J (2009a) A simplified yaw-attitude model for eclipsing GPS satellites. GPS Solut 13(1):1–12

Kouba J (2009b) Testing of global pressure/temperature (GPT) model and global mapping function (GMF) in GPS analyses. J Geod 83(3-4):199–208

Kouba J, Héroux P (2001) Precise point positioning using IGS orbit and clock products. GPS Solut 5(2):12–28

Kouba J, Springer T (2001) New IGS station and satellite clock combination. GPS Solut 4(4):31–36

Landau H, Chen X, Klose S, Leandro R, Vollath U (2007) Trimble's RTK and DGPS solutions in comparison with precise point positioning. In: Sideris MG (ed) Observing our changing Earth, Springer-Verlag, Berlin Heidelberg, pp 709–718

Langbein J, Bock Y (2004) High-rate real-time GPS network at Parkfield: Utility for detecting fault slip and seismic displacements. Geophys Res Lett 31:L15S20. doi:10.1029/2003GL019408

Larson KM (2009) GPS seismology. J Geod 83(3-4):227–233

Larson KM, Miyazaki S (2008) Resolving static offsets from high-rate GPS data: The 2003 Tokachi-oki earthquake. Earth Planets Space 60(8):801–808

Larson KM, Cervelli P, Lisowski M, Miklius A, Segall P, Owen S (2001) Volcano monitoring using the Global Positioning System: Filtering strategies. J Geophys Res 106(B9):19453–19464

Larson KM, Bodin P, Gomberg J (2003) Using 1-Hz GPS data to measure deformation caused by the Denali fault earthquake. Science 300(5624):1421–1424

Larson KM, Bilich A, Axelrad P (2007) Improving the precision of high-rate GPS. J Geophys Res 112:B05422. doi:10.1029/2006JB004367

Laurichesse D, Mercier F (2007) Integer ambiguity resolution on undifferenced GPS phase measurements and its application to PPP. In: Proceedings of ION GNSS 20th International Technical Meeting of the Satellite Division, Fort Worth, US, pp 839–848

Laurichesse D, Mercier F, Berthias JP, Bijac J (2008a) Real time zero-difference ambiguities fixing and absolute RTK. In: Proceedings of ION National Technical Meeting, San Diego, US, pp 745–755

Laurichesse D, Mercier F, Berthias JP, Broca P, Cerri L (2008b) Zero-difference ambiguity fixing for spaceborne GPS receivers. In: Proceedings of ION GNSS 21st International Technical Meeting of the Satellite Division, Savannah, US, pp 758–768

Laurichesse D, Mercier F, Berthias JP (2009a) Real time precise GPS constellation orbits and clocks estimation using zero-difference integer ambiguity fixing. In: Proceedings of ION International Technical Meeting, Anaheim, US, pp 664–672

Laurichesse D, Mercier F, Berthias JP (2009b) Zero-difference integer ambiguity fixing on single frequency receivers. In: Proceedings of ION GNSS 22nd International Technical Meeting of the Satellite Division, Savannah, US, pp 2460–2469

Laurichesse D, Mercier F, Berthias JP, Broca P, Cerri L (2009c) Integer ambiguity resolution on undifferenced GPS phase measurements and its application to PPP and satellite precise orbit determination. Navigation: Journal of the Institute of Navigation 56(2):135–149

Lawrence D, Bunce D, Mathur NG, Sigler CE (2007) Wide area augmentation system (WAAS) - program status. In: Proceedings of ION GNSS 20th International Technical Meeting of the Satellite Division, Fort Worth, US, pp 892–899

Lazio P (2007) Constraining network adjustment to OPUS-RS coordinate observations. J Surv Eng-ASCE 133(3):106–113

Le AQ, Lorga JFM (2006) Combining inertial navigation system with GPS precise point positioning: Flight trial results. In: Proceedings of ION GNSS 21st International Technical Meeting of the Satellite Division, Savannah, US, pp 3035–3042

Le AQ, Tiberius C (2006) Phase wind-up effects in precise point positioning with kinematic platforms. In: Proceedings of the 3rd ESA Workshop on Satellite Navigation User Equipment Technologies, Noordwijk, Netherlands

Le AQ, Tiberius C (2007) Single-frequency precise point positioning with optimal filtering. GPS Solut 11(1):61–69

Leandro R, Langley RB, Santos MC (2007) Estimation of P2-C2 biases by means of precise point positioning. In: Proceedings of the 63rd Annual Meeting of The Institute of Navigation, Cambridge, US, pp 225–231

Leandro R, Santos MC, Langley RB (2010) Analyzing GNSS data in precise point positioning software. GPS Solut doi:10.1007/s10291-010-0173-9

Li B, Shen Y (2010) Global navigation satellite system ambiguity resolution with constraints from normal equations. J Surv Eng-ASCE 136(2):63–71

Li B, Feng Y, Shen Y (2010) Three carrier ambiguity resolution: Distance-independent performance demonstrated using semi-generated triple frequency GPS signals. GPS Solut 14(2):177–184

Li M, Geng J, Shi C, Zhao Q (2008) Orbit determination of geostationary satellite during manoeuvres. In: Proceedings of the Society of Photographic Instrumentation Engineers, 7285, 728520. doi:10.1117/12.816380

Liu J, Ge M (2003) PANDA software and its preliminary result of positioning and orbit determination. J Nat Sci Wuhan Univ 8(2B):603–609. doi:10.1007/BF02899825

Liu X, Ditmar P, Siemes C, Slobbe DC, Revtova E, Klees R, Riva R, Zhao Q (2010) DEOS mass transport model (DMT-1) based on GRACE satellite data: Methodology and validation. Geophys J Int 181(2):769–788

Liu Z (2003) Development and analysis of a new ionospheric model. In: Proceedings of ION GNSS 16th International Technical Meeting of the Satellite Division, Portland, US, pp 1692–1703

Liu Z, Gao Y (2004) Ionospheric TEC predictions over a local area GPS reference network. GPS Solut 8(1):23–29

McCarthy DD, Petit G (eds) (2004) IERS 2003 Conventions. Verlag des Bundes für Kartographie und Geodäsie, Frankfurt am Main, Germany. pp 127

McDonald KD (2002) The modernization of GPS: Plans, new capabilities and the future relationship to Galileo. Journal of Global Positioning System 1(1):1–17

Melbourne TI, Webb FH, Stock JM, Reigber C (2002) Rapid postseismic transients in subduction zones from continuous GPS. J Geophys Res 107(B10):2241. doi:10.1029/2001JB000555

Melbourne WG (1985) The case for ranging in GPS-based geodetic systems. In: Proceedings of First International Symposium on Precise Positioning with the Global Positioning System, Rockville, US, pp 373–386

Melgard T, Vigen E, Ørpen O, Ulstein JH (2010) Pulling in all signals: PPP with GPS and

GLONASS: The new G2. GPS World 21(3):28–35

Mercier F, Laurichesse D (2008) Zero-difference ambiguity blocking properties of satellite/receiver widelane biases. In: Proceedings of European Navigation Conference, Toulouse, France

Mervart L, Lukes Z, Rocken C, Iwabuchi T (2008) Precise point positioning with ambiguity resolution in real-time. In: Proceedings of ION GNSS 21st International Technical Meeting of the Satellite Division, Savannah, US, pp 397–405

Meyer CD (2000) Matrix analysis and applied linear algebra. Society for Industrial and Applied Mathematics, Philadelphia, US. pp 718

Miyazaki S, Larson KM, Choi K, Hikima K, Koketsu K, Bodin P, Haase J, Emore G, Yamagiwa A (2004) Modeling the rupture process of the 2003 September 25 Tokachi-Oki (Hokkaido) earthquake using 1-Hz GPS data. Geophys Res Lett 31:L21603. doi:10.1029/2004GL021457

Mondal P, Tewari VK (2007) Present status of precision farming: A review. Int J Agr Res 2(1):1–10

Montenbruck O, Gill E (2000) Satellite orbits: Models, methods, and applications, 1st edn. Springer-Verlag, Berlin Heidelberg. pp 370

Montenbruck O, Gill E, Kroes R (2005) Rapid orbit determination of LEO satellites using IGS clock and ephemeris products. GPS Solut 9(3):226–235

Morujão DB, Mendes VB (2008) Investigation of instantaneous carrier phase ambiguity resolution with the GPS/GALILEO combination using the general ambiguity search criterion. Journal of Global Positioning System 7(1):35–45

Munekane H, Boehm J (2010) Numerical simulation of troposphere-induced errors in GPS-derived geodetic time series over Japan. J Geod 84(7):405–417

Musa TA, Lim S, Rizos C (2005) GPS network-based approach to mitigate residual tropospheric delay in low latitude area. In: Proceedings of ION GNSS 18th International Technical Meeting of the Satellite Division, Long Beach, US, pp 2606–2613

Niell AE (1996) Global mapping functions for the atmosphere delay at radio wavelengths. J Geophys Res 101(B2):3227–3246

Noll C, Bock Y, Habrich H, Moore A (2009) Development of data infrastructure to support scientific analysis for the International GNSS Service. J Geod 83(3-4):309–325

Ogaja C, Satirapod C (2007) Analysis of high-frequency multipath in 1-hz GPS kinematic solutions. GPS Solut 11(4):269–280

Øvstedal O (2002) Absolute positioning with single-frequency GPS receivers. GPS Solut 5(4):33–44

Park B, Kee C (2010) The compact network RTK method: An effective solution to reduce GNSS temporal and spatial decorrelation error. J Navigation 63(2):343–362

Peng WC, Lee YH, Chiang KW, Yang M (2008) The study of typhoon path in Taiwan region using precise point positioning technique. In: Proceedings of ION GNSS 21st International Technical Meeting of the Satellite Division, Savannah, US, pp 244–252

Petrie EJ, King MA, Moore P, Lavallée DA (2010) Higher-order ionospheric effects on the GPS reference frame and velocities. J Geophys Res 115:B03417. doi:10.1029/2009JB006677

Pratt M, Burke B, Misra P (1997) Single-epoch integer ambiguity resolution with GPS L1-

L2 carrier phase measurements. In: Proceedings of ION GPS 10th International Technical Meeting of the Satellite Division, Kansas City, US, pp 1737–1746

Puskas CM, Smith RB, Meertens CM, Chang WL (2007) Crustal deformation of the Yellowstone-Snake River Plain volcano-tectonic system: Campaign and continuous GPS observations, 1987-2004. J Geophys Res 112:B03401. doi:10.1029/2006JB004325

Ragheb AE, Clarke PJ, Edwards SJ (2007) GPS sidereal filtering: Coordinate- and carrier-phase-level strategies. J Geod 81(5):325–335

Revnivykh S (2008) Glonass status and progress. In: Proceedings of ION GNSS 21st International Technical Meeting of the Satellite Division, Savannah, GA, pp 431–452

Rizos C (2007) Alternatives to current GPS-RTK services and some implications for CORS infrastructure and operations. GPS Solut 11(3):151–158

Rocken C, Johnson J, van Hove T, Iwabuchi T (2005) Atmospheric water vapor and geoid measurements in the open ocean with GPS. Geophys Res Lett 32:L12813. doi:10.1029/2005GL022573

Rocken C, Lukes Z, Mervart L, Johnson J, Iwabuchi T, Kanzaki M (2006) Real-time ionospheric and atmospheric correction for wide area single frequency carrier phase ambiguity resolution. In: Proceedings of ION GNSS 19th International Technical Meeting of the Satellite Division, Fort Worth, US, pp 1208–1218

Rocken C, Iwabuchi T, Lukes Z, Mervart L, Fujita M, Kanzaki M (2008) Precise positioning of ships and buoys in the open ocean – results from a 3-month indian ocean cruise, and a tsunami buoy off Japan's coast. In: Proceedings of ION GNSS 21st International Technical Meeting of the Satellite Division, Savannah, GA, pp 2465–2472

Saastamoinen J (1973) Contribution to the theory of atmospheric refraction: Refraction corrections in satellite geodesy. Bull Gèod 107(1):13–34

Santerre R (1991) Impact of GPS satellite sky distribution. Manuscr Geodaet 16:28–53

Satirapod C, Homniam P (2006) GPS precise point positioning software for ground control point establishment in remote sensing applications. J Surv Eng-ASCE 132(1):11–14

Sato T, Miura S, Ohta Y, Fujimoto H, Sun W, Larsen CF, Heavner M, Kaufman AM, Freymueller JT (2008) Earth tides observed by gravity and GPS in southeastern Alaska. J Geodyn 46(3-5):78–89

Schmid R, Steigenberger P, Gendt G, Ge M, Rothacher M (2007) Generation of a consistent absolute phase-center correction model for GPS receiver and satellite antennas. J Geod 81(12):781–798

Schwarz CR (2008) Heuristic weighting and data conditioning in the National Geodetic Survey rapid static GPS software. J Surv Eng-ASCE 134(3):76–82

Schwarz CR, Snay RA, Soler T (2009) Accuracy assessment of the National Geodetic Survey's OPUS-RS utility. GPS Solut 13(2):119–132

Schweitzer J, Zheng B, Schwieger V, Kosmann D (2010) Evaluation of the TanDEM-X digital elevation model by PPP GPS analysis and intermediate results. In: Proceedings of XXIV FIG International Congress, Sydney, Australia

Senior KL, Ray JR, Beard RL (2008) Characterization of periodic variations in the GPS satellite clocks. GPS Solut 12(3):211–225

Shan S, Bevis M, Kendrick E, Mader GL, Raleigh D, Hudnut K, Sartori M, Phillips D (2007)

Kinematic GPS solutions for aircraft trajectories: Identifying and minimizing systematic height errors associated with atmospheric propagation delays. Geophys Res Lett 34:L23S07. doi:10.1029/2007GL030889

Shi C, Geng J, Liu J, Ge M (2006) Integrated adjustment of LEO and GPS with PANDA in precision orbit determination. In: Proceedings of ION GPS 19th International Technical Meeting of the Satellite Division, Fort Worth, US, pp 2579–2586

Shi C, Geng J, Meng X, Ge M, Teferle FN, Dodson AH (2008a) A novel real-time data screening approach in urban navigation. In: Proceedings of 12th European Navigation Conference, Toulouse, France

Shi C, Zhao Q, Geng J, Lou Y, Ge M, Liu J (2008b) Recent development of PANDA software in GNSS data processing. In: Proceedings of the Society of Photographic Instrumentation Engineers, 7285, 72851S. doi:10.1117/12.816261

Shi C, Lou Y, Zhang H, Zhao Q, Geng J, Wang R, Fang R, Liu J (2010) Estimating seismic displacement of the Mw8.0 Wenchuan earthquake from high-rate GPS observations. Adv Space Res 46(2):228–235

Skone S (2000) Wide area ionosphere modeling at low latitudes – specifications and limitations. In: Proceedings of ION GPS 13th International Technical Meeting of the Satellite Division, Salt Lake, US, pp 643–652

Skone S, Gao Y, Al-Fanek O, Tao W, Zhang Y, Héroux P, Collins P (2006) Atmospheric moisture estimation using GPS on a moving platform. In: Proceedings of ION GNSS 19th International Technical Meeting of the Satellite Division, Fort Worth, US, pp 1891–1900

Snay RA, Soler T (2008) Continuously operating reference station (CORS): History, applications, and future enhancements. J Surv Eng-ASCE 134(4):95–104

Sobolev SV, Babeyko AY, Wang R, Hoechner A, Galas R, Rothacher M, Sein DV, Schröter J, Lauterjung J, Subarya C (2007) Tsunami early warning using GPS-Shield arrays. J Geophys Res 112:B08415. doi:10.1029/2006JB004640

Soler T, Michalak P, Weston ND, Snay RA, Foote RH (2006) Accuracy of OPUS solutions for 1- to 4-h observing sessions. GPS Solut 10(1):45–55

Solheim FS, Vivekanandan J, Ware RH, Rocken C (1999) Propagation delays induced in GPS signals by dry air, water vapor, hydrometeors, and other particulates. J Geophys Res 104(D8):9663–9670

Steigenberger P, Rothacher M, Fritsche M, Rülke A, Dietrich R (2009) Quality of reprocessed GPS satellite orbits. J Geod 83(3-4):241–248

Stoew B, Nilsson T, Elgered G, Jarlemark POJ (2007) Temporal correlation of atmospheric mapping function errors in GPS estimation. J Geod 81(5):311–323

Teferle FN, Orliac EJ, Bingley RM (2007) An assessment of Bernese GPS software precise point positioning using IGS final products for global site velocities. GPS Solut 11(3):205–213

Teferle FN, Geng J, Meng X, Dodson AH, Williams SDP, Pennal N (2008) Possible detection of ocean loading deformation associated with the 9th November 2007 North Sea storm surge using GPS: Preliminary results. Presented at Amerimcan Geophysical Union Fall Meeting, San Francisco, US

Tétreault P, Kouba J, Héroux P, Legree P (2005) CSRS-PPP: An internet service for GPS user access to the canadian spatial reference frame. Geomatica 59(1):17–28

Teunissen PJG (1994) A new method for fast carrier phase ambiguity estimation. In: Proceedings of IEEE Position, Location and Navigation Symposium, Las Vegas, US, pp 562–573

Teunissen PJG (1996) An analytical study of ambiguity decorrelation using dual frequency code and carrier phase. J Geod 70(8):515–528

Teunissen PJG (1997) On the sensitivity of the location, size and shape of the GPS ambiguity search space to certain changes in the stochastic model. J Geod 71(9):541–551

Teunissen PJG (1998) Success probability of integer GPS ambiguity rounding and bootstrapping. J Geod 72(10):606–612

Teunissen PJG (2010) Integer least-squares theory for the GNSS compass. J Geod 84(7):433–447

Teunissen PJG, Kleusberg A (eds) (1998) GPS for Geodesy, 2nd edn. Springer-Verlag, Berlin Heidelberg. pp 650

Teunissen PJG, Verhagen S (2009) The GNSS ambiguity ratio-test revisited: A better way of using it. Surv Rev 41(312):138–151

Teunissen PJG, de Jonge PJ, Tiberius CCJM (1997) The least-squares ambiguity decorrelation adjustment: Its performance on short GPS baselines and short observation spans. J Geod 71(10):589–602

Titov VV, González FI, Bernard EN, Eble MC, Mofjeld HO, Newman JC, Venturato AJ (2005) Real-time tsunami forecasting: Challenges and solutions. Nat Hazards 35(1):41–58

Tregoning P, van Dam T (2005) Atmospheric pressure loading corrections applied to GPS data at the observation level. Geophys Res Lett 32:L22310. doi:10.1029/2005GL024104

Tregoning P, Herring TA (2006) Impact of a priori zenith hydrostatic delay errors on GPS estimates of station heights and zenith total delays. Geophys Res Lett 33:L23303. doi:10.1029/2006GL027706

Tregoning P, Watson C (2009) Atmospheric effects and spurious signals in GPS analysis. J Geophys Res 114:B09403. doi:10.1029/2009JB006344

Verhagen S (2004) Integer ambiguity validation: An open problem? GPS Solut 8(1):36–43

Wang CS, Liou YA, Yeh TK (2008) Impact of surface meteorological measurements on GPS height determination. Geophys Res Lett 35:L23809. doi:10.1029/2008GL035929

Wang J, Stewart MP, Tsakiri M (1998) A discrimination test procedure for ambiguity resolution on-the-fly. J Geod 72(11):644–653

Wang M, Gao Y (2006) GPS un-differenced ambiguity resolution and validation. In: Proceedings of ION GNSS 19th International Technical Meeting of the Satellite Division, Fort Worth, US, pp 292–300

Wang M, Gao Y (2007) An investigation on GPS receiver initial phase bias and its determination. In: Proceedings of ION National Technical Meeting, San Diego, US, pp 873–880

Webb FH, Zumberge JF (1997) An introduction to GIPSY-OASIS II. Jet Propulsion Laboratory, Pasadena, US

Weber G, Mervart L, Lukes Z, Rocken C, Douša J (2007) Real-time clock and orbit corrections for improved point positioning via NTRIP. In: Proceedings of ION GNSS 20th International Technical Meeting of the Satellite Division, Fort Worth, US, pp 1992–1998

Wielgosz P (2010) Quality assessment of GPS rapid static positioning with weighted ionospheric parameters in generalized least squares. GPS Solut doi:10.1007/s10291-010-0168-6

Wielgosz P, Kashani I, Grejner-Brzezinska DA (2005) Analysis of long-range network RTK during a severe ionospheric storm. J Geod 79(9):524–531

Wolf PR, Ghilani CD (1997) Adjustment computations: Statistics and least squares in surveying and GIS, 3rd edn. John Wiley & Sons, New York, US. pp 584

Wu JT, Wu SC, Hajj GA, Bertiger WI, Lichten SM (1993) Effects of antenna orientation on GPS carrier phase. Manuscr Geodaet 18(2):91–98

Wübbena G (1985) Software developments for geodetic positioning with GPS using TI-4100 code and carrier measurements. In: Proceedings of First International Symposium on Precise Positioning with the Global Positioning System, Rockville, US, pp 403–412

Wübbena G, Schmitz M, Bagge A (2005) PPP-RTK: Precise point positioning using state-space representation in RTK networks. In: Proceedings of ION GNSS 18th International Technical Meeting of the Satellite Division, Long Beach, US, pp 2584–2594

Xu G (2007) GPS: Theory, algorithms and applications, 2nd edn. Springer-Verlag, Berlin Heidelberg. pp 340

Xu P (2005) Sign-constrained robust least squares, subjective breakdown point and the effect of weights of observations on robustness. J Geod 79(1-3):146–159

Yang Y, He H, Xu G (2007) Adaptively robust filtering for kinematic geodetic positioning. J Geod 75(2-3):109–116

Yousif H, El-Rabbany A (2007) Assessment of several interpolation methods for precise GPS orbit. J Navigation 60(3):443–455

Yuan X, Fu J, Sun H, Toth C (2009) The application of GPS precise point positioning technology in aerial triangulation. ISPRS J Photogramm 64(6):541–550

Yuan Y, Tscherning CC, Knudsen P, Xu G, Ou J (2008) The ionospheric eclipse factor method (IEFM) and its application to determining the ionospheric delay for GPS. J Geod 82(1):1–8

Zhang X, Andersen OB (2006) Surface ice flow velocity and tide retrieval of the Amery ice shelf using precise point positioning. J Geod 80(4):171–176

Zhang Y, Gao Y (2008) Integration of INS and un-differenced GPS measurements for precise position and attitude determination. J Navigation 61(1):87–97

Zhu L, Lai YC, Shah M, Mahmood S (2007) Efficiency of carrier-phase integer ambiguity resolution for precise GPS positioning in noisy environments. J Geod 81(2):149–156

Zhu SY, Groten E (1988) Relativistic effects in GPS. In: Groten E, Strauß R (eds) GPS-techniques applied to geodesy and surveying, Springer-Verlag, Berlin Heidelberg, pp 41–46

Ziebart M, Cross P, Sibthorpe A, Arrowsmith P, Ochieng W, Feng S, Bhatti U, Niemann P (2007) Single epoch estimation of the Galileo integrity chain sensor station clock offsets. GPS Solut 11(4):227–237

Zumberge JF, Heflin MB, Jefferson DC, Watkins MM, Webb FH (1997) Precise point positioning for the efficient and robust analysis of GPS data from large networks. J Geophys Res 102(B3):5005–5017

Appendix A

Method Comparison

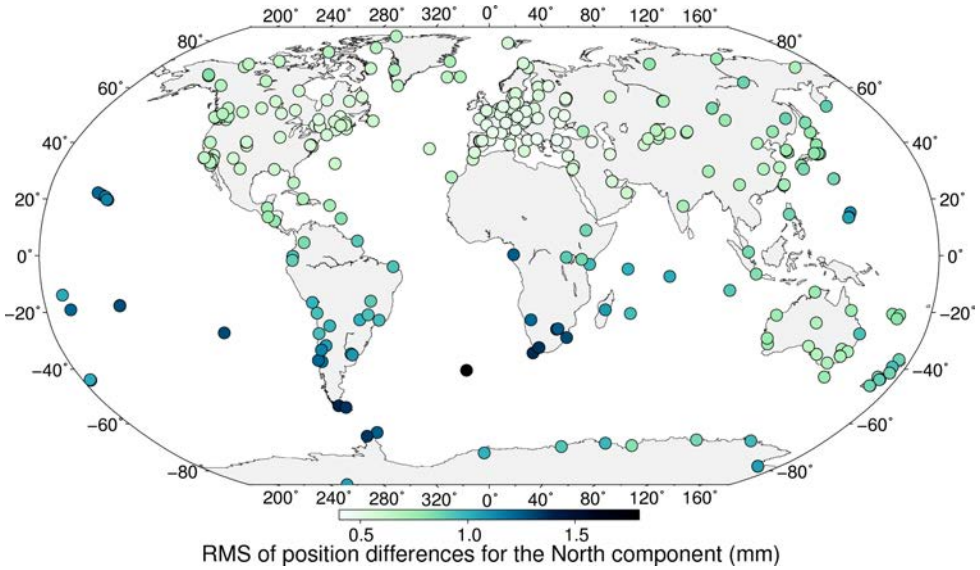

Figure A.1: Geographical distribution of the station-specific RMS statistics of the position differences over one year between the FCB- and IRC-based methods for the North component

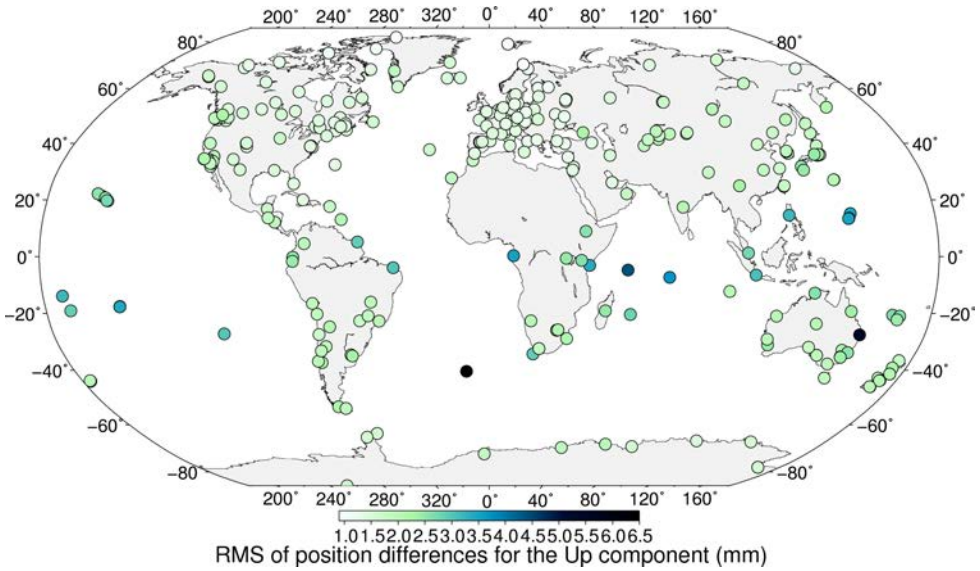

Figure A.2: Geographical distribution of the station-specific RMS statistics of the position differences over one year between the FCB- and IRC-based methods for the Up component

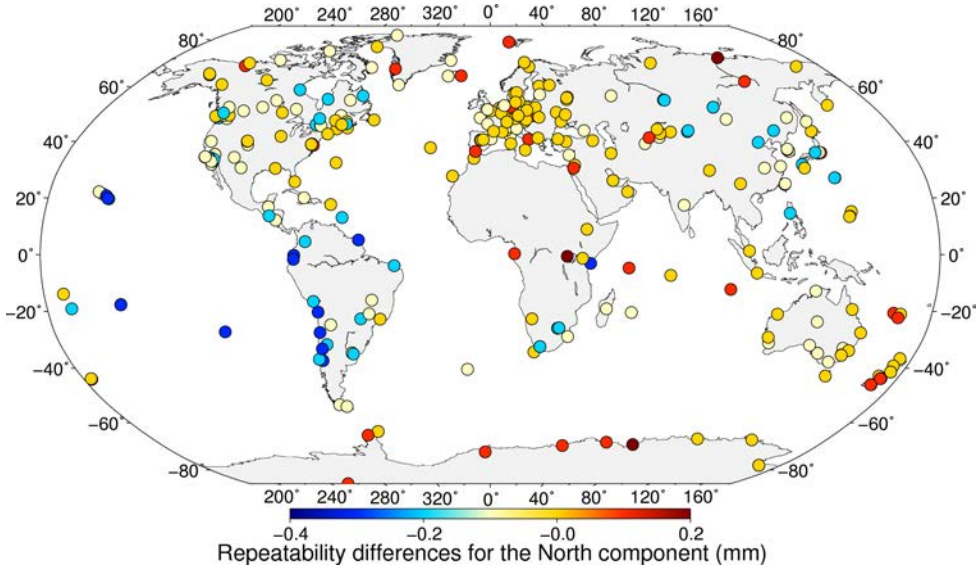

Figure A.3: Geographical distribution of the station-specific position repeatability of the FCB-based method minus that of the IRC-based method for the North component over one year

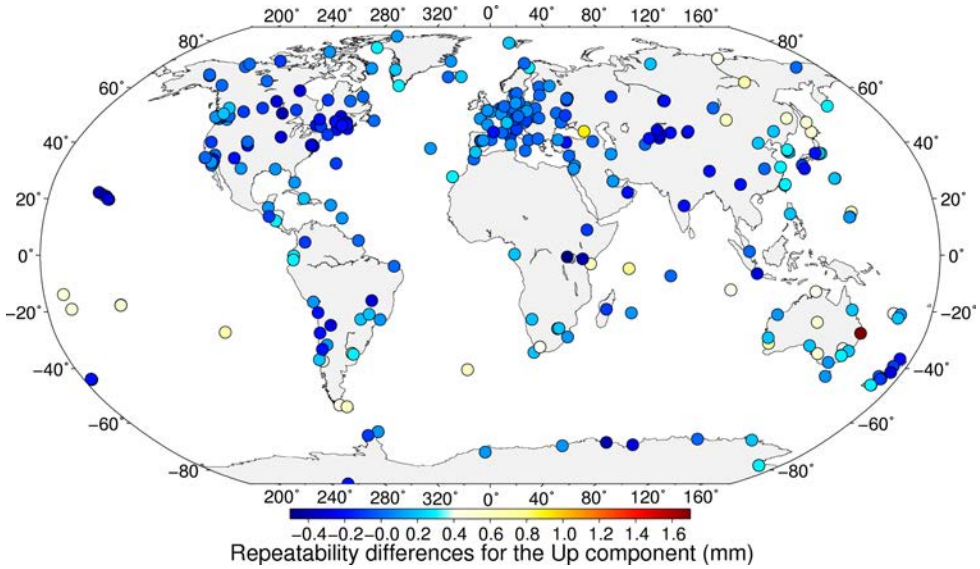

Figure A.4: Geographical distribution of the station-specific position repeatability of the FCB-based method minus that of the IRC-based method for the Up component over one year

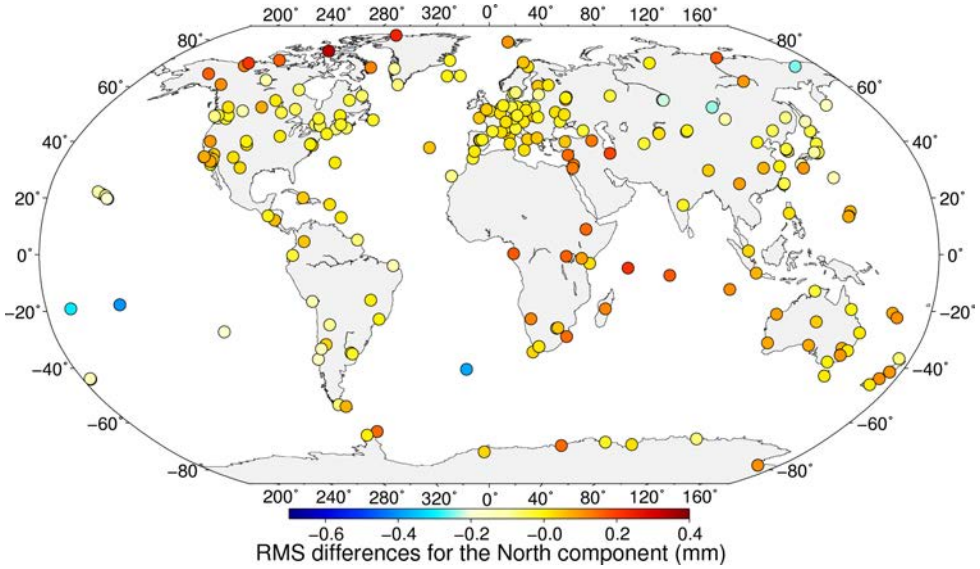

Figure A.5: Geographical distribution of the station-specific North RMS for the FCB-based method minus that for the IRC-based method. An RMS is computed over the residuals of ambiguity-fixed position estimates against the IGS weekly solutions for the North component over one year

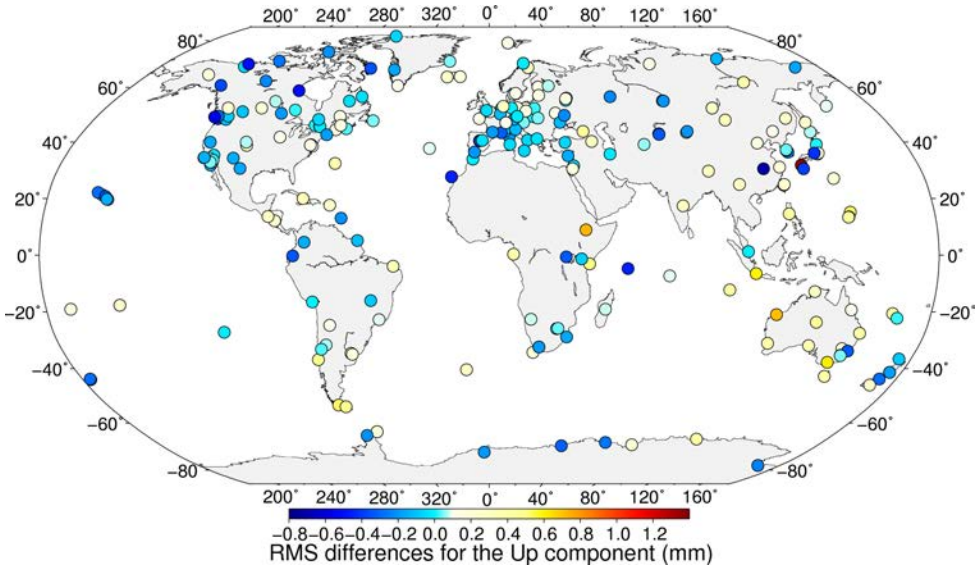

Figure A.6: Geographical distribution of the station-specific Up RMS for the FCB-based method minus that for the IRC-based method. An RMS is computed over the residuals of ambiguity-fixed position estimates against the IGS weekly solutions for the Up component over one year

Appendix B

Publications during this PhD study

Peer-reviewed journal publications

1. **Geng J**, Meng X, Dodson AH, Ge M, Teferle FN (2010) Rapid re-convergences to ambiguity-fixed solutions in precise point positioning. *J Geod* 84(12):705-714. doi:10.1007/s00190-010-0404-4

2. **Geng J**, Meng X, Dodson AH, Teferle FN (2010) Integer ambiguity resolution in precise point positioning: method comparison. *J Geod* 84(9):569-581. doi:10.1007/s00190-010-0399-x

3. **Geng J**, Teferle FN, Meng X, Dodson AH (2010) Towards PPP-RTK: Ambiguity resolution in real-time precise point positioning. *Adv Space Res.* doi:10.1016/j.asr.2010.03.030

4. Shi C, Lou Y, Zhang H, Zhao Q, **Geng J**, Wang R, Fang R, Liu J (2010) Estimating seismic displacement of the Mw8.0 Wenchuan earthquake from high-rate GPS observations. *Adv Space Res* 46(2):228-235. doi:10.1016/j.asr.2010.03.006

5. **Geng J**, Teferle FN, Meng X, Dodson AH (2010) Kinematic precise point positioning at remote marine platforms. *GPS solut.* doi:10.1007/s10291-009-0157-9

6. **Geng J**, Meng X, Teferle FN, Dodson AH (2010) Performance of precise point positioning with ambiguity resolution for 1- to 4-hour observation periods. *Surv rev* 42(316):155-165

7. **Geng J**, Teferle FN, Shi C, Meng X, Dodson AH, Liu J (2009) Ambiguity resolution in precise point positioning with hourly data. *GPS solut* 13(4):263-270

8. **Geng J**, Shi C, Zhao Q, Liu J (2007) GPS precision orbit determination from combined ground and space-borne data. *Geomatics and Information Science of Wuhan University* 32(10):906-909 (*in Chinese*)

Peer-reviewed conference publications

1. **Geng J** (2009) Rapid re-convergence in real-time precise point positioning with ambiguity resolution. In: Proceedings of the 22nd International Technical Meeting of the Satellite Division of Institute of Navigation, 22-25 Sep, Savannah, GE, US. (*best student paper*)

2. Gao R, Meng X, **Geng J**, Yu H-S, Xu L (2008) Application of real-time precise point positioning and GIS for rail track deformation monitoring of the Qinghai-Tibet railway. In: Proceedings of the 11th International IEEE Conference on Intelligent Transportation Systems, 12-15 Oct, Beijing, China

Other publications

1. **Geng J**, Meng X, Teferle FN, Dodson AH (2009) Continental centimetric real-time precise point positioning with ambiguity resolution. In: Proceedings of the European Navigation Conference, 3-6 May 2009, Naples, Italy

2. **Geng J**, Meng X, Teferle FN, Dodson AH, Ge M, Shi C, Liu J (2008) Performance of hourly precise point positioning with ambiguity resolution. In: Proceedings of the 21st International Technical Meeting of the Satellite Division of Institute of Navigation, 16-19 Sep, Savannah, GE, US

3. **Geng J**, Meng X, Teferle FN, Dodson AH (2008) Hourly precise point positioning with ambiguity resolution. In: Proceedings of the Navigation Conference & Exhibition NAV08/-ILA37, 28-30 Oct, London, UK

4. Shi C, Zhao Q, **Geng J**, Lou Y, Ge M, Liu J (2008) Recent development of PANDA software in GNSS data processing. In: Proceedings of the Society of Photographic Instrumentation Engineers, 7285, 72851S. doi:10.1117/12.816261

5. Li M, **Geng J**, Shi C, Zhao Q (2008) Orbit determination of geostationary satellite during manoeuvres. In: Proceedings of the Society of Photographic Instrumentation Engineers, 7285, 728520. doi:10.1117/12.816380

6. Shi C, **Geng J**, Meng X, Ge M, Teferle FN, Dodson A.H. (2008) A novel real-time data screening approach in urban navigation. In: Proceedings of the European Navigation Conference, 23-25 Apr, Toulouse, France

Appendix C

Awards and professional experiences during this PhD study

1. **Awards**
   (a) Chinese Government Award for Outstanding Self-financed Students Abroad, 2009
   (b) Best student paper prize, Institute of Navigation, US, 2009
   (c) Travel prize by Graduate School, University of Nottingham, UK, 2009
   (d) New Navigator prize for the best presentation, Royal Institute of Navigation, UK, 2008
2. **Professional experiences**
   (a) Journal Reviewer for *Journal of Geodesy*, *GPS solutions* and *Survey review*
   (b) Member of IGS work group on PPP ambiguity resolution
   (c) Student member of American Geophysical Union since 2008
   (d) Student member of European Geosciences Union, 2009
   (e) Student member of Royal Institute of Navigation, 2008
   (f) Invited guest scientist to Helmholtz Center of GeoForschungsZentrum, Potsdam, Germany, 2010
   (g) Invited talk at University of Glasgow, UK, 2009
   (h) Invited talk at General Assembly of European Geosciences Union, 2009